

AD A 114784

REPORT DOCUMENTATION PAGE

1. REPORT NUMBER JHU/APL DST-8		2. GOVT ACCESSION NO AD-A114 784		3. RECIPIENT'S CATALOG NUMBER	
4. TITLE (and Subtitle) Developments in Science and Technology				5. TYPE OF REPORT & PERIOD COVERED Annual Report Fiscal Year 1980	
				6. PERFORMING ORG. REPORT NUMBER JHU/APL DST-8	
7. AUTHOR(s) Various				8. CONTRACT OR GRANT NUMBER(s) N00024	
9. PERFORMING ORGANIZATION NAME & ADDRESS The Johns Hopkins University Applied Physics Lab. Johns Hopkins Road Laurel, MD 20707				10. PROGRAM ELEMENT, PROJECT, TASK AREA & WORK UNIT NUMBERS Various	
11. CONTROLLING OFFICE NAME & ADDRESS Naval Plant Representatives Office Johns Hopkins Road Laurel, MD 20707				12. REPORT DATE Fiscal Year 1980	
				13. NUMBER OF PAGES 189	
14. MONITORING AGENCY NAME & ADDRESS Naval Plant Representatives Office Johns Hopkins Road Laurel, MD 20707				15. SECURITY CLASS. (of this report) Unclassified	
				15a. DECLASSIFICATION/DOWNGRADING SCHEDULE	
16. DISTRIBUTION STATEMENT (of this Report) Approved for public release; distribution unlimited.					
17. DISTRIBUTION STATEMENT (of the abstract entered in Block 20, if different from Report)					
18. SUPPLEMENTARY NOTES					
19. KEY WORDS (Continue on reverse side if necessary and identify by block number) See attached list.					
20. ABSTRACT (Continue on reverse side if necessary and identify by block number) This is a compilation of brief accounts of the Laboratory's significant work during Fiscal Year 1980 that can be reported on an unclassified level. The following areas are covered: Surveillance and tracking systems; weapons technology; weapon control systems; command control and communications systems; space science and technology; ocean science and technology; computer technology applications; biomedical science and engineering; fundamental research; energy, environment, and urban technology; and special-purpose laboratories at APL.					

acoustic transmission loss
aluminum corrosion
AN/SYS-1 certification
APL/Data Dictionary System
APL/MVS Interactive Computing System
area tracking and correlation model
boresight errors
commutator feed
computer terminal control switch
copper concentration in the ocean
distributed processing system
duct fires
electromagnetic levitation
electromagnetic wave scattering
electronically steerable RF array
environmental assessments
fiber-optic contention bus network
fiber-optic data link
Guidance System Evaluation Laboratory
HF data communications
hybrid computer system
image display system
information management
infrared radiation of cornea
intercoastal bran translocator
Johns Hopkins Radiation Oncology Clinic
Johns Hopkins Equipment Quality Assurance Program
Jupiter plasma measurements
magnetic phases
Magsat
missile lethality models
modulation of short ocean wave spectra
oceanographic data acquisition system
OTEC cold-water pipe
OTEC heat exchanger
paravane system
Programmable Implantable Medicaiton System
radar performance prediction model
radar sidelobe suppression
radar signal processor
radomes
Raman scattering
remotely piloted atmospheric probe
Sensor Evaluation Laboratory
space shuttle relay link
stenosis hemodynamics
surface diffusion and ESP
switching and memory phenomena
vibrational frequencies

(12)

JHU/APL DST-8
FISCAL YEAR 1980



APPLIED PHYSICS LABORATORY

**DEVELOPMENTS
IN SCIENCE
AND TECHNOLOGY**

Approved for public release; distribution unlimited.

S DTIC
ELECTE **D**
MAY 24 1982
A

*THE JOHNS HOPKINS UNIVERSITY • APPLIED PHYSICS LABORATORY
Johns Hopkins Road, Laurel, Maryland 20707
Operating under Contract N00024-81-C-5301 with the Department of the Navy*

Technical Coordinators
 Chairman, M. W. Woods
 A. Brandt
 J. R. Champion
 L. L. Cronvich
 G. P. Gendron
 R. L. McCally

Managing Editor
 M. B. Gilbert

Associate Editor
 A. L. Machurek

Staff Artist
 K. D. Runkles



Accession For	
DTIC O&I	<input checked="" type="checkbox"/>
DTIC TAB	<input type="checkbox"/>
Unannounced	<input type="checkbox"/>
Justification	
By	
Distribution/	
Availability Codes	
Dist	Avail and/or Special
A	

FOREWORD

The Applied Physics Laboratory (APL), a division of The Johns Hopkins University, is located in Howard County, Maryland, midway between Baltimore and Washington. Its work is carried out under contractual agreements between the University and the federal, state, and local governments. APL employs a staff of more than 2500 including 1300 professional scientists and engineers, of whom more than half have advanced degrees. Their ideas are implemented and extended through several field activities and a network of associate contractors and collaborators from coast to coast.

The primary mission of APL is to enhance national security and welfare by applying advanced science and technology to the solution of problems important to national objectives. The Laboratory conducts programs in fundamental and applied research, exploratory and advanced development, component engineering, systems engineering and integration, and test and evaluation of operational systems. Approximately 85% of the Laboratory's effort is for the Department of Defense. The great majority of this effort (some 79%) is for the Department of the Navy. Approximately 15% of the effort is devoted to nondefense areas, including space research.

The current programs at the Laboratory cover a wide range of activities. Many are broad in scope, long term, and highly classified and therefore not reportable in this document. Nevertheless, the selected articles are examples of the type of R&D conducted. The articles are solicited annually from the whole Laboratory and cover the APL fiscal year. Respondents are individuals or small groups who have been personally involved in particular efforts and are motivated to report to a wider audience. For the above reasons, this publication does not represent all or even the most important accomplishments of APL during fiscal year 1980 (1 October 1979 through 30 September 1980), but it does give an exciting glimpse of the talent and versatility of the staff.

APL was organized in 1942 under the auspices of the Office of Scientific Research and Development to develop a proximity (VT) fuze for anti-aircraft defense; that was the principal effort during World War II. The success of the VT fuze in the Pacific and European theaters is a matter of history. The era of emerging guided-missile technology extended from about 1944 to 1956. During that time, APL concentrated on providing better air defense for the Fleet by developing a family of shipborne surface-to-air missiles. The Navy-sponsored "Bumblebee" program pioneered many basic guided-missile technologies later used in other air, surface, and submarine missile programs.

The era of systems engineering began in 1956 with the commissioning of the first guided-missile cruiser. The experience gained during that period has found application in many systems of interest to the Navy in various warfare areas and to other branches of the government. A number of significant activities are proceeding in areas of special APL competence, including missile propulsion, missile guidance, countermeasures, and missile systems integration. Current APL work of a broader nature supports a number of advanced Fleet

combat systems, including aviation countermeasures, Tomahawk and Harpoon cruise missiles, and the solution of current battle group defense coordination problems, including major developmental support to the Navy as Technical Advisor to the Aegis Shipbuilding Project. APL has a major role in the conceptualization of future command, control, and communications (C³) systems to facilitate the operation of Naval forces. Both strategic and tactical aspects of the C³ process are being examined.

In addition to the Laboratory's varied systems activities on behalf of the surface fleet, it continues to provide technical evaluation of the operational Fleet Ballistic Missile (FBM) System. Quantitative test and evaluation procedures are applied to every newly commissioned ballistic missile submarine. Similarly, APL currently provides precise evaluation of the Army's Pershing missile programs. Significant programs are also under way for Naval strategic communications and tactical targeting. Since 1976, APL has had responsibility for planning and conducting a significant technical program to ensure the security of the FBM submarine fleet against possible technological or tactical countermeasures. The approach is to quantify all physical and tactical means that might be developed to detect, identify, and track our submarines and to propose and evaluate suitable countermeasures and tactics.

The Navy Navigation Satellite System, originally known as Transit, is one of the most important accomplishments of APL since the wartime proximity fuze and the surface-to-air missile program. APL invented the concept, demonstrated its feasibility, designed and built the initial satellite constellation, set up and operated a worldwide satellite tracking network, extended the knowledge of the gravity field of the earth by orders of magnitude, and served as the Navy's agent in bringing the system into use. Expertise acquired through that program is applied to the design and construction of scientific satellites and spaceborne scientific experiments, primarily for the National Aeronautics and Space Administration.

With the encouragement of the Department of Defense, APL is applying its talent and the experience developed in DoD programs to a number of government-sponsored civil programs. Some examples of the areas to which attention has been devoted in recent years are biomedical research and engineering; transportation; fire research; reduction of pollution of the biosphere; ocean thermal, geothermal, and flywheel energy systems; air traffic control; leak detection in natural-gas distribution lines; and advanced education.

The role of computer applications within APL has become so interwoven in all of the Laboratory's technical, systems, and administrative functions that progress in that area is difficult to report as separate accomplishments. However, by extensive and intensive use of integrated circuits and microprocessor logic in satellites, in radar and other naval systems, and in biomedical engineering and other civil areas, APL has become a recognized leader in the area of computer technology. Furthermore, it continues to pioneer

in innovative applications of computers of all sizes to problems of national importance. This trend is underscored throughout the document by the frequent references to computing as an integral part of most of the accomplishments reported herein.

To support its R&D activities through knowledge and experience in advanced research, the Laboratory performs basic research in biological, chemical, mathematical, and physical sciences related to its various missions. Through unique applications of system engineering, science, and technology to the needs of society, APL has enhanced the University's tradition of excellence while gaining worldwide recognition of its own.

Experimental facilities are a vital part of APL's total technical capability. They include facilities for experimental design, fabrication, and test; central research laboratories; and special-purpose laboratories. The principal task areas supported by the special-purpose laboratories include information processing, propulsion systems, missile guidance systems (for guided missiles and tactical systems), combat systems and radar, strategic systems, space testing, and satellite tracking and communication. These laboratories have continually evolved in equipment, configuration, and interconnection in response to the technical requirements of APL's mission. They now provide unusual capabilities that are not readily available elsewhere in either industry or government laboratories. Some new capabilities of that sort are discussed in this report.

CONTENTS

SURVEILLANCE AND TRACKING SYSTEMS

Introduction	12
AN/SYS-1 Certification <i>S. F. Haase, E. C. Weitzlar, and B. K. Carter</i>	16
Surface Radar Processor <i>R. E. Thurber, R. Rzemien, S. M. Myers, G. W. Riffle, and R. J. Clevering</i>	18
Performance Prediction Model for Radar Suites <i>B. M. Kraus and C. E. Cole, Jr.</i>	21
Time Sidelobe Suppression and Signal Isolation for Binary-Phase-Coded Pulse-Compression Waveforms <i>D. A. Day</i>	24
A Wideband RF Commutator Feed Technique for a Scanning Circular Array Antenna <i>E. P. Irzinski</i>	26

WEAPONS TECHNOLOGY

Introduction	30
A Digital Simulation for Missile System Survivability Analysis in a Multiple ECM Environment <i>K. T. Plesser and L. W. Wald</i>	32
Remotely Piloted Atmospheric Probe <i>M. L. Hill</i>	34
Broadband Radome Boresight-Error Tolerances for Homing Missiles <i>B. E. Kuehne and H. Y. Chiu</i>	37
Bank-to-Turn Missile Guidance Performance <i>R. T. Reichert</i>	40
Simplified Lethality Models of SAM Warheads <i>C. R. Brown</i>	43

WEAPON CONTROL SYSTEMS

Introduction	46
A Fiber-Optic Data Link <i>J. B. Ferguson, R. L. Nelson, and A. E. Davidoff</i>	48
Design of a Fiber-Optic Contention Bus Network <i>S. A. Kahn, R. L. Stewart, and S. G. Tolchin</i>	51
A Highly Survivable Distributed Processing System <i>M. E. Schmid, R. L. Trapp, and A. E. Davidoff</i>	54

COMMAND, CONTROL, AND COMMUNICATIONS SYSTEMS

Introduction	59
Area Tracking and Correlation Model <i>T. G. Bugenhagen, B. Bundsen, and L. B. Carpenter</i>	60

SPACE SCIENCE AND TECHNOLOGY

Introduction	64
Completion of the Magsat Flight Mission <i>F. F. Mobley</i>	66
Hot Plasma Measurements at Jupiter <i>J. F. Carbary and S. M. Krimigis</i>	68
Computer Model for the MILA Shuttle Relay Link <i>S. C. Jones</i>	71
Magnetic Levitation Theory <i>J. F. Bird</i>	74
Optical Measurement of the Modulation of Short Waves by Long Ocean Waves <i>F. M. Monaldo</i>	76
PILOT, a Precision Intercoastal Loran Translocator <i>C. R. Edwards</i>	79

OCEAN SCIENCE AND TECHNOLOGY

Introduction	85
Development of an Adaptable Oceanographic Data Acquisition System <i>I. R. Hunter and J. W. Petersen</i>	86
The Paravane System <i>H. M. Grady, D. N. Qualkinbush, and S. J. Kundin</i>	89
A Towable System for Monitoring the Copper Concentration in the Open Ocean <i>D. G. Ondercin</i>	92
Comparison of Acoustic Transmission Loss Measurements in Convergence Zones <i>A. M. Diamant</i>	95

COMPUTER TECHNOLOGY APPLICATIONS

Introduction	100
Hybrid Computer System Based on the IBM 3033 <i>M. D. Lasky, F. W. Miller, T. G. Boland, P. F. Bohn, H. D. Pixler, N. K. Brown, and R. B. McDowell</i>	102

Interface of Image Display System to APL's Central Processing System	104
<i>T. G. Boland, D. Brocklebank, and R. E. Stovall</i>	
The APL/MVS Interactive Computing System	107
<i>D. Brocklebank and W. T. Renich</i>	
Application of REAS(ON) to ADP Acquisition Regulations	109
<i>B. W. Kuвшinoff and W. T. Renich</i>	
APL/Data Dictionary System	112
<i>B. J. Pride</i>	

BIOMEDICAL SCIENCE AND ENGINEERING

Introduction	119
Radiation Oncology Clinic	120
<i>D. G. Grant</i>	
High Technology Equipment Quality Assurance Program	121
<i>D. G. Grant (APL) and T. M. Judd and J. T. Lalmond (Johns Hopkins Hospital)</i>	
Structural Corneal Alterations from Exposure to Infrared Radiation	123
<i>C. B. Barger, R. L. McCally, and R. A. Farrell</i>	
Stenosis Hemodynamics and Endothelial Response	126
<i>V. O'Brien, O. J. Deters, F. F. Mark, and L. W. Ehrlich (APL) and K. Sagawa and G. M. Hutchins (JHMI)</i>	
The Programmable Implantable Medication System	128
<i>R. E. Fischell and W. E. Radford</i>	

FUNDAMENTAL RESEARCH

Introduction	132
Gases Evolved During the Pitting Corrosion of Aluminum	134
<i>C. B. Barger and R. C. Benson</i>	
Surface Diffusion and Spin Polarization	136
<i>L. Monchick</i>	
An Electrodynamic Mechanism of Surface Enhanced Raman Scattering	138
<i>F. J. Adrian</i>	
Vector Stochastic Variational Principles for Electromagnetic Wave Scattering	140
<i>J. A. Krill and R. H. Andreo</i>	
Vibrational Frequencies of Composite Structures	142
<i>D. W. Fox and V. G. Sigillito</i>	
Magnetic Phases in Disordered Alloys	145
<i>K. Moorjani</i>	
Switching and Memory Phenomena in Semiconducting Charge-Transfer Complexes	147
<i>T. O. Poehler and R. S. Potember</i>	

ENERGY, ENVIRONMENT, AND URBAN TECHNOLOGY

Introduction	153
Tests of the OTEC Core Unit Heat Exchanger as a Condenser <i>P. P. Pandolfini, J. L. Keirse, and J. A. Funk</i>	154
Developmental Testing of a Concrete Cold Water Pipe for OTEC Systems <i>R. W. Blevins and J. S. O'Connor</i>	157
The Environmental Assessment Group's Accomplishments in Fiscal Year 1980 <i>W. D. Stanbro and L. G. Phillips</i>	160
Duct Fires <i>L. W. Hunter</i>	163

SPECIAL-PURPOSE LABORATORIES AT APL

Introduction	166
GSEL Target Doppler Simulator <i>S. F. Buono and M. M. Soukup</i>	168
An Electronically Controlled RF Array <i>H. C. Davey and H. H. Knapp</i>	170
Microprocessor-Controlled Terminal Control Switch <i>C. F. Waltrip</i>	172

PATENTS

176

PUBLICATIONS AND PRESENTATIONS

180

AUTHOR INDEX

188

SURVEILLANCE AND TRACKING SYSTEMS

INTRODUCTION

APL's involvement in surveillance and tracking systems covers a wide spectrum of programs. However, the work described in this section is directed at improving the present and future capabilities of Navy surface combatant radars used in anti-air warfare (AAW). These radars perform the functions of maintaining surveillance of the air space surrounding the ship and those in company and of tracking engaged targets in support of the fire-control process. Functionally, surveillance includes detecting aircraft and missiles and tracking them for the purpose of developing and displaying a complete and accurate picture of air activity. The fire-control tracking function differs from surveillance with respect to the requisite precision and accuracy of target position and rate measurements. In general, tracking radars considered in this section are used to control Standard Missile engagements.

Historically, the first surveillance radars used a beam shape that was relatively narrow in the azimuth plane but fan shaped in elevation in order to cover all target altitudes of interest. Such radars became known as "2D" because they could measure the target's range and azimuth. Azimuth was determined from the mechanical position of the antenna as it rotated. The radar signals were presented to the operator in a range-azimuth format from which he could develop a plot of target-position histories. In order to engage a target, a fire-control tracker had to be assigned. Because of the unknown target elevation, the differences in azimuth resolution, and the imprecise range and range rate data, the acquisition of the designated track by the fire-control radar entailed considerable local search. The net result was a relatively long reaction time as measured from first observation of the target by the 2D operator until weapon launch. There could be only one engagement per tracker because the mechanical pointing of the tracker antenna axis was used both to control tracking and to update the fire-control solution.

The next major innovation in this process was the development of the "3D" air search radar, which used a beam that was narrow in both azimuth and elevation. While the beam scan in azimuth was still produced by a mechanical rotation of the antenna, scan in the elevation plane evolved rapidly from mechanical to electronic means. Such a radar could measure target elevation in addition to range and azimuth. The 3D measurement concept, combined with the higher angular resolution afforded by the trend toward higher operating frequencies for surveillance radars, significantly reduced the local search volume during fire-control tracker acquisition. Although this shortened the reaction time somewhat, the manual track plotting and designation process still took relatively long.

As the speeds of attacking vehicles increased and the target characteristics shifted from those of aircraft to cruise missiles, reaction time became a dominant consideration in weapon system design. APL took the lead in a two-pronged attack to reduce reaction time, one addressing existing systems and the other new designs.

For the existing systems based on rotating radars, the approach was to automate the track plotting process, to instrument the radars to provide full inherent measurement accuracy to the automated process, and to provide electrical transfer of track designation data to the fire-control radar. Before those things could be done, significant work in automatic threshold control was necessary to emulate the operator's ability to separate aircraft returns from background clutter and jamming. The result of that phase of the effort, SYS-1, has been evaluated operationally in a shipboard installation and has demonstrated the expected improvement in reaction time. However, reaction time was still a few tens of seconds.

It was soon recognized that the best a conventional system (i.e., a rotating surveillance radar designating to a dedicated fire-control tracker) could achieve in terms of reaction time and rate of engagement would not be adequate against future threats requiring a reaction time of less than 10 seconds for successful defense. It was apparent that a weapon system capable of completely automatic operation from detection through evaluation of the result of the engagement was needed. Further, neither the track initiation and evaluation delays inherent in the rotation-rate limitations of conventional surveillance radars nor the surveillance-to-track hand-over delays could be tolerated. Event-by-event beam placement control (made possible by the phased-array antenna) combined with advanced signal-processing features and modern computer technology were required to achieve the necessary reaction time. The multifunction phased-array radar merged the surveillance and fire-control tracking functions so that track information of sufficient quality for threat evaluation and engagement support was available less than a second after initial target detection. The same features that led to fast, automatic reaction also resulted in the capability to track a large number of targets with accurate fire control, thereby increasing the number of engagements per unit time that such a system could prosecute significantly compared with conventional, dedicated tracking radar systems. In the mid 1960's, APL began the design of an advanced development radar to demonstrate these principles. Known as AMEAR, that radar was operational in 1968. The demonstrated principles formed the basis for the Aegis weapon system. The first Aegis-equipped ship is scheduled to be operational in early 1983.

Within the context of AAW radars, the programs described in this section are diverse; however, they are roughly separable into those supporting the continuing evolution of conventional, rotating, surveillance-dedicated tracker systems and those supporting multifunction phased-array weapon system radars. The tasks are directed toward providing the Navy with radar performance to meet current and future AAW requirements. As a part of this objective, studies are done to interpret new threat characteristics in terms of their impact on existing radars and on requirements for future equipment.

The several programs addressing evolutionary improvements to conventional radar equipments, as a class, seek to improve the surveillance function

by applying modern automation technology to better use the outputs of the radars by means of a process known as integrated automatic detection and tracking (IADT). The equipments that perform this function have been assigned the nomenclature SYS-(). SYS-1 is in production for use on DDG class ships, and SYS-2 is being developed for use by Terrier CG class ships. To achieve the current, demonstrated level of SYS performance, a number of video processing developments were needed in order to provide automatic control of the detection process and to be resistant to changes in the clutter environment. This work is continuing; it is described in the paper on a processor for surface search radars.

The region between those evolutionary improvement tasks and those directed at new, advanced-technology radars is bridged by analytical work of the type described in the paper on performance prediction for radar suites. The surveillance system is modeled as a collection of radars tied together by an IADT function. The unit radars are generally considered to be relatively conventional in that mechanical rotation is used to obtain the azimuth component of the radar beam scan. The analytical approach allows the evaluation of proposed new radar designs of the conventional type on a surveillance system level.

Phased-array multifunction radars capable of satisfying both surveillance and fire-control tracking needs may be considered *unconventional*, or *futuristic*, in that the first combatant equipped with such a radar, the *Ticonderoga* (CG-47) equipped with Aegis, will be commissioned in early 1983. Nevertheless, APL has been assisting the Navy in reaching the goal represented by this ship for over 15 years.

The final category of tasks is that directed at assuring that the new class of equipment remains technologically current. The core weapons system programs for which the above radar work is intended (the DDG 2/15 upgrade, CG new threat upgrade, and Aegis) have been under way for a number of years. APL's role has varied with time for each program, but the cycle has been relatively consistent beginning with the definition of a concept for a system to meet some observed or anticipated change in the nature of threat or for the provision of some new functional capability. APL's strong role in concept definition and subsequent equipment development and test has led to the position of technical advisor to the Navy while the technology is transferred to industry and production equipment is designed and tested. APL's role has reached the latter stage in the three major weapon system programs. In the case of Aegis, however, concept definition has begun anew for the sequence of technology upgrades for phased-array radars that appear to be made necessary by the threat and to be made possible by advancing technology.

AN/SYS-1 CERTIFICATION

S. F. Haase, E. C. Wetzlar, and B. K. Carter

The operational computer program for the AN/SYS-1 Integrated Automatic Detection and Tracking (IADT) system, which automatically combines radar detections from several radars to form target tracks, has been tested extensively at system level in preparation for integration with the combat system. Testing has been accomplished at APL by using a separate computer to simulate the remainder of the combat system, including target trajectories, the radar detection process, command and control, and weapons control. Successful completion of the testing and certification of readiness represents a significant step toward the deployment of the major new combat system.

BACKGROUND

As part of a recent modernization program, the Navy designated six ships of the DDG 2/15 Class for upgrade using the IADT approach to sensor integration along with improved versions of the tactical data system, the weapon direction system, and the fire control system. The IADT system developed at APL, formally designated AN/SYS-1, was subjected to extensive testing, including land-based testing at APL, followed by Technical Evaluation and Operational Evaluation at sea by Navy personnel.

The Operational Evaluation in 1978, was highly successful, and the system was approved for service use. A few relatively minor modifications were requested by the Navy to further improve performance and reliability. With the development phase essentially completed by APL, the SYS-1 computer program was turned over to Norden Systems for implementation of the requested modifications in preparation for formal acceptance by the Navy. The requirement that the modified SYS-1 computer program be certified by the Navy prior to combat system integration resulted in comprehensive certification testing, which took place at APL between January and June of 1980.

A Certification Test Team was appointed by NAVSEA-62X to conduct the test and report the results. The team, led by APL, included members from the Naval Sea Systems Command Detachment, Norfolk, and Vitro Laboratories, with support provided by Norden Systems.

The system under test consisted of two operational computer programs, a full-capability Normal

program for two AN/UYK-20 computers, and a reduced-capability Casualty program for one. Enough displays and controls were provided for efficient operator control of the detection and tracking processes as well as to monitor communications between SYS-1 and the remainder of the combat system.

The approach used in SYS-1 is to combine all available sensor data into a comprehensive data base of target information. The sensor data are used to update a single unduplicated track file, thereby reducing storage requirements and improving track continuity. Track initiation and update are automatic, which improves track accuracy, reduces reaction time, and increases target capacity compared with manual tracking. To avoid overloading the system, the radar detection process is monitored and controlled so that the false alarm rate remains low and relatively constant while optimum sensitivity is maintained for any radar environment encountered.

DISCUSSION

The principal objective of certification testing was to ensure that the SYS-1 Normal and Casualty programs met the performance requirements of the IADT system specification¹ and the various interface design specifications, as well as the software quality requirements of NAVMATINST 5230.5A.² The requirements of those documents were assembled into a test specification that identified 17 individual tests (Table 1), each with its own pass/fail criteria. Procedures were developed for each test, including a scenario

Table 1

TESTS CONDUCTED DURING SYS-1 CERTIFICATION TESTING

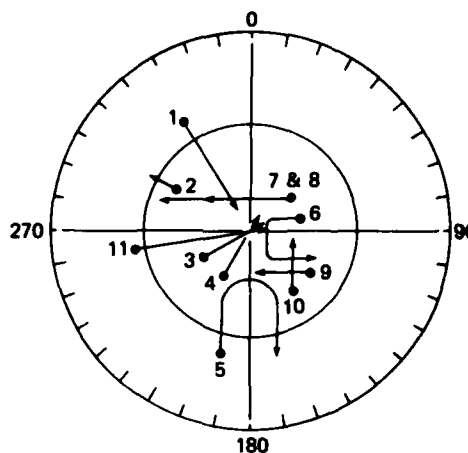
Instrumented volume of coverage
Performance volume of coverage
Track capacity
Track classification and automatic drop criteria
Track resolution
Track continuity
False track performance
Track accuracy
Designation accuracy
Multiradar alignment
Track acquisition
Long range track acquisition
Reaction time
Casualty mode operation
AN/SYS-1 interface functions
Displays and controls
Software quality

of about 20 simulated targets to exercise SYS-1 and to determine whether the system responded as required. For example, the scenario shown in Fig. 1 was used to check the maneuver tracking capability of SYS-1 in the track continuity test.

In order to exercise SYS-1 in the combat system environment and with a specific scenario of targets, a separate computer simulation, known as the AN/SYS-1 Wrap Around Simulation Program (WASP), was used to simulate the remainder of the combat system. WASP could simulate three-dimensional target trajectories and the radar detection process, including the effects of measurement noise, detection probability, and target radar cross section. It also simulated the interfaces with the tactical data system and the weapon direction system to verify communications with them.

Most data were provided by the SYS-1 data extract feature, which was part of the Normal program. Data extraction was controlled by the SYS-1 operator according to the requirements of each test. Extracted data were stored on magnetic tape and later processed to determine if SYS-1 responded as required. A test observer log was also maintained to supplement the data extract. No data extract feature was available to test the Casualty program, and the pass/fail criteria were based on observation of the various operator displays.

Program problems revealed during testing were documented with Program Trouble Reports and recommended solutions, which were submitted to a Local Configuration Control Board for review and approval. Approved Trouble Reports were returned to Norden Systems for preparation of Engineering Change Proposals. Completed Change Proposals were submitted to the Navy for final approval. Close cooperation among all parties concerned gave the



Notes: Not drawn to scale.
Target numbers are indicated.

Fig. 1 Target scenario for track continuity test, shown on PPI display.

necessary control over the computer program while resolving problems rapidly.

Based on the intensive nature of the certification testing and the results of the data analysis, it has been concluded that the SYS-1 operational programs meet the performance requirements of Ref. 1. The SYS-1 system is now being integrated with the rest of the combat system at the Integrated Combat System Test Facility at San Diego.

REFERENCES

- ¹System Specification for the Integrated Automatic Detection and Tracking System, WS-19879, Appendix I.
- ²NAVMATINST 5230.5A (TADSTAND 9), 094/WAP, Ser. 260 (18 Aug 1978).

SURFACE RADAR PROCESSOR

R. E. Thurber, R. Rzemien, S. M. Myers, G. W. Riffle,
and R. J. Clevering

A signal processor was developed as part of an in-house research and development project in semicoherent Doppler processing techniques. The processor demonstrates the advantages of Doppler processing for surface surveillance radars and provides markedly improved detection in clutter.

BACKGROUND

The complexity of digital signal processing, particularly Doppler processing in noncoherent radar systems, has limited the application of Doppler techniques in several important classes of radars, including shipboard surface surveillance radars, coastal surveillance radars, and ship collision-avoidance radars. Each of these would benefit significantly from Doppler processing because of the better detection of small surface targets in sea clutter and the better discrimination of moving and stationary surface contacts.

A signal processor was developed that accepts radar video as an input, performs Doppler filtering, and formats detection data for recording on a digital magnetic tape system. The design is versatile enough to handle the parameters of most surface surveillance radars. The purpose of the development was to demonstrate the advantages of Doppler processing on surface surveillance radars by recording and analyzing actual sea surface surveillance data.

In addition to front end radar signal processing, a data processing technique was developed that significantly reduces the false alarm rate (FAR) of the output data so that long-term scan history displays can be provided for an operator and reliable data can be provided for automatic detection and tracking. The retrospective data processor has the unique property of reducing the FAR by five or six orders of magnitude while causing practically no loss in target detectability. The front end processing can be run at a high, yet well regulated, FAR for maximum target detectability in a clutter environment. The data can then be filtered by the retrospective data processor to yield an output with a very low FAR.

The signal processor has been used in the field to process and record data from two different types of sea-surface surveillance radars in actual operating environments. It has also been used to process analog radar data recordings from shipboard surface surveillance radars. The results of the data collection and analysis to date indicate that the signal processing techniques developed as part of this program can provide significant advances in the display and use of data from surface surveillance radars.

DISCUSSION

Figure 1 shows the signal processor and the associated data recording equipment. The processor

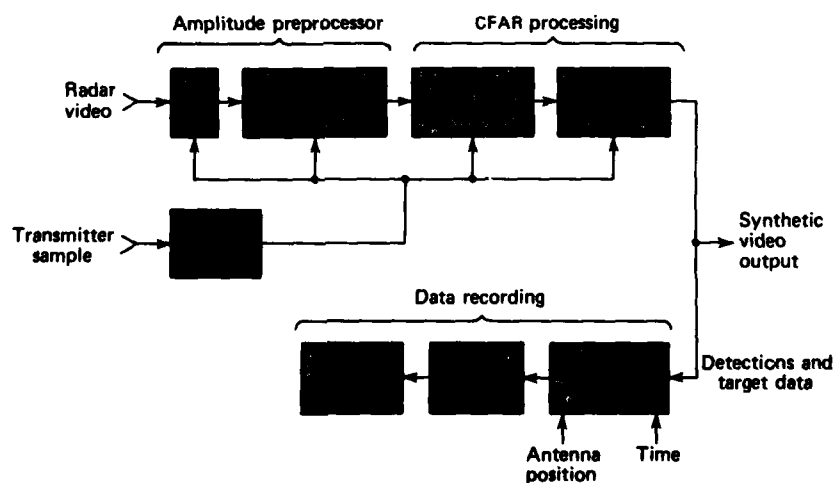


Fig. 1 Signal processor and data recording equipment.

consists of an amplitude preprocessor where input video is digitized and filtered, a CFAR processing section where filtered data are detected with a low and well-regulated FAR in all environments, and data formatting circuits for interfacing with the digital magnetic tape system.

Three features of the processor make it exceptionally well suited for processing data from sea surface surveillance radars. The first is the use of a very wide dynamic range in the processing circuits. A dynamic range of at least 60 dB is required to perform effective Doppler and CFAR processing in the presence of sea clutter. This range is obtained by using the output from the radar logarithmic receiver and digitizing it to 8 bits. The 8 bit log data are then converted to 12 bit linear data for Doppler processing.

The second feature is the programmable filter in the amplitude preprocessor. It is a digital nonrecursive or transversal type and can be programmed for each range sweep to provide outputs with different filter weights. This allows Doppler data and moving window integrated data to be processed on the same circuits.

The third unique feature is the two-stage CFAR processing. The first stage works on a local basis and determines the two mean levels of the 16 range cells on either side of the target cell of interest. The greater of the two means is subtracted from the target cell to produce a CFAR output. The two range cells immediately adjacent to the target cell are excluded from the mean estimate to prevent the target from corrupting the estimate. Both the target amplitude and the background amplitude are sent to the recording system as part of the data field recorded for each detection.

The target-minus-mean is input to the slow CFAR control loop, which works on a regional basis. The

value is compared to a threshold that is regulated in a closed loop to produce detections with a 10^{-5} probability of false alarm. Operation at a high FAR produces many samples over the region of control and allows for precise regulation. The slow CFAR loop is segmented in both range and bearing to allow independent false alarm control in 64 separate regions of the radar plan view.

The closed loop threshold value for each segment is multiplied by a constant and is compared to the target-minus-mean to produce detections at a low FAR. Multiplication of the closed loop threshold by a constant keeps the output FAR at a constant value determined by the scale factor, regardless of the input clutter distribution, as long as the distribution is in the Weibull family.

The final output detection goes to the data buffer for digital recording and also to an analog buffer for display as synthetic video. The range, bearing, amplitude, and amplitude of the background about the contact are recorded for every contact.

Figure 2 represents the data collection and reduction process on the host radar. The plan position indicator (PPI) display is used for viewing both the raw radar video and processed video from the collection system. The radar interface includes antenna synchro, system trigger, and radar log video.

Digital recordings of the contacts are made and returned to APL for reduction. The tapes are played through a reconstruction system on the PDP 11/70 computer, which unpacks the contact data and computes the centroids of the contacts. The centroids are displayed in polar form on a graphics display where the range of the display and also the desired number of scans of data can be selected. This allows a history for

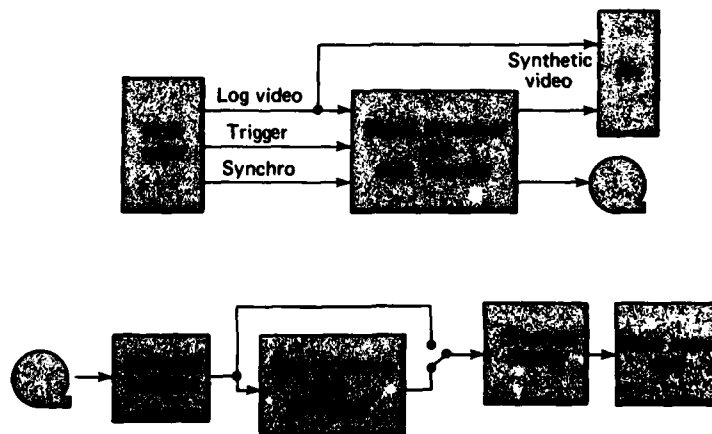


Fig. 2 Data collection and analysis system.

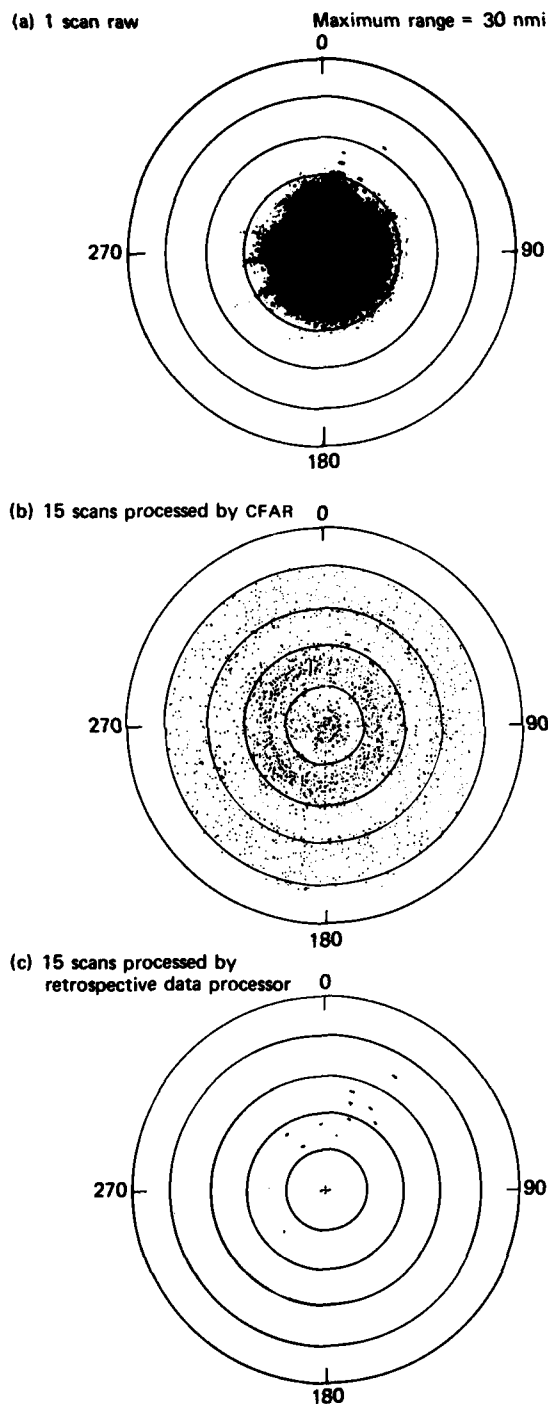


Fig. 3 Centroid history displays, AN/SPS-67 radar, open ocean, sea state 5, 11 ships in convoy.

any number of scans to be presented on the graphics display. A hard copy of that display can be obtained through a Tektronix hard copy unit.

For targets in clutter, the detectability is excellent using the processor. However, for even a moderate FAR of 10^{-6} or 10^{-7} , the scan history displays soon become cluttered with false alarms because of the large number of sample cells present. A total of 25 to 50 scans (2 to 4 min) of data is about all that can be displayed at the normal FAR before the display becomes cluttered.

To obtain good surface target tracks for an operator on a scan history display, 150 or more scans are desirable. To obtain a clutter-free scan history display for hundreds of scans, the retrospective data processor was developed. This processor examines each centroid and compares it with centroids from the previous seven scans if they fall within a certain range and bearing window about that centroid. The centroid of interest is displayed only if it forms a "probable track" with centroids from the previous seven scans. The range and bearing windows are set to allow examination of all prior contracts that could result from a target moving at up to 35 kt in any direction.

An example of data obtained with the signal processor and data reduction routines is shown in Fig. 3. The data were produced from an analog radar video recording taken aboard the USS *Marvin Shields* on the AN/SPS-67 surface surveillance radars. *Marvin Shields* was in a convoy with 10 other ships in the open ocean with heavy seas. The radar was transmitting a $0.1 \mu\text{s}$ pulse with a scan time of 4 s. The sea clutter extended to 12 nmi, making the detection of close-in ships by raw video very difficult (Fig. 3a).

The signal processor was run with the lowest threshold setting to produce the highest FAR and the best target detectability. The effect of the segmented CFAR can be seen in the uniform FAR over the radar plan view (Fig. 3b). The plot is for 15 scans (1 min) of centroid data.

The retrospective data processor output plot in Fig. 3c shows that the probability of a false alarm, P_{fa} , of 10^{-4} for the input is reduced to about 10^{-12} for the output, with little or no loss in target detectability. The plot is of the same 15 scans of data. The 10 other ships in the convoy are clearly visible; only a few false targets were caused by the ship's mast reflection.

REFERENCE

- ¹ R. E. Thurber, *Data Collection and Analysis, AN/FPS-114 Surface Surveillance Radar*, JHU/APL FS-80-210 (Aug 1980).

PERFORMANCE PREDICTION MODEL FOR RADAR SUITES

B. M. Kraus and C. E. Cole, Jr.

A software simulation package that models the operation of Navy shipboard surveillance radar systems has been successfully designed, developed, and tested at APL. The simulation encompasses a system, the radar suite performance prediction model, that provides the ability to predict the detection and tracking performance of a multiradar suite in an integrated automatic detection and tracking (IADT) configuration against a multitude of expected enemy threat scenarios.

BACKGROUND

The need for the model arises from IADT implementation and procurement cost reduction. The IADT concept is an integral part of the radar surveillance and track generation processes of a combat system. It is relatively new in the Fleet and is basically a synergistic integration of radar detection data from several complementary radar sets. Procurement costs for Navy shipboard surveillance radar systems are reduced by contractor competition, and contractors may be asked to propose conceptual designs for radar suites. A generic and flexible system was needed to model various radar suites and to incorporate IADT processes, and the Navy required quantifiable simulated performance data for a thorough evaluation and screening of the competing contractor proposals. This model satisfies both needs.

DISCUSSION

The radar suite performance prediction system is composed of two major elements (Fig. 1). The first,

which was developed for the Navy by Technology Service Corp., is called the single radar performance prediction system. It models the operation of a selected radar, in a specified mode, against a selected scenario with an associated environment. The outputs include detection plots, tabular data, and magnetic tape data. The magnetic tape contains the data outputs for several runs of the system and enables a group of selected radars, which constitute a shipboard radar suite, to be modeled by the second element, called the sensor integration and control performance prediction system (SI&C).

Each shipboard radar suite will provide the necessary level of surveillance to support the group of Naval warfare mission areas assigned to the ship. Threat/environment sets reflect the scenarios associated with an assigned mission and also reflect the surveillance requirements for the radar suite in terms of detection/disclosure ranges. The single radar performance prediction system can be adjusted to model each radar in a proposed radar suite. The magnetic tape output provides inputs to the SI&C; then the suite's performance is plotted and printed for evaluation.

Figure 2 illustrates the operation of the SI&C. The control element simulates the operation of the radars in the suite by accessing precomputed values of the probability of detection, P_d , and deciding statistically whether P_d is translated into an actual radar detection or into no radar detection. For the model, P_d is a function of the radar being simulated, the radar operating mode, environment parameters, target size and range. Figure 3 is a graph of P_d versus ground range for the radars in the suite.

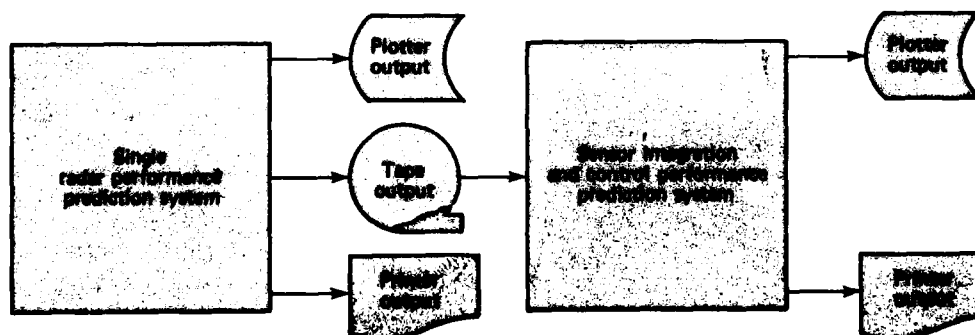


Fig. 1 Radar suite performance prediction model.

The control element performs the functions of user interaction, antenna beam coordination, radar mode selection, contact opportunity validation, and tracking algorithm interface.

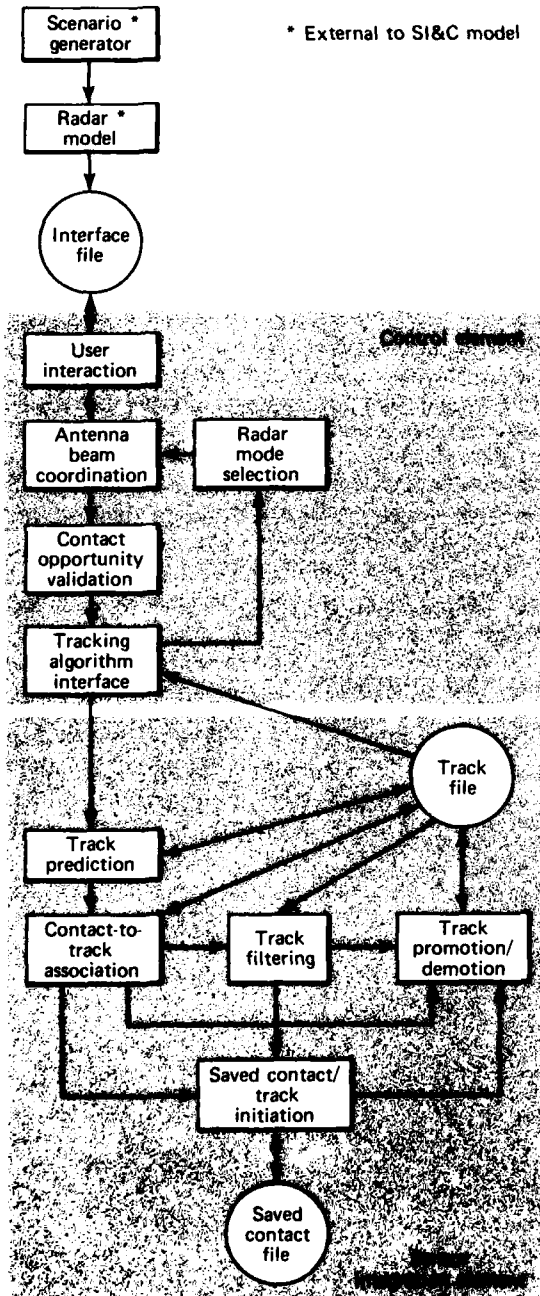


Fig. 2 Functional diagram of sensor integration and control.

User interaction, the interface between the user and the model, allows variables to be selected that affect the P_d . As many as three radars can be simulated in a run: a two-dimensional surface search radar, a two-dimensional air search radar, and a three-dimensional air search radar. To complete the suite description, an antenna azimuth rotation rate and an initial operating mode for each simulated radar must be selected. The user also selects the scenario in which the radar suite is to operate. Scenario is defined here to mean one target defined by a single radar cross-sectional value, a trajectory, and the environmental conditions imposed on the suite. Environmental conditions can be non-benign (any combination of rain, sea state, and electronic countermeasures) or benign.

Antenna beam coordination randomly initializes each radar's antenna beam in azimuth and uses the radar's azimuth scanning rate to simulate the azimuth scan. The simulated azimuth scan and initial azimuth beam position are used to determine the time each radar's main beam illuminates the target as the target moves along its trajectory. These times translate directly into radar-to-target ranges, which are the final variables needed to determine the P_d that results when a radar illuminates a target in the presence of particular environmental factors at some range. The P_d values are accessed in a monotonically increasing time sequence.

Radar mode selection automatically varies the radar's initial operating mode in a preprogrammed fashion as the scenario progresses, by means of radar processing control gates and track gates. Radar processing control gates modify mode and detection thresholds to accommodate clutter in the threat profile. Track gates change a radar's detection level in an area where a track is known to exist.

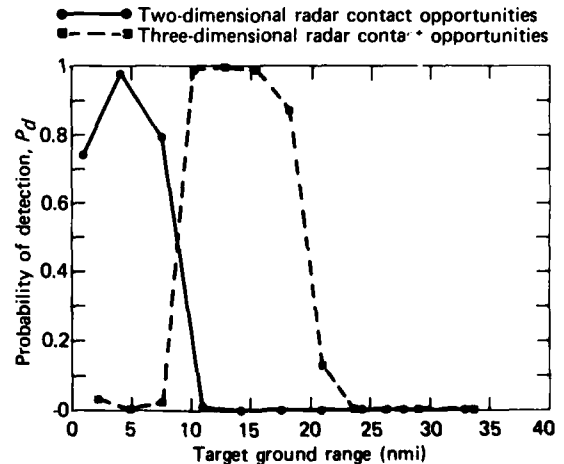


Fig. 3 Probability of detection versus ground range.

Contact opportunity validation incorporates a uniform random number generator to determine if the selected P_d value should be passed to the sensor integration element as a radar detection or as a missed detection.

The tracking algorithm interface transfers detection (contact opportunity) and track data between the control and the sensor integration elements. The contact opportunity data consist of an identification code, position measurement data, measurement accuracies, and an indication of detection/missed detection. The sensor integration element maintains two files of track data: air track and clutter track. Track status data are the feedback required by the control element to implement the mode changing schemes.

The sensor integration element of the SI&C determines the disclosure range for surveillance radar suites. Disclosure range is defined as the range at which the surveillance radar suite (continuously) indicates the presence of a new contact with high confidence. For a crossing or closing target, it is the range at which radar returns, when processed through the automatic detection and tracking initiation logic, provide a 90% probability of maintaining system track. Within this range, track continuity with specified accuracies must be maintained.

The disclosure range is established after completing the target scenario and observing the range interval where continuous track is maintained. If it is maintained from the required disclosure range to some specified minimum range, then the run is successful. A Monte Carlo approach shows whether 90% of the runs have the prerequisite continuous track interval.

The sensor integration element performs the following major functions:

1. Track prediction, which extrapolates the position of tracks to some future time for the purpose of association.
2. Contact-to-track association, which determines if a contact belongs to a group of contacts, called a track (clutter and air), that the sensor integration element decided previously is from the same target.

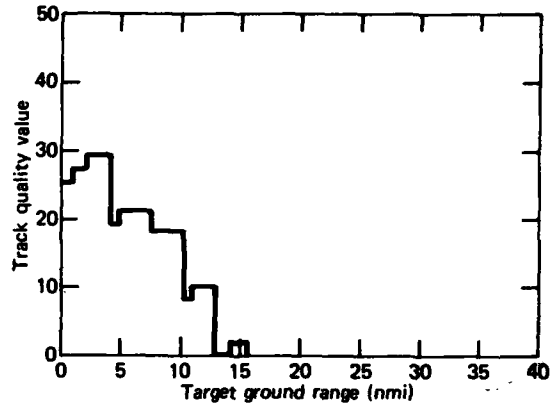


Fig. 4 Sample graph of track quality, corresponding to values in Fig. 3.

3. Track filtering, which incorporates a Kalman filter algorithm to estimate a track's position when additional data become available as a result of the association function.
4. Saved contact/track initiation, which saves new contacts that might be from a newly detected target. The saved contacts are used subsequently when attempting to form new tracks. This function also discards saved contacts that, after a certain number of scans of the initiating radar, have not been used to form a new track because they probably were false alarms.
5. Track promotion/demotion, which incorporates a sequential log-likelihood ratio test to compute the probability that a track is from a real target as opposed to false contacts (tracks generated from clutter returns and thermal noise).

Figure 4 is a sample track quality graph corresponding to the P_d values in Fig. 3. Examination of Figs. 3 and 4 shows the benefits of IADT. When P_d is low for the two-dimensional radar, it is high for the three-dimensional radar and vice versa. This results in a track quality that is essentially a monotonically increasing function.

TIME SIDELobe SUPPRESSION AND SIGNAL ISOLATION FOR BINARY-PHASE-CODED PULSE-COMPRESSION WAVEFORMS

D. A. Day

Time sidelobes of radar pulse-compression waveforms are key design parameters. Conventional linear approaches to pulse compression allow sidelobe levels to be transformed by an amplitude-weighting derivable, using simple techniques. However, time sidelobes of pseudorandom phase codes favored for pulse compression in weapon system radars oriented to electronic counter-countermeasures cannot be controlled by conventional amplitude-weighting approaches. Therefore, linear programming techniques have been used to derive amplitude weighting that can reduce random time sidelobes.

BACKGROUND

Pulse-compression waveforms have been used in radar and communication systems to improve the effective signal-to-noise ratio (S/N) while maintaining high time resolution. A long pulse with low peak power will result in high total energy but poor time resolution. Pulse compression maintains the long pulse and high energy while yielding a time resolution comparable to that achieved with a short pulse length.

One method of pulse compression is to code the pulse pseudorandomly. The received pulse is demodulated to yield the transmitted coded sequence, which is then correlated with a reference code sequence. The result of the correlation is a single peak response when the two code sequences are aligned in time. The peak response is of much shorter duration than the transmitted pulse, thereby providing time resolution better than that attainable by the uncompressed long pulse.

The reference and the transmitted code sequences used in the correlation are usually the same. The output of the correlation is the autocorrelation of the code sequence that results in the maximum S/N. The ideal output of the correlation would be a zero response for all times except when the codes are time aligned; then the peak response would result. For finite-length code sequences, the correlation results in non-zero outputs, known as time sidelobes, at times other than when the peak response occurs (Fig. 1). When the time sidelobes are large enough to exceed the detection threshold, multiple detections occur for a single target. The detections resulting from the time sidelobes are erroneously identified as returns from small targets. To

detect small targets reliably in the presence of large targets, it therefore is necessary to reduce the time sidelobes.

Two valued (binary) code sequences, Barker and pseudorandom codes, have levels of time sidelobes that are low relative to the correlation peak. It was shown¹ that the time sidelobe levels of these codes could be greatly reduced by correlating them against a reference code that was different from the transmitted code, resulting in a cross correlation between the transmitted and the reference code. The result is that the S/N is no longer maximized; however, the time sidelobes are greatly reduced at the expense of a small loss in S/N.

The reference code is computed to maximize the ratio of the peak response to the peak time sidelobe. To do this, the reference code is no longer constrained to be binary valued but can assume any real value. The real value code is referred to as a filter, mismatched when the transmitted code and reference code are not identical. The filter optimization was shown to be a linear problem that could be solved using linear programming techniques.¹

This capability has been extended in order to design a filter with a nearly ideal correlation output for the signal code and a nearly zero output for the interference code. The constraints on the filter design for rejecting the interference code double the number of constraints needed for producing the desired output for the signal code alone.

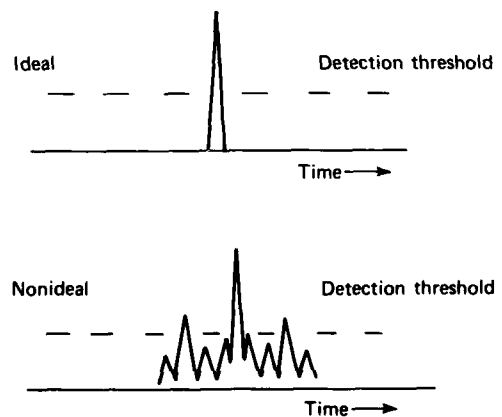


Fig. 1 Examples of ideal and nonideal autocorrelation functions.

A filter designed to pass one code and reject another can be used to sort two pulses, with different codes, that overlap in time. They can be sorted using two filters, one to pass the signal code and reject the interference code and the other to pass the interference code and reject the signal code (see Fig. 2). S_1 and S_2 are the two codes and F_1 and F_2 are the corresponding filters. If the two signals are applied to the filter inputs, the output at F_1 will correspond to the arrival time of S_1 , and the output at F_2 will indicate the arrival time of S_2 .

A high degree of isolation between the signal code and the interference code would permit the simultaneous reception of two different signals. The signals can be separated by the filters (F_1 and F_2) for processing in independent channels. The ability to separate the signals that are normally sent sequentially in radar and communications systems allows them to be sent in parallel, overlapping in time.

DISCUSSION

Reference 1 provides the results for filters optimized to produce the maximum ratio of mainlobe to peak sidelobe (M/PS) for selected phase codes. The length of the codes varied from 15 to 127. In the signal rejection study, the code lengths were restricted to 15 and 31.

The filters generated solely for time sidelobe suppression are subject to fewer constraints than are the filters designed to perform both sidelobe suppression and interference signal rejection. The addition of the interference-signal-rejection capability imposes additional constraints on the filter and reduces the size of the region (range of filter coefficients) over which the optimization can be performed. Therefore, the performance of the sidelobe suppression filter represents an upper bound on the performance that can be achieved for the dual-function filter.

Table 1 shows the effects of different constraints on filter performance. The first entry shows the performance of a length 127 filter for time sidelobe suppression for a length 15 signal code. The M/PS is 38.2 dB, the best that can be expected for this filter and code combination for time sidelobe suppression. Next, the interference-code rejection constraints are added for a length 15 interference code, reducing the M/PS to 14.5 dB. Leaving the signal-code time sidelobes unconstrained and maximizing the signal-code-mainlobe to peak-interference-code output results in an M/PS of 22.6 dB for the interference code. This case shows the maximum level of rejection that can be obtained for this signal and interference code pair. The 22.6 dB level of rejection was obtained at the expense of the signal

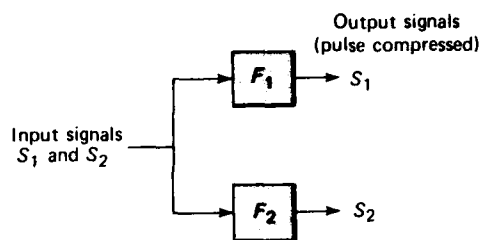


Fig. 2 Filter configuration for signal separation.

Table 1

FILTER PERFORMANCE FOR A SPECIFIC SIGNAL INTERFERENCE LENGTH 15 CODE PAIR AND LENGTH 127 FILTER

Constraint	M/PS (dB)
Signal-code sidelobe suppression only	38.2
Signal-code sidelobe suppression and interference code rejection (filter F_1)	14.5
Interference code rejection only	22.6
Signal-code sidelobe suppression and interference code rejection, when the signal and interference codes have been reversed (filter F_2)	15.1

code time sidelobes, which increased greatly to yield an M/PS of 3.1 dB for the signal code. Reversing the roles of the signal and interference codes (designing filter F_2 rather than F_1) yields an M/PS of 15.1 dB, which is comparable to the original M/PS of 14.5 dB.

The filters were designed for many length 15 and 31 signal and interference codes. The length 15 code pairs produce M/PS's that typically are in the range of 14 to 16 dB for length 127 filters. The length 31 code pairs produce M/PS's ranging from 17 to 20 dB for the length 127 filter.

The effect of filter length on filter performance was also observed in this study. Increasing the filter length improves the performance by increasing the M/PS, but performance is only slightly improved in the case of the dual function filter. For a specific length 15 code pair, a length 15 filter produced an M/PS of 12.0 dB. Increasing the filter length to 127 gave 14.5 dB. Longer filter lengths will yield slightly better performance.

The filters were implemented as transversal filters, which are easily implemented using a surface acoustic wave (SAW) device. The SAW device allows wide bandwidth signals to be processed with much less hardware than a filter implemented with digital elec-

tronics. The digital implementation traditionally had the advantage that the filter coefficients could be changed readily for different code pairs. The SAW devices are generally fixed, and a new one is required for each filter. To remove this limitation, a programmable SAW device is being constructed. It will be used to demonstrate the two filter types and also to determine the quality of SAW design.

SUMMARY

A method of reducing time sidelobe levels for binary-phase-coded waveforms has been described.¹

Using linear programming, the method has been extended to permit signals to be isolated or sorted by means of their phase code.

REFERENCE

¹K. P. Davis, *Final Report, Time Sidelobe Reduction Study*, JHU/APL FS-79-108 (Jun 1979).

A WIDEBAND RF COMMUTATOR FEED TECHNIQUE FOR A SCANNING CIRCULAR ARRAY ANTENNA

E. P. Irzinski

A coaxial-waveguide amplitude-commutation feed system has been developed for the scanning circular array antenna. The major advantages of the coaxial commutator feed compared to other types of circular array feeds are the broad bandwidth and small insertion loss achieved simultaneously with a simple feed geometry. The functional and measured performance capability of a 30% RF bandwidth, low-sidelobe RF commutator feed design are described.

BACKGROUND

The RF feed network design has long been recognized as the critical design area in electronically scanning circular array antenna systems. A fundamental requirement of the feed system is to commutate a desirable amplitude distribution about the periphery of the circular array so that a given number of radiating elements in a 180° or smaller sector is excited at any instant of time. The network implementation problem is practical rather than theoretical since one or more undesirable physical or performance attributes are usually associated with a particular design. Most frequently these problems reside in the areas of design

complexity, control of RF output amplitude and phase tolerance, insertion loss, or bandwidth limitations. The design of the circular array feed network, reported in this paper, is characterized by simplicity and a resultant overall improvement in critical performance areas.¹ A dominant transverse electromagnetic (TEM) mode and a pair of orthogonal transverse electric (TE₁₁) modes excited within the coaxial waveguide are used to generate a commutable low-sidelobe amplitude distribution about the circular periphery of the RF feed output. The unique features of the coaxial-waveguide amplitude-commutation network are an extremely simple input excitation network and the capability for large RF bandwidth operation. The resultant antenna efficiency of a communication or radar circular phased array using this feed design will be relatively high because of the small insertion loss (≈ 0.5 dB) of the commutation network.

DISCUSSION

Figure 1 is a schematic of the coaxial-waveguide commutation network. The RF input is divided into two outputs via the K_{dB} coupler. One of these outputs is the input to the sum port of the monopulse comparator.

RF outputs to switches and phasors of circular array

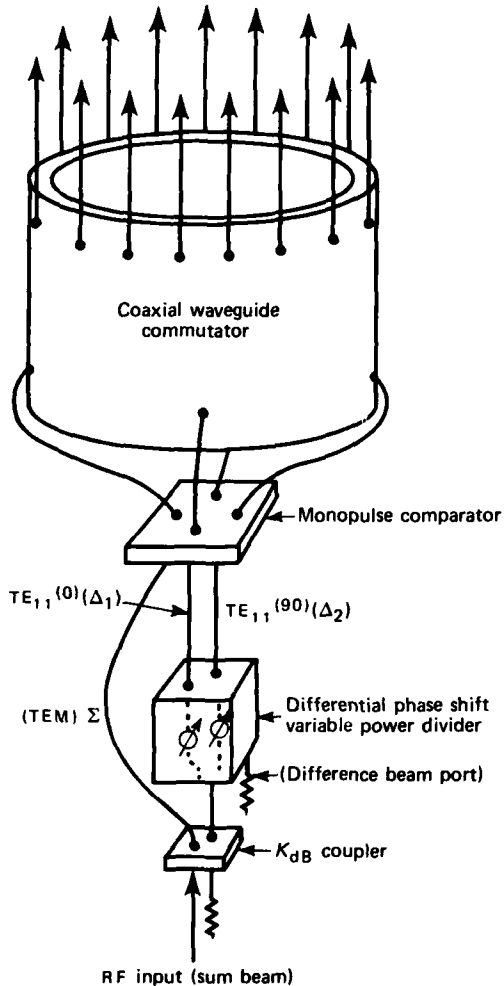


Fig. 1 Coaxial waveguide commutation network.

The four outputs of the monopulse comparator are connected to four symmetrically disposed input probes of the coaxial-waveguide commutator. Thus, the sum input to the monopulse comparator excites the TEM mode in the coaxial waveguide. The second output from the K_{dB} coupler is the input to the differential-phase-shift variable-power-divider network, as shown.

A special and desirable feature of this variable power divider design is that the output ports phase-track each other. The power divider outputs are the inputs to the difference ports of the monopulse comparator. Consequently, the variable power divider excites a pair of spatially orthogonal TE_{11} modes in the coaxial waveguide. The coaxial-waveguide commutator is terminated in N arbitrary output ports symmetrically disposed with respect to the four input ports. In the

region of the coaxial-waveguide annular output, a radial electric field intensity of the form

$$V(\phi) = A + (1 - A) \cos^2 \frac{1}{2}(\phi - \alpha) \quad (1)$$

exists by a superposition of the functionally orthogonal TEM and TE_{11} mode pairs. Equation 1 has been written in the recognizable cosine-squared-on-a-pedestal form, where A is the pedestal magnitude that is simply related to the input coupling value, α is the differential phase shift of the variable power divider, and ϕ is the angular coordinate in the coaxial annulus region.

Inspection of Eq. 1 reveals that a tapered amplitude distribution proportional to $V(\phi)$ may be discretely commutated about the output periphery of the coaxial-waveguide amplitude commutator by a digital variation of α . A variation of α in discrete equal increments will provide the coarse commutation capability needed for this type of feed system. Thus the RF outputs of the coaxial commutator interface with an RF switch and phase shifter network as shown in Fig. 1 prior to final termination at the radiating element inputs of the circular array. The RF phase shifters are used for the dual functions of plane wave collimation of the cylindrical wavefront and fine beam steering between the coarse discrete beam positions provided by the amplitude commutation and switching network.

An experimental L band model of a coaxial-waveguide amplitude commutator was designed, fabricated, and tested to verify the feasibility of this circular array feed technique. A design with 16 output ports was chosen somewhat arbitrarily; however, it would be compatible with a 64 element circular array with 16 RF switches (type IP4T) and 16 phase shifters for the excitation of a sector of 16 radiating elements at a given instant of time. The initial stage of the development was devoted to impedance matching the commutator input and output probes for the TEM and the pair of orthogonal TE_{11} modes. For the 30% bandwidth optimization, the measured TEM mode voltage standing wave ratio was less than 1.6:1; it was less than 1.8:1 for the TE_{11} modes. The isolation between the input ports of the monopulse comparator was better than 25 dB throughout the band. The insertion loss of the RF feed commutator network was small and did not exceed 0.5 dB in the 30% frequency band.

The second part of the test program was primarily concerned with verifying the operating principle of the commutation network by measuring the complex output voltages of the waveguide commutator. The phase shifters in the circuit of Fig. 1 were simulated by coaxial line stretchers, and a 6 dB directional coupler was used at the RF input. Figure 2 presents the complex amplitude measurements of the coaxial waveguide commutator output port for the differential phase shift

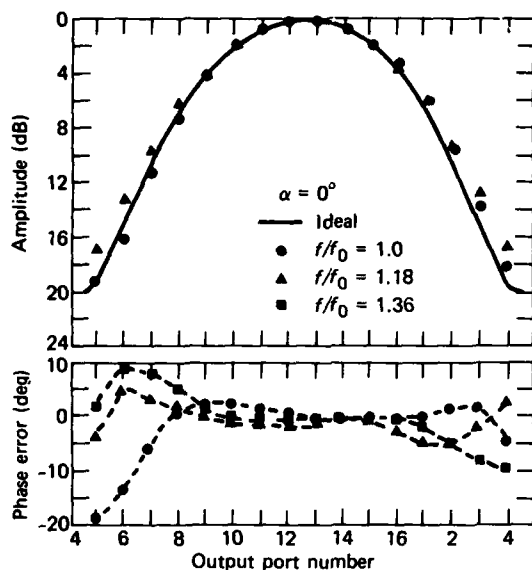


Fig. 2 Amplitude and phase measurements of the commutator output.

condition of $\alpha = 0$. The measurements were made at three frequencies in the 30% frequency band as indicated in Fig. 2; an ideal, continuous, cosine-squared-on-a-20-dB-pedestal distribution is shown for comparison. The degree of deviation of the measured voltage magnitudes from the ideal case indicates qualitatively the extent to which undesirable spurious mode generation (primarily due to input probe amplitude and phase imbalance) compositely affects the ideal commutator output voltages.

Linear array patterns were generated using the measured data for the complex amplitude element excitation condition. A linear array geometry was chosen because we wanted to determine the effect of array excitation error on the ideal low-sidelobe antenna

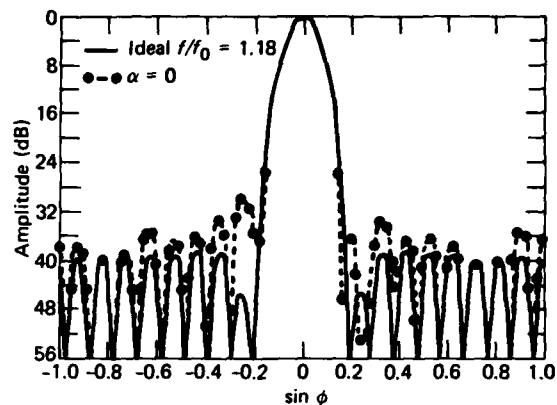


Fig. 3 Array antenna pattern for ideal and measured commutator outputs.

pattern structure, and the introduction of a finite radius of curvature was deemed an unnecessary complication. A single representative computed pattern for the midband data set of Fig. 2 is shown in Fig. 3; the ideal pattern is shown for comparison. The array element spacing was 0.55 wavelength at the low frequency end of the 30% band. An isotropic element pattern was assumed so that the off-axis sidelobe structure would not be muted with a directive element gain pattern. The sidelobe structure of this typical computed pattern deviates somewhat from the ideal errorless case, but the results nevertheless indicate excellent low-sidelobe performance over a large frequency band.

REFERENCES

- 1 E. P. Irzinski, "A Wideband Coaxial Waveguide Commutator Feed for a Circular Communication or Radar Scannable Array Antenna," JHU/APL F2A-0-308 (29 Sep 1980).
- 2 E. P. Irzinski, "A Coaxial Waveguide Commutator Feed for a Scanning Circular Phased Array Antenna," *IEEE Trans. Microwave Theory Tech.* (Mar 1981).

WEAPONS TECHNOLOGY

INTRODUCTION

Since World War II, APL has been actively involved in the development of the Navy's surface- and subsurface-launched missiles. The effort included the development of the Talos, Terrier, and Tartar missiles, the evolution of Standard Missile, the flight development of Long-Range Typhon, and the test and evaluation of Polaris, Poseidon, and Trident. Supporting these efforts have been exploratory and advanced development programs in all aspects of weapons technology, including the design, fabrication, and testing of guidance system components, propulsion systems, and aerodynamic models. The objectives of these weapons technology efforts are to advance the state of the art and to contribute to the timely evolution of operational systems.

Although APL's involvement in weaponry began with the proximity fuze and progressed primarily into anti-air-warfare systems, since the late 1960's APL has been strongly involved in offensive missilery, specifically in the Harpoon and Tomahawk tactical and strategic missile developments. Much of the Harpoon guidance system feasibility demonstration was undertaken by APL, and the early analysis of the terrain contour matching (TERCOM) scheme used by Tomahawk was also performed at APL.

With the introduction of the Soviet Backfire bomber, the air threat to the surface Navy has intensified. In addition to the high performance of the backfire, its antiship weapons and electronic countermeasures capability represent significant challenges to weapons systems development. Significant APL effort has been devoted recently to the concept development of new long-range SAM's to augment fighter aircraft in the outer air battle.

Stresses on the area and point defense zone SAM's continue to increase with the Soviet introduction and evolution of supersonic antiship missiles. APL continues to support the improvement of existing point and area defense

weapons through the development of the RAM Missile and Standard Missile Block II. These systems will significantly upgrade the kinematic and homing performance of existing weapons.

The first article discusses the development of a digital simulation that can be used to evaluate the performance of Harpoon in a multiple target and countermeasures environment.

The second article describes APL's participation in the development of a remotely piloted vehicle for probing the lower atmosphere. The electric field sensing system, previously shown to be useful for the vertical stabilization of the vehicle, now has been shown to provide a guidance method that has inherent terrain-avoidance features.

The development of a broad frequency band with small boresight errors is the topic of the third article. It discusses the maximum boresight errors that can be tolerated by an HOJ guidance system without significant system performance degradation.

The fourth article discusses the potential implementation of bank-to-turn steering control for long-range SAM's. Recent airframe/propulsion investigations have highlighted the desirability of chin inlets for the propulsion system; chin inlets require bank-to-turn steering. This effort has shown that bank-to-turn steering is feasible if the autopilot can be designed to provide sufficient airframe roll response.

The fifth article describes simple mathematical models that do not require the use of a computer. They have been developed to calculate the effectiveness of a surface-to-air missile when it encounters a missile target.

A DIGITAL SIMULATION FOR MISSILE SYSTEM SURVIVABILITY ANALYSIS IN A MULTIPLE ECM ENVIRONMENT

K. T. Plesser and L. W. Wald

A fully digital, launch-to-impact simulation model has been developed for the Harpoon missile system. The simulation can process the seeker response characteristics of hundreds of targets and countermeasures simultaneously, while providing a stochastic capability for the statistical determination of system performance by a Monte Carlo method.

BACKGROUND

A continued program to evaluate the survivability of Navy antiship missile systems is necessary if such systems are to remain effective in the face of an evolving threat. In particular, an assessment of missile vulnerability to electronic countermeasures (ECM) is of critical importance. This article discusses the development of a digital simulation as an analytical tool to evaluate the survivability of the Harpoon antiship missile system in a multiple target and countermeasures environment.

DISCUSSION

Evaluation Methods

Missile system test and evaluation methods can be broadly divided into three types. The first, most direct and obvious, is an actual firing against real targets on an instrumented range. This technique is extraordinarily expensive but leaves the least doubt as to the validity of the results. The other two techniques, a hybrid and a fully digital simulation method, are more compatible with a laboratory environment.

A hybrid hardware/software simulation, of which the APL Guidance System Evaluation Laboratory¹ is representative, is normally constructed with one or more items of actual missile hardware (such as a radar seeker) interfaced by appropriate analog-to-digital devices to a software simulation of the remainder of the missile system. This type of hybrid simulation is of particular value in evaluating hardware but, because of geometric limitations, may be unsatisfactory for certain kinds of dynamic analyses, including scenarios involving large numbers of targets.

The fully digital simulation gives the analyst full control over a wide range of variables and does not need to be run in real time (i.e., 20 seconds of flight may be simulated in, perhaps, 1 second of computer time). The associated disadvantage is that it is not possible to simulate analog hardware (such as RF processing equipment) explicitly unless wide simulation bandwidths are used, thus negating the time and cost gains. One must also be particularly cautious to validate such a simulation thoroughly prior to its application; telemetry data from actual firings are ideal benchmarks for such a purpose. However, with carefully selected assumptions and acceptably small iteration rates, digital techniques can and do yield accurate results.

Digital simulation techniques have been widely recognized and applied to a broad class of problems ever since the advent of sufficiently powerful computing machinery. APL has been involved extensively in the evaluation of missile dynamic characteristics by means of six-degree-of-freedom aerodynamic models of surface-to-air missiles. In general, these simulations provide deterministic results to questions far too intractable for manual solution. Typical uses include verifying the effects of hardware and/or software changes on the flight profile and examining in detail the final moments of flight before impact (endgame analysis).

Survivability Assessment Simulation

The general structure of the antiship missile simulation program is shown in Fig. 1. Targets are generated and moved about in accordance with input parameters that define a target's initial position, course, and speed. Missile motion is determined by a five-degree-of-freedom (roll excluded) aerodynamics model. From these, the relative missile-target geometry is computed and used in the radar range equation to calculate mean signal and noise powers. Commands to the missile airframe and to the antenna gimbals are under the control of the midcourse guidance unit, which, in turn, is under the control of the radar seeker. The seeker output is driven by the results of stochastic tests performed on the mean signal-to-noise ratio. This closes the loop and permits the simulation program to "fly" until impact.

Electronic countermeasures are conceptualized as potential targets with certain unique signal characteristics that depend on the nature of the countermeasure.

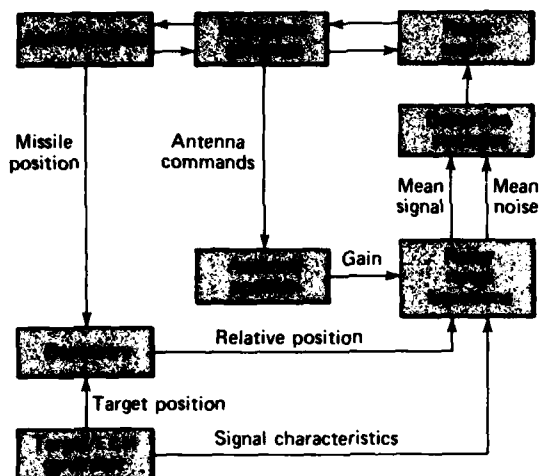


Fig. 1 Structure of the antiship missile simulation.

A full spectrum of countermeasures may be modeled, given an *a priori* knowledge of their influence on the radar seeker.

A significant feature of the simulation is the recognition of the fact that the physics of the situation gives rise to a large number of stochastic processes, each characterized by a unique probability distribution. Examples of some of these phenomena are given in Table 1.

A Monte Carlo technique is used wherein each replication of a missile flight is initialized by selecting a single realization of the random variables that vary from flight to flight but remain fixed during any given flight. Random variables that vary during flight (e.g., target fluctuations or wave height) are sampled from the parent population each time a computation is required. Since each replication of a missile flight is independent, a sequence of simulated flights may be considered as a series of Bernoulli trials. In this manner, one may calculate (based on the binomial distribution) an estimate of the hit probability associated with each target and the limits of the expectation at any confidence level.

Implementation and Application

The stochastic simulation just described has been documented, and the software is resident in the Labora-

Table 1
TYPICAL STOCHASTIC PHENOMENA IN A MISSILE SYSTEM SIMULATION

Example	Probability Distribution
Hardware tolerances Gyro bias Thrust misalignment	Gaussian Gaussian
Environmental Wind direction Sea surface	Uniform ($0 \leq \theta \leq 2\pi$) Gaussian
Target characteristics Small ships Some large ships Some large ships Clutter Noise	Chi-square (2 degrees of freedom) Chi-square (4 degrees of freedom) Lognormal Weibull or lognormal Gaussian

tory's IBM 3033 computer system. The basic cycle rate of the simulation is 50 Hz; i.e., discrete computations are performed every 20 milliseconds of simulated flight. It is possible to simulate a 5 minute flight in about 10 seconds at a cost of less than three dollars. As more targets and countermeasures are added, the required processing time increases. Because only 100 replications are required to narrow the relative error to a few percent at the 90% confidence level, reliable statistics of missile performance can be generated at a cost of a few hundred dollars, a small fraction of the cost of an actual missile firing.

This simulation technique has been used extensively to model the effects of a wide variety of ECM against the Navy's Harpoon antiship missile system. Data on ECM vulnerability obtained in this manner are combined with data on vulnerability to other defensive systems in order to assess the overall survivability of the missile and, thus, the likelihood of the missile achieving its intended purpose. Because of the success in modeling the Harpoon system, an effort is currently under way to perform a similar analysis on the antiship variant of the Navy's Tomahawk cruise missile.

REFERENCE

- ¹W. M. Gray and R. W. Witte, "Guidance System Evaluation Laboratory," *Johns Hopkins APL Tech. Dig.* 1, No. 2 (1980).

REMOTELY PILOTED ATMOSPHERIC PROBE

M. L. Hill

The performance of electro-optical devices used in military systems is affected by atmospheric turbulence, aerosol and particulate content, temperature gradients, and other meteorological variables. The investigation of these effects using manned aircraft is expensive and, on occasion, impossible if data are needed from hazardous areas. To overcome these difficulties, the Laboratory, in cooperation with the University of Texas at El Paso (UTEP) has developed a small remotely piloted vehicle (RPV) for probing the lower atmosphere. Personnel at UTEP are responsible for instruments related to meteorological measurements, whereas APL is responsible primarily for the vehicle's operation and for instruments to record its aerodynamic performance. Included in the instrumentation is a complement of atmospheric electric field sensors that previously were shown to be useful for the vertical stabilization of such vehicles. This report is limited to a brief description of the vehicle and some results obtained in recent tests in which the electric field sensing system was shown to provide a guidance method that has inherent terrain-avoidance features.

BACKGROUND

The effectiveness of electro-optically guided weapons can be degraded by adverse meteorological conditions that cause attenuation, scattering, and diffraction of line transmission in the infrared, visible, and ultraviolet portions of the spectrum. Among the most serious offenders are dust particles, aerosols, and refractive index gradients associated with turbulence and temperature inhomogeneities. The extent and nature of such degradation are not fully documented, particularly for systems that are to be operated in the lower atmosphere. Considerable research on this problem is being done using special ground ranges and instrumented manned aircraft. It was recognized by the Army's Atmospheric Sciences Laboratory that there was a need for a small remotely piloted vehicle that could be flown in hazardous areas — for example, near exploding projectiles on an artillery range or close to mountain cliffs and peaks where turbulence presents a severe hazard to manned aircraft. Accordingly, the Laboratory has developed a Maneuverable Atmospheric Probe (MAP) vehicle.

In addition to developing a method for probing hazardous areas, the objectives have also included keeping the costs of the vehicle and its operation below

This work was supported by the Army Research Office and the Army Atmospheric Sciences Laboratory.

those for manned aircraft, and providing a slower, more maneuverable vehicle so that fine-scale meteorological factors in confined regions could be measured more thoroughly. Still another objective was to gather data about the performance of a so-called electrostatic autopilot that was invented at APL¹ and used on several previous RPV's developed at APL.² The autopilot derives its vertical reference from measurements of the vector of an electric field in the atmosphere that is usually vertical in fair weather.

DISCUSSION

The MAP vehicle is shown in a three-view drawing (Fig. 1) and a photograph (Fig. 2). The mountain in the background is North Oscura Peak (7999 ft) located 1.3 mi east of the dirt runway (5800 ft altitude) that served as the operations base for the tests in July 1980. The aircraft has a 10 ft wingspan and is

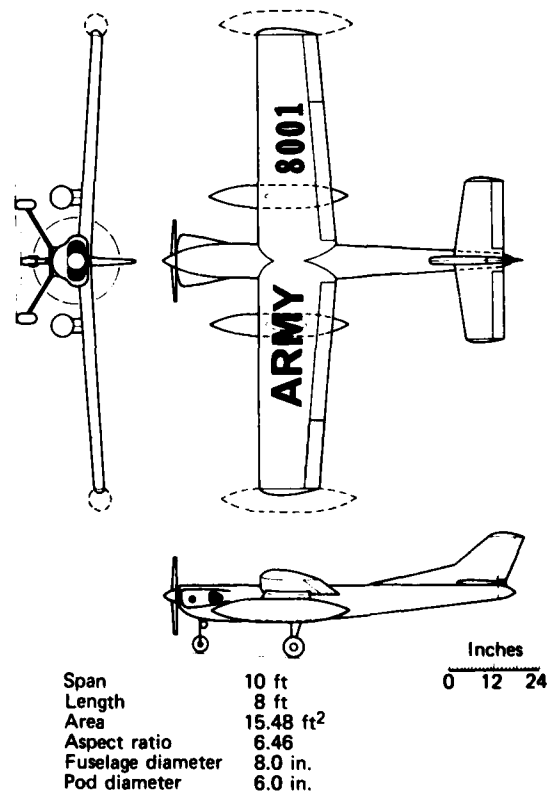


Fig. 1 Three views of the MAP vehicle.



Fig. 2 MAP vehicle at North Oscura Peak test site, July 1980.

powered by a 10 hp, 2 cycle reciprocating engine. It has high-lift flaps on the wing and can fly at speeds of about 35 to 110 mph at sea level. It has been flown to 13,000 ft altitude and has a computed ceiling of 25,000 ft. Its gross weight is about 95 lb when it is carrying 25 lb of payload and enough fuel for 1½ hours. The vehicle is fitted with two independent autopilots, one based on fluidic gyros and the other on the atmospheric electric field; either can be enabled by ground commands.

The instruments and telemetry normally carried record the following data: temperature; pressure; humidity; high-frequency, fine-scale turbulence; low-frequency yaw and pitch gust directions; three components of angular rate (yaw, pitch, and roll); altitude; heading; engine speed; air speed; and electric field in the x , y , and z directions. Devices to collect aerosol and dust samples are carried in the pods slung under the wing. A radar transponder provides for accurate tracking when flying in regions of strong clutter.

About six hours of data tapes were recorded during the North Oscura Peak operation. Examination of the data is still in progress. Here we will describe only one of the significant sections from a flight on July 10, 1980. During this last flight of the series, it was possible to schedule several tests near the cliff face to determine whether the electric field autopilot would provide outputs that would prevent the aircraft from colliding with the mountain. This possible use of electrostatic sensing for terrain avoidance had been recognized previously³ but had not been demonstrated.

The flight paths of four special test runs made near the mountain peak are shown in Figs. 3a and 3b. The basic procedure for each pass was the same. The pilot, who was located atop the peak, steered the aircraft to a heading essentially parallel to the cliff face

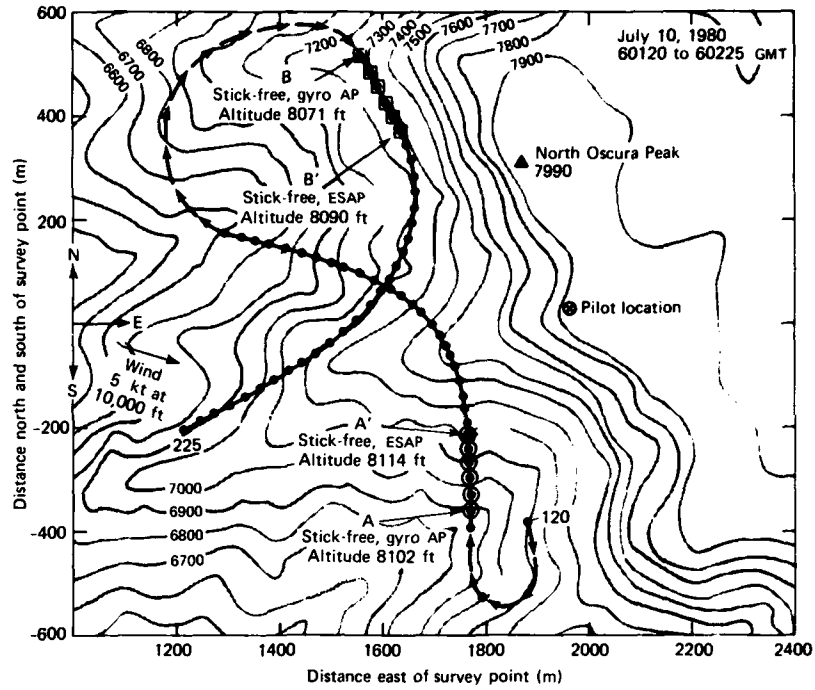
and then allowed the aircraft to fly stick-free on an open-loop heading under the control of the gyro autopilot for a period long enough to define a straight path. The start of one such path is at point A. At point A', the pilot merely pushed the switch that transferred control from the gyros to the electrostatic autopilot (ESAP). It can be seen that at A' the aircraft made a distinct left turn from its south to north heading to a nearly east to west heading. As the aircraft became more distant from the mountain, the turn radius diminished until the aircraft was again essentially flying on a straight path. The procedure was repeated at B and B', where the initial course was north to south, or nearly opposite the course of the previous pass. At B', under the influence of the electric field, the aircraft made a distinct right turn away from the mountain. Similar turning effects are seen in the next two passes (Fig. 3b). A sharper left turn occurred at A' because the aircraft was closer in and headed more directly toward the mountain than in the other passes.

All of the passes were made at an altitude of about 8100 ft (100 ft above the peak height) for safety reasons. At that time, the wind at 10,000 ft was 5 kt from slightly north of west. The pilot atop the peak judged the wind at his location to be 5 kt from due west. Considering this wind and the initial heading, the aircraft would have drifted eastward across the mountain peak if it had been left to its whims on the gyro autopilot. However, the flight paths clearly show that the electrostatic sensing system introduced turns to guide the aircraft away from the mountain peak.

These effects are expected to be considerably stronger and more positive if the aircraft is flown below peak height rather than above. We hope to perform such tests soon because this kind of sensing could be quite valuable in RPV systems that must navigate in mountainous regions.

Figure 4 is a photograph of the MAP vehicle lifting off from the runway and turning toward the broad valley to the west of North Oscura Peak. Tests of the electrostatic autopilot were done over this area in a region 1.5 to 3 mi from the peak. No influence of the peak on the verticality of the electric fields could be detected there, and it was demonstrated, while the aircraft was being flown on the gyro autopilot, that this simple, lightweight, electrostatic system can detect bank angles of the order of 0.5°. Also, data recorded during aerobatic maneuvers such as loops and axial rolls show the rudiments of a way to measure the roll and pitch angles at any angle, from upright to fully inverted. The results will be described in a separate publication. The possibility of developing this device into a simple, lightweight, tumble-free attitude sensor is clearly evident. Such a device could be a valuable asset in many

(a) Runs 1 and 2



(b) Runs 3 and 4

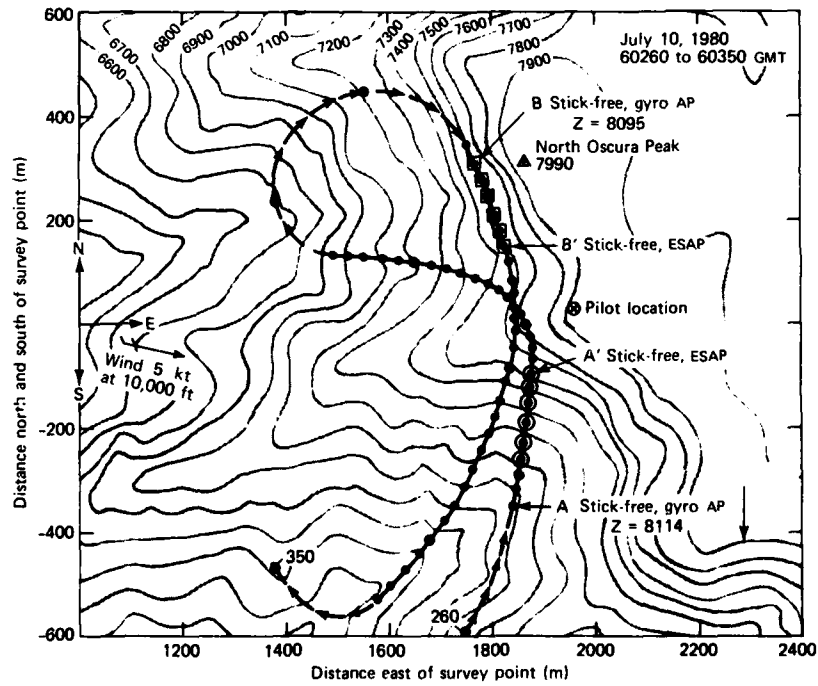


Fig. 3 Flight path near North Oscura Peak.

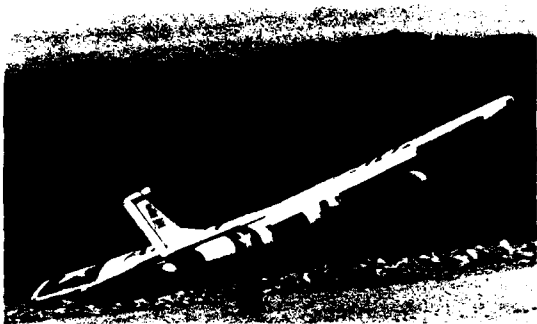


Fig. 4 MAP vehicle lifting off and turning west.

BROADBAND RADOME BORESIGHT-ERROR TOLERANCES FOR HOMING MISSILES

B. E. Kuehne and H. Y. Chiu

The potential performance of a surface-to-air homing missile using a broadband passive-guidance mode is constrained by the large boresight error slopes associated with a broadband radome. The maximum boresight error slopes that can be tolerated without a significant degradation in performance have been determined for a prospective wide-area-defense missile using broadband home-on-jamming (HOJ) guidance for a postmidcourse/preterminal homing transition-guidance mode. The results provide a much needed measure for evaluating candidate multimode radome/sensor configurations.

BACKGROUND

The capability for broadband or multiband homing guidance may be necessary for future surface-to-air missile systems, particularly those intended for a wide-area-defense role. A broadband guidance mode would allow the missile to home passively against aircraft jamming at search and targeting radar frequencies. Such broadband HOJ guidance would be used principally during a transition portion of flight, following an inertially guided high-altitude cruise phase

This work was supported by NAVSEASYSKOM, SEA-62R1.

R&D aerodynamic tests, and it is hoped that we will soon be able to pursue this work further.

REFERENCES

- ¹M. L. Hill, "Introducing the Electrostatic Autopilot," *Astronaut. Aeronaut.* **10**, No. 1 (1972).
- ²M. L. Hill, "Design and Performance of Electrostatically Stabilized Delta Planform Remotely Piloted Vehicles," *Proc. Military Electronics Defence Expo.*, Weisbaden, Germany, 1977, Interavia S.A. Geneva (1978).
- ³C. S. Leffel and M. L. Hill, *Use of the Atmospheric Electric Field for Terrain Avoidance*, JHU/APL TG 1271 (Mar 1975).

and preceding a short-range active or infrared-guided terminal homing mode. During this transition guidance phase, gross heading errors are nulled but precision homing is not required.

One potential problem with HOJ guidance involves the large boresight-error slopes associated with a broadband radome. Radome boresight error arises from the distortion of the incoming target-tracking radar's signal by the nonhemispherically shaped radome that protects the missile's seeker and antenna (Fig. 1). Effectively, this distortion results in an apparent perturbation, ϵ_r , in the missile/target line-of-sight vector, which is the primary source of missile guidance information. The boresight error is a function of the look angle, β , between the missile's centerline and the missile/target line-of-sight vector. In a missile using proportional navigation guidance, this functional dependence effectively introduces an undesirable feedback path into the missile guidance system. If the boresight-error slope, which is the derivative of ϵ_r with respect to β , becomes excessive, the feedback path may cause an instability in the missile guidance loop.

Boresight-error effects are constraining the design of current semiactive (narrowband) terminal-homing missile guidance systems. For the broadband

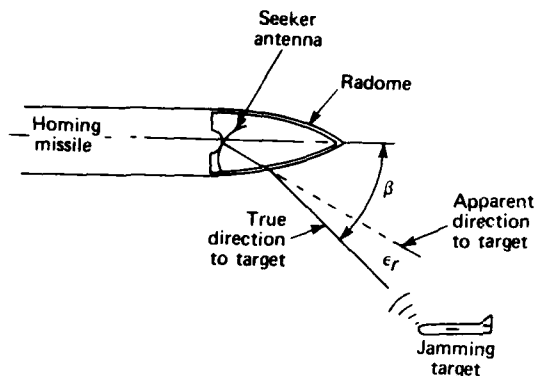


Fig. 1 Perturbation of the apparent missile/target line-of-sight vector by radome boresight error.

case, the radome design cannot be optimized for some predetermined nominal operating frequency, and therefore boresight-error slopes are expected to be an order of magnitude more severe. Fortunately, if used only for a transition guidance phase of flight, the HOJ mode can be dynamically less responsive than a terminal guidance mode, and a less responsive guidance loop is less sensitive to boresight-error effects. Consequently, tolerance to large boresight-error slopes can be designed into the HOJ guidance law.

The analysis described here quantifies the level of boresight-error slopes that can be tolerated by a broadband HOJ guided missile. The tolerances are based on maintaining a given level of system performance rather than on the traditional small signal stability criterion.

DISCUSSION

The study was divided into two phases. First, a guidance law that would be applicable to the transition guidance mode was defined. Then the guidance law was incorporated into a detailed missile simulation that contained a realistic parametrical representation of actual boresight error. The simulation was used to determine the relationship between tolerable slope magnitudes and the area of the radome over which the slopes extend.

The initial phase of the study (i.e., the determination of an appropriate HOJ transition-mode guidance law) had two primary considerations. The guidance law is required to compensate for expected large, broadband boresight-error slopes. Therefore, the magnitude of the boresight-error slope at which system instability occurs (called the critical boresight-error slope, r_c) should be as large as possible. This can be accomplished by decreasing the effective guidance gain,

λ_E , and increasing the effective guidance time constant, τ_E , hence slowing down the dynamics of the guidance loop. However, missile performance will be unsatisfactory if too much sluggishness is introduced into the guidance system in this manner. Consequently, the goal was to develop a transition-mode guidance law that permits the critical boresight-error slope to be as large as possible and at the same time maintains a required level of system performance.

The first step in defining the transition guidance law was to quantify the range of values for λ_E and τ_E that allows satisfactory transition guidance. By definition, satisfactory performance gives a terminal-acquisition heading error that can be successfully nulled with a dynamically responsive terminal-homing guidance system. Both nonmaneuvering and maneuvering targets were considered in determining the maximum acceptable acquisition heading error. Wide-area-defense scenarios probably will involve multiple jammers whose individual locations may not be initially identifiable. The time when the target jammer can be resolved from other jammers in the engagement was left as an independent parameter for this study. Using a simplified homing missile simulation, the relationship between λ_E and τ_E for satisfactory performance was derived. The solid lines in Fig. 2 show, for three different jammer resolution times, the bounds on λ_E and τ_E that maintain satisfactory HOJ transition guidance.

Figure 2 also shows (dashed lines) the relationship between the guidance responsiveness parameters (λ_E and τ_E) and r_c , based on analysis of the system eigenvalues at a high altitude flight condition. Clearly, for each jammer resolution time, there is an optimal set of λ_E and τ_E values that gives the required system performance as well as a maximum attainable r_c . For example, if the target jammer is resolved 23 s prior to intercept (a reasonable value, based on candidate signal processing proposals), the optimal set will be $\lambda_E = 2.2$ and $\tau_E = 8$ s. The corresponding value of r_c will be ± 0.026 deg/deg. If the guidance law for the transition mode is assumed to be in the structure of proportional navigation,¹ then approximate analytical expressions² are available to relate λ_E and τ_E to the corresponding parameters of proportional navigation.

The critical slope data shown in Fig. 2 are dependent on flight conditions. The complete analysis encompassed the altitudes expected for an HOJ transition guidance trajectory. Because the boresight-error slopes associated with a radome can be considered invariant with missile altitude, the critically stable slope should also be independent of altitude. Hence, the guidance law parameters were determined as functions of flight conditions so that the critically stable slope was the same at all missile flight conditions.

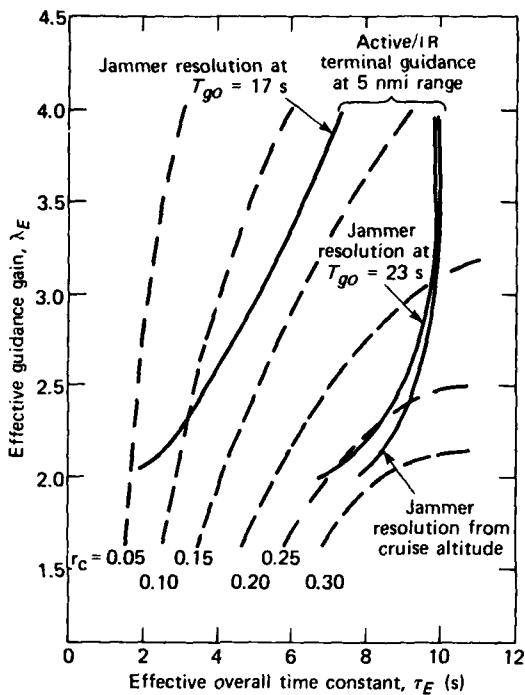


Fig. 2 Relationship between performance (solid lines) and boresight error slope stability requirements (dashed lines). The jammer resolution times range from 17 s time-to-go (T_{go}) before intercept to resolution from cruise altitude before initiation of the transition guidance mode.

In the second phase of the study, the resulting transition guidance law was incorporated into a six-degree-of-freedom (6-DOF) homing missile simulation. The detailed digital model contained three-dimensional boresight error characteristics.³ The boresight-error data were implemented so that different areas of the radome could be exercised conveniently without modifying the engagement geometry. In addition, the boresight error data could be multiplied by an arbitrary gain so that various possible slope magnitudes could be generated easily.

With the 6-DOF simulation, a homing geometry was selected that caused the missile to follow a typical wide-area-defense transition guidance trajectory. Satisfactory transition guidance performance was defined as in the previous phase of the study. Different regions of boresight-error slope and various slope-multiplying gains were exercised to relate the maximum tolerable boresight-error slope to the size of the radome area over which the slope occurs. This radome area size is defined as the extent of the look angle region, $\Delta\beta$, over which the slope is approximately constant.

The resulting trends are plotted in Fig. 3. This figure should be interpreted as follows: If the

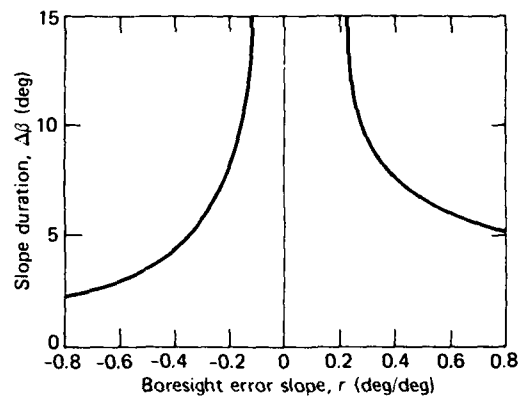


Fig. 3 Guidance system tolerance to large radome boresight error slopes for a broadband home-on-jamming transition guidance mode.

characteristics of a region of large boresight-error slope lie below the curves, that region of slope can be tolerated. However, if the slope characteristics lie above the curve, that region of large slope may contribute to degraded system performance for some homing engagements. In general, boresight error slopes of 0.4 deg/deg and larger can be tolerated in a broadband transition guidance mode only if they occur over small regions of the radome. This is in contrast to allowable slopes for a terminal-homing guidance mode, which previous studies have shown must be less than about 0.05 deg/deg.

The boresight-error slope tolerances shown in Fig. 3 were derived for a particular candidate wide-area-defense missile configuration that uses skid-to-turn steering. By accounting for airframe lift characteristics and engine air inlet constraints, the broadband boresight-error slope tolerances were modified to pertain to other candidate airframes, and the results of this analysis can therefore be used to evaluate the prospective multimode radome/sensor designs for each of the proposed airframes.

ACKNOWLEDGMENT

The authors wish to acknowledge the efforts of C. Ronnenburg, who provided the three-dimensional boresight error data used in the second phase of this study.

REFERENCES

- H. L. Pastrick, S. M. Seltzer, and M. E. Warren, "Guidance Laws for Short Range Tactical Missiles," presented at AIAA Aerospace Sciences Meeting, New Orleans, La., 15-17 Jan 1979.
- B. E. Kuehne, "Relationship Between Guidance System Responsiveness and Critical Boresight Error Slope for Broadband Homing Missiles," JHU/APL FIC(1)-79-U-033 (Sep 1979).
- B. E. Kuehne, "An Assessment of Radome and Aero/Control Models for Simulating Boresight Error in Homing Missiles," presented at AIAA Guidance and Control Conf., Danvers, Mass., 11-13 Aug 1980.

BANK-TO-TURN MISSILE GUIDANCE PERFORMANCE

R. T. Reichert

The agility and range of tactical missiles must be improved to satisfy increasingly severe mission requirements. Recent analysis has shown that bank-to-turn (BTT) steering offers several potential advantages that might be exploited to provide the needed improvement. Despite these potential advantages, the homing guidance performance of a BTT missile system has not been studied in depth. Therefore, the NASA Langley Research Center has sponsored a program to study the homing guidance performance of several candidate BTT configurations.

BACKGROUND

BTT steering offers several potential advantages that may be exploited to improve the performance of future missile systems.¹ For example, a planar missile airframe can be designed to have very high lifting capability in one direction without the weight and drag penalties associated with orthogonal lifting surfaces. This high-lift vector can then be directed using BTT control. In the case of cruciform configurations, the angle-of-attack capability is often limited by roll-yaw aerodynamic stability considerations or control surface effectiveness. These constraints can be relieved by rolling or banking the airframe to an orientation with optimum stability and control effectiveness.

In addition to its potential advantages, BTT steering introduces some technical concerns that must be evaluated carefully. For example, the methodology for designing a BTT autopilot is not well developed. Such a

design must take into account the aerodynamic and kinematic coupling terms as well as allow for operation at low signal levels (i.e., small angles of attack) when the preferred roll orientation is poorly defined. Other technical concerns include the coupling of body motion into the guidance signal and the interaction of BTT control with such missile subsystems as the seeker, guidance signal processing, and control servo.

All of these concerns must be investigated before BTT steering can be considered a viable method to control high performance tactical missiles. However, the technical concern addressed in this study is guidance performance. BTT steering is inherently a three-dimensional phenomenon because acceleration components will be directed out of the desired plane of maneuver while the missile is banking. The study investigated whether or not the coordination of the banking maneuver and the resulting out-of-plane motion negate the potential advantages of BTT steering.

DISCUSSION

Comparative performance assessments have been made of a moderate-lift cruciform airframe (with low-aspect-ratio wings) configured with both skid-to-turn (STT) and BTT steering and a high-lift planar airframe (with larger wings) configured with only BTT steering. The control features of the four steering policies investigated in this study are summarized in Table 1. The performance of the moderate-lift

Table 1

STEERING POLICY CONTROL FEATURES

Steering Policy	Pitch Channel	Yaw Channel	Roll Channel
STT	Develop commanded acceleration. Equal positive and negative angle-of-attack capability.	Develop commanded acceleration. Equal positive and negative angle-of-sideslip capability.	Maintain roll attitude at fixed reference position.
BTT-45	Develop commanded acceleration. Equal positive and negative angle-of-attack capability.	Develop commanded acceleration. Equal positive and negative angle-of-sideslip capability.	Roll airframe to effect a combined plane maneuver. Maximum roll-attitude error of 45°.
BTT-90	Develop commanded acceleration. Equal positive and negative angle-of-attack capability.	Coordinate with roll channel to minimize sideslip. Limited angle-of-sideslip capability.	Roll airframe to direct lift vector. Maximum roll-attitude error of 90°.
BTT-180	Develop commanded acceleration. Positive angle-of-attack capability only.	Coordinate with roll channel to minimize sideslip. Limited angle-of-sideslip capability.	Roll airframe to direct lift vector. Maximum roll-attitude error of 180°.

This work was supported by the NASA Langley Research Center.

cruciform airframe was assessed for four policies: one STT and three BTT policies (BTT-45, BTT-90, and BTT-180), identified by the maximum roll-attitude error. The high-lift planar airframe was evaluated for two policies (BTT-90 and BTT-180). Two sets of subsystem time constants were selected to be representative of a fast and a slow system response (Fig. 1) so that the effect of parameter variations could be assessed. The results are categorized as a comparison of steering policies, a comparison of airframe configurations, and an identification of subsystem parameter dependencies.

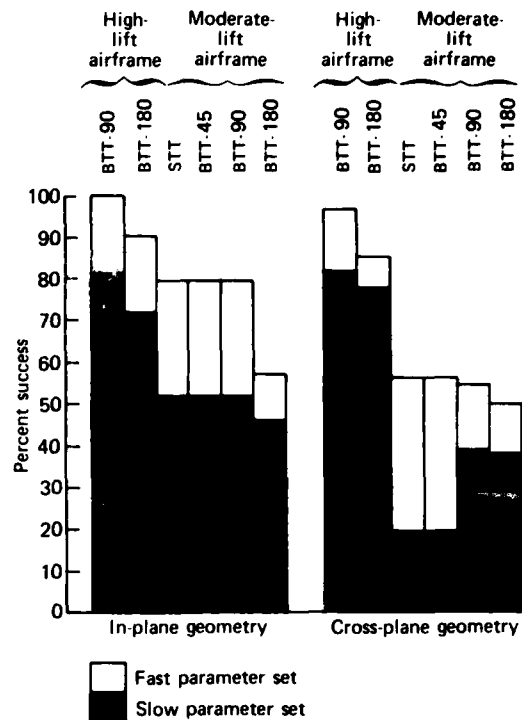
In order to focus the study and develop meaningful results, two missions were selected for which BTT steering is applicable, a long-range raid-suppression mission and a medium-range, or area-defense, mission. The characteristics of these missions define the particular engagement and parameter values used. The area-defense assessment is summarized in this article.

Area defense, as considered here, is a medium-range engagement against a high-altitude air-to-surface enemy missile. Figure 2 illustrates the engagement geometry used in the study. Anticipated target characteristics suggest a target velocity corresponding to Mach 3 at 80,000 ft altitude with a 3 g turndown maneuver to a constant flight-path-angle descent. The surface-to-air missile typically followed a midcourse profile uplinked by the ground control navigation facility prior to target acquisition. The missile followed the prescribed midcourse trajectory, regardless of target location, until the range between the missile and the target (the acquisition range) was 10 nmi. Both in-plane and cross-plane midcourse trajectories were considered.

The selected measure of performance was the length of the target trajectory along which the target could be intercepted successfully, where a successful intercept is defined as a miss distance of less than 50 ft. Figure 1 summarizes performance results for this area-defense engagement. The performance measure, expressed as percent success, corresponds to the ratio of the length of the target trajectory that is successfully intercepted to the total length of the trajectory investigated. Two sets of results comparing the performance of the various configurations for the in-plane and cross-plane engagement geometries are shown.

RESULTS

The results from all four steering policies can be compared using the moderate-lift configuration. For the in-plane engagement geometry, the performances of STT, BTT-45, and BTT-90 are similar and better than that of BTT-180 for both the slow and fast sets of system parameters. The BTT-180 interceptor performance is limited by the slow response time associated with the



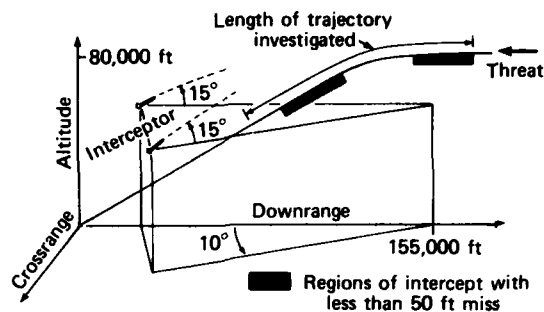
Parameter	Fast set	Slow set
Aero/control time constant (s)	$12\sqrt{q}$	$18\sqrt{q}$
Guidance filter time constant (s)	0.3	0.6
Roll rate limit (deg/s)	$\left\{ \begin{array}{l} 150 \\ 250 \end{array} \right.$	$q < 800 \text{ lb/ft}^2$ $q > 5000 \text{ lb/ft}^2$
Dynamic pressure, q (lb/ft ²)		$800 < q < 5000$

Fig. 1 Summary of results of the area-defense assessment.

bank system, relative to the steering system, under the conditions for this engagement. In general, the maximum allowable roll rate capability should be sought when designing a BTT system.

For the cross-plane engagement, the performances of STT and BTT-45 are nearly identical. When configured with the set of system parameters corresponding to a fast system response, the performance ranking of the steering policies is as follows:

1. STT and BTT-45 (equivalent) (55.7%)
2. BTT-90 (54.1%)
3. BTT-180 (49.3%)



Interceptor initial velocity = Mach 4.5
 Threat velocity = Mach 3
 Threat acceleration = 3 g

Fig. 2 Area-defense engagement geometry.

For the slow set of system parameters the ranking is:

- | | |
|--------------------------------|---------|
| 1. BTT-90 | (38.3%) |
| 2. BTT-180 | (37.5%) |
| 3. STT and BTT-45 (equivalent) | (19.3%) |

The change in performance ranking for the two sets of system parameters reflects the greater degradation in performance exhibited by STT and BTT-45 in shifting from the in-plane to the cross-plane engagement geometry.

The moderate-lift and high-lift airframe configurations were compared using the BTT-90 and BTT-180 steering policies. As expected, the performance of the high-lift configuration is better. The difference is greater for the more difficult cross-plane engagement geometry.

For each case, subsystem parameters corresponding to a faster system result in better performance. Increasing the maximum roll rate capability of the BTT-90 and BTT-180 configurations improves the performance of these systems by reducing the overall maneuver response time. In addition, the effective response time in the plane of the desired maneuver is affected not only by the subsystem responses but also by the amount the airframe must bank to achieve the commanded orientation.² For the cross-plane engagement, the effective time constant of the response in the plane of maneuver is smaller than for the in-plane engagement because the commanded maneuver plane is closer to the initial orientation of the interceptor's maneuver plane. This explains why the degradation in performance from the in-plane to the more difficult cross-plane engagement is not as severe for the BTT-90 and BTT-180 steering policies as it is for those of the STT and BTT-45.

SUMMARY

The results of this study indicate that BTT steering can provide acceptable performance provided the assumed subsystem responses can be achieved. A follow-on investigation is studying the BTT autopilot design problem.

REFERENCES

- ¹F. W. Riedel, *Bank-to-Turn Control Technology Survey for Homing Missiles*, NASA CR-3325 (Sep 1980).
- ²R. T. Reichert, *Homing Performance Comparison of Selected Airframe Configurations Using Skid-to-Turn and Bank-to-Turn Steering Policies*, NASA CR (to be published).

SIMPLIFIED LETHALITY MODELS OF SAM WARHEADS

C. R. Brown

Relatively simple mathematical models not requiring the use of a computer were developed for calculating the effectiveness of a surface-to-air missile (SAM) warhead when it encounters a missile target. The application of these models can provide approximations to kill probability, P_k , that are accurate enough for preliminary weapon system analysis.

BACKGROUND

Although computer models are usually more precise for calculating the P_k of a warhead, the weapon system analyst frequently needs less sophisticated techniques. Force level studies of advanced weapons, for example, may lack accurate input data so that approximations to P_k based on simple numerical models will suffice.

Both head-on and crossing encounters between a fragmentation warhead and a missile target are of particular interest. In a perfect fuze model, the fragments are assumed always to strike the most vulnerable region of the target; therefore, the P_k has the highest possible value. A more realistic P_k is found with a fuze/warhead model having nonperfect fuzing.

DISCUSSION

Figure 1 shows the intercept geometry for a head-on attack just before warhead detonation. The fuze radiation pattern is represented as a frustum of a cone having a sharp cutoff range and a half angle, ψ_F . The miss distance, ρ , and orientation angle, ϕ , locate the position of the missile in the x, y plane. The probability of killing the target is

$$P_k = \frac{1}{2\pi} \int_0^{2\pi} \int_{\rho_{min}}^{\rho_{max}} P_c f(\rho) d\rho d\phi. \quad (1)$$

In this equation, P_c is a conditional kill probability, given a hit by the fragment beam spray, $f(\rho)$ is the probability density function for a Rayleigh distribution of miss distances, and ρ_{min} and ρ_{max} are the minimum and maximum miss distances within which a fragment hit can occur.

When the density of the fragment beam spray is inversely proportional to the square of the distance to the target (spherical dispersion), a numerical solution to

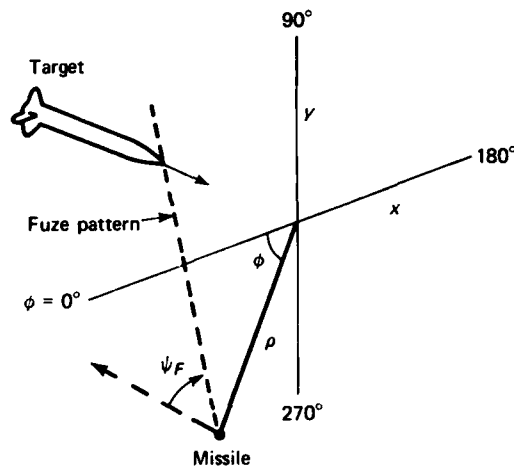


Fig. 1 Intercept geometry for a missile/target head-on encounter.

Eq. 1, in the case of perfect fuzing, is closely approximated by a function of a lethality parameter, u :

$$P_{k/c} = P_{k/c}(u), \quad (2)$$

where

$$u = \frac{N_s A_v \sin I_a}{\sigma^2 \sin \psi}, \quad (3)$$

and

- $P_{k/c}$ = kill probability for perfect fuzing,
- N_s = fragment beam density (number of fragments per steradian),
- σ = guidance error,
- A_v = effective vulnerable area of target,
- I_a = impact angle of fragments at the target's center, and
- ψ = average dynamic ejection angle of fragments.

A similar approach to $P_{k/c}$ was taken for cylindrical fragment dispersion.

The effective vulnerable area is the total vulnerable area if the fragment beam spray is large enough to cover the target. For smaller beam sprays, A_v is calculated as some fraction of the total.

This work was supported by the Chief of Naval Operations, OP-96.

The perfect fuzing model was modified to include the contribution of blast and to show the effects of warhead weight, W (in pounds), and guidance error, σ (in feet), on kill probability (Fig. 2). In the new lethality parameter, u_0 (Fig. 2), h is the weight of each fragment in grains and B is a half-angle of the static fragment beam spray. F is a design factor that is the fraction of the total weight used in the fragment beam, including the explosive and the metal case; in most cases, it lies between 0.80 and 0.90. The effective vulnerable area, A_V , depends on the striking velocity and mass of the fragment. The ratio of explosive charge weight to metal casing weight, C/M , was assumed to be 1.2; other values of C/M can be used in Fig. 2 by multiplying u_0 by $2.2/(1 + C/M)$.

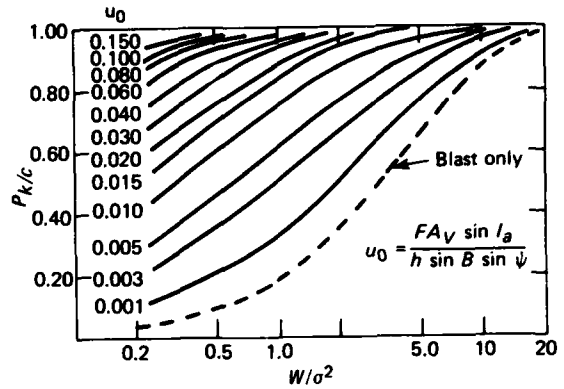


Fig. 2. Warhead kill probability, assuming head-on encounter and perfect fuzing.

Table 1

COMPARISON OF MATHEMATICAL AND COMPUTER MODEL RESULTS

σ	Aspect*	Computer Model		Simplified Model	
		$P_{k/c}^\dagger$	P_k^\dagger	$P_{k/c}$	P_k
10	H	0.996	0.996	0.980	0.980
	S	-	0.927	-	0.967
20	H	0.927	0.921	0.891	0.882
	S	-	0.829	-	0.785
30	H	0.774	0.734	0.768	0.695
	S	-	0.646	-	0.612

* H = head-on

S = side-on

† $P_{k/c}$ = kill probability, perfect fuzing

P_k = kill probability, realistic fuzing

The addition of realistic fuzing in the model for spherical dispersion gives P_k as the function

$$P_k = P_k(\rho_B, \sigma, \rho_{min}, \rho_{max}, P_{k/c}), \quad (4)$$

where the effect of the warhead blast is provided by the blast radius ρ_B , and where ρ_{min} and ρ_{max} depend on the fragment ejection angles, the fuze angle (ψ_f), and the fixed time delay (t_D) set by the fuze. Formulas for calculating ρ_{min} and ρ_{max} were derived for both head-on and crossing target encounters. P_k is calculated at four orientation positions ($\phi = 0, 90, 180, \text{ and } 270^\circ$, Fig. 1), and the results are averaged. Several sample calculations of $P_{k/c}$ and P_k showed good agreement with the results from a more sophisticated computer model (see Table 1).

WEAPON CONTROL SYSTEMS

INTRODUCTION

As an outgrowth of the program to develop the proximity (VT) fuze in World War II, APL became actively involved in the improvement of gun directors and, by the end of the war, was engaged in the application of new technology to the problem of directing anti-aircraft weapons. During the initial development of the anti-aircraft guided missile and its early introduction for service use, the APL staff worked with the Navy's equipment contractors to acquaint them with the characteristics of these new weapons. The role of the Laboratory in weapon control necessarily expanded with the assumption of responsibility for technical direction of the Navy's AAW guided missile systems in the late 1950's.

The challenge to the Fleet posed by manned supersonic bombers attacking en masse under the cover of electronic countermeasures required a radical departure from the relatively primitive, human-intensive control procedures that grew out of World War II.

Working first with analog and then digital electronic computational techniques, the Navy has produced tactical data and weapon control systems that relieve weapons personnel from much of the routine bookkeeping associated with a fighting ship. APL made important contributions in this evolution, particularly in the area of threat evaluation and weapon assignment. In addition to the characteristic drive to discover and apply the basic principles underlying a problem, the Laboratory brought to the Navy weapon control community an understanding of the potential capabilities of the then-emerging world of electronic computation and automation.

APL has contributed to defining the basic structure of shipboard combat systems and to allocating functions consistently among the sensor, command support, and weapon control elements of these very complex systems. Such consistency of structure has aided technical interchange among major

developments in which APL has played a role, including the Aegis Weapon System, Terrier and Tartar New Threat Upgrades, and, most recently, the DDGX Combat System. APL initiatives supporting the development of weapon control systems have included Combat Information Center design, computer program development, management techniques, human control of automated system responses, and scheduling of weapons engagements in a complex threat environment.

Anticipating the potential threat of antishipping missiles, the Laboratory has focused its recent efforts in the area of weapon control on the definition and development of techniques that allow weapon systems to respond to a threat in minimum time while providing the requisite control capability for the several levels of tactical command. Integral to Laboratory efforts in this and other areas of weapon control is the identification of data processing and distribution approaches that enable the implementation of practical and economical designs — designs that provide requisite hardness to equipment casualty or battle damage.

The articles in this section describe several related exploratory efforts directed at the application of emerging technology in the areas of fiber optics and computer science to provide highly capable and flexible networks of computational elements and displays that can be used economically in weapon control systems. The first article describes the experimental demonstration of the use of fiber optics to provide high speed/high capacity digital communication as an improvement over and replacement for copper wire. The next discusses a design approach to the combination of fiber optic cables and electronics to form a highly reliable, multiuser, common communication network — a data bus.

The third article describes the demonstration of techniques to implement and manage a distributed processor network that can transfer tasks among several linked computers in order to maintain a minimum level of functional capability, despite the loss of one or two of the linked computer elements.

A FIBER-OPTIC DATA LINK

J. B. Ferguson, R. L. Nelson, and A. E. Davidoff

A proof-of-principle investigation to determine the practicality of a fiber-optic data link interconnecting standard Navy interfaces has been undertaken. As a result of the study, a Naval Tactical Data System (NTDS) fiber-optic data link has been designed and tested, with success.

BACKGROUND

The Navy's Aegis Weapon System, a fully automatic, shipboard, surface-to-air missile system, is being installed in a new class of cruiser. The first ship of the class, USS *Ticonderoga* (CG 47) will be delivered in early 1983. The Aegis New Computer Technology Applications Program has been established to investigate new computer-related technological developments whose application to the Aegis Weapon System and its support equipment could lead to reduced costs or improved system performance for follow-on upgrade programs.^{1,2} The application of serial fiber-optic transmission technologies to digital communication systems is a promising new technology because of the numerous advantages of data transfer by serial fiber optics rather than the current parallel copper cabling. The advantages include high bandwidth, low signal attenuation, inherent freedom from electromagnetic and radio frequency interference and emissions, immunity to electromagnetic pulse effects, electrical isolation, and communications security as well as size, weight, and cost benefits when compared with using bulky, heavy, high-signal-loss parallel copper cable.

A fiber-optic NTDS output data link has been developed as part of an investigation of the Aegis New Computer Technology Applications Program, with support from the New Threat Upgrade project. It

demonstrates to the Navy the utility of fiber-optic technology and serves as a working testbed for detailed validations within APL's Combat System Evaluation Laboratory and possible Navy environments.

DISCUSSION

The fiber-optic data link was designed to duplicate the functional operation of a standard NTDS output cable. According to NTDS specifications, a computer communications channel consists of a pair of input and output cables, each consisting of 45 pairs of twisted copper wires with common shielding. Information composed of four "handshaking" controlled bits and up to 36 data bits is transmitted through each cable as a parallel connection; i.e., each bit has a dedicated line. The activity associated with an output cable is characterized by requests originating at a peripheral and acknowledgments generated by the computer.

The data link contains two interface boards, two power supplies, and three optical fiber cables (Fig. 1). The computer interface board is located close to the computer and transforms the computer's conventional parallel output into a serial data stream of light pulses propagating through an optical fiber. The peripheral interface board executes the complementary function and converts the serial stream of information into a parallel format data word for presentation to the peripheral. Two interface boards are event-driven, the initiating events being the rising and falling edges of the four control lines.

Operation of the two interface boards is synchronized by a 40 MHz master clock on the computer interface board and transmitted to the peripheral in-

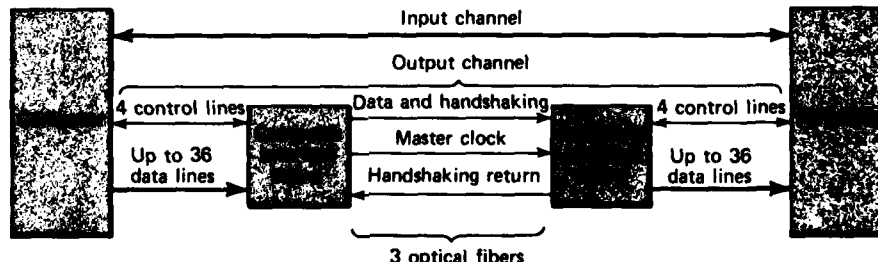


Fig. 1 Computer channel implemented with a fiber-optic output cable.

terface board by one of the optical fibers. Because of the bandwidth limitations of the specific optical transmitter/receiver pairs used, the 40 MHz master clock on the peripheral interface board is actually synthesized from a transmitted 20 MHz square wave.

Two types of information may be transferred on an NTDS output channel: output data and external functions. The associated control signals indicate to the peripheral that a valid data word is available on the channel. Either event will cause the computer interface board to load a 44 bit shift register with synchronizing, handshaking, parity, and data word information. The register, operating as a parallel-to-serial converter (Fig. 2), is then right circular shifted at a 40 MHz rate, thereby generating the serial data stream. When the first bit returns to its original position, the shifting operation is terminated. A circular shift is necessary so that the register can repeat the process in the event of a parity error signal from the peripheral interface board.

Four parity bits are generated before each transmission; three are from the 36 data bits and the fourth contains the total parity of the message. The 36 data bits (0 through 35) are rearranged for parity checking so that the possibility of undetected consecutive data errors is minimized. The last parity bit is calculated from the first three parity bits and the two control lines.

As an additional feature, the number of data bits transferred by the fiber-optic data link is switch programmable in increments of four. This permits the data link to be operated at a faster rate for computers with data words that contain fewer than 36 bits.

Upon reception of serial data stream synchronization bits, the peripheral interface board (Fig. 3)

prepares the shift register counter to the expected number of bits in the transfer stream. The completion of this count sequence signals the shift register to terminate the sampling operation. The parity of the received data stream is then compared with the received parity bits to determine if a sampling error has occurred. If an error does exist, a resend request is transmitted to the computer interface board, which responds with a retransmission of the original data stream. Otherwise, the shift register data are clocked into latches and presented to the voltage translators and NTDS drivers. Regeneration circuitry is incorporated to generate the proper acknowledge pulse, which drives the peripheral's output cable to indicate that data are available for sampling.

A similar scheme is used to transfer handshaking return control lines from the peripheral to the computer. The transfer is initiated by a rising edge of the resend request signal or a change of state in either of two peripheral control lines. Any one of these events causes a five bit data stream, consisting of synchronizing bits, control signals, and a possible resend bit, to be transmitted.

TESTING

The single-direction fiber-optic NTDS data link has been tested successfully in a number of computer-to-peripheral configurations within the Combat System Evaluation Laboratory. The initial testing was carried out for the purposes of trouble-shooting, debugging, and checking.² Figure 4 shows one such test of an early version of the fiber-optic channel hardware. The primitive test programs transferred blocks of data and

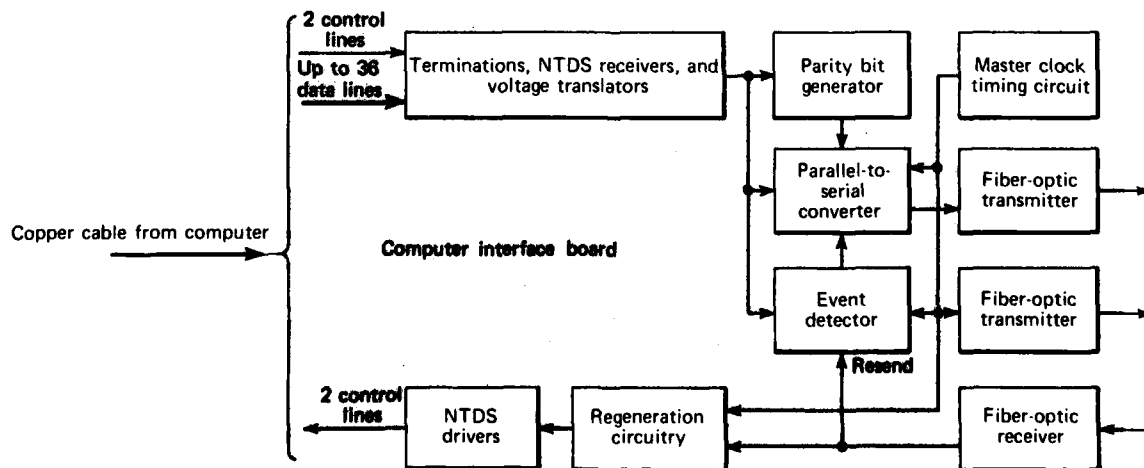


Fig. 2 Functional diagram of computer interface board.

handshaking control lines to a specified peripheral over the fiber-optic output channel and checked for errors by reading the data back over the copper input channel. Those "end-around" test programs were used extensively and exhaustively to determine the bit error rate of the link.

When the operational checkout had been completed, error-detection and resend circuitry was added to the fiber-optic data link in order to ensure the very high reliability of data transmission. To verify the operation of the resend capability, deliberate error injection circuitry was incorporated into the computer interface board. It selectively injected a single bit error in the serial data stream without altering the correct information in the shift registers, thereby permitting thorough testing of the serial data stream, the fiber-optic data link, and the error detection and resend feature.

The final phase of testing was performed with a high speed computer and various high speed peripherals such as equipment for buffering video and display information, a military tape drive unit, and a commercial rigid data disk. The test programs that were successfully executed included a magnetic tape diagnostic test program, a stand-alone disk test, and a display demonstration program written for the battle group anti-air-warfare coordination (BGAAWC) project. The BGAAWC demonstration program required some software timing changes to accommodate delays caused by the external conversion process. Table 1 lists the specific link configurations that were tested successfully. The single-direction fiber-optic NTDS data

link will be installed in a local facility for long-term sustained operation, evaluation, and demonstration.³

SUMMARY

As a result of the fiber-optics investigation, a working fiber-optic NTDS data link has been developed to demonstrate to the Navy the utility of this technology. The data link has undergone extensive testing with a variety of computer and peripheral configurations. The results indicate that a fiber-optic data link can successfully replace conventional parallel copper cables in most communication systems. However, external serial converters cause additional delays that may necessitate more tolerant software to achieve system transparency. On the other hand, embedding the fiber-optic channel inside the computer or peripheral can achieve an interconnection that does not introduce additional delays, providing its bandwidth is high enough.

There are significant economic and performance implications that make fiber optics attractive and practical. The reduced size and weight and the successes of



Fig. 4 Testing of early version of the NTDS fiber-optic data link.

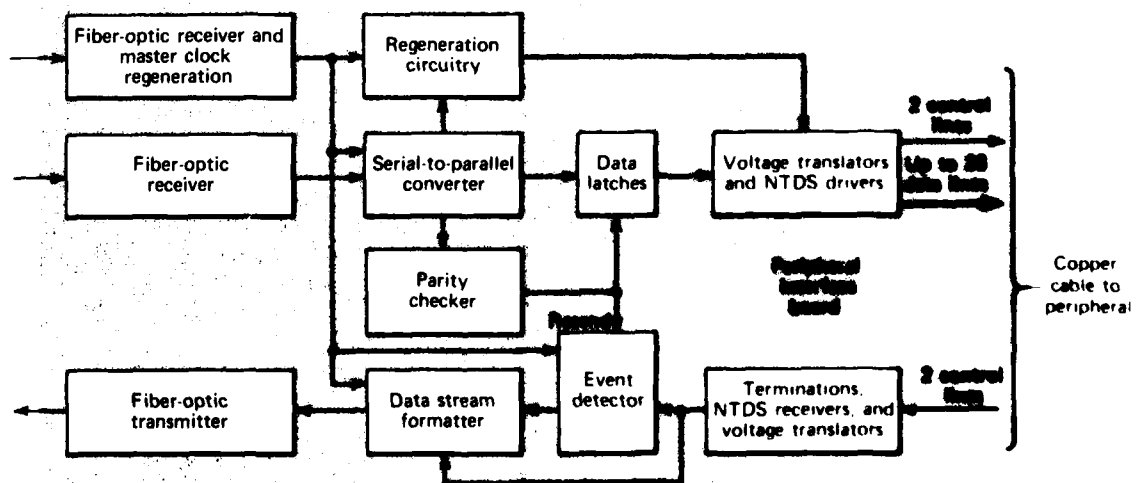


Fig. 3 Functional diagram of peripheral interface board.

Table 1
SUCCESSFUL FIBER-OPTIC DATA LINK TESTING

Computer	Peripheral	Description of Test
AN/UYK-20	1840 magnetic tape unit	Random data test programs
AN/UYK-20	Central data buffer	Interface test programs
1230	Output-to-input channel NTDS fast and slow	End-around test program
1230	Ramtek	Ramtek test program
AN/UYK-7 (4-bay)	Central data buffer	BGAAWC BADG (DM-1A) computer program (with changes to software timing required)
AN/UYK-7 (4-bay)	RD 358 magnetic tape unit	RD 358/UYK (1840M) test
AN/UYK-7 (4-bay)	SI 9762 rigid data disk	Stand-alone disk test for CDC 976X series disks using System Industries Model 9500 controller

the fiber-optic NTDS data link demonstrate the utility and promise of these communication links in future Navy systems. As a result of the successful prosecution of this project and the lessons learned regarding external serial data transmissions, plans are under way for the implementation of an embedded fiber-optic converter as a demonstration candidate at sea in the first engineering development model (EDM-1) of the Aegis Mk 7 Weapon System. The Aegis EDM-1 has been installed

and operating in USS *Norton Sound*, the Navy's floating proving ground, since December 1973.

REFERENCES

- ¹A. E. Davidoff, "Aegis Program for Application of New Computer Technology," *Developments in Science and Technology, Fiscal Year 1978*, JHU/APL DST-6.
- ²J. B. Ferguson, *Fiber Optic New Technology Proof of Principle Checkout*, JHU/APL F2F-2-237 (Apr 1979).
- ³A. E. Davidoff, *Status of NTDS Fiber Optic Link Development Efforts*, JHU/APL F2F-2-349 (Aug 1980).

DESIGN OF A FIBER-OPTIC CONTENTION BUS NETWORK

S. A. Kahn, R. L. Stewart, and S. G. Tolchin

The logical and physical design of an intelligent communications support system, based on fiber optics, for interconnecting diverse computers and devices is described. The networking system, called the Duplex Bus Communications Service (DBCS), is being developed to support local area communications networking.

The DBCS facilitates system integration by means of a multilayered protocol structure, a directed and branching fiber-optic bus, and microprocessor-based intelligent interface units. The system architecture includes high-level protocols resident within the network interface units, reliable encrypted communications free from electromagnetic interference, ease of cable installation, ease of maintenance and growth, and full-duplex transfer capability.

This work was supported by Indirectly Funded R&D.

BACKGROUND

Several efforts are under way to design communication networks that will connect computers and computer devices manufactured by different companies and serving different communities of users. However, no local area (spanning a few kilometers) communications technology for interfacing heterogeneous computers, terminals, and peripherals is now available. Also, no local network has network-resident high-level protocols to assure protocol standardization, ease of maintenance in a complex environment, and ease of adding new members. The implementation of a network providing these features can provide an expansion of user services in several multicomputer system environments.

The DBCS network¹ being developed at APL is aimed at providing an extensive but inexpensive communications service. The fiber-optic medium affords simple installation as well as freedom from easy tapping and electromagnetic interference. By using microprocessors and comprehensive software support at each network connection, DBCS provides a range of communications services, from simple message exchange to the management of the temporary integration of processes in different computers. The physical architecture of the network is reliable with respect to overcoming localized component failures (e.g., link or node failures). The software provides assured and secure data communications. In addition, the DBCS is an "open" system in the sense that new members may be added easily without having to modify existing members.

The DBCS networking technology will be able to support a wide range of applications, including

1. Information, data processing, and sensor systems integration^{2,3};
2. Office automation;
3. Electronic mail memorandum routing and retrieval;
4. Remote access to computer graphics, word processing, and other special resources or software packages;
5. Distributed data base development; and
6. Distributed data processing research.

DISCUSSION

The DBCS architecture consists of interface units to connect devices to the network, dual-strand fiber-optic cable links, and junction boxes that direct all

data incoming on a given fiber (encoded as light pulses) to all other outbound fibers.

Figure 1 illustrates a possible network configuration. Computers or devices such as terminals or printers are connected to the network by means of the programmable network interface units (NIU). These units are interconnected by means of junction boxes (J) and the fiber-optic cables. Note that network growth is easily accomplished by adding junction boxes and fiber-optic cable segments.

An NIU transmits data from its computer or terminal to the receiver of its junction box. The junction box retransmits the data to all the other outgoing fibers but not back to the originating source. Because all junction boxes follow the same rule, data are transmitted to all nodes on the network except back to the sender. Data are passed on the network in discrete packets that contain source and destination addresses. Only packets addressed to a given NIU are read by that NIU.

Each NIU competes with all others to use the common communication channel. By listening on the bus until no signal is detected, it can determine when to begin transmitting data. Another may attempt to transmit at approximately the same time, which could result in the superposition of two or more messages on the common channel. Such an event, called a collision, is detected by the sending NIU, which issues a network abort. The abort floods the network with a pulse of light that directs all receiving NIU's to disregard the packet. The sending NIU then waits a randomly determined delay time before attempting retransmission, to avoid recurrence of the collision.

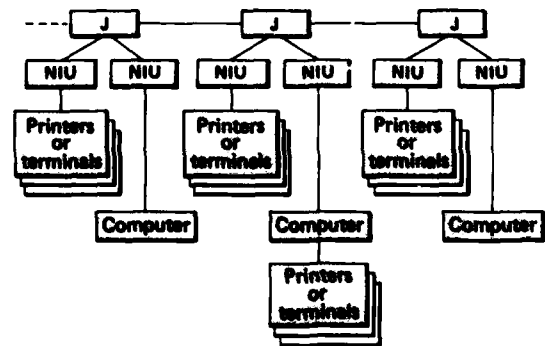


Fig. 1 A typical network configuration. Data and control signals are exchanged among host computers and user terminals under control of microprocessor-based NIU's via pathways consisting of fiber-optic cables and junction boxes (J). Data, encoded as light signals, enter a junction box and are redirected to all other outbound cables. Data originating from a given NIU are heard by all other NIU's but not by the originator.

Two data packets may exist simultaneously without causing a collision, for example, when two NIU's are sending messages to each other. In this case, the receive lines of the two NIU's do not contain superposed data. The scheme permits a simultaneous exchange, or full duplex, within the DBCS architecture. The basic bus access scheme described above has been modified in DBCS to permit full-duplex communications to improve data transfer efficiency, to permit close coupling between two computers when necessary, and to support such applications as feedback control.

Data communications in DBCS will be reliable in two different ways. First, the integrity of bits, bytes, packets, and complete messages transferred across the network will be assured because software is embedded in each NIU to perform error detection, correction, and reporting. Second, the basic network is not vulnerable to single-point catastrophic failures because NIU's on either side of a failed junction box can continue to communicate with all NIU's linked by operative junction boxes. Communications control is distributed among NIU's to avoid or minimize the effects of NIU or junction box failures on network members.

Communications functions are performed according to rules known as protocols. The functions range from managing the physical transfer of bit streams at the low level through high-level functions such as the control of integrated and structured data exchanges among cooperating programs in different computers.⁴ The protocol functions are accomplished within each NIU, and distributed network control is achieved by means of a common network protocol system design.

The design decision to perform most protocol functions within the NIU's rather than within the host computer provides significant advantages, including a resulting simplification of development and maintenance activities. Rather than having to develop protocols within each host computer for every other host with which it may need to communicate, only one interface (to the network) is needed. Future changes may include protocol revision, changes of computers in various user areas, or changes in the applications designs supported by the network. Rather than having to implement new software in all computers on the network to accommodate the new environment, only changes to DBCS software will be required since the protocols are within the NIU's. The changes can be made in a uniform, controlled manner by the network manager, thereby easing protocol maintenance.

The protocols provide various communications services. A simple message exchange without receipt acknowledgment (like a letter dropped in a mailbox) is known as "datagram service." The next level of service

is called "virtual circuit service"; message sequencing and delivery are assured. Finally, to link two computing devices across the network, the content and time reference of messages as well as their associated virtual circuit must be monitored. The administration of such an event-oriented circuit is called "session management." Unlike other networks, DBCS has been designed to provide session management services by a negotiation process between the initiating computer (or person at a terminal) and its NIU. That NIU then assumes responsibility for establishing and maintaining the required virtual circuits with other NIU's.

Major protocol program modules are depicted in Fig. 2 in their relative functional location within an NIU. Briefly, communications protocol functions are performed asynchronously by two separate microcomputers. Higher level "management" protocols, such as control of processing sessions between two network hosts, data encryption, and input/output of complete sequenced messages, are implemented by the upper half of the NIU. The incoming and outgoing messages are buffered in shared memory. The lower half of the NIU partitions outgoing messages into smaller, more efficient packets and "prepends" destination and source

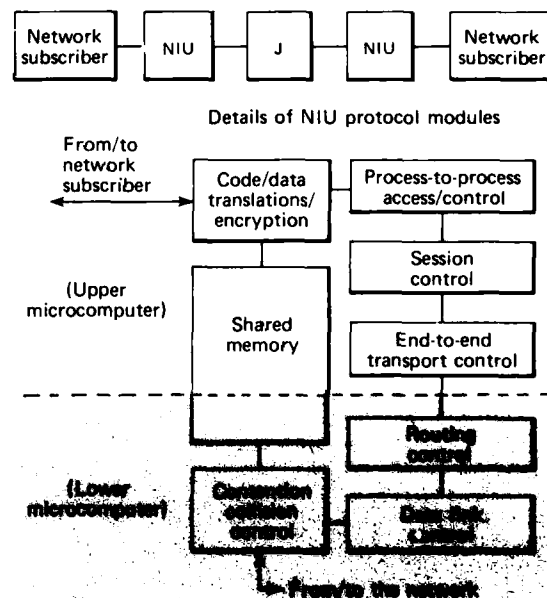


Fig. 2 NIU protocol modules. Two microcomputers execute program modules to control data transfer. The upper microcomputer handles data translations, program access control, session management, and end-to-end message sequencing. Data messages from and to the attached subscribers are stored in a shared buffer area. The lower microcomputer in the NIU works independently to address, deliver, and acknowledge delivery of data exchanged among NIU's.

addresses. When the network is quiet, the packets are sent (and resent as necessary) to their destination until error-free delivery is acknowledged by a return packet. Incoming packets are similarly assembled into messages.

The following is an example of an NIU protocol operation involving a user at a terminal and a remote computer. The terminal's data code is converted to a single network code, and then a connection and processing session between the user and the computer is negotiated across the network. After this establishment phase, data are exchanged interactively between the terminal and the computer under the control of the lower level protocol modules.

Summarizing, a local area communications network technology has been developed to support a wide range of potential applications and to provide a test bed for continuing research in distributed data processing. The components of an initial network, based on the DBCS architecture, have been designed, fabricated, and

tested. The overall system is designed to provide several new features: (a) a new fiber-optic-based branching contention bus, (b) embedding of high-level communications protocols within the network to permit extensive subscriber services and to simplify development and maintenance activities, (c) full-duplex communications capabilities, (d) implementation of open system concepts, and (e) secure and reliable data communications among various computers and computer devices.

REFERENCES

- ¹S. A. Kahn, R. L. Stewart, S. G. Tolchin, and S. J. Healy, "Functional and Logical Description of a New Fiber-Optic Contention Bus Network," presented at COMPCON 80, Sep 1980.
- ²S. G. Tolchin and R. L. Stewart, "The Distributed Processing Approach to Hospital Information Processing," presented at Fourteenth Annual Hawaii International Conf. on System Sciences, Jan 1981.
- ³R. L. Stewart and S. G. Tolchin, "A Distributed Processing Fiber-Optic Hospital Information System," presented at Fourth Annual Symp. on Computer Applications in Medical Care, Nov 1980.
- ⁴"Reference Model of Open Systems Interconnection," ISO/TC 97/SC16/N227 (Jun 1979).

A HIGHLY SURVIVABLE DISTRIBUTED PROCESSING SYSTEM

M. E. Schmid, R. L. Trapp, and A. E. Davidoff

A novel strategy for computer system survivability has been implemented using a distributed system of homogeneous microcomputer elements. The system has demonstrated the ability to perform high speed transfers of function from elements with simulated failures to backup elements. It will become a testbed for implementing failure detection and recovery strategies in distributed systems.

BACKGROUND

In the past, the high cost of computer hardware forced designers to think in terms of highly centralized computer systems. Today, on the other hand, many

small computers can be linked together, forming a decentralized computer system with the equivalent power of a large central computer but at potentially less aggregate cost (see Fig. 1). The overall system is less vulnerable to failure because computing power is no longer confined to a single compartment. With the relative isolation of each system, the availability of any one system is less dependent on the others. Decentralization can also help simplify design requirements and allows for more flexible resource allocation.

The realization of these advantages presents problems that have yet to be fully solved. One problem is to retain computer system functionality despite component failures. In large centralized computer complexes, hardware failures are known centrally and are accommodated by using the remaining functional

hardware to run as much of the required work as possible. A decentralized system must rely on different principles to accommodate failures since the knowledge of hardware failures is inherently distributed along with the computing capability.

DISCUSSION

Three major objectives characterize the design approach to a survivable distributed processing system:

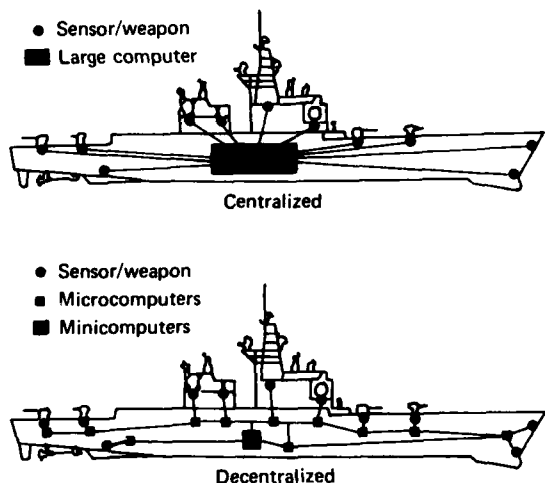


Fig 1 Differences between centralized and decentralized computer systems.

(a) implement system survivability at a level that will minimally affect task software development; (b) achieve system control through the participation of all the active elements rather than through the use of a central controller that could become a single point of failure; and (c) focus on system recovery strategies rather than on methods to detect different types of errors (the more traditional approach usually taken in fault-tolerant computer research).

The resultant working model, the failure isolation and recovery survivable system testbed (FIRSST), is shown in Fig. 2. It consists of six identical microcomputers that either run tasks or operate as backup elements. Typically, three are run as tasks and three as backups. Two system busses provide communications between computers, to simulated sensor/weapon devices, to the maintenance log, and to the secondary memory. System software has been developed to automatically transfer a task processing function from a faulted computer to a backup computer.

The backup computers have been designed to respond to two categories of faults. If a correctable fault occurs, an operational transfer is performed. However, if an uncorrectable fault occurs, a restart transfer is performed.

An operational transfer is defined as the transfer of an active function from a task microcomputer to a backup microcomputer without corruption of the executing task. Such a transfer may occur upon indication that a correctable fault has been detected by a

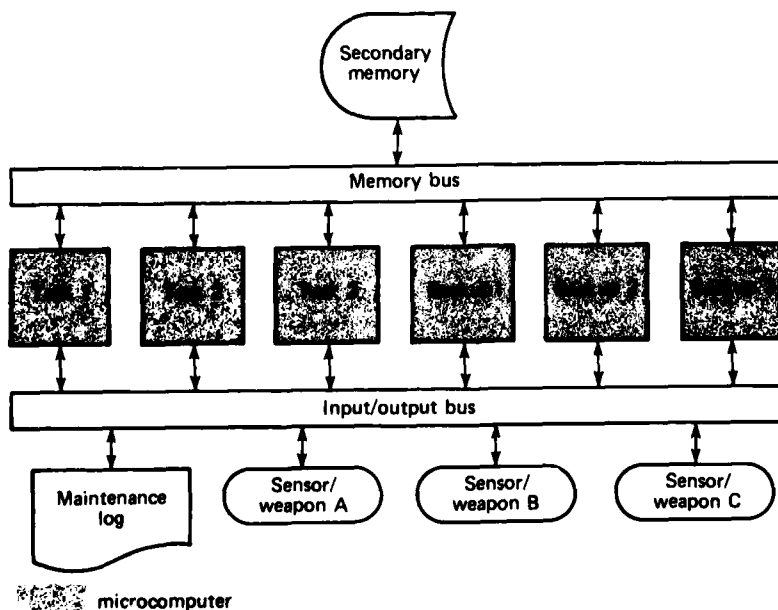


Fig. 2 FIRSST six-computer three-task system.

particular backup microcomputer. When this happens, a backup microcomputer transfers the complete memory and register set of the faulted microcomputer into its own internal store. Upon completion of the transfer, the backup computer begins operation of the task precisely where the faulted computer had been interrupted for the transfer. Thus, the task function is completely unaffected (with the exception of the transfer delay). The active transfer of function is possible because a correctable failure comes from a microcomputer that is still executing proper results but may soon fail entirely. Operational transfers may also be used to reallocate tasks among the working computers in order to permit maintenance or diagnostic tests on a computer.

A restart transfer is defined as one in which the task must be "cold" started from task software stored in the system's secondary memory. It frequently occurs as the result of the detection of an uncorrectable failure, which necessitates the interruption and reinitialization of only the specific faulted task. In this case, the backup loads the required task from secondary memory. The transfer causes a discontinuation in the task function because the backup microcomputer must restart the task at the beginning. To prevent possible interference, the failed microcomputer may be electrically isolated from the system communication lines and designated "dead."

The demonstration system, completed on September 30, 1980, is shown in Fig. 3. Both cold restart transfers and operational transfers were performed repeatedly without system malfunction. Typical recovery times for both types of transfers range from 0.01 s for small programs to 0.25 s for large programs.

The FIRSST system demonstrates an effective architecture for reliable and quick recovery from faulted functions. Its survivability is enhanced by the fact that the modular nature of the system allows microcomputer elements to be repaired or replaced while the system is fully operational. Furthermore, the system was designed so that its survivability would be totally independent of any specific task. This also means that the design and programming of a task occurs without the added burden of having to design and implement survivability into each unique application of the computer system.

FIRSST has been very useful in emphasizing the concept that survivability can be designed in at the beginning of a project to provide a cost-effective survivable system. FIRSST will also be used in the future research of fault detection methods.



Fig. 3 FIRSST demonstration system.

ACKNOWLEDGMENT

The authors wish to thank Professor G. M. Masson, of The Johns Hopkins University Electrical Engineering Department, for his many constructive suggestions concerning the design and testing of FIRSST.

REFERENCES

- ¹A. E. Davidoff, *CY 81 IR&D Documentation for Distributed Processing Project (Survivable Systems) — Updated*, JHU/APL F2F-2-401 (19 Dec 1980).
- ²A. E. Davidoff, *IEEE Workshop Presentation*, JHU/APL F2F-2-304 (16 Jan 1980).
- ³R. L. Trapp, M. E. Schmid, and A. E. Davidoff, *Exploratory Development Status: A Highly Survivable Distributed Processing System*, JHU/APL F2F-2-220 (5 Feb 1979).

COMMAND, CONTROL, AND COMMUNICATIONS SYSTEMS

INTRODUCTION

Command, control, and communications (C³) are required to support the several military commanders in the integrated use of available service forces in the deterrence of war or, should such deterrence fail, in the prosecution of warfare to achieve national objectives. C³ supports this mission by assembling and formatting the information needed to make decisions, rendering decisions as required, developing and promulgating orders to implement the decisions, and monitoring the course of events resulting from the promulgated orders.

AS²L became involved in the C³ program in 1971 when the Chief of Naval Operations requested an evaluation of the performance of TACAMO, the airborne strategic communication link to Fleet Ballistic Missile submarines. That successful test program led to an ever-increasing participation in test and evaluation, methodology development, equipment design, and the development of computer software in strategic naval communications. In 1976, additional facets of C³ were added to APL's task, including evaluation of Fleet Command Centers, study of requirements for Tactical Flag Command Centers afloat, and testing of C³ support for the Army's Pershing missile system.

In 1977, the Naval Electronic Systems Command (NAVELEX) requested APL's assistance in the system engineering of a tactical C³ system for the U.S. Navy in the year 2000. The objective of the program is to provide NAVELEX with engineering design guidance and transition planning for the development of this future system. In 1978, another increase in effort occurred with the addition of tasks in the fields of electronic warfare, surveillance, and over-the-horizon detection, classification, and targeting. The latter are closely related to APL work in the cruise missile programs, Tomahawk and Harpoon. A year later, a strategic connectivity study defined required improvements to the communications support of sea-based strategic forces of the future.

APL is continuing activity in all the areas discussed. In addition, major new projects have been assigned, including derivation of the command and control architecture for the future Navy, evaluation of U.S. Army Electronics Research and Development Command development programs, and support for the analytical evaluation of the Navy Integrated Tactical Surveillance System.

From the work in progress, almost all of which is classified, one article has been selected for this section of the report. It describes an ocean surveillance analysis model for simulating the ship traffic situation in a defined ocean area.

AREA TRACKING AND CORRELATION MODEL

T. G. Bugenhagen, B. Bundsen, and L. B. Carpenter

A simulation model of the surface ocean surveillance situation has been developed. Using the model, the requirements for producing surveillance pictures accurate enough for over-the-horizon targeting were determined.

BACKGROUND

APL has conducted an engineering analysis of over-the-horizon detection, classification, and targeting (OTH/DC&T). The objective of the program was to formulate system concepts, select and validate a specific system, and provide an engineering description of the selected system. The OTH/DC&T capability is intended to support long-range engagements of surface, sub-surface, and airborne targets with weapons fired from surface ships, submarines, and aircraft.

As a part of this analysis, it was necessary to define the requirements that would allow targeting of long-range antiship weapons in a realistic environment, and therefore an ocean surveillance analysis model was needed. Previous analyses assumed that merchant ship traffic was uniformly distributed throughout an area, with the number of ships in the area given by the Poisson distribution. This is different from the actual situation where ships travel in shipping lanes. The area tracking and correlation (ATAC) model was developed to resolve this discrepancy.

DISCUSSION

The ATAC model is a simulation of the surface ocean surveillance situation. It generates ship tracks across an arbitrarily defined ocean area, simulates sensor reports, correlates reports, and measures the accuracy of the correlations by comparing them with ground truth. It uses Kalman filtering and probabilistic decision-making to perform multisensor, multitarget tracking in an arbitrary ocean area. New sensor reports are correlated optimally with existing tracks because the best fit of the reports over all the tracks is determined. Detection misses and false alarms are included in the model.

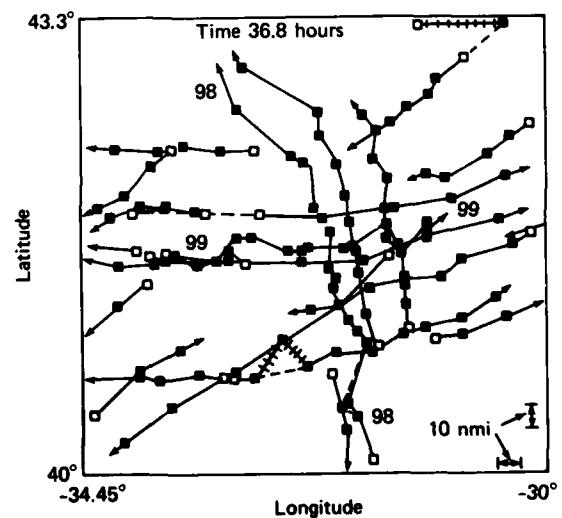
In the present version of the ATAC model, three different sensors were modeled and used in the analysis: two active sensors (radar) and a passive sensor that is assumed to give location reports only on high-interest ships. The passive sensor is also assumed to furnish a

unique identity of the ships on which it reports. Of the two active sensors, one is assumed to give only position reports and the other position and velocity measurements. Future versions of the ATAC model will use sensors that give line-of-bearing measurements. In addition, the correlation of reports by attribute matching is planned as an extension of the unique identification technique now used.

To keep computer processing time and costs within bounds, a threshold reduction technique was incorporated into the model. It limits the size of the uncertainty areas and, therefore, the number of hypotheses that may be generated, at a cost of more errors in correlation.

Several measures of effectiveness (MOE's), developed to determine the quality of the surveillance picture and track file produced by the correlator, included the average track purity and the mean error in the prediction of track position at a specified future time.

Figure 1 gives an example of the output of the ATAC model used in a mid-Atlantic ocean area to



The two high interest ships are Nos. 98 and 99. Incorrect associations are highlighted as follows:

- ++++ Incorrect associations
- Association omitted
- Sensor report at track initiation
- Subsequent sensor reports

Fig. 1 Correlator associations.

correlate reports from two different sensors. Table 1 gives the general scenario. An active sensor that gives hourly reports on background ships and two maneuvering high-interest ships and a passive sensor that gives reports only on two high-interest ships are assumed. The reports from the passive sensor are assumed to include unique identification.

In order to fill the shipping lanes with enough ships to approximate the desired intensity, the ship generation part of the model is run for a period of time before the sensor models are used. The period in this example is 27 hours. Then, the sensor models and the correlator are used in the next 10-hour period from

$t = 27$ to 37 hours. The tracks of the two high-interest ships in Fig. 1 are numbered 98 and 99. The other tracks are of background ships. Crossed lines show where incorrect associations were made by the correlator. Dashed lines show where a correct association was omitted. One error was made in the high-interest ship tracks, and four were made in the background ship tracks.

Similar scenarios, with the density raised to 50 ships per 100,000 nmi², were used in a parameter sensitivity analysis to establish the requirements. In this study, the ATAC model was run in a Monte Carlo loop. As the sensor update intervals and location accuracies

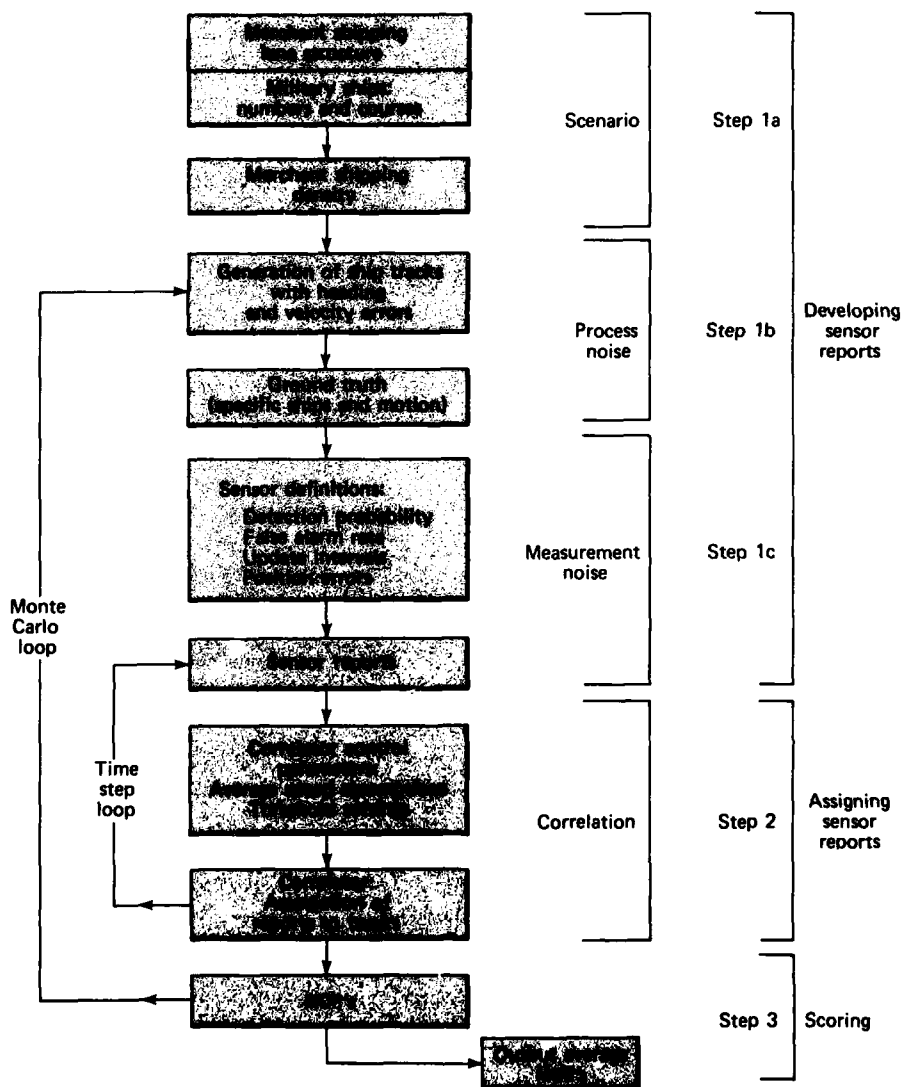


Fig. 2 Functional flow when ATAC model is used in a Monte Carlo loop.

Table 1
**SCENARIO FOR AREA TRACKING
AND CORRELATION MODEL***

Mid-Atlantic ocean area (40,000 nmi ²) shipping density	40 ships/100,000 nmi ²
Active sensor (position reports on background ships and two high-interest ships)	
Update interval	1 h
Location accuracy	2 nmi
Passive sensor (position report on two high-interest ships only)	
Update interval	1.8 h
Location accuracy	3 nmi

* Ten-hour time period

were varied, several MOE's were recorded. Thus, the surveillance parameters needed to achieve high MOE values were established.

Figure 2 illustrates the functional flow when the ATAC model is used in a Monte Carlo loop with the simulation of ship traffic and sensor reports. The three basic steps of the model are (1) developing sensor reports, (2) assigning sensor reports, and (3) scoring.

Step 1 is subdivided into scenario, process noise, and measurement noise. In the scenario subdivision, the ocean area is defined (by four corners in latitude and longitude), the structure of the shipping lanes is established, and the density of the merchant shipping is set. In the process noise subdivision, the ship heading errors and velocity errors are defined, after which specific simulated ships and their motions are generated. Measurement noise takes into account the sensor parameters to generate sensor reports, which are perturbed from the ground truth (actual) positions according to the associated position errors.

In the correlation phase, which makes up all of step 2, the sensor reports are associated (correlated) with existing ship tracks in a track file by means of Kalman filtering and probabilistic decision-making. The time step loop in the block diagram is meant to show that as sensor reports are periodically generated and received (based on the sensor update interval), the correlator associates the reports with tracks. At each time step, certain MOE's are calculated and then averaged at the end of the time period for which the model was run.

After the ATAC model is run with one set of process noise and sensor parameters, a new set is chosen. The process is repeated, as shown by the Monte Carlo loop. The MOE's are collected for each such iteration and are used to determine the grand averages for the analysis (step 3).

ATAC is currently programmed in the PL-1 programming language and run on an IBM 3033 computer. It uses about 1.5 megabytes of storage and about 10 seconds of computer processing time for one iteration involving roughly 20 ship contact reports every hour over an area of 40,000 nmi² in a given 10-hour time period.

ACKNOWLEDGMENT

The following people also contributed to the development of this model: J. S. Culbertson, D. E. Corman, and H. G. Tornatore.

REFERENCES

- ¹T. G. Bugenhagen and L. B. Carpenter, *OTH/DC&T Engineering Analysis, Volume 5, A Kalman Filter Rhumb-Line Ship-Tracking Algorithm*, JHU/APL FS-79-032 (Mar 1979).
- ²T. G. Bugenhagen, B. Bundsen, and L. B. Carpenter, *OTH/DC&T Engineering Analysis, Volume 11, Area Tracking and Correlation Model*, JHU/APL FS-80-170 (Aug 1980).

SPACE SCIENCE AND TECHNOLOGY

INTRODUCTION

The Laboratory's involvement in space programs began in the postwar years when Aerobee and captured V-2 rockets carried Geiger tubes, magnetometers, and optical spectrometers high above the earth's surface. The flights provided the first high-altitude measurements of cosmic rays, the geomagnetic field, and atmospheric constituents such as ozone and were conducted by pioneers James A. Van Allen, John J. Hopfield, and S. Fred Singer (who were then APL staff members). In 1946, a V-2 rocket carried the first camera, installed by APL, to look at the earth from an altitude of 100 miles. From these distinguished beginnings, APL's record of accomplishments proceeds, and includes the conception, design, and development of the Transit Navigation Satellite System and the Sattrack Missile Tracking System for the Navy.

The satellite activities spawned a multitude of firsts by APL, including the development of the first gravity-gradient satellite, the first photographs of the entire earth from synchronous-altitude satellites, the first solid-state particle detectors flown on a satellite, and the first extremely accurate measurements of the geomagnetic field.

The space activities at APL have been supported by an active program of basic research directed toward understanding the chemical and physical processes involved in the earth's atmosphere, ionosphere, and magnetosphere and in interplanetary phenomena. Some significant Laboratory achievements include the first detection of solar cosmic rays with satellite-borne solid-state detectors, the design and construction of one of the longest lived and most productive scientific satellites ever launched (1963-38C), the first measurement of short-period magnetohydrodynamic waves near synchronous altitude, the discovery of heavy ions trapped in the earth's radiation belts, the experimental confirmation of large-scale field-aligned currents in the auroral regions, the demonstration of the effect of stratospheric pressure variations on the ionosphere, and the development of radio astronomy techniques for predicting geomagnetic storms that can disturb terrestrial radio transmissions. The research activities have involved international collaborations with scientists from more than a dozen academic and defense organizations.

Other research programs include scholarly investigations of ancient astronomical records, which led to the suggestion that Ptolemy was a fraud; the discovery of plasma acceleration regions behind the earth that can generate charged particles with energies up to hundreds of thousands of electron volts; and the discovery that Jupiter is a prominent source of energetic particles in the earth's vicinity that previously were thought to originate in the sun.

NASA has selected scientists and engineers from APL to participate in a record number of interplanetary missions including Voyagers 1 and 2; Galileo, which is scheduled to orbit Jupiter; and Solar Polar, which will orbit over the

poles of the sun. The Laboratory supports the joint APL/Max-Planck Institute Active Magnetospheric Particle Tracer Explorer for NASA and the Federal Republic of Germany. Its purpose is to create an artificial ion cloud outside the earth's magnetosphere in order to investigate the mechanisms responsible for forming the Van Allen radiation belts.

The articles in this section discuss the following six topics.

The successful completion of the Magsat flight is reported. The Magsat satellite was built by APL to support NASA and the U.S. Geological Survey requirements for measurements to be used for magnetic field charts, maps, and research. Magsat was launched on October 30, 1979. Attitude control worked properly, the magnetometer boom was extended, and measurements were made of the earth's magnetic field. The satellite reentered the atmosphere and burned up on June 11, 1980. APL continues to be involved in analyzing scientific data from Magsat.

During March and July 1979, Voyagers 1 and 2 passed by the planet Jupiter, carrying a Low Energy Charged Particle experiment developed at APL. Plasma temperatures of approximately 350×10^6 K, densities of 10^{-1} to 10^{-3} ions/cm³, and corotational convection speeds to 900 km/s were measured in the magnetosphere of Jupiter. In addition, volcanic products from Io were detected.

In support of the Space Shuttle mission, APL has developed a computer model for the NASA Shuttle/Tracking and Data Relay Satellite communications relay link. The model shows the effects of waveguide phase dispersion and amplitude and phase distortion.

A contribution to magnetic levitation theory was made at APL by extending the theory to treat biaxial suspension systems. It was then applied to analyze the magnetic suspension of the proof mass in the disturbance compensation system used in recent Navy Transit satellites.

Another APL study deals with theories of wind-wave generation and the problem of remotely sensing long ocean waves by monitoring short waves. A technique was refined to obtain ocean short-wave slope spectra by the optical Fourier analysis of sea surface photographs. The short-wave spectra were used to measure the modulation of short waves by long waves for a specific wind and long-wave condition.

PILOT (a Precision Intercoastal Loran Translocator) is an electronic aid to piloting vessels in harbors and rivers. The system processes information obtained from a Loran-C receiver, the ship's gyro, and prerecorded magnetic tape cartridges. Data are presented graphically and digitally with respect to a local way point and as a horizontal bar graph to aid channel-keeping.

COMPLETION OF THE MAGSAT FLIGHT MISSION

F. F. Mobley

The design, development, and testing of Magsat by APL was completed with its successful launch on October 30, 1979. APL supported the flight mission by assisting Goddard Space Flight Center (GSFC) in control operations and by analyzing Doppler data to yield very accurate satellite positions. The work continued until the satellite reentered the earth's atmosphere and burned up on June 11, 1980, as expected.

BACKGROUND

The primary purpose of the Magsat program was to survey the earth's magnetic field from a low satellite altitude in order to prepare new magnetic field charts and to detect magnetic anomalies in the earth's crust. A new three-axis vector magnetometer was developed by GSFC, and a new scalar magnetometer that uses optical pumping of cesium-133 gas was developed by Ball Bros. These instruments were integrated with systems for power, command, telemetry, attitude control, and Doppler tracking by APL. A detailed description of the satellite is given in Ref. 1.

The full go-ahead for the Magsat program was received by APL in April 1977. The design was completed by November 1977, subsystems were completed by January 1979, and testing of the 183 kg satellite was finished in October 1979.

DISCUSSION

The satellite and test equipment were delivered to Vandenberg Air Force Base on October 8, 1979. Final testing was completed, the satellite was joined with the fourth-stage rocket, and the combination was spin-balanced. Before launch, the command system was loaded with about 160 commands that were to be implemented automatically during the first two orbits. Those commands turned off the tape recorder to save power, turned on the Doppler transmitters at the proper time for the signal to be received by a station at Winkfield, England, fired two pyrotechnic bolts to release the optical bench, and operated the attitude control system to change the satellite's orientation in space so that full solar power could be generated.

The satellite was launched at 1416 hours UT on October 30, 1980. A Scout rocket put the satellite into

This work was supported by the National Aeronautics and Space Administration.

an orbit of 97° inclination (i.e., 7° off polar). That orbit had been chosen in order to produce a precession rate of the orbit plane of about 1° per day to make the orbit sun-synchronous. The perigee of 352 km was exactly as desired; the apogee of 578 km was higher than was initially planned because of the weight-saving achieved in the spin balance. Figure 1 is an artist's conception of the satellite in orbit.

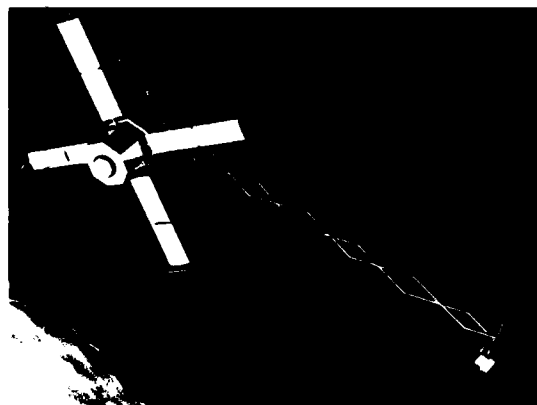


Fig. 1 Artist's concept of Magsat in orbit.

The performance of the 6 m extendible boom is of particular interest. The mechanical stability of the boom after extension was critical to the success of an optical system called the attitude transfer system (ATS). The system used two mirrors attached to the sensors on the end of the boom to measure the relative angles between the vector magnetometer sensor and the star cameras. The allowable angle range for the mirrors was only ± 3 arc-min. To achieve this high level of mechanical stability, the boom was made of graphite-fiber/epoxy links, laminated to achieve a near-zero coefficient of thermal expansion. The results were very gratifying. ATS signals were captured when the boom was extended and were not lost thereafter until the ATS was turned off near the end of the mission. Figure 2 shows the boom partially deployed.

Attitude control of Magsat was difficult because of aerodynamic torques at low altitudes. Furthermore, the very short passes over ground stations limited the opportunities for direct control from the ground. An autonomous attitude control system was designed using

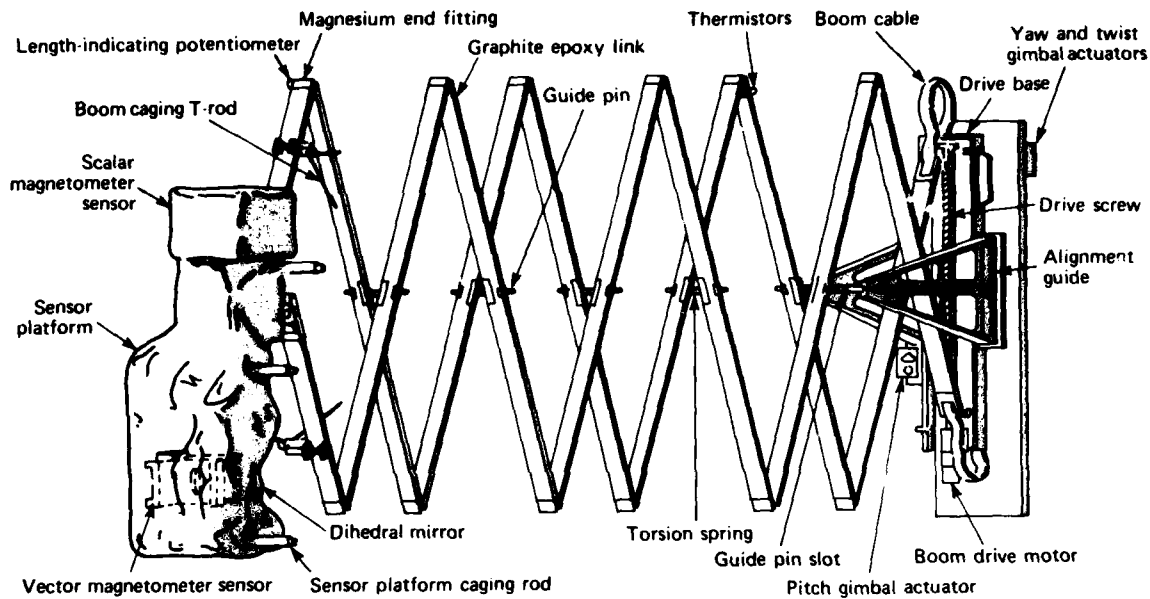


Fig. 2 Partially extended magnetometer boom.

an RCA 1802 microprocessor. Pitch was controlled by sensing the earth's horizon with an infrared scanner and modulating the speed of an internal wheel. Roll and yaw were corrected up to four times per orbit by magnetic torquing. The system was very successful. Attitude control was maintained throughout the Magsat mission until a few hours before burnup. A tubular boom, 1.2 cm in diameter by 5 m long, was extended in orbit to trim the aerodynamic torque in yaw. This aerotrim boom concept was very successful in reducing control activity to a minimum.

Doppler tracking of the satellite was accomplished by analyzing the signal received from satellite transmitters operating at 162 and 324 MHz. The signals were stabilized to one part in 10^{11} by a thermally controlled quartz crystal oscillator inside the satellite. The signals were received by the ground stations of the Defense Mapping Agency. The received frequency was shifted slightly by the Doppler effect as the satellite approached and receded from the station. This Doppler shift was analyzed by APL to yield satellite positions versus time accurate to 50 m root mean square (rms). The tracking accuracy results are shown in Fig. 3.

With the launch of the satellite, the Laboratory's efforts in the design and development of Magsat were essentially completed. APL's participation in the flight mission was limited to (a) providing technical assistance to GSFC in satellite operations and attitude control, (b)

analyzing unexpected behavior, and (c) analyzing Doppler data to determine the precision satellite ephemeris. The collection of data from the satellite began on November 1, 1979, and continued until a few hours before reentry and burnup on June 11, 1980. A detailed description of the postlaunch activity is given in Ref. 2.

FUTURE PLANS

APL's future participation in the Magsat effort will be limited to the work of Dr. T. Potemra in analyzing the magnetic field data to determine the

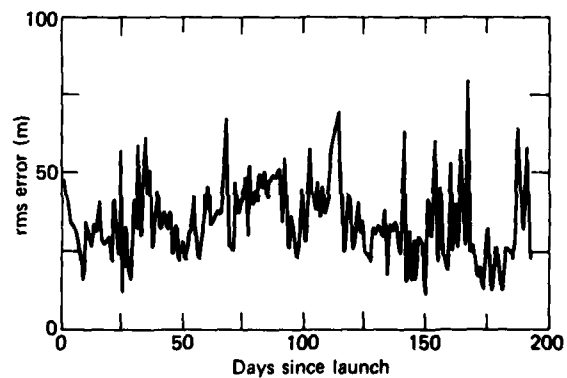


Fig. 3 Accuracy of Doppler tracking of Magsat.

effect of electric currents associated with auroral phenomena. The Magsat data will be correlated with similar data from APL's Triad satellite, launched in 1972 and still producing important magnetic field measurements.

REFERENCES

- ¹M. M. Schaefer, "MAGSAT Spacecraft Description," JHU/APL SDO-5146 (Mar 1979).
- ²Johns Hopkins APL Tech. Dig. 1, No. 3 (Jul-Sep 1980).

HOT PLASMA MEASUREMENTS AT JUPITER

J. F. Carbary and S. M. Krimigis

The observations made by the Low Energy Charged Particle (LECP) experiment on board the Voyager 1 and 2 spacecraft during the recent flybys of Jupiter constitute the first measurements of hot, convecting plasma within the magnetic environment of the planet. The results provide valuable experimental constraints for investigations not only of Jupiter but also of astrophysical objects such as pulsars and stellar magnetospheres.

BACKGROUND

In addition to imaging cameras, the twin spacecraft carried a full array of instruments designed to measure the particle and field environment (or magnetosphere) of Jupiter and its interaction with the solar wind. Designed and built by APL in collaboration with other institutions, the LECP instrumentation can measure ions of energies greater than about 28 keV and electrons of energies greater than about 15 keV. The detectors provide compositional information about the ambient plasma and, being mounted on a rotating scan

platform, they can measure actual flows of the plasma.¹

The Voyager 1 and 2 spacecraft were launched from the earth in 1977 and encountered the planet Jupiter in March 1979 and July 1979, respectively. The encounter trajectories were essentially confined to the equatorial plane of Jupiter (Fig. 1) and allowed the probes to sample an extensive part of the Jovian magnetosphere, a tear-drop-shaped cavity formed by the interaction of the solar wind and Jupiter's magnetic field.

DISCUSSION

During the Voyager flybys of Jupiter, the LECP experiment was able to measure the properties of the hot, convecting plasma within the Jovian magnetosphere (Fig. 2). The data revealed that Jupiter's plasma has temperatures of 20 to 30 keV ($\approx 300 \times 10^6$ K) and has number densities of 1×10^{-1} to 1×10^{-3} ion/cm³ (Refs. 2, 3, and 4). This hot tenuous plasma apparently pervades the entire Jovian magnetic environment, which has a scale size of approximately 10 million kilometers. The plasma convects in the sense of

This work was supported by the National Aeronautics and Space Administration.

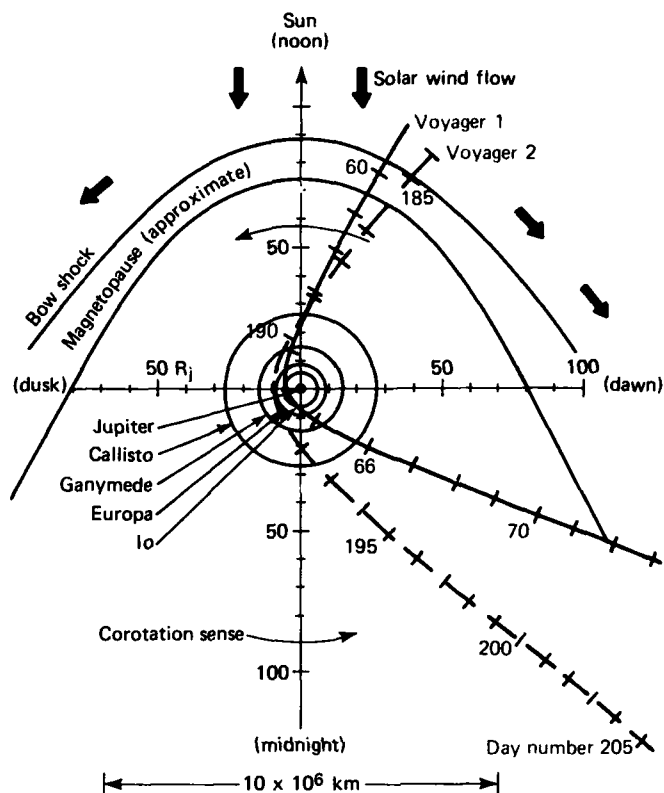


Fig. 1 The Voyager encounter trajectories in the equatorial plane of Jupiter. The bow shock and magnetopause curves show approximate plasma boundaries formed by the solar wind interaction with the Jovian magnetic field. Also shown are the orbits of the four principle satellites of Jupiter. Tick marks on the spacecraft trajectories indicate days (day 60 is March 1; day 185 is July 4). The arrow marked "corotation sense" indicates the motion of plasma within the magnetosphere.

planetary rotation at speeds up to 1000 km/s.^{4,5} The experiment obtained compositional information indicating that ionized volcanic products (oxygen and sulfur) from the satellite Io permeate the magnetosphere.^{3,4} In places, the plasma pressures are high enough to exceed the confining pressure of the magnetic field. When this occurs, the satellite ions form an outward-flowing magnetospheric wind similar to the solar wind and escape from Jupiter into interplanetary space.^{4,5} The "planet bursts" were detected by both spacecraft well outside the Jovian magnetosphere.

These observations constitute the first *in situ* measurements of hot plasma in Jupiter's magnetosphere, an environment that resembles in many ways more exotic astrophysical objects. For example, the disk-like structure of the Jovian magnetosphere and its hot plasma are thought to resemble the environment surrounding a pulsar. Both possess hot, rapidly rotating

plasma and/or outwardly expanding winds of ionized gas. Thus, the Jupiter observations provide valuable experimental constraints for the modeling of truly cosmic phenomena.

The Voyager 1 spacecraft reached the planet Saturn in November 1980, and Voyager 2 will reach Saturn in August 1981. The LECF instrument will take measurements similar to those made at Jupiter. If all goes well, Voyager 2 will encounter the planet Uranus in 1986.

REFERENCES

1. S. M. Krimigis, T. P. Armstrong, W. I. Axford, C. O. Bostrom, C. Y. Fan, G. Gloeckler, and L. J. Lanzerotti, "Low Energy Charged Particle (LECP) Experiment on the Voyager Spacecraft," *Space Sci. Rev.* 21, pp. 329-354 (1977).
2. S. M. Krimigis, T. P. Armstrong, W. I. Axford, C. O. Bostrom, C. Y. Fan, G. Gloeckler, L. J. Lanzerotti, E. P. Keath, R. D. Zwickl, J. F.

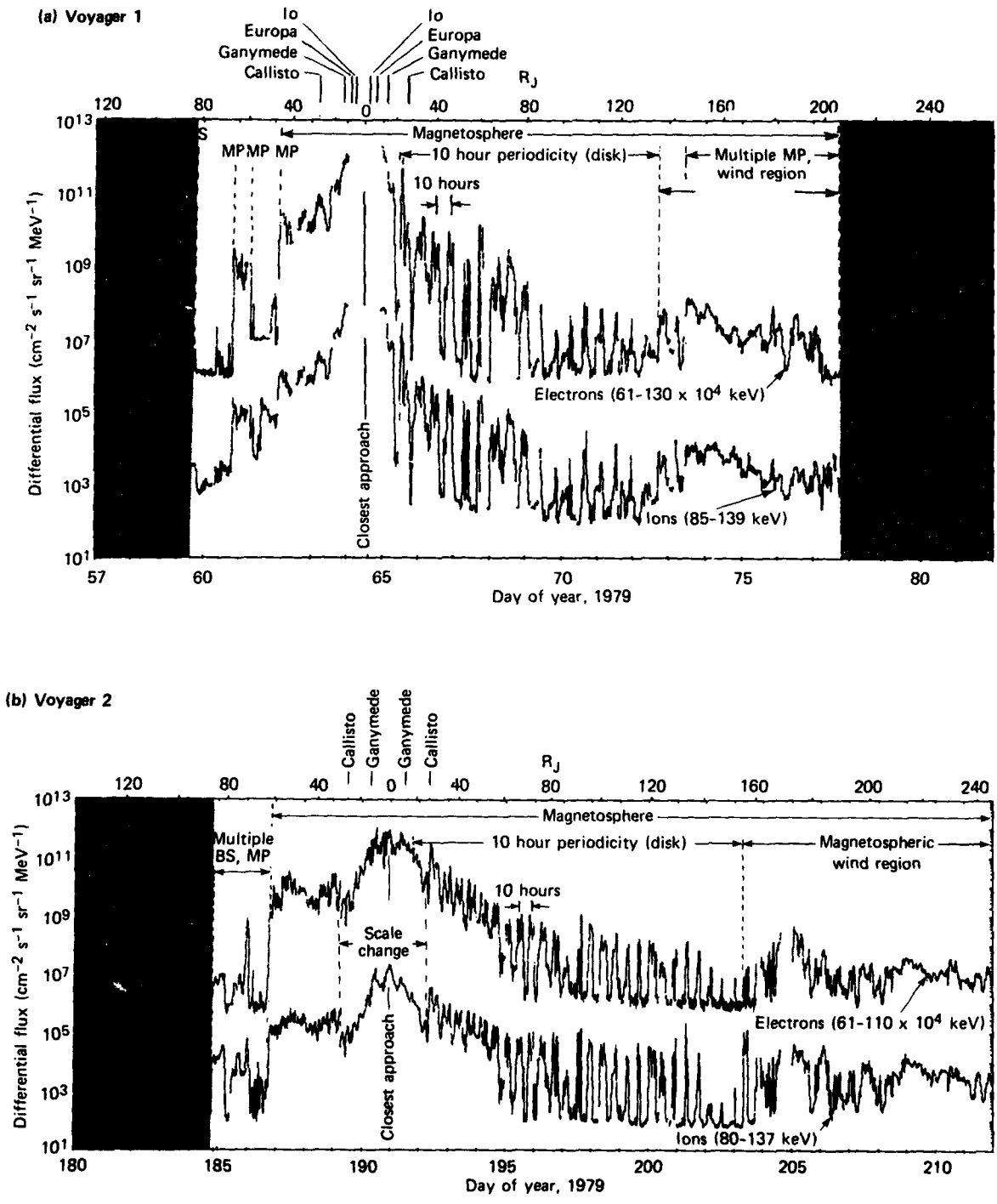


Fig. 2 Summary of low energy charged particle observations by Voyager 1 (a) and Voyager 2 (b). BS indicates a bow shock encounter; MP indicates a magnetopause encounter (see Fig. 1). The strong 10-hour modulations in the particle fluxes after closest approach are caused by the rocking motion of the magnetic axis of Jupiter relative to the spin axis. These modulations are disrupted in the outflow or wind region beyond distances of 140 to 160 Jupiter radii.

Carbary, and D. C. Hamilton, "Low Energy Charged Particle Environment at Jupiter: A First Look," *Science* **204**, pp. 998-1003 (1979).

³S. M. Krimigis, T. P. Armstrong, W. I. Axford, C. O. Bostrom, C. Y. Fan, G. Gloeckler, L. J. Lanzerotti, E. P. Keath, R. D. Zwickl, J. F. Carbary, and D. C. Hamilton, "Hot Plasma Environment at Jupiter: Voyager 2 Results," *Science* **206**, pp. 977-984 (1979).

⁴S. M. Krimigis, J. F. Carbary, E. P. Keath, C. O. Bostrom, W. I. Axford, G. Gloeckler, L. J. Lanzerotti, and T. P. Armstrong, "Characteristics of Hot Plasma in the Jovian Magnetosphere: Results from the Voyager Spacecraft," *J. Geophys. Res.* (in press).

⁵J. F. Carbary, S. M. Krimigis, E. P. Keath, G. Gloeckler, W. I. Axford, and T. P. Armstrong, "Ion Anisotropies in the Outer Jovian Magnetosphere," *J. Geophys. Res.* (in press).

COMPUTER MODEL FOR THE MILA SHUTTLE RELAY LINK

S. C. Jones

A computer model has been developed by APL of the communications relay link at Cape Kennedy, Fla., between the NASA Shuttle and the Tracking and Data Relay Satellite (TDRS). The model has been used to predict the performance of the relay link and also to assess and design equipment to correct problems that have been found. Written in APL "pseudo code" modules, the model is flexible and is generally applicable to other problems involving distortion of phase shift keyed communications links.

BACKGROUND

When the shuttle is in the Orbiter Processing Facility at the Cape Kennedy Merritt Island Launch Area (MILA) being prepared for flight, special relay links will enable two-way communications between it and the TDRS. The TDRS, in turn, will relay the data to and from the NASA/Johnson Space Center in Houston through other communications links via a TDRS ground station at White Sands, N. Mex.

The MILA relay links will operate at S and Ku bands and will use long (about 1000 foot) runs of waveguide to separate the antennas and reduce cross coupling between them. The phase dispersion resulting from this waveguide and the distortion effects of the many cascaded filters used in the relay can result in severe degradation of wideband data.

At the request of the NASA/Goddard Space Flight Center, APL developed a computer model¹ of

This work was supported by the NASA/Goddard Space Flight Center.

the relay link that analyzes and displays the effects of all amplitude and phase distortion. The model was used in a design evaluation of biphase shift keyed (BPSK), quadriphase shift keyed (QPSK), and staggered quadriphase shift keyed data transmission through the relay at rates as high as 300 megabits per second.^{2,3}

DISCUSSION

Figure 1 is a conceptual model of data transmission through the MILA relay link. The center frequency of the signal is $\omega_c = 2\pi f_c$ rad/s. The input data, $x(t)$, are expressed in terms of a real I channel input, $c_i(t)$, and an imaginary Q channel input, $c_q(t)$. The input signal is convolved with the relay impulse response, $g(t)$, to produce a distorted output, $y(t)$, which is separated into I and Q channel outputs, $c'_i(t)$ and $c'_q(t)$, respectively. The distorted output is then input to a pair of "matched" integrate and dump detectors to produce the output data.

The performance of such a communications link is characterized by a plot of bit error probability versus signal-to-noise ratio. The degradation introduced by the relay at a given noise level can be expressed as the increase in input level that would be required to obtain the same bit error probability as when distortion-free data are input directly to the integrate and dump detectors.

Figure 2 is a block diagram of the computer model. It is a low pass model, all bandpass functions being expressed in terms of their equivalent complex envelopes. The data generator module generates maximal-length, pseudorandom-bit sequences up to 31

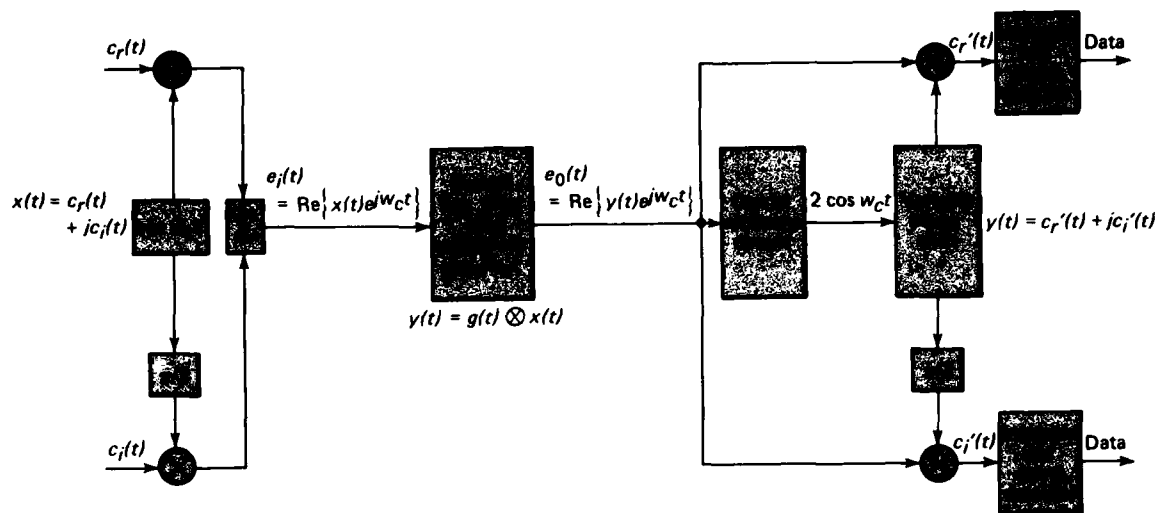


Fig. 1 Conceptual model for QPSK data transmission through the MILA relay link.

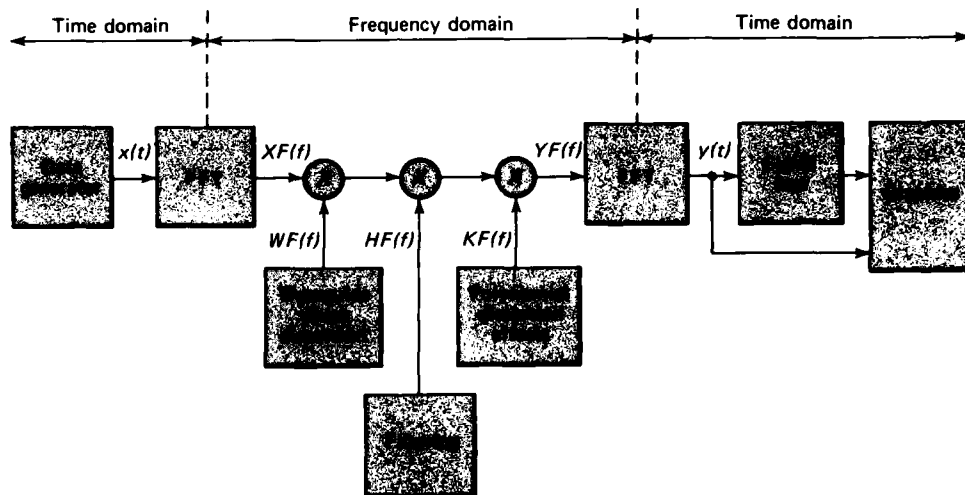


Fig. 2 Computer model program modules.

bits long. To avoid the complexity of convolution, the input data are transformed to the frequency domain and are multiplied by the composite transfer function of the relay link elements. The frequency domain representations of the input data, $x(t)$, and the output data, $y(t)$, are denoted $XF(f)$ and $YF(f)$, respectively. The relay link transfer functions are denoted $WF(f)$, $HF(f)$, and $KF(f)$ in Fig. 2. These transfer functions result from cascaded sets of devices, filters, and propagation effects and need not be restricted to realizable devices. A polar fast Fourier transform (FFT) algorithm was prepared to perform the frequency domain trans-

formation because experimental data for the relay link are only available in polar form.

The computer model has program modules to introduce filtering distortions that result from Butterworth and Tchebychev filters with an arbitrary number of poles, bandwidths, and ripple amplitudes. A module also is used to add polynomial amplitude and phase distortion terms.

When the transformed data have been converted back to the time domain, the model computes the signal

degradation for integrate and dump detection and provides for output display.

Figure 3 is a computer plot of an I channel 150 megabits per second BPSK input and the resulting I and Q channel output waveforms for transmission through the MILA relay. The model computes output signal degradation on both a bit-by-bit and an overall basis. The overall degradation of the waveform of the biphasic shift keyed data transmission of the I channel output is 2.2 dB.

For the BPSK input signal shown in Fig. 3, there is, of course, no Q channel input. Therefore, the Q channel output signal indicates the high leakage of I channel signal into the Q channel. This cross coupling between channels is the major reason that quadriphase shift keyed data transmission signals are more severely degraded by the MILA relay than are BPSK signals. The primary cause of the cross coupling is the nonconjugate quadratic-phase (equivalent to linear group delay) component of the waveguide transfer function.

Although the biphasic mode turned out to be fairly insensitive to the expected amplitude and phase distortion, the computer model showed that the two quadriphase data modes are severely degraded by the expected phase dispersion. The pseudo code modules were rearranged and modified, and the model was then used for the preliminary design of a waveguide equalizer to correct the phase dispersion.⁴

The MILA relay computer model is composed of modules that can be rearranged so that it can be applied to any phase shift keyed communications link problem involving amplitude and phase distortion. Its accuracy and flexibility make it applicable to a number of problems where direct analytic approaches are not feasible.

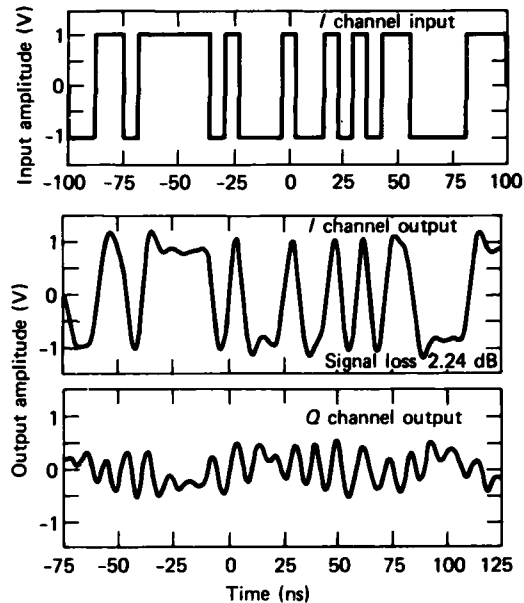


Fig. 3 MILA relay input and output waveforms.

REFERENCES

- ¹S. C. Jones, *MILA Relay Link Model*, JHU/APL S3C-5-018 (20 Nov 1979).
- ²S. C. Jones, *Distortion of 100 Mbps PSK through the MILA Relay Ku-Band Return Link*, JHU/APL S3C-5-020 (21 Nov 1979).
- ³S. C. Jones, *Distortion of 300 Mbps QPSK and SQPSK through the MILA Relay Ku-Band Return Link*, JHU/APL S3C-5-023 (19 Feb 1980).
- ⁴S. C. Jones, *Equalization of the MILA Relay Ku-Band Return Link Using Tapered Waveguide*, JHU/APL S3C-5-026 (31 Mar 1980).

MAGNETIC LEVITATION THEORY

J. F. Bird

The theory of electromagnetic levitation was extended to treat biaxial systems and was applied to analyze various proof-mass suspensions for the disturbance compensation system (DISCOS) used in Navy Transit satellites. The biaxial magnetic levitation theory and the end-effect approximations derived therefrom represent new contributions to electromagnetic theory; the application to DISCOS assisted in diagnostic and design studies, in particular suggesting significant simplification in proof mass fabrication.

BACKGROUND

Recent Transit satellites have incorporated a type of DISCOS that compensates only for along-track disturbances, as required for accurate orbital ephemeris prediction.¹ This single-axis DISCOS has a magnetic suspension of the proof mass along the two uncompensated axes. The biaxial suspension system consists in essence of a cylindrical metal shell (the proof mass) encircling a straight wire. The wire carries alternating current that induces magnetic fields that levitate the proof mass about the wire.²

The problem was to calculate the magnetic force-torque system acting on the proof mass. Such levitation calculations were needed by the APL Space Department to support their ongoing efforts to diagnose malfunctions in the DISCOS aboard the TIP-II satellite. Furthermore, a suspension theory was desirable to aid in optimizing the DISCOS design for subsequent Nova satellites. Existing suspension calculations² were based on a simplified eddy-current model deduced from currents in the equilibrium (coaxial) configuration, which gives a misleading physical picture of the levitation behavior. Vector-field theory would permit precise and complete formulation of the problem, but so far such calculations had been carried out successfully only for uniaxial³ or, at best, infinite paraxial⁴ geometries.

Therefore, we extended the vector-field theoretic approach to biaxial suspensions, with arbitrary relative orientation of shell and current axes, and calculated the induced magnetism, associated eddy-currents, and resulting force-torque systems for a variety of proof mass designs.⁵ An important conclusion was that levitation depends predominantly on the *innermost*

shell layer, with the corollary that the eddy-currents responsible for levitation are confined largely to this inner layer. Hence, the difficult fabrication of isotropic end caps on nonhomogeneous shells, as considered in some proof mass designs to provide radial current paths, was deemed unnecessary.

To facilitate the comprehensive computations in Ref. 5, the effects of the finite length of the proof mass were set aside, as is usual in electromagnetic calculations. While this does not vitiate the qualitative design studies and their conclusions, it is desirable to calculate the end effects for accurate comparison with quantitative measurements. Therefore, vector-field theory was further extended to treat levitational end corrections, which yielded an effective analytic approximation that agrees well with experiments.⁶ In addition, kinetic effects resulting from motions of the proof mass, which may affect the secular stability of the system, can be analyzed exactly by the field theoretic approach.⁷

DISCUSSION

The theoretical calculations encompassed a variety of shell constructions that were under consideration for the DISCOS proof mass: a solid (homogeneous annular) shell, a hollow shell (with an evacuated annular region), and a composite shell (made up of insulated layers of different metals). To illustrate the levitation in the different systems, we consider here just the force constant, k_F , which is defined as the limit of the force/displacement ratio near equilibrium. Other indexes of comparison like the torque and acceleration constants, as well as force at all displacements, are detailed in Ref. 5.

A universal plot (Fig. 1) of k_F as a function of all shell and current parameters for the solid shell is of prime interest for design studies. Figure 1 shows that with increasing metal thickness, the force rises at first but flattens out as additional layers become ineffective — or even regresses for the larger ratios of radius to skin depth.

Figure 2 illustrates k_F for hollow shells as a function of various radii, metals, and suspension frequencies. The range of hollow-region dimensions (a' , b') corresponds to inner and outer shell thicknesses from 0.1 mm to 1.5 or 1.6 mm. The crossover behavior between different outer thicknesses in the upper panels of Fig. 2 corresponds to the peaking in the curves of Fig. 1.

This work was supported by Indirectly Funded R&D and the U.S. Navy Special Projects Office.

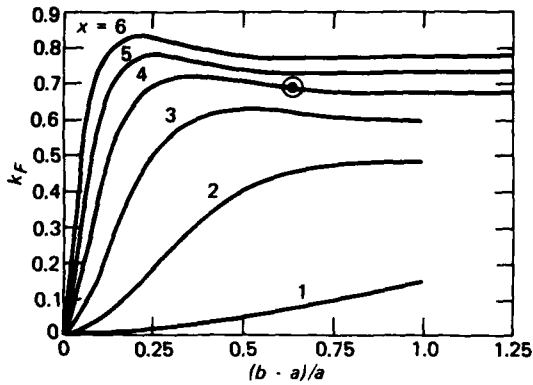


Fig. 1 Solid-shell force constant, k_F , as a function of shell geometry, $b/a - 1$, for a range of skin-depth parameters, x . k_F is in units of $10^{-7} I_0^2 L/a^2$ N/m, where I_0 is current amplitude, L is shell length, and a is shell inner radius. $(b - a)/a$ is shell thickness/inner radius and x is $\sqrt{2}$ times inner radius/skin depth. The circled point represents the DISCOS suspension in TIP-II.

Table 1
COMPOSITE SHELLS

Inner Layer*	Middle Layer*	Outer Layer*	Insulator Thickness (in.)	Force Constant† (units of Fig. 1)
Ag	Al	Ag	10^{-4}	0.7397
Ag	Al	Ag	0	0.7399
Ag	Al	Ag	2×10^{-3}	0.7375
Ag	Al	Al	10^{-4}	0.7469
Ag	Ag	Ag	10^{-4}	0.7449
Ag	Al	none	10^{-4}	0.7635
Ag	none	none	-	0.7087
Al	none	none	-	0.4745

*Radii: $a = 5.21$, $a' = 5.88$, $b' = 7.76$, $b = 8.52$ mm.

†Sinusoidal current at 2080 Hz.

Table 1 summarizes some k_F computations for composite shells with different arrangements of two metals (Al and Ag) in insulated layers. The first three entries correspond to a recent DISCOS design and show the minute effects of insulation thickness. The next two entries indicate the slight effect of the middle and outer layers; the next two show that even the removal of those layers makes only a 3 to 4% difference. In contrast, the final entry illustrates the dominance of the inner layer's constitution for the levitation.

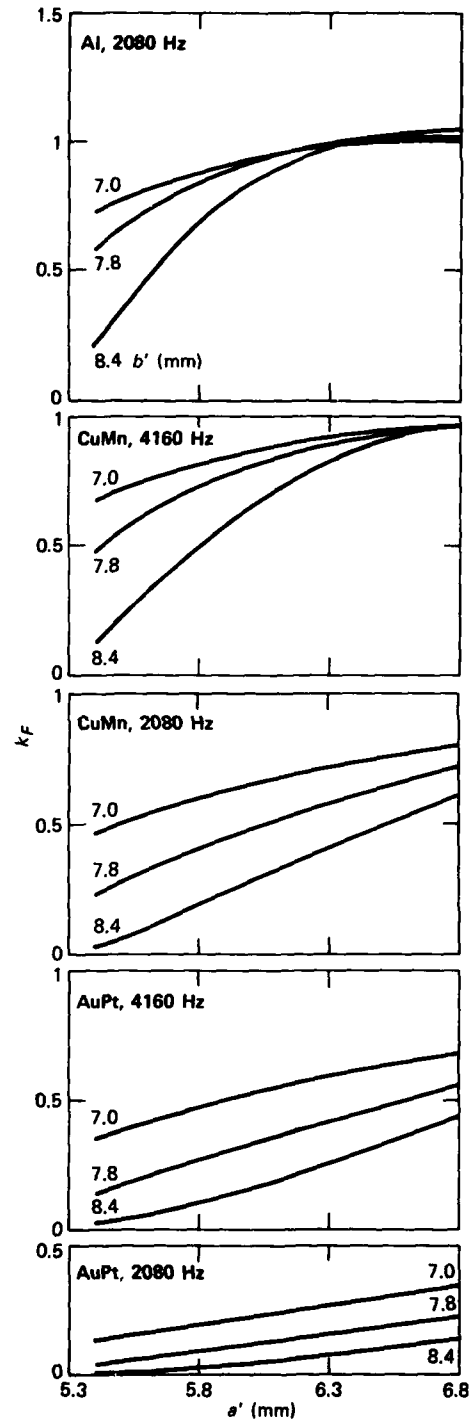


Fig. 2 Hollow-shell force constants, k_F , for various metals and frequencies as a function of internal radii, a' , b' , with external radii fixed ($a = 5.2$ mm, $b = 8.5$ mm). k_F ordinates are relative to solid Al values.

The results clearly demonstrate the "inner-dominant" conclusion and its current-path corollary, as cited above. A further consequence is that parameter effects may be largely discerned from the universal Fig. 1 for shells more elaborate than the simple solid shell.

The levitation end corrections, even when quite large, are given well by the approximation formulas that were derived in Ref. 6. For example, the end-less result from Ref. 5 for a thin Al alloy shell is reduced 47% by just the lowest-order correction from Ref. 6, which already brings the calculated k_F to agree with the measured value within the measurement's few percent precision. For shells closer to actual flight designs, the end-corrections are less severe and readily calculated, e.g., 14% for TIP II (circled point in Fig. 1). In any

event, these end effects do not change the qualitative conclusions of Ref. 5 as summarized above.

REFERENCES

- ¹J. C. Ray, "Partially Drag-Free Satellites with Application to the TIP-II Satellite," Stanford University Center for Systems Research Report, SUDDAR 498 (1976).
- ²F. F. Mobley, G. H. Fountain, A. G. Sadilek, P. W. Worden, Jr., and R. Van Patten, *IEEE Trans. Magn. MAG-11*, p. 1712 (1975).
- ³C. V. Dodd, C. C. Cheng, and W. E. Deeds, *J. Appl. Phys.* **45**, p. 638 (1974) and references therein.
- ⁴J. A. Tegopoulos and E. E. Kriezis, *IEEE Trans. Power Appar. Syst. PAS-90*, pp. 1278 and 1287 (1971). (Subsequent papers in this series are erroneous.)
- ⁵J. F. Bird, "Theory of Magnetic Levitation for Biaxial Systems," *J. Appl. Phys.* **52**, 58 (Feb 1981).
- ⁶J. F. Bird, "Levitational End-Effects in a Cylindrical Magnetic Suspension" (to be published in *J. Appl. Phys.*).
- ⁷J. F. Bird, "Kinetic Torque and Dynamic Behavior in a Magnetic Levitation Device" (submitted to *J. Appl. Phys.*).

OPTICAL MEASUREMENT OF THE MODULATION OF SHORT WAVES BY LONG OCEAN WAVES

F. M. Monaldo

Photographs of the sea surface have been obtained that yield the spatial wave slope spectrum of waves imaged within the photographs. By correlating short wave spectra (3 to 30 cm wavelengths) determined in this manner with long wave (greater than 5 m wavelengths) slopes, we can determine the modulation of short wave spectral energy by long waves.

BACKGROUND

The study of the short-wave/long-wave interaction has generated a growing interest on the part of persons dealing with remote sensing and oceanography. Of particular interest has been the role of this interaction in allowing long gravity waves to be imaged by the Seasat satellite synthetic aperture radar (SAR) on a synoptic basis.

At large incidence angles, a microwave radar interacts with the ocean surface by means of a Bragg in-

teraction mechanism with waves whose lengths are on the order of the radar wavelength. The magnitude of the backscattered power is linearly related to the amplitude squared or to the spatial spectral energy of such waves. For the Seasat SAR, the ocean interaction wavelength is approximately 30 cm. Variations in spectral energy at 30 cm induced by long waves can thus make waves visible on SAR imagery.

The manner in which long gravity waves on the ocean affect short wave spectral energy and the extent of this effect determine how and under what conditions spaceborne SAR's can be used to monitor long ocean waves routinely. Moreover, the question arises as to which short wave spectral region is the most isotropically and strongly modulated by long waves. The design parameters of future spaceborne SAR's could depend on the answer.

Also of interest to oceanographers is the fact that the wave/wave interaction question is significant in the understanding of wind-wave growth mechanisms. Specifically, the interaction of long waves and short waves provides an energy transfer mechanism that is

This work was supported by the Office of Naval Research and the National Science Foundation.

relevant to the explanation of the rate of wind-wave growth. If short wave spectral energy is modulated in phase with the long ocean waves, the long wave energy may be augmented appreciably.

DISCUSSION

Despite the importance of the short-wave/long-wave interaction problem, ocean data on the short wave spatial spectrum and its modulation are scarce because *in situ* measuring in that regime is difficult for two reasons.

First, the act of *in situ* measuring actually tends to modify the short wave spectrum being measured. Second, these are point measurements that are used to measure the temporal spectrum. To convert to the spatial spectrum, since microwave radars interact spatially with the short waves, correction must be made for the orbital velocity of the long waves. This requires the use of the dispersion relationship, which in this wavelength regime is uncertain at best.

Photography permits the circumvention of these problems because visible radiance does not modify the ocean surface, and only spatial coordinates in an instant of time are measured in a photograph.

The photographic technique we used to measure short wave spectra relies on surface-reflected skylight for imaging ocean waves. Methods developed at APL allow for the selection of optimum camera viewing angles and film characteristics. Under these optimum

circumstances, the wave slope on the ocean surface maps linearly into film transmittance (see Fig. 1). (In the figures, k is the wave number.) When coherent monochromatic light such as that from a laser is projected through a piece of film, the resulting diffraction pattern is the two-dimensional power spectrum of the transmittance variation on the film. The optical Fourier transform of the transmittance variation on the film can therefore be considered proportional to the short wave ocean slope spectrum in the patch of ocean circumscribed by the photograph.

A one-dimensional slice is cut from this optically derived, two-dimensional, short wave spectrum. The slice corresponds to the spectral slope energy along the camera pointing azimuth. From this slice, three spectral regions are isolated, corresponding to the slope spectral energy at 3, 11.5, and 30 cm wavelengths on that section of the long wave within the photograph (see Fig. 2). The

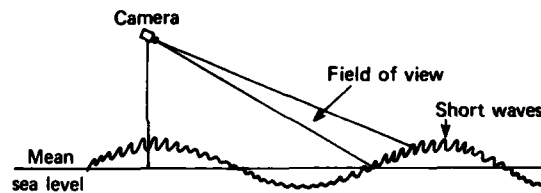


Fig. 1 Diagram showing how an ocean photograph images short waves riding atop the long ocean waves. Time series short wave spectra are derived from time series photographs and correlated with the long wave slope.

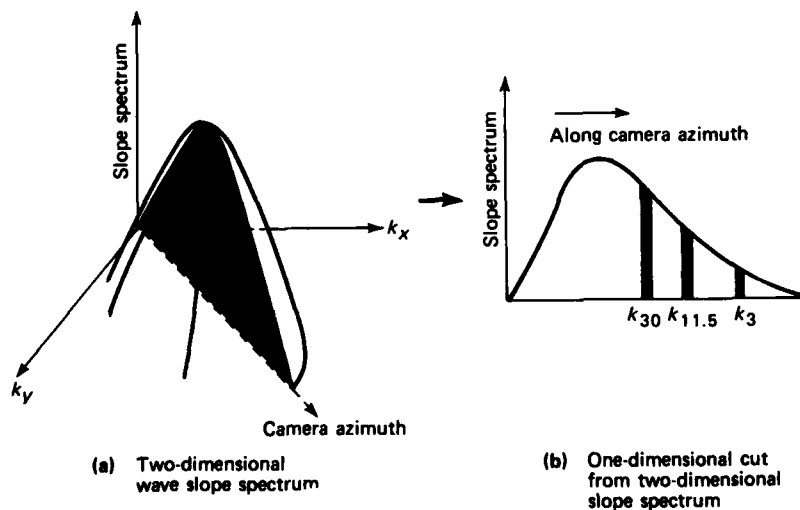


Fig. 2 Slice taken from the optically derived, two-dimensional short wave spectrum. From this slice, three spectral regions around wave numbers k_{30} , $k_{11.5}$, and k_3 are isolated. The wave numbers correspond to wavelengths of 30, 11.5, and 3 cm, respectively.

30 cm spectral region was examined because it corresponds to the Bragg interaction wavelength of the Seasat SAR, and the 3 cm region corresponds to our limit of resolution. The 11.5 cm region was selected simply because it was between 3 and 30 cm.

A time series of photographic sea images is Fourier transformed and processed in this way to generate the time series variation in the short wave spectral energy. By correlating the time series with the time variation in a long wave slope (also photographically obtained), the modulation of short spectral energy in the three isolated spectral regions by long waves is determined.

These techniques have been used recently to analyze photographic data from two experiments: the Joint North Sea Waves Project (JONSWAP), conducted in the North Sea off the coast of West Germany in 1975, and Duck-X, conducted in 1978 off the Coastal Engineering Research Center Pier in Duck, N.C. Although all the photographic data were processed on an automated optical bench at APL, much of the time series analysis of JONSWAP data was performed by APL personnel in Hamburg, Germany, as part of a joint effort with the Max-Planck Institute for Meteorology. All the Duck-X data have been analyzed within APL.

RESULTS

Although this short wave modulation by long waves must be determined for a large array of wind and sea conditions before conclusive statements can be made concerning that modulation, significant results have already been obtained from the two current data sets.

For the situation in which short and long waves are propagating along the same direction in moderate winds, the JONSWAP data have demonstrated that the short wave spatial spectrum is modulated by the long waves by as much as 15% at wavelengths between 3 and

30 cm. There appears to be no significant difference in the magnitude of modulation within that spectral region.

The short wave modulation was 90° out of phase with the long wave crest, suggesting that the maximum amount of spectral energy is not at the crest of the long wave. This result is important because the phase of the short wave modulation is used in theories of wind-wave growth.

The analysis of the Duck-X data addressed more explicitly the directionality of this short-wave/long-wave interaction. There were clear examples in this data set of the modulation of short wave energy propagating perpendicularly or nearly perpendicularly to the long wave. This suggests that microwave radars, particularly the SAR, are able to image long waves by a Bragg interaction mechanism, even when the electromagnetic waves are propagating normally to the long wave train. This result comes as somewhat of a surprise.

Further analysis of the Duck-X data indicates that the short wave spectrum becomes more isotropic as the spatial frequency of the short wave increases.

FUTURE PLANS

Future efforts will include using this photographic technique to analyze the short wave spectral modulation in a variety of wind and long wave conditions to get a better grasp of short wave modulation.

REFERENCES

- ¹F. M. Monaldo and R. S. Kasevich, "Wave-Wave Interaction Study Using Fine Time Series Optical Spectra," JHU/APL SIR-80U-016 (Jun 1980).
- ²F. M. Monaldo and R. S. Kasevich, "Daylight Imagery of Ocean Surface Waves for Wave Spectra" (to be published in *J. Phys. Oceanogr.*).
- ³D. Stilwell, "Directional Energy Spectra of Sea Surface Photographs," *J. Geophys. Res.* 74, pp. 1974-1986 (1969).

PILOT, A PRECISION INTERCOASTAL LORAN TRANSLOCATOR

C. R. Edwards

The Precision Intercoastal Loran Translocator (PILOT) system is an electronic aid to piloting vessels in harbors and rivers. Its purpose is to provide accurate navigation information in a format that can be used immediately without significantly increasing the workload of the bridge personnel. Eight preproduction systems have been built and five are undergoing shipboard evaluation on the St. Mary's River between Lake Superior and Lake Huron.

BACKGROUND

The present PILOT terminal is the product of a long evolution of special-purpose loran processors developed at APL. In 1968, a loran assist device (LAD) was developed for a unique military aircraft requirement; it was followed by several other military versions. In 1970, a Coast Guard loran assist device (COGLAD) was developed to evaluate loran as an aid to positioning buoys. With the development of microprocessors in 1973, a small, simple processor (CLAD) was developed and tested by the Coast Guard. The original COGLAD was upgraded and tested on the St. Mary's River in 1976. Each new system used increasingly sophisticated data processing techniques, required less operator training and attention, and represented a lower potential production cost. These improvements were largely the result of the phenomenal developments in integrated circuits and microprocessors in the last decade.

The design objective of the PILOT system was to demonstrate that loran repeatability (i.e., returning to presurveyed way points) could be used successfully to pilot harbors and rivers without significantly increasing the workload of the bridge personnel, and that the system could be mass produced by industry for an affordable price. To minimize development and production costs, a commercially available microprogrammable graphics terminal (Hewlett-Packard 2649A) was selected as the nucleus of the PILOT system. Significant hardware modifications were required but most are of the plug-in or bolt-on type and do not change the basic HP terminal.^{1,2} The loran receiver currently used with the system is an unmodified commercial item. Extensive new software was developed for this application, in-

cluding sophisticated data filtering and transformation techniques.³

DISCUSSION

The PILOT terminal obtains its information from a loran-C receiver, the ship's gyro, and prerecorded magnetic tape cartridges. The data are edited for accuracy, filtered for smoothness, and mathematically transformed into various display formats. The data are presented graphically and digitally with respect to a local way point and as a horizontal bar graph to aid channel-keeping. The startup procedure for the PILOT system consists of selecting the appropriate tape cartridge and, after the receiver has automatically acquired the loran signals, commanding the PILOT terminal to start navigation. Once started, the system will compute position and velocity information continuously and select new area charts as necessary, without further operator action. The operator may select optional features and the enhancement of displays if desired.

Prerecorded tape cartridges containing charts and other navigation information provide the PILOT terminal with a degree of "local knowledge." The vessel's present position, speed, and heading, continuously determined from a loran receiver and the vessel's gyro, are displayed on the current area chart. Charts of two different scales (master and detail) are always available for operator selection. Position, speed, and time to go relative to way points are displayed to the left of the chart. A horizontal bar graph representing the vessel's cross-track position relative to the track line can be shown along the bottom of the display.

Other features available to the operator include the capability for projecting the vessel's expected track line, a continuous readout of range and bearing from own ship to any point on the displayed chart, a time-of-day clock, and the ability to zoom in, zoom out, and pan on the displayed chart. The operator can enter time difference (TD) bias values to compensate for seasonal variations, select from three types of vessel projections, select from four data filter time constants, and display ship's gyro and loran receiver data. Using a special diagnostic tape cartridge, the operator can perform self-tests on the PILOT terminal. When used with a line printer, the terminal can print position information at a fixed time interval or can be used as a survey system to measure the mean and standard deviation of the TD's of the vessel's present position.

This work was supported by the Department of Transportation, U.S. Coast Guard.

All coordinate conversion constants and navigational reference information, as well as a mosaic of harbor charts, are contained on a cartridge that is, in effect, a loran-C harbor chart on a magnetic medium. A single cartridge contains as many as 200 of these charts, representing about 200 miles of river or harbor.

Each cartridge contains an index file, master files, and detail files. The index file, which contains a title block and a list of all master charts on the cartridge, is always displayed before the PILOT terminal begins the navigation mode and whenever the terminal is reset.

Each master file contains the graphics for a master chart showing 8 to 16 miles of track (a scale of about 1:50,000), area transformation coefficients, transmitter coordinates, and supplemental data such as display origin, scale, and rotation. Master charts provide "look ahead" by showing the next several way points and the identities of a few prominent features. Because a master chart is generally too small for piloting in narrow channels, it is associated with one or more detail charts.

Each detail file contains the graphics for a detail chart showing 1 to 2 miles of track (a scale of about 1:12,500), the TD's, the coordinates of the current way point, the bearing angles to and from the way point, and supplemental data. Detail charts provide a closer view of the vessel's current situation and include many of the fixed aids to navigation and an outline of the channel, if applicable.

The process for producing chart cartridges was developed at APL, where the original cartridges for the St. Mary's River were produced. The Coast Guard R&D Center, Groton, Conn., has now taken over the production of the cartridges. Beginning with the appropriate National Oceanic and Atmospheric Administration (NOAA) charts, the process for producing cartridges includes: (a) selecting appropriate chart areas and way points for the river or harbor; (b) digitizing

NOAA charts and adjusting them to the proper scale, rotation, and origin (this step determines whether the chart displayed on the PILOT terminal will be north-up or track-up); (c) computing transformation coefficients for the geometry of the loran-C chain to be used; (d) conducting a loran survey of the river or harbor; and (e) combining the above data into the proper format and recording it on magnetic cartridges. The Coast Guard R&D Branch, Washington, D.C., has developed new techniques for surveying the loran coordinates of each way point. Using the actual measured TD's rather than theoretical ones greatly enhances the accuracy of the PILOT system.

The PILOT terminal is shown in Fig. 1 and the system block diagram in Fig. 2. Normal shipboard installation consists of the PILOT terminal, a loran receiver (currently the Internav 404 receiver), and a cable connection to the ship's gyro. Optional equipment includes a second loran receiver (for cross chain opera-

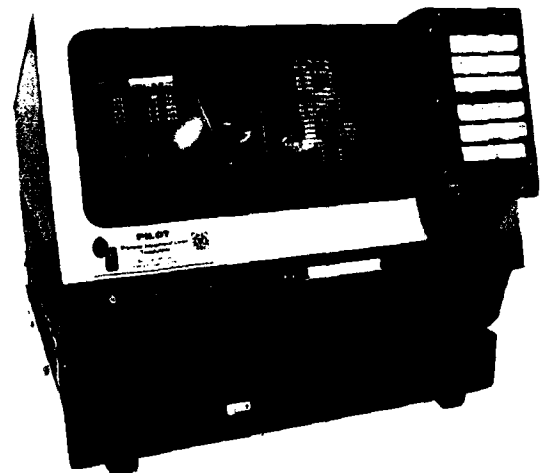


Fig. 1 PILOT terminal.

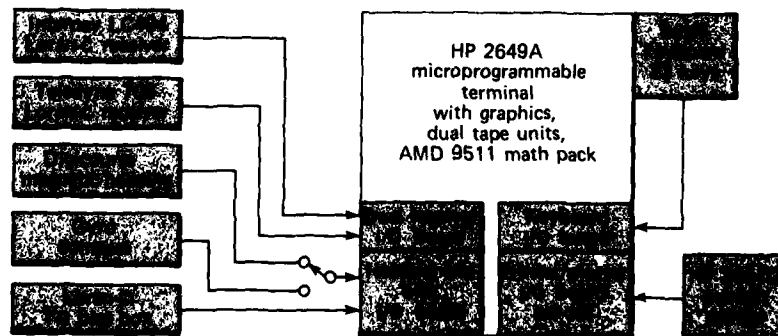


Fig. 2 Block diagram of the PILOT system.

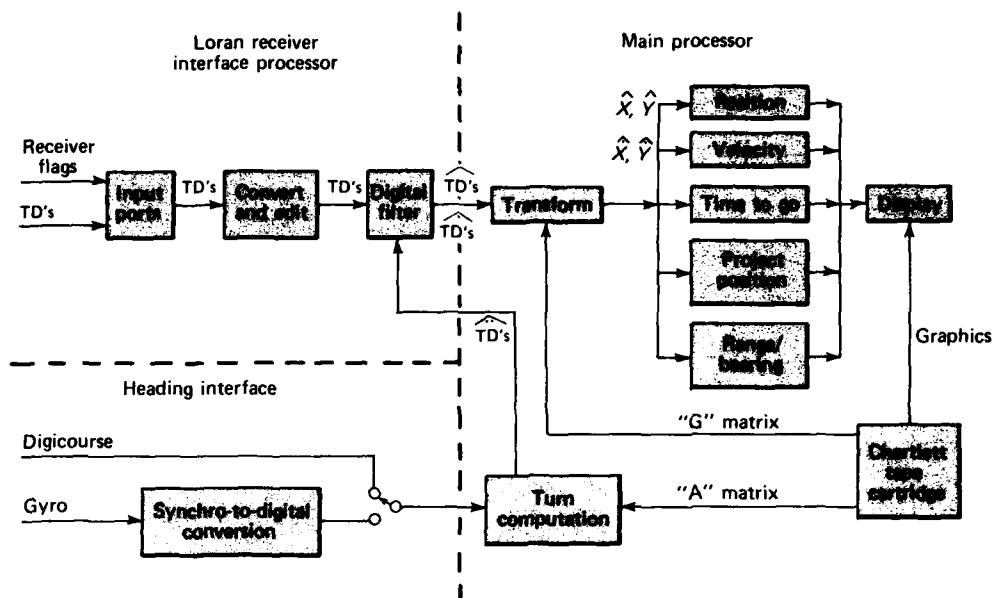


Fig. 3 Functional data flow diagram.

tion), an interface or modem for remotely entering TD bias values, and a printer.

The nucleus of the PILOT system is the Hewlett-Packard 2649A microprogrammable graphics terminal, which was selected because it has a separate graphics processor with memory, dual tape cartridge units, and an Intel 8080 microprocessor that can be modified and programmed as required. Modifications to the terminal included: (a) converting the 8080 microprocessor from software arithmetic to hardware arithmetic by adding an Advanced Micro Devices 9511 arithmetic processing unit, (b) developing an interface board to preprocess loran data from two loran receivers, (c) developing an interface board to connect to the ship's gyro and to a TD bias modem or box, (d) replacing the large general-purpose keyboard with a small predefined keypad, and (e) building a short base for the terminal to serve as a cable junction box.

Figure 3 is a functional data flow diagram of the PILOT terminal. Approximately 17,000 bytes of machine language code were developed at APL for the terminal and an additional 40,000 bytes of the original Hewlett-Packard code were retained. Structured programming and assembly language were used for maximum efficiency.

REFERENCES

1. C. R. Edwards, *PILOT, A Precision Intercoastal Loran Translocator, Volume I — Users' Manual*, JHU/APL SDO 5699 (Sep 1980).
2. J. E. Tarr, J. W. Eifert, and J. H. Starkes, *PILOT, A Precision Intercoastal Loran Translocator, Volume II — Hardware*, JHU/APL SDO 5699.1 (Jul 1980).
3. G. E. Baer, W. D. Kelley, B. S. Ogorzalek, and S. Mantel, *PILOT, A Precision Intercoastal Loran Translocator, Volume III — Software*, JHU/APL SDO 5699.2 (in preparation).

OCEAN SCIENCE AND TECHNOLOGY

INTRODUCTION

An understanding of the physics of the ocean environment is essential for APL to perform its mission in support of the Fleet. This area of physics includes the propagation of electromagnetic and acoustic radiation; absorption and scattering both within and at the surface of the ocean; hydrodynamic phenomena such as surface waves, internal waves, and currents; and the effects of such physical variables as water temperature, pressure, salinity, and density on ocean dynamic phenomena. Central to APL's effort is the development of sensing and data-processing systems to detect and characterize signals propagated through or at the surface of the ocean. Analysis, simulation, and laboratory research are extremely useful, but many phenomena of interest must be studied at sea. Accordingly, APL has developed the ability to conduct large-scale scientific studies in the open ocean.

Much ocean research is not reported here for security reasons, but the selected sample will illustrate some of the current areas of investigation. The first article describes a high-speed data acquisition system developed to meet the needs of many of the oceanographic research programs. The Modular Adaptive Recording System uses the most recent advances in microprocessor and high-density digital recording technology to provide the required flexibility in sensor control, signal conditioning, and data acquisition. It incorporates real-time computer data processing as well as high-volume data storage. Its modular design allows its use in the wide range of experiments of current interest.

In the measurement of acoustic signals using a linear hydrophone array, it has been found that knowledge of the straightness of the array is critical to obtaining accurate data. The second article describes a paravane system developed to measure the deviation from a straight line of a linear acoustic array and to groom the beamforming equations while processing the array data. This technique results in narrower beams and improved sidelobe performance. The paravane system transmits high-frequency, pulsed signals that are received by the array and processed by the associated system electronics.

A sensor capable of continuous, real-time monitoring of seawater for changes in the concentration of copper ions is described in the third article. The system uses ion-selective electrodes installed on a submersible body that can be towed at sea. Data obtained with this instrument should aid chemical oceanographers in determining the distribution of this trace metal.

To interpret acoustic signals properly, background noise levels and transmission losses must be understood. Transmission loss in convergence zones, based on ocean measurements, is discussed in the fourth article. These measurements demonstrate the statistical similarities in the transmission loss in convergence zones at corresponding frequencies.

DEVELOPMENT OF AN ADAPTABLE OCEANOGRAPHIC DATA ACQUISITION SYSTEM

I. R. Hunter and J. W. Petersen

An oceanographic data acquisition system has been developed for the APL Submarine Technology Division. The Modular Adaptable Recording System (MARS) can satisfy the data requirements of oceanographic test programs to be conducted during the next several years.

BACKGROUND

APL has conducted a series of oceanographic experiments using a variety of developmental sensors. A series of data acquisition systems was developed, each tailored to a specific sensor or experiment within the constraints of existing recording capabilities. Limited funding and a restricted schedule precluded a system engineered for flexibility and adaptability. Many of the experiments were conducted on submarine platforms, which necessitated instrumentation systems designed for limited space. There also were installation access problems associated with the platforms. In September 1977, APL personnel, along with specialists in data acquisition and submarine instrumentation from Interstate Electronics Corp. (IEC), began to investigate the development of a field deployable data acquisition system to satisfy the following general requirements:

1. Expandable data acquisition and processor capabilities,
2. Flexible sensor control, signal conditioning, and data acquisition from inboard and outboard sensors, and
3. Real-time computer data processing.

IEC was contracted by APL to develop technical specifications¹ for data acquisition and playback systems that could meet these requirements. A detailed requirements document² was prepared by a team of specialists at APL in May 1978, and IEC was contracted to design and fabricate the systems. A paper on the system³ was presented at the Second Working Conference on Oceanographic Data Systems. The two MARS configurations, acquisition and playback, were factory acceptance tested⁴ in the spring of 1980 and have successfully supported the initial data acquisition mission.

The development and design of the MARS system was the result of technological advances in microprocessors and high-density digital recording. The micro-

processor enabled the implementation of a bus-architecture, distributed-microprocessor system design. Each MARS module is controlled by a 6800 microprocessor programmed to perform a specific function. Variable parameters within the microprocessor firmware provide a way to change module operations in response to new data acquisition requirements. If the module variability is insufficient, a new module may be added. The high-density digital recording technology enabled the storage of up to 14 hours of data at 125,000 words per second on a single tape. This efficient recording method reduces data loss resulting from changing tapes and minimizes the number of tapes required per deployment. A modified MIL-SPEC AN/USH-24 tape recorder/reproducer was selected for its reliability and compact design.

The deployment of the MARS system on submarines imposed size and weight constraints on the system units. Each unit must be sized to fit through a 26 in. diameter hatch and must weigh no more than 200 lb. Fault recognition and maintenance were additional design considerations. During a deployment, the system must be operated and maintained by senior level technicians. When feasible, automatic self-diagnostics are useful, along with fault alarms and a visual indication of module faults. Repairs are made by replacing a module.

DISCUSSION

MARS is designed around a bus architecture with distributed microprocessors. The bus structure combines features of both a commutation and a protocol system to provide speed and flexibility in a single data acquisition system. The bus format is defined by the data requirements of each mission, and the modular design provides the adaptability required by various test programs. Modules are decoupled using first-in first-out (FIFO) buffering techniques to allow independent module design and system integration. Only firmware changes in programmable read-only memories (PROM) are necessary to integrate a new module.

The MARS bus structure consists of four independent buses controlled by the microprocessor bus controller module (Fig. 1). The source code bus and the data bus are 16-bit parallel synchronous buses. The source code generator is used to identify the source (module and channel) of the data that will appear on the data bus during the next clock period. Each module

contains a source detector interfaced to the source code bus. When a source code is detected, the module is enabled to either write on or read from the data bus.

Seven clock signals are generated by the clock generator, which drives the rate bus. The system data rate is 960 kHz; a parallel bus operation is performed each clock cycle, resulting in 960,000 bus slots each second. The source code generator outputs one unique source code for each bus slot, and each code is generated at one of 16 rates, i.e., 1 Hz to 480 kHz. The rate assignments are made according to mission data requirements. This bus format is repeated each second. The clock generator also places time of year on the data bus.

The control bus is a serial, asynchronous, communication bus interfaced to the microprocessor in each

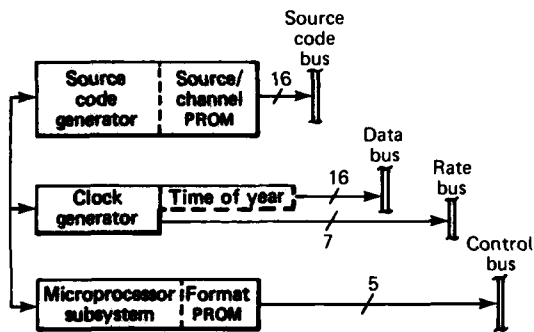


Fig. 1 The microprocessor bus controller.

module. Data transfer can take place in a block transfer mode at a rate up to 240,000 bits per second. The control bus is used to transmit intermodule messages such as operator's commands and status data. The microprocessor bus controller downloads module format data via that bus each second to refresh volatile memory in each module.

A typical data acquisition module is illustrated in Fig. 2. Each module is interfaced to the four buses. The microprocessor receives its control program (format) on the control bus from the microprocessor bus controller each second, and controls the order and rate at which the data from an external source enter the FIFO buffer. Upon receiving the source code from the source code bus, the source detector enables the FIFO to drive the data bus on the next bus slot. Module timing and system synchronization are provided by the clocks on the rate bus. The module also accepts commands from the control bus and writes module status on the control bus each second.

MARS can be configured for either an acquisition system or a playback system by means of plug-in modules. Two basic units are used. One is configured for at-sea deployments (see Fig. 3); the other, the playback unit, contains the basic system modules (i.e., modules below the bus system) plus a computer system interface module (CSI). The CSI is interfaced to a Digital Equipment Corp. PDP-11 through two DR-11B boards.

Status words are generated by each module that contains current mode of operation and error conditions for system, module, and channel levels. The status

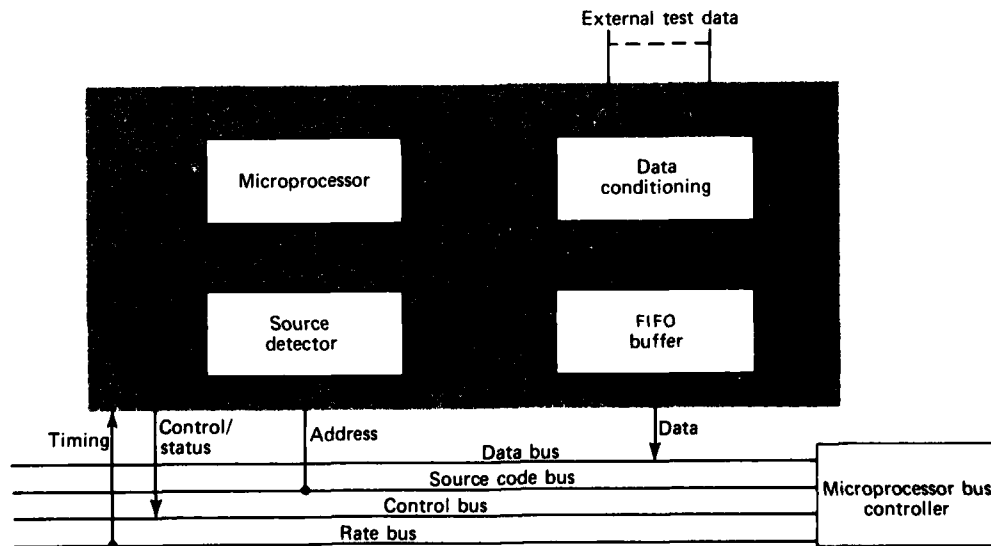


Fig. 2 Typical data acquisition module.

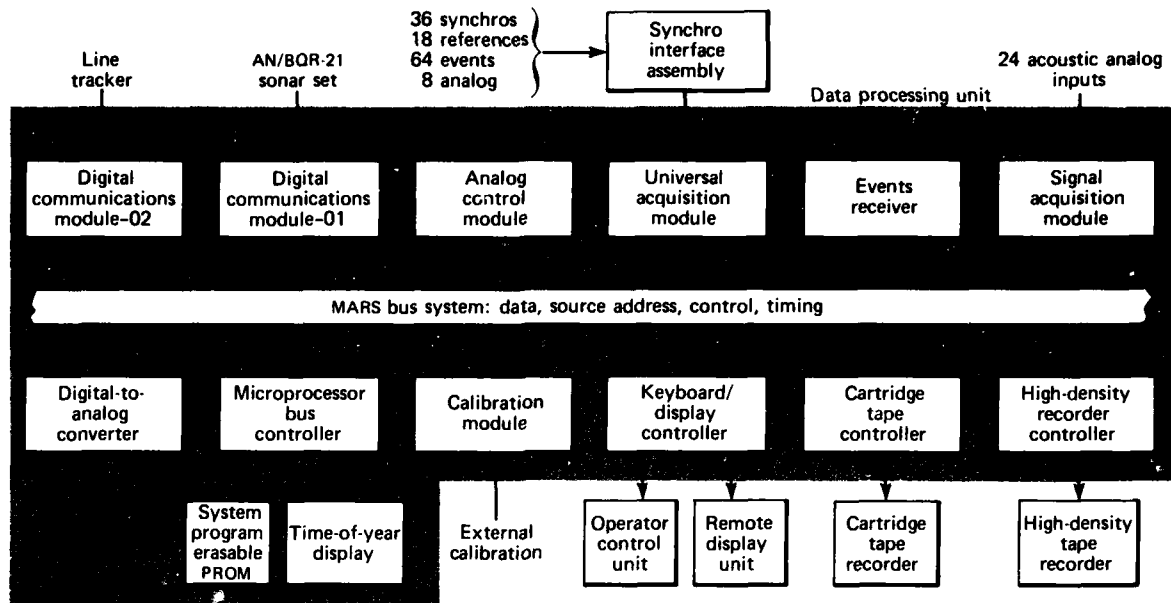


Fig. 3 Configuration for at-sea deployment.

words, along with time of year and all external data sources, are recorded on the high-density tape recorder. Source codes are not recorded but are regenerated during playback by the source code generator.

The keyboard/display controller can access and process selected data from the data bus. The operator interfaces with the system through the operator control unit. It has a panel for system mode control and status alarm lights; system status and processed data can be displayed on a 12-line by 40-character self-scanning plasma display. A full ASCII alphanumeric keyboard can be used by the operator to input commands and select data for display. The operator can also perform automatic or manual calibration via the calibration module.

The Bell and Howell AN/USH-24(v) high-density tape recorder has 28 tracks and uses serpentine recording serial by track on 1 in. tape at a bit-packing density of 33,300 data bits per linear inch. Tape speeds from 3-3/4 to 60 in./s provide about 224 to 14 hours, respectively, of recording/playback time per 9200-ft tape. Data recorded at low speed can be played back at speed ratios up to 16:1. The data capacity is approximately equivalent to 280 nine-track digital tapes at 1600 bits per inch.

A dual-cartridge drive unit records selected data (e.g., status words) for quick-look playback. Data can be recorded from the data bus at a maximum rate of

100 16-bit words per second. Buffering during rewind prevents loss of data.

Twelve analog output channels are available via digital-to-analog converters for strip chart or oscilloscope presentation. The desired data are selected by the operator on the operator control unit and are picked off the data bus in acquisition or playback mode.

The CSI is designed to interface MARS with a PDP-11 via two DR-11B interface boards. One transfers commands from the PDP-11 software to MARS. The other transfers MARS data to the PDP-11. Data

Table 1

MARS INITIAL DEPLOYMENT DATA REQUIREMENTS

Data Type	Number of Channels	Total Words per Second
Synchro	27	54
DC low-frequency analog	5	40
Switch closure events	1	10
Wideband analog	16	42,000
Low-rate digital	8	8
High-rate, asynchronous digital	6	9,550
Time of year	1	2
MARS status	N.A.	84
MARS data bus check codes	N.A.	8
Total		51,756 words/s

transfer rates of up to 125,000 16-bit words per second have been demonstrated. Any data selected from the MARS data bus may be transferred under computer software control to the PDP-11 computer. The CSI may be used either in the acquisition system for real-time data processing or as part of a playback configuration for postexercise data processing.

Table 1 lists the types of data and the rates acquired by MARS during the initial deployment.

THE PARAVANE SYSTEM

H. M. Grady, D. N. Qualkinbush, and S. J. Kundin

A paravane system featuring shipboard control and data collection from two simultaneously towed, underwater sound-source paravanes has been developed. The paravane system is part of a system to measure the deviation from a straight line of a linear acoustic array while under tow. Measurements thus made are used to trim the beamforming equations while array data are processed to provide narrower beams and better sidelobe performance.

BACKGROUND

It is currently accepted by most users of long towed arrays that hydrodynamic forces maintain adequate straightness of the array to allow acceptable beamforming on the received acoustic signals. That this is not always true was demonstrated by APL in a 1976 sea test using paravanes similar to those described herein. The test also demonstrated the need for a paravane system with greater flexibility in control and in data collection. The present system provides this flexibility.

DISCUSSION

Figure 1 depicts the relative deployment geometry for the array and the paravanes. The system uses

This work was supported by the Department of the Navy.

REFERENCES

- ¹ *Specifications for MARS*, APL Subcontract 600638 (Nov 1977).
- ² APL MARS Review Team, *Modular Adaptable Recording System (MARS) Requirements Document* (May 1978).
- ³ J. W. Petersen and E. L. Brickner (APL) and R. A. Robinson (IEC), "Adaptable Data Acquisition and Processing System," presented at Second Working Conf. on Oceanographic Data Systems, Woods Hole Oceanographic Institution, 26 Sep 1978.
- ⁴ *MARS Acceptance Procedure*, IEC 7033507 Rev. E (26 Nov 1979).

12,000-ft-long paravane tow cables, this length affording acceptable geometry for acoustic arrays of up to 10,000 ft. Several high-frequency hydrophones are interspersed with the acoustic low-frequency hydrophones along the length of the array to receive the 25-kHz pulse transmitted (alternately) by each paravane. Each paravane also receives the pulse from its companion. Propagation delays, measured along the paravane-to-paravane and paravane-to-array high-frequency hydrophone paths, are combined with depth measurements of the array and of the paravanes to provide relative position information for each array high-frequency hydrophone. Interpolation between those hydrophone positions provides position data for each acoustic lower-frequency hydrophone. These position data are used to correct the beamforming equations to compensate for distortions in hydrophone position (deviations from a straight line).

Figure 2 is a block diagram of the paravane electronics. The only standard cable suitable for towing paravanes was an armored cable, 0.5 in. in diameter, containing seven conductors. Paravane power, downlink commands, and uplink data must be carried by this limited number of conductors. Uplink and downlink data are carried separately on wire pairs. Those pairs also carry positive and negative ix power to the paravane; a single ground wire is provided.

The downlink waveform provides dwell timing, range count clocks, uplink clocks, and encoded com-

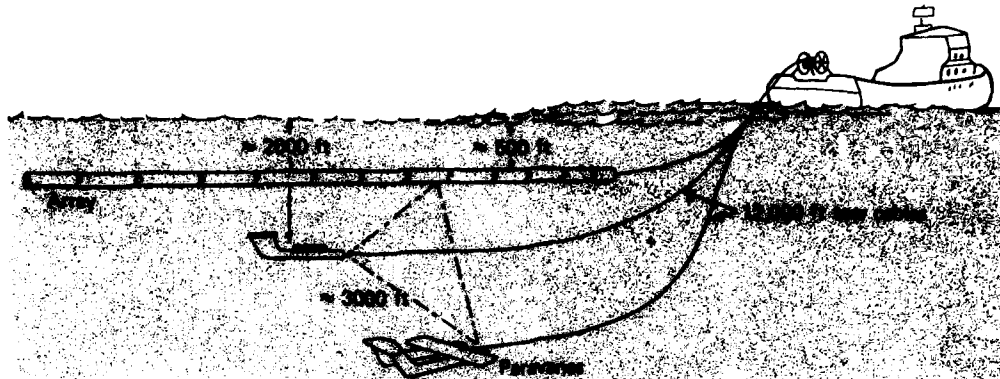


Fig. 1 Geometry of paravane deployment.

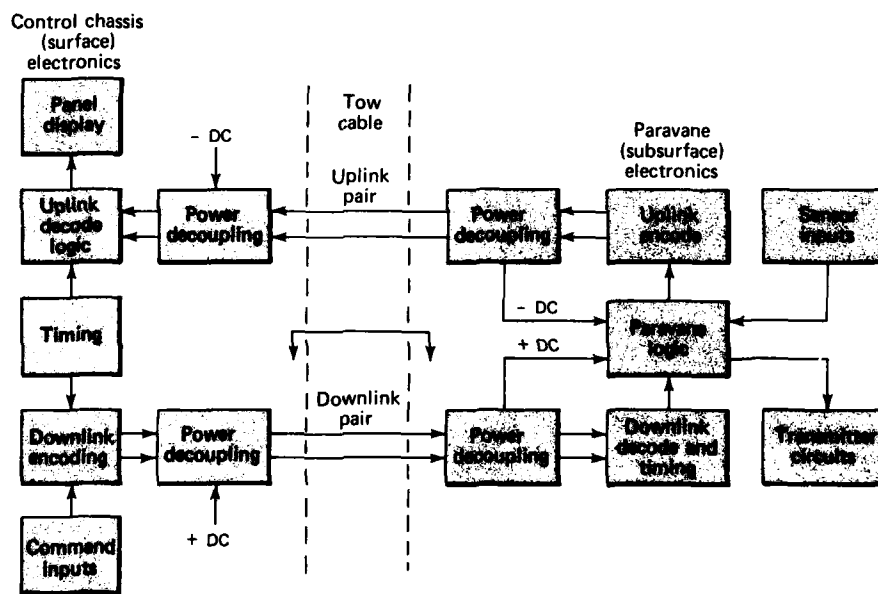


Fig. 2 Block diagram of electronics for paravane system.

mands for mode, pulse length, power level, receive gains, and attitude control. The uplink waveform returns the following digitally encoded data: depth, base range, surface range, temperature, roll fin position, attitude (roll and pitch), and a digitized monitor of the transmitted waveform.

Timing is split into alternating dwell periods of port-transmit/starboard-receive and starboard-transmit/port-receive. The downlink for each dwell is a balanced waveform comprising a 20-ms period of command code (40 bits at 2000 bits per second, self-clocking symmetrical waveform), a 10-ms no-signal (reset) in-

terval, a variable-duration (mode- and dwell-dependent) 200-kHz count clock, and a variable-duration (mode-dependent) 10-kHz clock that provides uplink data clocking. The uplink is a 128-bit serial data stream that is biphase encoded. Digitized paravane data are multiplexed into this data stream. Reference 1 provides detailed system logic and electronic specifications. CMOS logic is used in the subsurface unit to minimize power drain.

The surface electronics chassis and the subsurface electronics chassis are shown in Figs. 3a and 3b. The subsurface electronics is housed in a pressure-proof

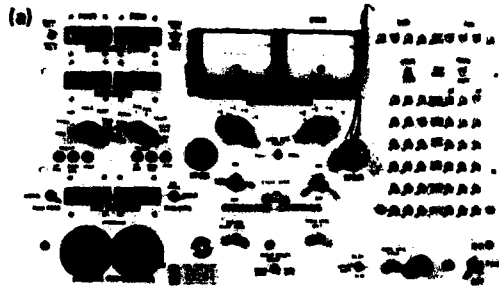


Fig. 3 Paravane electronics hardware, surface (a) and subsurface (b) electronics chassis.

instrumentation module located inside one of the paravane body tubes. Port or starboard towing sense is achieved by the choice of location of the instrumentation module and an equivalently sized flotation module in the opposite tubes plus added roll weights under the wing. Towing depths and offsets are determined roughly by paravane balance and wing and tail incidences. Roll trim, provided by controllable fins at the wing tips, controls the depth of the paravane. Figure 4 shows a paravane being deployed.

The system was used in a 1980 sea test, data from which are now being evaluated, and it is being updated for use in the another sea test scheduled for 1981.

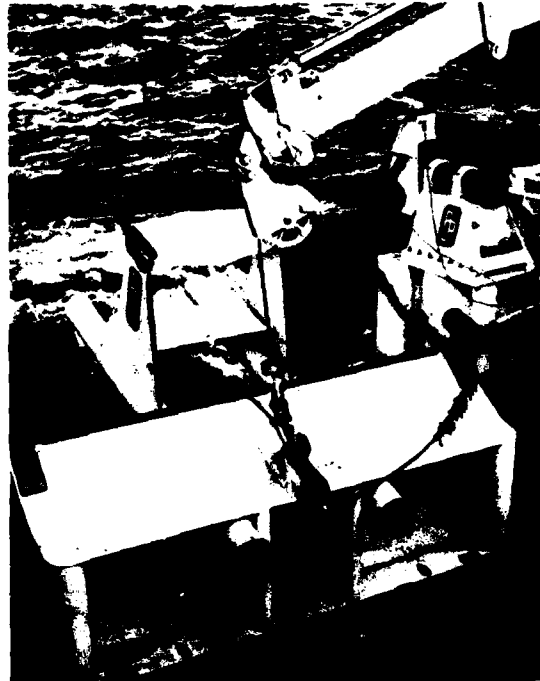


Fig. 4 Deployment of paravane.

REFERENCE

- ¹D. N. Qualkinbush and C. B. Cooperman, *Paravane Electronics for Array Deformation Measurement*, JHU/APL STA-80-035 (Aug 1980).

A TOWABLE SYSTEM FOR MONITORING THE COPPER CONCENTRATION IN THE OPEN OCEAN

D. G. Ondercin

APL has developed a sensor that can monitor seawater continuously, in real time, for changes in the concentration of copper ions. The sensor should aid chemical oceanographers in determining the distribution of trace metals, in this case copper, in the world's oceans.

BACKGROUND

A review of the chemical oceanography literature reflects the considerable difficulty in finding accurate and precise methods to analyze trace metals in the ocean. Specific sampling techniques, container contamination, and analytical techniques all have to be considered when one assigns a confidence level to the results.

In a typical scenario for the analysis of seawater, a discrete sample is obtained using a sampling bottle (for example, Go-Flow or Niskin). The sample is acidified and may then be concentrated and stored in another bottle until analysis in the laboratory, usually by flameless atomic absorption spectrometry. The disadvantages of this system are numerous. Contaminants can be introduced during any or all of the steps, from sampling to analysis; only discrete samples of seawater can be analyzed; and the results may not be known for days, weeks, or even months after the sample was taken.

The need for an analytical method that could monitor the seawater continuously and in real time was apparent. The APL Environment Group has developed such a sensor for the detection of copper ions. It uses ion selective electrodes (ISE) that may be installed in a submersible body and towed at sea.

DISCUSSION

Ion selective electrodes produce a potential, E , that is proportional to the log of the concentration of the ion of interest¹:

$$E = E^{\circ} + 0.099T \log [\text{Cu}^{++}] \quad (1)$$

Here E° is a constant, T is the absolute temperature, and $[\text{Cu}^{++}]$ is the copper ion concentration. If the temperature is held constant, changes in the copper ion concentration will be reflected by the electrode's potential.

Electrodes for detecting copper ions are available commercially. It was determined² that the silver ISE was more sensitive to copper ions than was the copper ISE. The former electrode and a fluoride ISE reference electrode were modified for use at sea (Fig. 1). The silver ISE was simply a pressed pellet of silver sulfide onto which a conductive lead was epoxied. The pellet was epoxied into an inert polyvinyl chloride body, as was the lanthanum fluoride (LaF_3) sensing element of the reference electrode. This electrode requires an internal filling solution, which was sealed in place with epoxy. Both electrodes were about 3 in. long and 0.5 in. wide. A platinum electrode was used to establish a ground for the electronics.

The three electrodes were plugged into the faceplate of the underwater electronics (Fig. 2), and a Plexiglas flow cell was added to the underwater package. Water enters the center of the flow cell, impinges directly onto the copper-sensitive electrode, and is de-

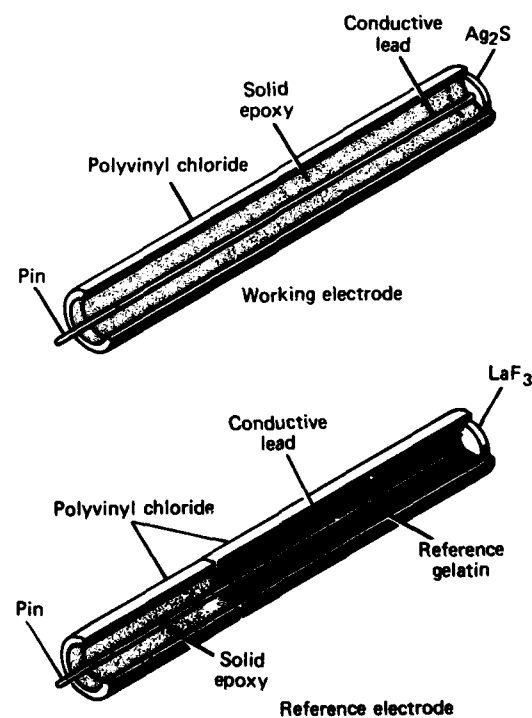


Fig. 1 Modified commercial electrodes.

flected to either side. This design permits complete flushing of the flow cell. The assembled package was installed in a tray (Fig. 3) that was inserted into a towed body. Water is fed to the electrodes by means of a circulating pump located in the front of the tray. A normal flow rate of four liters per minute was established. Two

syringe pumps were modified for underwater use so that known quantities of standard solution could be injected into the flow for calibration.

The first at-sea test of the system was conducted off Grand Bahama Island in January 1980. The sensor

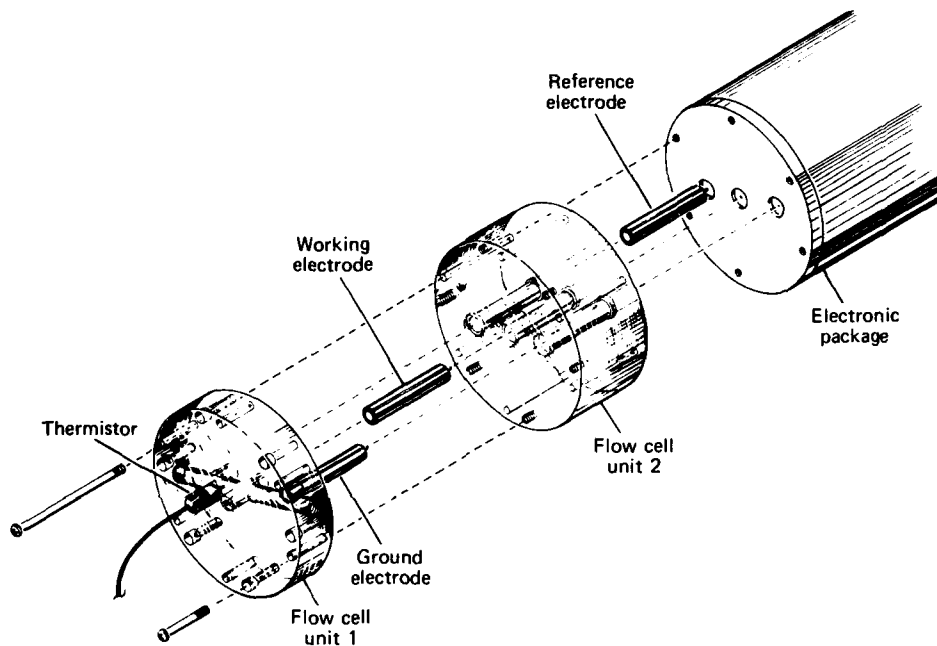


Fig. 2 Flow cell assembly.

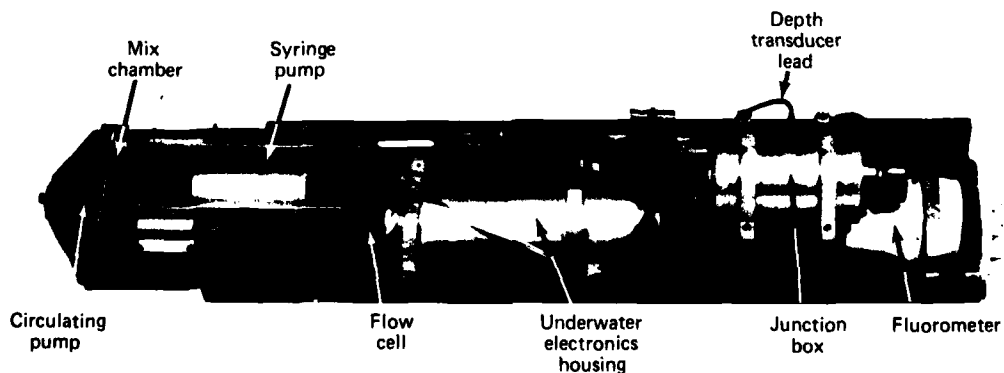


Fig. 3 Underwater tray.

was towed at a depth of 50 ft and a speed of 4 kt. Copper ion curtains, one mile long (Fig. 4), were laid to simulate copper ion fluctuations in the ocean. The towed body was passed through the curtain to determine if the electrode could sense the fluctuations. The concentration of the curtain was varied by adjusting the concentration of the cupric nitrate added to the shipboard curtain-laying solution.

The test showed that a system for continuously monitoring trace metals in the ocean can be deployed. Concentration changes as low as 0.2 part per billion were detected. This concentration is within the range one would normally find for a background copper level.^{3,4} Testing done several months later dockside on St. Croix, U.S.V.I., showed that concentration increments as low as 0.02 part per billion could be observed easily.

The system does have two serious drawbacks. Its response time is very slow (on the order of five to ten minutes). Also, the electrodes do not follow Eq. 1 at these low concentrations; they respond linearly with concentration change. These two facts prevent the system from monitoring the copper content in the open ocean quantitatively. However, the system can highlight qualitative changes. In a continuous tow mode, it can pinpoint anomalous regions of high or low concentrations that may otherwise go undetected by conventional batch-sampling techniques. A chain of these electrodes could be used to profile the anomalous regions, and this, in conjunction with conventional batch sampling techniques, would permit the regions to be mapped quantitatively.

The system has demonstrated the feasibility of monitoring trace elements continuously in the open ocean. If it is towed near shore or near the mouth of a river, the trace metal concentration probably would be several orders of magnitude higher. At such concentrations, the electrodes are again obeying Eq. 1, and quantitative results can be obtained without the aid of batch analysis.



Fig. 4 Deployment of dyed copper curtain.

REFERENCES

- ¹ R. A. Durst, "Ion Selective Electrodes," *Proc. Symp. National Bureau of Standards*, Gaithersburg, Md., Jan 1969.
- ² G. K. Rice, *An Evaluation of Ion Selective Electrode Response in Copper (II) in Seawater*, Final Report, Texas Instruments Contract No. 600591 (May 1977).
- ³ R. E. Pellenberg and G. M. Leone, *Dissolved Trace Metals in Seawater*, U.S. Naval Oceanographic Office TN 3005-1-78 (Feb 1978).
- ⁴ K. W. Bruland et al., "Sampling and Analytical Methods for the Determination of Copper, Cadmium, Zinc and Nickel at the Nanogram per Liter Level in Seawater," *Anal. Chim. Acta* **105**, pp. 233-245 (1979).

COMPARISON OF ACOUSTIC TRANSMISSION LOSS MEASUREMENTS IN CONVERGENCE ZONES

A. M. Diamant

The evaluation of the capability of passive acoustic systems requires the knowledge of sound propagation loss in the sea. Some information on the statistical behavior of acoustic transmission loss was obtained from measurements made during the 1976 sea test.

BACKGROUND

A major difficulty in predicting passive sonar performance is assigning appropriate values to transmission loss (TL), which is the measure of acoustic power loss resulting from spreading and attenuation. TL, one of the parameters determined by the medium in the sonar equation,¹ varies in space and time as a function of the sound-velocity structure in the ocean.

Historically, sound-velocity profiles (SVP's), which are measures of sound velocity versus depth, have shown changes with time and with ocean region, especially in the first 1000 ft or so of depth.² The question at issue is whether the perturbations in the SVP's have a significant effect on sound propagation as it is reflected in TL statistics.

A 1976 sea test included an experiment to measure TL across an extent of the Pacific Ocean. The goal was to determine if there were stable statistical patterns in the TL, in spite of fine structure variations across distance and time.

DISCUSSION

The 1976 test took place in a deep-water region of the Pacific, about 450 nmi northwest of San Diego, within an area of about 10,000 mi². Two surface research vessels were used. One towed an array of hydrophones at a depth of about 600 ft, and the other towed an acoustic signal transmitter at a depth of about 300 ft. Among the transmitter emissions were three tones in the midrange of acoustic frequencies.

Over a period of about two days, there were two test runs in which the vessels closed on each other at a uniform rate from about 100 to 2 nmi separation. The runs took place along widely separated tracks within the test area. Wind and sea state varied over the period of the test, and SVP's measured along the courses showed the expected variations in the sound-velocity structure.

This work was supported by the Department of the Navy.

During the runs, continuous readings were made of the transmitted and received signals.

In the log or decibel domain, TL is the difference between the transmitted and the received signal levels. In the Laboratory, the recorded data were used to generate plots of TL in decibels versus range in nautical miles for each of the three tonals. One such plot (Fig. 1) covers 22 to 37 nmi for the lowest frequency tone, for each of the two runs. The first convergence zone (CZ) is indicated on the plot. A CZ is a region of significant signal enhancement as a result of focusing; it occurs at range intervals determined by the position of the source and the physics of the sea channel.¹ The width of a CZ is proportional to its range. In this exercise, three CZ's were traversed within the maximum range of approximately 100 nmi. The analysis of TL was restricted to the areas of convergence gain.

A visual comparison of the plots in Fig. 1 reveals general structural similarities within the CZ, although at any particular range the TL values may differ by several decibels. To compare the TL values in the two runs statistically, cumulative relative frequency distribution functions were constructed. Figure 2 is a set of distribution functions for the two runs and the first three CZ's, at the lowest frequency. There is generally good agreement between the distributions of TL values within the same CZ. The offsets between CZ's are to be expected because of spreading and attenuation with range.

Table 1 presents the means and standard deviations, in the decibel domain, of TL for the three frequencies, three CZ's, and two runs. The similarities between runs are evident in parts (a) and (b) of the table. Part (c) gives the averages of the two runs. The differences in the means from the lowest to the highest frequency are about what would be expected because of increasing attenuation with frequency.

To address the question of how consistent the distributions of TL values were, the distribution functions for the two runs were compared for the different CZ's within each run and for like CZ's in the two runs. The Kolmogorov-Smirnov (K-S) goodness-of-fit test³ was applied to pairs of distribution functions to get a statistical measure of how closely related the members of each pair were to each other. Inputs to the test are the number of samples in each distribution being compared and the maximum distance, D , along the percentage scale between the two functions. The output of the test is the significance level, α , which is the probability of a

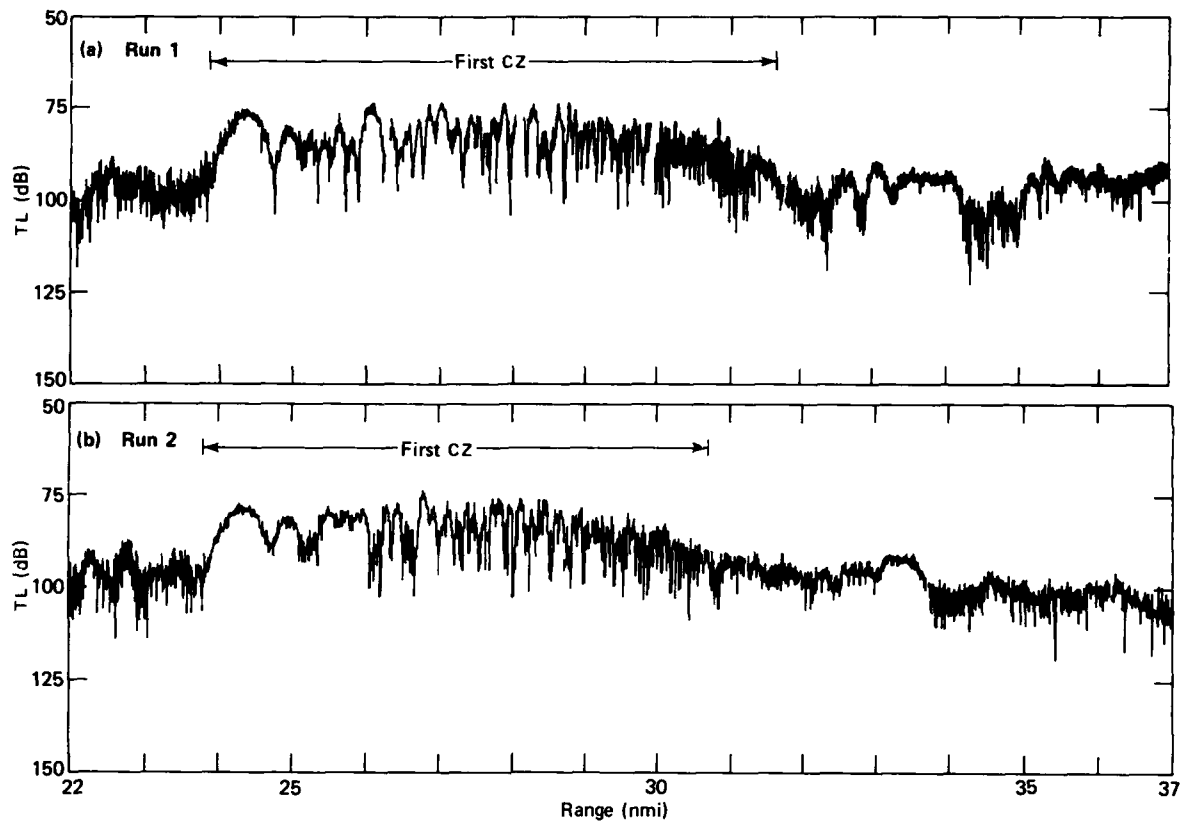


Fig. 1 Transmission loss versus range, lowest frequency.

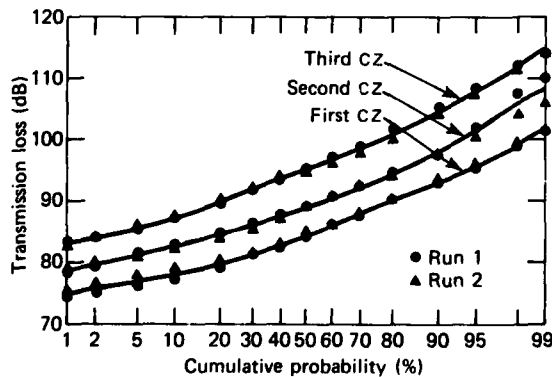


Fig. 2 Transmission loss distribution functions, first through third CZ, lowest frequency.

separation, D , occurring if the two distributions were constructed of samples from the same parent population. In other words, a large α (close to unity)

indicates a good fit. If, for example, the measured TL distributions in a CZ for two different runs score high in the K-S test, that outcome supports the assumption of similar statistics, in general, in sets of samples from that CZ.

Since the K-S test demands that the distributions be constructed of independent samples, autocorrelation functions were constructed to determine the decorrelation range interval and thus the minimum separation between valid data points. The decorrelation distance was found to be 1 or 2% of the CZ extent.

Table 2 gives the results of applying the K-S test to pairs of the data sets to compare like and unlike CZ's within and between the two runs at the lowest frequency. Part (a) of the table compares like CZ's in the two runs. The two second CZ's compare well with each other, as do the two third CZ's. The first CZ's do not, with a value of α of 0.30. However, if one of the first CZ distributions is shifted along the decibel scale to minimize D , the comparison is good. The amount of

Table 1
MEAN (M) AND STANDARD DEVIATION (σ) OF TRANSMISSION LOSS IN THE DECIBEL DOMAIN VERSUS RUN, FREQUENCY, AND CZ

CZ	550 Hz		750 Hz		1050 Hz	
	M	σ	M	σ	M	σ
(a) Run 1						
1	84.8	6.0	84.8	5.9	86.0	6.2
2	90.1	6.3	90.6	6.3	92.9	7.2
3	95.8	7.0	96.7	7.0	98.3	6.9
(b) Run 2						
1	85.4	5.6	86.1	6.0	86.5	5.7
2	89.7	6.1	89.6	6.4	91.3	6.2
3	95.4	6.6	96.6	6.6	98.7	6.5
(c) Average of Runs 1 and 2						
1	85.1	5.8	85.4	6.0	86.2	6.0
2	89.9	6.2	90.1	6.4	92.1	6.7
3	95.6	6.8	96.6	6.8	98.5	6.7

Table 2
KOLMOGOROV-SMIRNOV DISTRIBUTION TEST APPLIED TO PAIRS OF TL SETS BETWEEN CZ'S AND RUNS

(a) Like CZ's, Run 1 versus Run 2			
CZ		α without Mean Removal	α with Mean Removal
1		0.30	0.78
2		0.98	0.98
3		0.77	0.98
(b) Unlike CZ's, with Mean Removal			
CZ	vs. CZ	α of Run 1	α of Run 2
1	2	0.93	1.00
2	3	1.00	0.97
1	3	0.99	0.79

relative shift is about the same as that caused by the removal of means, in this case about 1 dB.

Part (b) of Table 2 compares different CZ's within each of the two runs. The removal of the mean is expected and necessary because of spreading and attenuation losses with range. The CZ's compare well: first to second, second to third, and first to third.

CONCLUSION

A visual comparison of the TL distribution functions in the two runs shows similar statistics in corresponding CZ's and at corresponding frequencies. Offsets between unlike CZ's and frequencies can be attributed largely to predictable spreading loss and attenuation differences.

A mathematical comparison of the TL distribution functions at the lowest frequency, using the K-S test, supports the visual impression of similar statistics across runs and CZ's provided, in general, that there is mean removal.

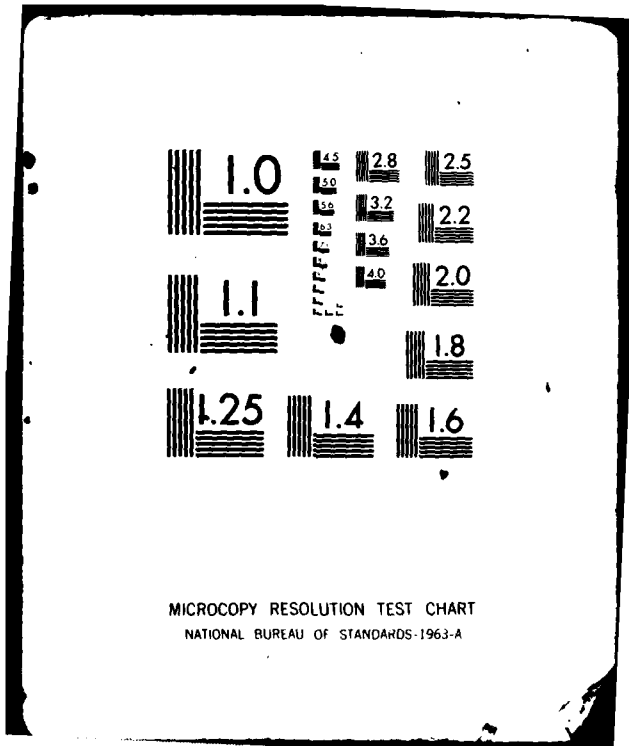
Autocorrelation functions show a pattern of longer correlated range intervals with farther CZ's, the correlated interval being on the order of 1 or 2% of the CZ extent.

The analysis results show the TL statistics to have been insensitive to the SVP variations in the test area. This evidence helps in the design of models to set detection thresholds.

REFERENCES

- ¹R. J. Urick, *Principles of Underwater Sound for Engineers*, McGraw-Hill, New York (1967).
- ²E. M. Podeszwa, *Sound Speed Profiles for the North Pacific Ocean*, NUSC Technical Document No. 5271 (2 Feb 1976).
- ³A. M. Diamant, *Applying the Kolmogorov-Smirnov Goodness-of-Fit Test to Help Compare a Model and a Data Set, or Two Data Sets*, APL/STA-1-1050/DM-3866 (4 Jan 1978).

COMPUTER TECHNOLOGY APPLICATIONS



MICROCOPY RESOLUTION TEST CHART
NATIONAL BUREAU OF STANDARDS-1963-A

INTRODUCTION

Computer systems play an important role in APL's contributions both to national defense and to the solution of civil problems. Extensive computational facilities are maintained by the Laboratory to support the work of its scientists and engineers.

The central digital computer facility consists of an IBM 3033 multiprocessor with high-speed large-scale dual processors. The 3033 has a basic machine cycle time of 58 ns with overlapped instruction execution and has an advanced virtual memory operating system. Its main memories contain 16 million bytes. This capability is supplemented by auxiliary direct access storage totaling 115 billion bytes (disk and mass storage). The facility serves a wide variety of tasks including large-scale simulations, complex analyses, and data processing and reduction. Extensive use is made of interactive processing for the real-time solution of problems; about 700 remote terminals are available.

APL also supports two analog/hybrid computer laboratories. Analog and hybrid computations are essential to the solution of complex problems, particularly when large numbers of simultaneous differential equations must be solved. Hybrid facilities can economically simulate large physical systems composed of continuous and discrete processes as well as real-time simulations that include hardware in the loop. APL's two hybrid computer laboratories are the Interactive Simulation Laboratory (ISL) and the Guidance System Evaluation Laboratory. The EAI 680 analog computers in the ISL are interfaced with an IBM 3033 digital machine that is part of the multiprocessor configuration. The other hybrid system, consisting of an EAI PACER 600 system interface to missile hardware and a radio-frequency test-chamber darkroom, is used primarily to test missile guidance hardware.

This section contains five articles representative of the computer-related projects at the Laboratory. The first article describes the new hybrid computer implemented in the ISL and interfaced to the IBM 3033. The new computer system incorporates an intelligent hybrid interface that significantly improves the digital sample rate, allowing for more efficient use of the digital computer. This will improve existing airframe, attitude control, and other simulations run on the system.

The second article describes an image display system that has been interfaced to the IBM 3033. It consists of both hardware and software interfaces that allow for the storage and display of complex image data. Examples of Navy research involving digital image processing include target recognition studies, wide-area guidance and control, and cruise-missile scene-matching studies.

Three articles describe software systems implemented on the IBM 3033. The first, an interactive system for the APL language, allows full use of the IBM 3033 multiple virtual storage operating system, permitting use of this large-scale computing environment under control of APL-coded algorithms. A regulatory environment assessment system, described in the next article, provides a general approach for the management of moderately sized document collections and also the ability to retrieve information rapidly. A data dictionary developed to support the INQUIRE Data Base Management System is discussed in the final article. The data dictionary allows for the flexible and efficient use of this system by providing essential definition maintenance and definition extraction functions.

HYBRID COMPUTER SYSTEM BASED ON THE IBM 3033

M. D. Lasky, F. W. Miller, T. G. Boland, P. F. Bohn,
H. D. Pixler, N. K. Brown, and R. B. McDowell

A new hybrid computer has been implemented by APL personnel as a necessary part of APL's transition from an IBM 360/91 to an IBM 3033 central digital computer. The analog computer has remained the same. The opportunity afforded by this transition has been taken to develop an original design of an intelligent hybrid interface that allows substantially greater efficiency in the digital computer. The improved efficiency allows a closed-loop sampling rate of 1000 samples per second as opposed to the previous 400 samples per second. Key simulations that have benefited are the six-degree-of-freedom (DOF) rolling airframe missile and the 6-DOF satellite attitude control.

BACKGROUND

The first hybrid computer at APL, completed in 1970, was a combination of a large Electronic Associates, Inc. Model 680 analog computer tied to an IBM 360/91, the Laboratory's main digital computer. The system grew out of needs characterized by large physical system simulations involving many simultaneous differential equations, hardware tie-ins, and a need for real-time interactive control. Then, as now, those needs could only be met by a large-scale hybrid computer.

When the IBM 3033 was planned to replace the 360/91, plans were also made to redesign and minimize the hybrid program synchronization and the input/output (I/O) software, functions that would be handled by an intelligent interface adapted to the different architecture and operating system of the 3033. Implementation of the new hybrid system was effectively completed in September 1980; however, limited operations began in February 1979.

The real-time workload imposed by the hybrid system on the 3033 has been accommodated without noticeable effect on the normal concurrent operations of the digital computer. No other hybrid computer system is known to be able to run concurrently with all other operations of a large-scale, general-purpose central digital computer.

The hybrid computer largely supports missile performance studies for the Navy but is also used for submarine performance studies, the design and development of NASA earth satellite control systems, and

automotive vehicle studies for the Department of Transportation.

DISCUSSION

Most, if not all, large aerospace contractors use hybrid computers for a variety of large system-development programs. The applications are well established in the literature, in particular, in the journal of the Society for Computer Simulation. Examples of specific applications at APL include the 5-DOF Standard Missile-1 and -2, the 3-DOF signal processor for Standard Missile-2, the 6-DOF rolling airframe missile, the 6-DOF satellite attitude control, the 6-DOF Harpoon missile, the 3-DOF Pershing missile, and automotive vehicles with up to 17 DOF.¹⁻⁴

The work reported here is the improvement of a large-scale hybrid computer not only by means of a very powerful third-generation digital computer but also by performing many operations in the I/O channel hardware that were formerly done by software in the central processing unit (CPU). Using the I/O channel as a "smart" device improves the effective speed more than two-fold. The improvement is effected by removing much of the system control from the CPU and having it carried out in a simultaneous or parallel manner by the interfaces between the digital and analog computers. This parallelism in hardware minimizes contention between hybrid jobs and other digital computer work, eliminating the usual practice (in the industry) of acquiring two digital main frames, one for hybrid and the other for general-purpose work.

Figure 1 illustrates the major hardware features of the 3033-based hybrid. The single most important component in the new system is the hybrid system synchronizer (HSS), which, as a part of the interface, takes over the synchronization of digital and analog functions. These functions were CPU-based in the previous system using a real-time monitor. Conventional dedicated digital computer systems also manage synchronization using a real-time monitor. Working in parallel with the CPU, however, the HSS allows two substantial improvements:

1. Elimination of hybrid-related synchronization and I/O overhead, thereby allowing more efficient processing of all jobs on the digital computer; and

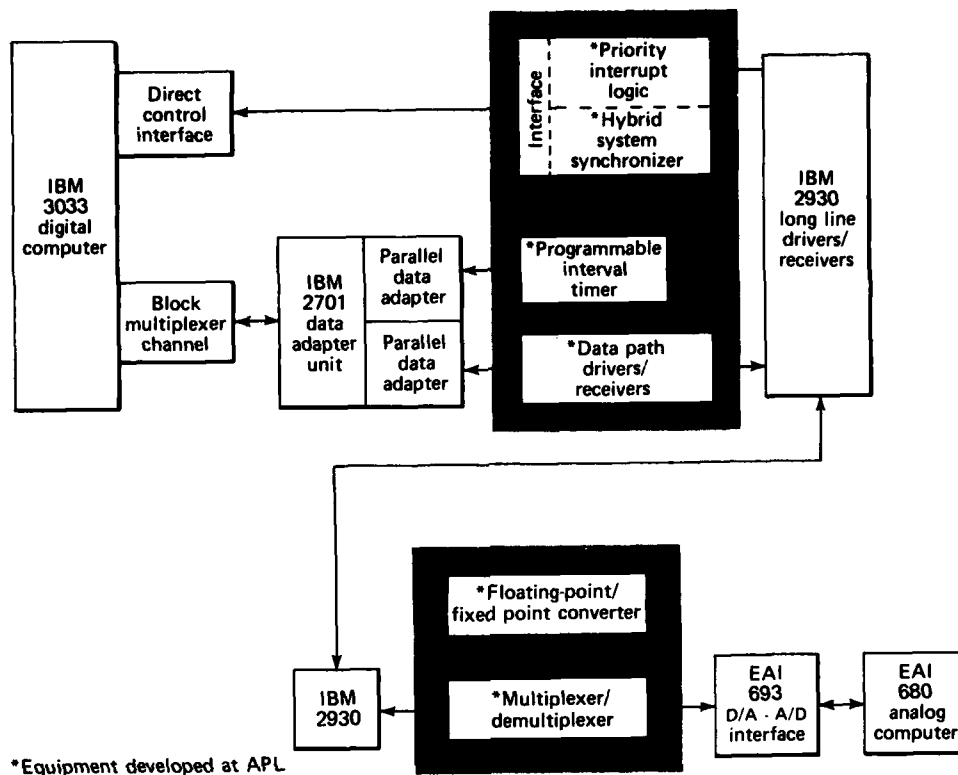


Fig. 1 APL hybrid computer digital subsystem.

2. A near-zero likelihood of hybrid malfunctions affecting the 3033 because most hybrid functions are prevented from running in the privileged state as part of the operating system.

Along the same lines, another key function has also been off-loaded from the digital computer — the need to issue start I/O commands to transfer data and commands between the analog and digital computers. This time-consuming operation is now handled by software in the I/O channel itself, synchronized by the HSS. The technique, called a chained channel program, is not new but is new to hybrid systems.

Another important feature, not found in most other hybrid systems, is the conversion in interface hardware of the fixed point analog data to floating point digital data and vice versa. In the 360/91-based

system, this was done by software in the CPU. Again, substantial overhead has been eliminated.

References 5 and 6 detail the previous system. A forthcoming paper will detail the 3033-based system.

REFERENCES

- ¹ C. S. Kuehne and H. D. Dunkle, *RAM Control Test Vehicle Hybrid Simulation (CTV-2)*, JHU/APL BCE-T-0846 (Jan 1980).
- ² C. S. Kuehne, *Hybrid Simulation to Determine Launch and Reflood Forces*, JHU/APL BCE-T-0741 (17 Nov 1978).
- ³ P. F. Bohn and R. J. Keenan, *Improved Hybrid Computer Vehicle Handling Program*, JHU/APL CP 049A (Oct 1978).
- ⁴ G. H. Fountain, B. E. Tossman, F. F. Mobley, and C. E. Williams, "A Sampled Data Attitude Control System for MAGSAT Spacecraft," presented at Ninth Annual Pittsburgh Conf. on Modeling and Simulation, Apr 1978.
- ⁵ R. B. McDowell, A. G. Witte, N. K. Brown, P. F. Bohn, and D. M. White, "Development of Computer Technology for Simulation," *Simulation* 17, No. 1 (1971).
- ⁶ R. B. McDowell, P. F. Bohn, N. K. Brown, P. M. Kirk, and A. G. Witte, "A Real-Time, Interactive, Multiple Computer System," *APL Tech. Dig.* 11, No. 2 (1971).

INTERFACE OF IMAGE DISPLAY SYSTEM TO APL'S CENTRAL PROCESSING SYSTEM

T. G. Boland, D. Brocklebank, and R. E. Stovall

Hardware and software interfaces have been developed for use between an image display system and the Laboratory's IBM 3033MP computing system. The display system features storage, processing, and display capabilities that have been combined with the extensive resources of the IBM 3033MP. Together they provide APL scientists and engineers with a powerful and versatile image analysis tool.

BACKGROUND

All branches of the Armed Services are investigating a variety of imaging systems (radar, forward-looking infrared, and optical) for weapon delivery applications. APL is participating in Navy research programs involving digital image processing including autonomous target recognition, wide-area guidance and control, and the Tomahawk Cruise Missile Program. Principal among these is the cruise missile program, which is directed at developing and analyzing optical scene-matching algorithms. The algorithms are used to compare sensed optical images of the terrain below the missile with stored reference data to provide location information for the missile during the terminal segment of flight.

Each program involves extensive computer analysis of digital image data and requires some means to display the images. There are several display-hardware alternatives, but selection must be guided by the needs of all users in diverse programs. The common factor (and driving element) of the programs is their analytical and experimental nature, which imposes restrictions on the configuration of the image display hardware. First, digital image data stored within a computer and operated on by it must be displayed for visual assessment within a reasonable time interval. Display on an off-line device, although possible, is too slow to be useful. Second, it is important to connect the display system to a computer with which all users are familiar and to which all have access. In so doing, user training is reduced substantially and program results are achieved more quickly.

The overall system configuration that meets these and related restrictions is the direct, local connection of image display hardware to the Laboratory's

IBM 3033MP central processing system. Display monitors are located at the user's work sites. Image display at near real-time speeds allows the user to develop programs and analyze data interactively by means of the widely used IBM Time Sharing Option (TSO).

DISCUSSION

The basic components of a digital image display system are a digital memory, a video monitor, and a display controller. An image is stored in the memory as a matrix of intensity values that the controller converts to an analog video signal for display on the monitor.

The APL display system includes a Grinnell GMR-270 image processing/display system. It contains four banks of eight-bit image memory at a 512 by 512 display resolution and has two independent display monitors. It has a powerful image processor that can be used for image manipulation and enhancement, two 512 by 512 four-bit overlay memories, a video image digitizer, two joystick input devices, and full color capabilities. The overlay memories store an image that can be superimposed on an image generated from the other memories.

The requirement for nearly instantaneous image display was satisfied by local attachment to a high-speed, parallel data path (input/output (I/O) channel) in the IBM 3033MP system. Figure 1 is a block diagram of the major hardware components. An IBM 2701 parallel data adapter serves as the link between the IBM channel and the non-IBM image display system hardware. The 2701 handles all channel control functions and presents a parallel demand-response interface to the display memory interface (DMI). The DMI, developed at APL, multiplexes data between the 2701 and multiple external parallel devices. The GMR-270 is the only external device currently attached. It resolves data exchange protocol differences and electrical interface incompatibilities. Display system software running in the IBM 3033 manages the flow of data to and from the display hardware. Software control is accomplished through a TSO or APL terminal session.

Restrictions on cable lengths in the parallel data paths required that the 2701, DMI, and GMR-270 be located near the 3033. However, because low-loss CATV coaxial cable was being used, it was possible to

This work was supported by NAVSEASYSOM and the Joint Cruise Missiles Project Office.

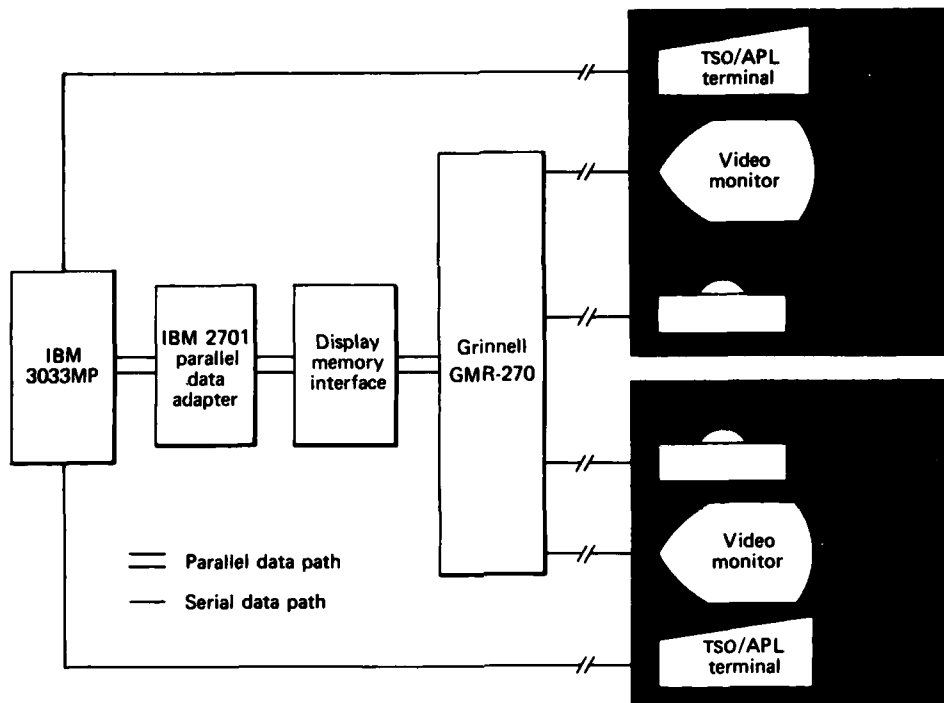


Fig. 1 Hardware of the image display system.

locate the video monitors and graphic input devices for the GMR-270 at the users' work sites.

Figure 2 shows the major functional components of the DMI. The bus interface module converts the 2701 signal interface to another form called the DMI bus, which is a high speed parallel path on which data are multiplexed to the DMI control module and to as many as seven external device modules. DMI control provides power-on and programmed reset functions, controls the selection of external device modules, and manages asynchronous interrupts to the IBM 3033MP from the external device modules. These modules, when enabled by DMI control, transfer data between the DMI bus and the external device, perform other necessary device-dependent functions, and provide the proper electrical signal interface to the device. The self-test module, a microcomputer that can perform diagnostic tests off-line from the 3033 and the 2701, can exercise all functions of the DMI and GMR-270 by mimicking command/data sequences from the 3033. This capability allowed hardware testing to proceed concurrently with 3033 software development.

The software system that controls the DMI and the GMR-270, APLIMAGE, was developed to meet several design objectives: concurrent access to the facility by multiple users, dynamic allocation of the

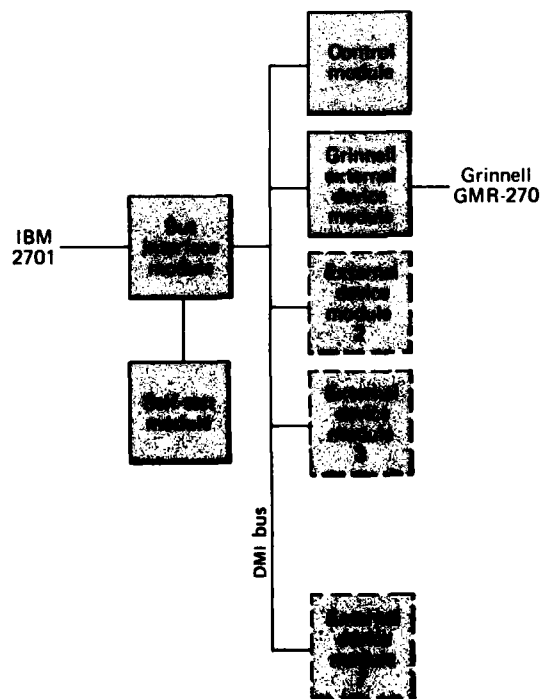


Fig. 2 Block diagram of the display memory interface.

various components of the hardware, high reliability and performance levels, and interfaces to the two most widely used programming languages, PL/I and APL (Iverson's language). APLIMAGE functions and the overall software structure are shown in Fig. 3.

Although the Grinnell system may be controlled by PL/I programs operating in a batch mode, it is most conveniently used interactively with the APL language. A set of simple APL functions permits loading of image memories, configuration of image processing hardware, cursor and joystick control, and resource management. The APL language itself offers the possibility for considerable image manipulation, file processing services, and, most importantly, an excellent environment for developing and experimenting with algorithms.

The user of the display system must understand the general design of the Grinnell hardware in order to command it appropriately, because the software system has not attempted to generalize the hardware to a point

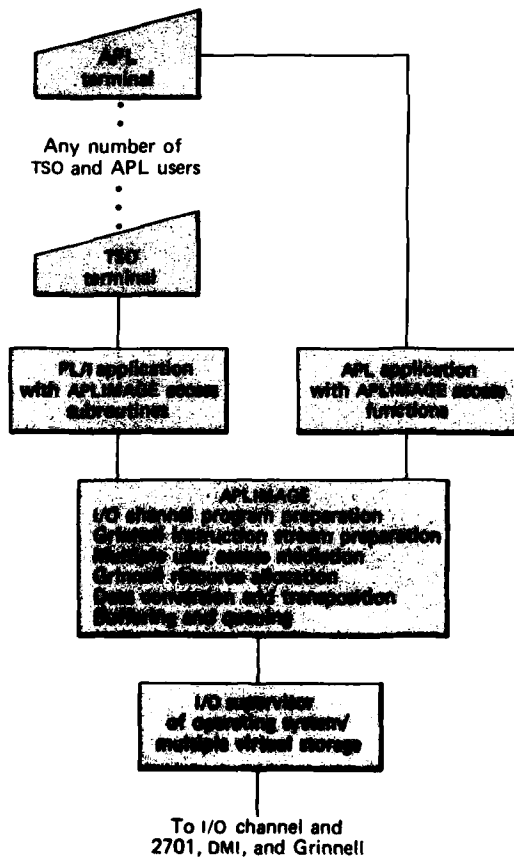


Fig. 3 Structure of the software system.

where its special image-handling capabilities would be lost. The programmer interface seeks only to make it convenient to control the hardware fully and to handle images and subimages as conventional data arrays in whichever language is chosen.

AN APPLICATION OF THE GRINNELL SYSTEM

The Tomahawk Cruise Missile Program is representative of programs that are currently using the Grinnell image processing/display system. During flight, the cruise missile cross-correlates a sensed image against a larger stored reference image. The location of the maximum correlation indicates the missile's true position relative to that estimated by the navigation system.

One concern of the cruise missile program is that the true fix peak in the correlation surface may recede to a level near that of competing false fix maxima. Conversely, the false fix peaks may get too large. Studies have begun of peak degradation caused by sensor distortions such as incorrect scale and rotation. Enhancement algorithms can lower the level of the false fix maxima, and many algorithms have been implemented in the Grinnell system. Figure 4 contrasts a desert scene before and after application of an enhancement algorithm. The first and third vertical bands show the original image, and the second and fourth bands show the enhanced image.

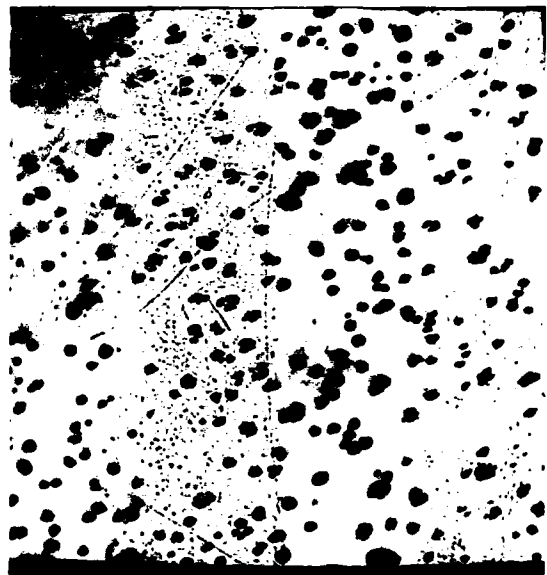


Fig. 4 Desert scene before and after application of an enhancement algorithm.

SUMMARY

The components of the image display system hardware and software have been integrated and tested. The system has already proven its value in the display and visual analysis of image data for the cruise missile program. Work is proceeding rapidly on the develop-

ment of applications software that will use the full image processing and manipulation capabilities of the Grinnell hardware. New applications of image processing and display are being explored, and we anticipate interest and vigorous activity in this area at the Laboratory.

THE APL/MVS INTERACTIVE COMPUTING SYSTEM

D. Brocklebank and W. T. Renich

Although it has been in widespread use for over a decade, the notation known as A Programming Language (APL) has been of limited practical value as implemented within computing systems. The APL/MVS (Multiple Virtual Storage) Interactive Computing System makes it practical to use this exceptionally powerful notation to address computing applications of considerable size, complexity, and variety.

BACKGROUND

APL was designed by Kenneth Iverson (in collaboration with Adin Falkoff) as an aid to the development and expression algorithms (independent of any computer machinery); it was subsequently implemented within early IBM systems so that one could experiment with algorithms and observe the results. The notation is a remarkably concise, highly general language, reminiscent of a rigorously conceived algebra. It has a few rules that are applied in a uniform manner, and it is rich in interesting identities.

The original APL implementations for IBM 360 computers provided interactive access from remote typewriter terminals in a way that made it convenient to enter, revise, and execute algorithms using small quantities of data. Only a small portion of the capability of the computer itself could be harnessed; typically one could handle no more than 4000 real values at a time (even though a Fortran programmer using the same computer could easily handle 60,000 real values). Addi-

tionally, the early implementations had no mechanism for access to data files or for input/output other than to the interactive terminal.

In spite of these engineering restrictions, APL has become recognized for its intrinsic qualities and for several important byproducts of its usage: greatly improved programmer productivity, more reliable and more convincingly correct programs, and very high levels of program generality. It has been said that the quality of the APL notation is a model for quality of thought in algorithm design, and that it tends to elevate the activity of programming (even by someone with little understanding of computers) to a highly professional level.

The Frank T. McClure Computing Center at APL has a large-scale complex with an IBM 3033MP computing system; the operating system for the complex is known as Multiple Virtual Storage (MVS). The APL/MVS Interactive Computing System was developed by the authors to make the capabilities of the full computing system available to the APL user. Thus it permits the large-scale computing environment to be exploited under control of APL-coded algorithms.

DISCUSSION

Within the context of an organization like APL, the use of Iverson's notation can significantly improve the productivity of people needing to do computing. Exploratory calculations otherwise requiring weeks of program development in Fortran, PL/I, or Pascal can be accomplished in a matter of hours using APL.

This work was supported by Indirectly Funded R&D.

In order to make APL available to staff members, the Computing Center has pursued a series of evolutionary APL software systems. As a major computing center, it usually obtains its software systems from commercial and government sources; it was therefore natural to install on the IBM 360/91 the best available APL software system, known as APLSV (1974).

APLSV offered Iverson's notation in an interactive manner to multiple, time-shared terminals. It was shown to be highly responsive and was used successfully by Laboratory staff members. However, like its predecessors, APLSV permitted users to have workspaces of a limited size (approximately 100,000 8-bit bytes of usable memory) and therefore limited the size of the problems that could be solved conveniently using APL.

With the APLSV system came the introduction of shared variables, a concept that permits orderly communication between processes whether coded in APL or not, for example, between APL and Fortran, APL and PL/I, or APL and the operating system. Through shared variables, APLSV offered users of the system access to disk-resident data files having the same data formats used by other languages. This file access was achieved by building an auxiliary processor, a system program written in non-APL that provides services to the APL user.

APL was implemented in the IBM operating systems of the 1960's and early 1970's. Through advances in operating system design, IBM produced the MVS operating system, which provided an evolutionary change for its users and gave them greatly expanded capabilities of virtual storage so that only the active portion of a program needed to reside in the main computer memory. "Swapping" or "paging" kept only the active portions in real memory. It became obvious that the users of APL would not be able to enjoy the advantages of the new technology unless an entirely new software system were developed. Thus we began a study of the available APL systems that would exploit virtual memory technology.

Several seemingly adequate systems were available from software vendors. They all offered virtual memory workspaces of up to several million bytes in size, and they all offered some variety of data file processing. The user had to learn the operating system and the needed job control languages. The functions of the operating system were not made part of the APL notation. We decided to design and build our own APL

system to replace APLSV. We wanted to take advantage of the engineering features of virtual memory and the operating system and have the features used automatically in the APL notation.

To do this, we obtained a totally abstract APL software product that is independent of any operating system. We then intergrated that software with the MVS operating system. The new APL/MVS provided the following capabilities in APL notation: terminal input/output, virtual workspace management (up to four million bytes per workspace), a library system for workspaces (including long-term mass storage facilities), a complete shared-variable subsystem for communication between software processes, and an auxiliary processor offering efficient data file processing and bulk output to line printers, microfiche, etc. The system is now in production use on the IBM 3033MP and has totally replaced the old APLSV service. One of the most beneficial aspects was that APL/MVS was compatible with APLSV so that users could execute their previously written APL algorithms without significant revision. As the need arose, the users could then take advantage of the new extensions.

There are now more than 600 people enrolled as users of the APL/MVS service, and the system is currently holding nearly 7000 workspaces for them. Among the saved workspaces are several hundred of a public nature — available to all users of the system. Many of those workspaces implement powerful capabilities using the APL language itself instead of the more traditional assembly language implementation: bulk report generation and routing, inverted data base management, and interactive inquiry software, to mention a few. APL/MVS has proved to be an extremely reliable system offering much better performance than its predecessor.

By means of a technology-transfer agreement with a commercial software organization, the APL/MVS system software is available on a license basis to both government and private organizations.

REFERENCES

- ¹ K. Iverson, *A Programming Language*, John Wiley and Sons, Inc., New York (1962).
- ² L. Gilman and A. J. Rose, *APL: An Interactive Approach*, John Wiley and Sons, Inc., New York (1971)
- ³ G. H. Foster, "APL: A Perspicuous Language," *Comput. Autom.* (Nov 1969).

APPLICATION OF REAS(ON) TO ADP ACQUISITION REGULATIONS

B. W. Kuvshinoff and W. T. Renich

The Regulatory Environment Assessment System (ONline) (REAS(ON)) is an ensemble of components that provides two capabilities: a solution to an information management problem that arises in the acquisition of automated data processing (ADP) technology in the Department of Defense (DoD), and a tool for analyzing the dynamics of the regulatory process as reflected in the policy documents and regulations that govern ADP acquisition.

REAS(ON) is at once a general approach to the management of small or medium-sized document collections, a practical means for retrieving information quickly in critical situations, and a working model that can help define special requirements for such systems in other applications.

REAS(ON) may be viewed as a way to eliminate a large part of the paperwork burden that now encumbers regulatory documentation in DoD by centralizing the updating function; only one machine file needs to be kept current instead of the multiplicity of document files presently maintained manually at the Pentagon.

BACKGROUND

The acquisition of ADP equipment by the executive agencies of the Federal Government is controlled by numerous regulations that stem from laws passed by Congress, from Presidential Executive Orders, and from rules promulgated by executive offices such as the Office of Management and Budget (OMB) and the General Services Administration (GSA). Instruments issued by the higher levels of government set overall policy that must be implemented by lower level executive agencies. In DoD, for example, policies and broad-based requirements are passed to the respective military services in the form of directives and instructions, which are implemented by the services through regulations and detailed instructions to subordinate commands. The latter, in turn, issue further, more detailed instructions and guidelines tailored to suit the particular needs and missions of specific command units.

These rules and regulations concern such things as the definition of need for ADP resources, planning, budgeting, reporting, contracting, testing, evaluating,

This work was supported by the Office of the Undersecretary of Defense.

and a host of other activities involved in the acquisition of complex systems.

Including public laws, six levels of regulatory documents are in effect in the Executive Branch, complicated by parallel hierarchies of instructions of three military services and a maze of command-level rules and guidelines. Altogether, over 30,000 pages of regulations are in effect in DoD alone, and 11,000 pages of new regulations or changes to existing ones are issued annually (not counting supplementing and implementing documents issued by units below the command level). Although a relatively small proportion of these pages apply directly to ADP acquisition, the figures show the scope of the paperwork problem that REAS(ON) can help mitigate.

Another complication, one that applies specifically to large ADP systems, is that each acquisition, even of a replacement system, is a new exercise. Because a number of years pass before a system is replaced, one finds that the technology has changed, the rules have changed, and the original acquisition team has been dispersed.

DISCUSSION

The Problem

The problem to be solved is how to select from the large mass of regulations only those that apply to a given computer acquisition program or, on a finer scale, to determine what rules should be followed to carry out a specific task. For example, what are the current rules for evaluating a proposal for contract award? Is cost/price the main criterion, or are other factors more important? Such questions arise frequently in practice, and a great deal of time may be spent searching for answers.

What is needed is an information management system for regulations that would make it possible to

1. Maintain a complete collection of regulatory documents, containing all of the latest changes;
2. Identify documents that govern the major phases of ADP acquisition or broad areas of responsibility as they apply to various organizational units at different levels; and

3. Provide specific answers to specific questions during the course of an ADP acquisition program.

The Solution

The REASON system was developed to satisfy these needs. Its software components are three sets of commercially available computer programs. One set is used to establish an input file of regulatory documents, another is used to convert the input file to a form suitable for information retrieval, and the third provides and controls online retrieval. The software is installed on an IBM 3033 computer.

The Database

The database comprises more than 200 regulatory documents, including a few public laws, several key OMB circulars, and large numbers of DoD directives and instructions, Air Force regulations, and Navy instructions. Army documents may be added in the future.

Most of the documents contain fewer than 10 pages; if so, the entire document is keyboarded into the database. Some, however, may have well over 100 pages; in that case, an extended abstract is prepared and entered along with a table of contents.

Documents were selected in two stages. A core group of documents was gathered by scanning printed indexes for titles that were obviously relevant to ADP equipment acquisition. Then other documents were identified through citations in the core documents.

Document Input Format

As might be expected, documents prepared by different organizations differ widely in style and content. To facilitate retrieval, a certain amount of structure was overlaid on the original documents. For example, exceptions to rules were gathered into a paragraph named "EXCEPT" in order to make them readily available in one place. The same procedure was applied to definitions of special terms that are crucial to the proper understanding of requirements in regulatory documents.

The Online Search System

Information is retrieved from the database by formulating search queries consisting of words that are expected to occur in the desired text. Boolean operators AND, NOT, and OR may be used to link query terms and thereby make searches more specific. In addition, proximity operators, ADJ, SAME, and WITH can relate

query terms spatially, respectively, next to each other, in the same sentence, and in the same paragraph. Also, searches can be restricted to particular portions of documents — for example, titles or abstracts.

To illustrate the retrieval capabilities of the system, let us try to find the answer to the question posed above: "What are the factors to be considered in contract award?" We could formulate the search query as follows (where the query numbers are provided by the program):

00001 factors or considerations
with contract same award

where "factors" or "considerations" is to be in the same paragraph as "contract," which is to be in the same sentence as "award." Twenty-six documents are retrieved. To narrow the search, we add more terms, thus:

00002 1 source adj selection

which tells the program to include "source selection" in the initial query. The result is two documents. One is DoD Directive 4105.62, "Selection of Contractual Sources for Major Defense Systems," which states in part:

In developing the (source selection) criteria the proper balance shall be established among technical, cost, schedule, management, and other factors.

Text preceding and following this statement in the original document adds further relevant information. Selected pages or entire documents may be printed if desired. The system is described in detail in Ref. 1.

The Inventory System

Supporting the REASON database but independent of it is an inventory system that was established to produce lists of database documents by accession number and document number. Such lists are convenient to check document currency when new indexes are received or to check whether a document has already been included in the database. The programs for the inventory system are written in APL (A Programming Language). The inventory system database consists of the accession and document numbers of documents in the REASON database as well as the numbers of the documents cited in them. As the inventory began to take shape, it was found that several interesting features could be built in to make it useful to policy makers and DoD managers in general.

With few exceptions, regulatory documents make important citations of other documents. For example, most regulatory documents cite authority documents. Also, rather than detail a procedure or a requirement, a document will reference another that describes the procedure or requirement. Documents amend, supplement, reference, cancel, supersede, replace, and otherwise relate to other documents by citation. In all, eleven relationships were defined and programmed into the inventory system, together with their reciprocals. Reciprocal relationships exist because for every amending document there is an amended one, for every supplemented document there is a supplementing one, and so on.

As a result, citation networks can be displayed for each document in the database. It now becomes possible to map the extent of the role played by a given document in the regulatory process. Most interesting of the citation networks are authority chains and trees. Heretofore, except through prodigious effort, there was no way to determine to what extent a given policy document was implemented by lower echelons. Now, simple commands in the inventory system construct and display authority trees upward from low-level implementing documents or authority chains downward from high-level policy documents. For the first time, one can visualize the documents that implement a given document or the network of documents that may be affected if a substantive change is made in one of them. Clearly, this is a potent analytical tool for regulatory officials.

Several self-adjusting features have been built into the inventory system to facilitate database maintenance; two are of particular interest. Whenever a document is renumbered, replaced, consolidated into another document, or cancelled, its surrogate is automatically moved to an archival list and every citation to it in the entire database is tagged to show that it is no longer in effect. The other feature concerns changed and revised documents. In certain document series, a suffix or change number is added to the document's number when it is revised. A semiautomated function is available to change all citations in the database to the current document number.

Original documents cannot keep up with changes easily. Many instances have been found where obsolete and cancelled documents are cited as if they were still in force. Changes that are issued to correct individual documents are unsatisfactory because they become lost or, because of the tedium involved in inserting pen and ink changes, are ignored. With REAS(ON), every user

may be assured of access to the most current version of each document in the database.

SUMMARY

REAS(ON) and its adjunct inventory system can serve both Federal acquisitions personnel and regulatory policy officials. Some of the features are useful to both groups, others are of more interest to one or the other.

In a practical operational situation, anyone planning an ADP acquisition can, at will, gather all mentions of a given topic in every relevant document so that he can deal with all requirements related to that topic at once, rather than piecemeal. Knowing in advance the full scope of the requirements that exist for each detail of a proposed acquisition program is a valuable asset to effective planning.

The retrieval of parallel texts from the set of regulatory documents affords important advantages to regulatory officials. It becomes possible to collect all texts dealing with a given requirement to compare them, side by side, for redundancy, conflicts, and other difficulties. The ability to display relationship paradigms facilitates the study of the anatomy of the regulatory documentation system.

Finally, a considerable reduction in paperwork and probability of error, together with a saving in time, may be realized through REAS(ON) and the inventory system because the maintenance of regulatory document files is centralized. As an example of an immediate application, the Pentagon operates a number of self-service document distribution centers. On a recent visit to one, at least half of the documents sought were out of stock. Several that were obtained had one or more pages of changes appended to them. Aside from the mentioned difficulty with pen and ink changes, one can never feel certain when dealing with such a system that all changes are in hand.

REAS(ON), or a similar system, could eliminate redundant files and the manual entry of changes by document users, and could ensure that each document is as current as the most recent update of the single master file.

REFERENCE

- ¹ B. W. Kuvshinoff, *REAS(ON) Manual (Regulatory Environment Assessment System (ONline))*, JHU: API SR 81-2 (Feb 1981).

APL/DATA DICTIONARY SYSTEM

B. J. Pride

Data dictionary systems are usually closely related to one or more database management systems. The INQUIRE Database Management System, installed at APL, lacked an adequate data dictionary system, and therefore the APL/Data Dictionary System (APL/DDS) was developed.

BACKGROUND

A data dictionary is primarily a documentation tool that centralizes and clarifies data definitions and specifications. For example, each field in a database record has the characteristics of name, length, type, position, etc. (A field is a named piece of information in a file or database, and a record is a collection of fields whose values relate to a specific person or thing, such as a personnel record.) This information would be stored in a dictionary along with the field's contextual definition (how data values are to be interpreted). Bringing this information into a central dictionary often reduces the ambiguity that may occur when a field apparently has multiple uses or is associated with multiple databases. For example, suppose an organization has two databases that deal with employees. In each there is a field designated ADDRESS. However, in one database it refers to an employee's home address while in the other it is the employee's office location. In this case, ADDRESS refers to two different pieces of information.

Data dictionary systems have been widely accepted by the data processing industry as the best way to organize information pertaining to the definitions and specifications of a company's data resources. The systems are available commercially, but usually they are designed to have a symbiotic relationship with a target database management system (a set of computer programs that provides an environment for organizing, storing, retrieving, and securing data). For example, the IBM's Data Dictionary DB/DC supports only an IMS database management system and is implemented as an IMS database (IMS is a computer program).

The INQUIRE Database Management System is available to users of APL's IBM 370/3033 computer if their problems are best solved by a database approach (see Ref. 1 for an overview of the system capabilities).

Although data dictionary software was supplied with the INQUIRE system, it was weak in many areas

considered by the Computing Center to be vital for general Laboratory use:

1. The INQUIRE dictionary was not implemented as a database but as a flat file (a flat file has only one data retrieval strategy while a database has many).
2. There was no maintenance program to ensure that the integrity of the dictionary data would be maintained.
3. No facility for securing data was provided.
4. The dictionary report software was inflexible; that is, there was little or no choice of report format or content.

Unfortunately, no commercially available data dictionary system supports the INQUIRE system. To purchase a commercial system would also require the purchase, installation, and maintenance of a second database management system. Thus, the APL/DDS was designed and written as a companion to the INQUIRE system.

DISCUSSION

APL/DDS is a data-resource information-management tool comprising a set of computer programs (software) written in the PL/I programming language and a set of INQUIRE databases, which the software manipulates. The system is divided into two functional areas, definition maintenance and definition extraction.

The APL/DDS database contains information about fields and databases that can be divided into two categories: attributes (such as the physical attributes of length and type) and definitions.

A field's definition is a description of what the value stored in a field represents. For example, suppose there is a field called *X* in a database called *Y*. Further, suppose that the value for *X* in a particular record is 1.5. What can be said, then, about *X*? It is not clear at all what *X* represents. It could be a measurement, an amount, or a code. The field definition information in the APL/DDS will explain to anyone analyzing data from database *Y* how to interpret field *X*.

The definition of a database is a general description of its contents and a statement of the information storage/retrieval problem that the database was intended to solve.

The APL/DDS maintenance program provides the mechanism for storing attribute and definition information in the dictionary database. It examines the attributes, such as field type, for correctness and prompts the operator to correct erroneous information, thus improving the probability that the dictionary's information is correct. The maintenance program is interactive and makes use of the electronic "form-fill-in" capability of the IBM 3270 series cathode ray tube terminal. This capability allows the terminal operator to fill in attribute and definition information with a single prompt. This approach simplifies the use of the maintenance program and further reduces the possibility of errors because the operator has a chance to correct typographical errors before they can enter the dictionary. Also, since it is independent of system response time, there is no loss of train of thought as when the operator must wait for a prompt for each unit of information. Figure 1 is an example of a data dictionary prompt.

Once a database and its fields have been defined to the data dictionary, that information is used in a number of ways by APL/DDS reports and utilities.

Reports

Five standard dictionary reports were written using the INQUIRE query language.* They have three

*One of the attractive features of the INQUIRE system is its query/report-generation language. With this easy-to-use, easy-to-learn, English-like language, users of INQUIRE can produce rather sophisticated reports from their databases (in this case the dictionary) without having had previous data-processing experience.

potential audiences: the Database Administrator, the computer programmer/analyst, and the end user (usually a non-data processing individual who uses data from the end-product database). The standard reports are designed to serve as database documentation, to be used in guides for database usage, and to aid in identifying and preventing data redundancy wherever feasible.

The dictionary documents where fields are used (reports, programs, etc.), so the reports can be used to study the potential impact of planned changes to field attributes.

Database Design and Creation

There are three steps to the implementation of an INQUIRE database: designing it, gathering the data with which it will initially be loaded, and creating it. The data dictionary software can help perform two of these steps.

The Database Administrator designs a database to solve a specific information storage/retrieval problem. Often some of the information he needs in order to solve that problem is not new and already resides in a database. Using dictionary reports, he can determine what data fields already exist and what fields are completely new. He can then decide what new databases must be created, how existing ones can be used in conjunction with the new ones, and whether to duplicate a particular field in the new ones. (This creates what is called controlled redundancy; since it is a known redundancy, programs can be written to ensure the integrity of all occurrences.) Thus the dictionary can

```

COMMAND:                               KEYWORD:
ATTRIBUTE FOR COST      IN FINANCE      DATE:790610
                                ADD PANEL
FIELD FORMAT: n  TYPE OF KEY:          ITEM REQUIREMENT:  FIELD LENGTH: 6
PRINT FORMAT: $k  FIELD TYPE:          PARENT FIELD OR MAX. BOUND:
OFFSET OR CURRENT BOUND:              UPPER LIMIT:
ENGLISH NAME: project cost in thousands of dollars
ORDER IN FDT: 5      DATA DEFINITION CODE: $  ELEMENT STATUS: P
INITIALIZING GROUP: afc  MAINTAINING GROUP: afc
VALIDATION CRITERIA:
SOURCE:

```

Upper case letters: information to be provided
Lower case letters: data that have been filled in

Fig. 1 Sample of an APL/DDS maintenance program prompt.

be used as a decision-making tool as well as a documentation tool (see Fig. 2).

The INQUIRE system keeps the physical attributes of the fields in a special portion of the database called the field definition table (FDT). This table must be supplied by the Database Administrator when he creates a database. All the information required to form the FDT is stored in the APL/DDS database; therefore, a PL/I dictionary utility was written to extract the physical attributes of the fields from the dictionary.

A second dictionary utility (also written in PL/I) uses this FDT and the physical attribute information from the dictionary along with some user-supplied parameters (such as how many records the database will eventually contain) to calculate magnetic storage device (disk) requirements and the control language required to actually create and load the database.

Uses of APL/DDS

More than 50 databases are defined for the APL/DDS, including those that comprise a management information system developed by the Computing Center for Laboratory use, one to track personnel applications, a personnel locator, an IBM 370/3033 computer system log, a hydrogen maser parts inventory, and the two databases that make up the data dictionary itself. These databases were designed and created using the APL/DDS maintenance and utilities programs. Dictionary reports are included as part of the documentation of the management information system.

A generalized maintenance program has been written² that uses data attribute and validation information from the dictionary and IBM 3270 screen layout descriptions from a "screen" database. The program creates an interactive environment that allows a

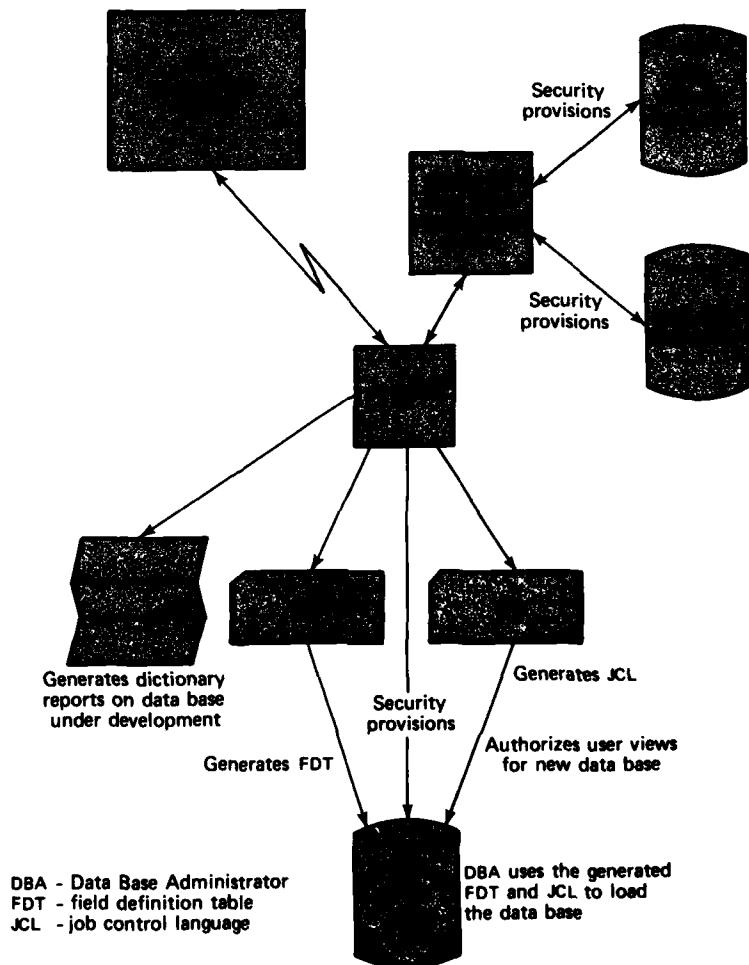


Fig. 2 Example of how the Database Administrator uses the dictionary.

terminal operator to key in additions or modifications; performs any required validation; and then adds, replaces, or deletes records in the target database. Almost any INQUIRE database can be maintained by this one program. Because non-INQUIRE flat files can be defined to the dictionary, the program will maintain those as well.

APL/DDS, like other dictionary systems, is a tool to aid the Database Administrator, the programmer/analyst, and the end user. It is a documentation tool but also paves the way for the effective use of

information, as demonstrated by its interrelationship with the INQUIRE system and the generalized maintenance program.

REFERENCES

- ¹ *INQUIRE Concepts and Facilities*, Infodata Systems Inc. (Dec 1977).
- ² R. R. Potter and B. J. Pride, *Generalized Full Screen Input Package (GFSIP)*, JHU/APL BCS-1-018-80 (12 Jun 1980).
- ³ B. J. Pride, *Applied Physics Laboratory Data Dictionary System (APL/DDS)*, JHU/APL BCS-1-100-79 (1 Oct 1979).

BIOMEDICAL SCIENCE AND ENGINEERING

INTRODUCTION

It was recognized early by The Johns Hopkins University that there had been a dearth of successful efforts to bring organizations with expertise in the physical sciences and engineering, gained from defense and space programs, into medical research and development. It was further recognized that the University was in a unique position to bring this about because three divisions of the University — the Applied Physics Laboratory, the School of Hygiene and Public Health, and the Medical School — are highly competent in their own areas of expertise, spanning the sciences, systems technology, and medicine. It was therefore decided more than a decade ago to institute a collaborative multidisciplinary program on a more general and systematic basis than had existed in the past. This interaction has resulted in many sponsored programs in ophthalmology, neurosensory research, cardiovascular systems, prosthetic devices, radiology and nuclear medicine, biomedical engineering, and health-care delivery.

APL contributions to these collaborative medical programs have been in the areas of instrumentation, theoretical modeling, systems engineering, experiment design, simulation, technique development, and computer applications. The collaborative program runs the gamut from basic physiological research to direct engineering support of the health-care delivery systems at the Johns Hopkins Hospital.

The results of the research and development are reported in the open literature, principally in biomedical, biological, and medical journals. During the program's relatively short life, over 200 papers and book chapters have been published and many instruments for research and clinical application have been developed. APL staff members have assumed line responsibility for Johns Hopkins Medical Institutions in areas where technology can make specific contributions to patient care and to health-care delivery, including radiation physics, clinical information systems, and clinical engineering.

The articles selected for this section show the wide range of APL efforts. There is a report on providing technical guidance for expanding the radiation oncology wing of the Johns Hopkins Oncology Center. An operating system is described for a High Technology Equipment Quality Assurance Program that has been developed for the Johns Hopkins Hospital. In the area of fundamental medical research is a report on studies of structural alterations to the cornea of the eye from exposure to infrared radiation. There is a discussion of biofluid mechanics experiments that are being conducted to appraise the relationship of hemodynamics to the progress of atherosclerosis. The final article describes a programmable implantable medication system for the delivery of medicines in the human body.

Further details of this and other work are reported in the *Biomedical Research, Development, and Engineering Annual Report (JHU/APL MQR)*, which is published in November of each year.

RADIATION ONCOLOGY CLINIC

D. G. Grant

The Division of Radiation Therapy of the Johns Hopkins Oncology Center has recently undergone a major expansion. Three additional therapy treatment rooms were added to the existing facility and new major therapy equipment was installed, resulting in a considerable expansion of the Radiation Oncology Clinic's patient load capability. Major efforts in engineering design by APL were required to complete the expansion.

DISCUSSION

The Division of Radiation Therapy conducts a major cancer therapy clinic that provides both inpatient and outpatient care to approximately 120 patients per day. Therapy sources include two 4 MeV linear accelerators, a dual-mode (X-ray, electron) 10 MeV linear accelerator, a dual-mode 15 MeV linear accelerator, and a cobalt-60 teletherapy source. The clinic also provides major isotopic implant services using radium and radioactive iridium.

To support this project, a radiation shielding design consistent with national standards and the State

of Maryland code had to be developed. Basic requirements were established based on anticipated patient workloads, use and occupancy factors, and material guidelines for a maximum exposure for nonradiation workers of 10 mR per week. The principal concerns were primary radiation barriers and the barriers required to protect against spurious neutron production. Typical barrier requirements were 6 ft of concrete with 8 in. of embedded steel. The neutron barriers were designed into the room doors (i.e., 6 in. of borated polyethylene and 1 in. of lead).

Radiation surveys conducted in the facility in June 1980 (Fig. 1) indicated that all levels are well within facility design goals and national recommendations.¹ Certification for use of the facility has been obtained from the State of Maryland.

As a part of the radiation therapy expansion, three additional machines were purchased: two high-energy linear accelerators (Fig. 2) and a therapy simulator. The APL Physics Group was responsible for all technical aspects of room preparation. Complete engineering requirements for installation (electrical power, heating, ventilating, air conditioning, etc.) as well as

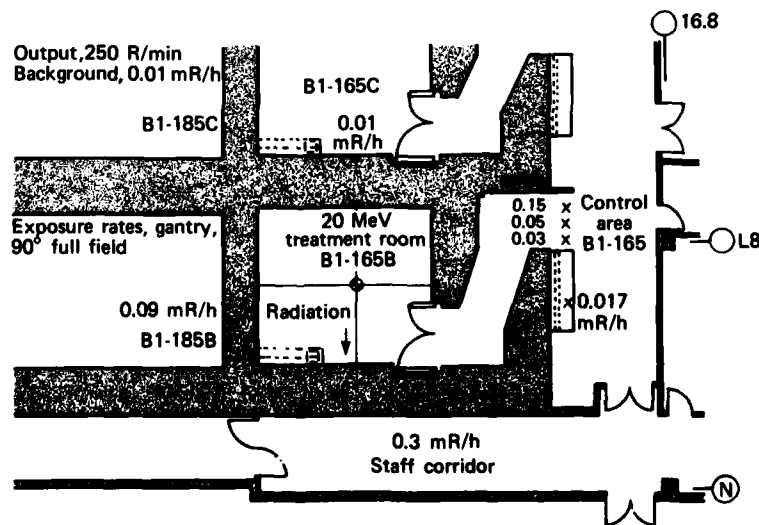


Fig. 1 Radiation survey results, Clinac-20 room.

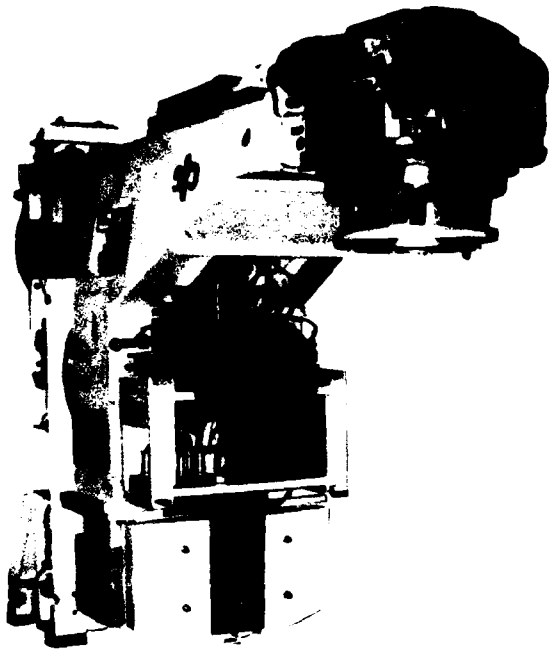


Fig. 2 Varian Clinac-20 dual-mode linear accelerator after completion of the engineering installation.

physical and functional layouts were developed and provided to the architects and engineers for integration into the facility design. This project required considerable coordination among vendors, architects, plant engineers, hospital administrators, construction project managers, and contractors.

As of September 1980, all major equipment had been installed, calibrated, and certified and is now in use.

REFERENCE

- ¹ *Structural and Shielding Design and Evaluation for Medical Use of X-rays and Gamma Rays of Energies up to 10 MeV*, National Council on Radiation Protection report 49 (1976).

HIGH TECHNOLOGY EQUIPMENT QUALITY ASSURANCE PROGRAM

D. G. Grant (APL) and T. M. Judd and
J. T. Lalmond (Johns Hopkins Hospital)

The Johns Hopkins Hospital (JHH), in collaboration with The Johns Hopkins University Department of Biomedical Engineering and APL, has established an institution-wide High Technology Equipment Quality Assurance (HTE/QA) Program. The program was established to assure the hospital that the high technology devices and systems used directly in patient care are both safe and effective.

The program has achieved operational status and was officially turned over to the JHH Clinical Engineering Services group on July 1, 1980.

This work was supported by the Johns Hopkins Hospital.

BACKGROUND

Modern health care is a technology-intensive activity that requires comprehensive control policies to assure the safe and effective use of medical equipment. Although Federal legislation in recent years has addressed the problems associated with the design and manufacturing processes of such equipment,¹ it is recognized that many of those problems are related to maintenance and user procedures.² The impetus for a program addressed to the problems came as a result of concepts developed by Richard J. Johns, Director of the Department of Biomedical Engineering, and Joe T.

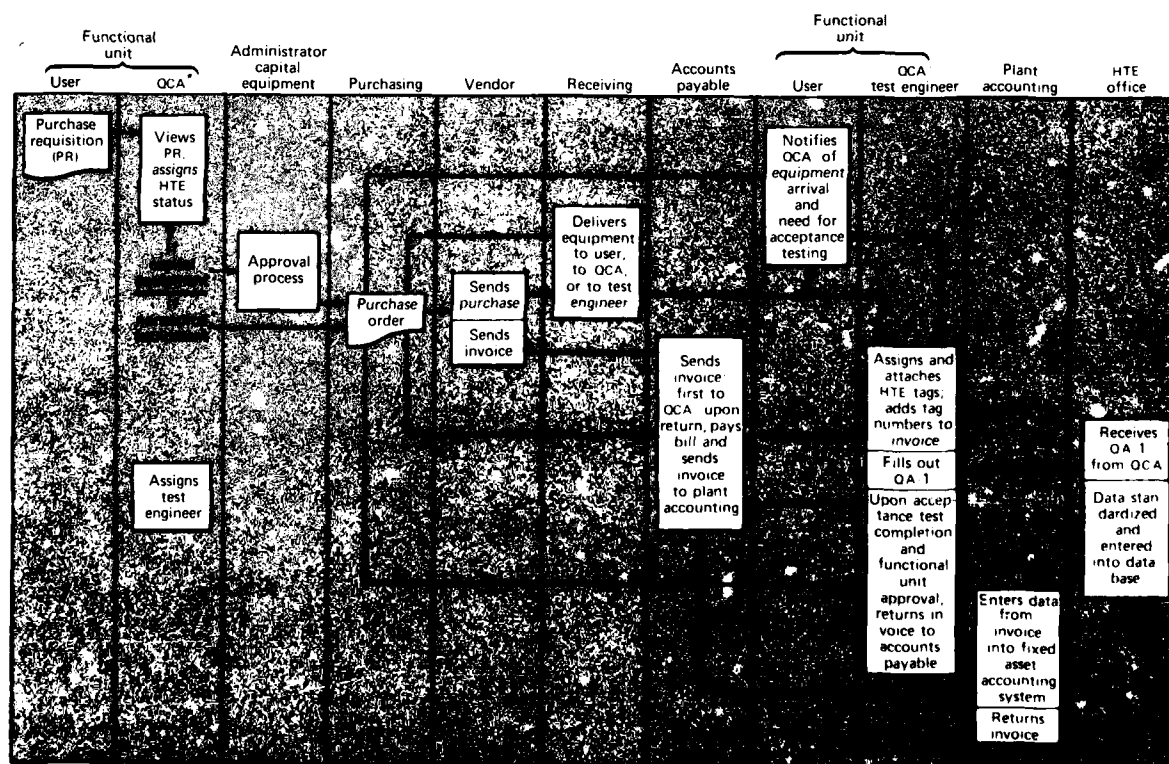
Massey, Director of the Biomedical Programs Office of APL. Their efforts, along with those of Richard W. Trompeter of Facilities Management and Engineering Services (JHH) and Donald J. Manchak of Materials Management (JHH), led the Johns Hopkins Medical Board in 1977 to recommend the establishment of the HTE/QA program. Close collaboration among the JHH administration and functional unit administrators, the Department of Biomedical Engineering, and APL has been maintained throughout the effort.

DISCUSSION

Establishment of the HTE/QA program required the development of a number of resources not previously available to the hospital. A comprehensive inventory of all patient-related high technology equipment was first developed using the hospital's computing system. All equipment has been physically tagged, and specific equipment identification/classification information has been entered into the data base. The inventory and the associated new equipment data capture system (Fig. 1) form the basis for the program's scheduled service-verification reporting system and the

equipment history file. Considerable effort has been devoted to updating and certifying data base entries, which currently comprise more than 4800 active items.

Each month, clinical functional units receive a computerized statement indicating which equipment is scheduled for a quality assurance transaction (e.g., preventive maintenance). The list is generated automatically based on acceptance test dates and scheduled service intervals in the basic inventory record. Entries in the monthly statement must be verified by the functional unit as having been completed, the statement is returned to the program office, and the new information is then incorporated into the data base. The reporting system provides the functional unit with a complete current inventory of the high technology equipment, a comprehensive status report relative to the HTE/QA program, and a detailed maintenance history on each piece of equipment. Equipment failure rates and maintenance costs can be determined as a management aid for making informed capital procurement decisions. The phase of the program described above became operational for all clinical functional units in May 1980.



* Quality Control Administrator

Fig. 1 Flow chart of the HTE/QA data capture system.

For a successful program, functional units must be in a relatively high state of compliance. However, the heart of the program lies in the written standards and procedures used to maintain equipment and verify its performance. This represents an enormous undertaking to cover the entire data base. Many standards have been written by the hospital's engineering staff while others have been obtained from vendors and engineering service groups. The acquisition and maintenance of these records is essential if the HTE/QA program is to have a positive effect on the hospital. At present, 250 written procedures have been obtained for a thousand different kinds of equipment. A manual containing all written procedures used hospital-wide is maintained in the HTE/QA office.

Computer operating costs for the system are extremely low. Based on the first several months of opera-

tion, a cost of \$900 per year for the entire institution is projected, which is about 20 cents per item per year.

In summary, the HTE/QA program has provided the institution with a low cost, effective, quality assurance tool. A detailed summary of the program is contained in Ref. 3.

REFERENCES

- ¹ *Medical Device Amendments of 1976*, House of Representatives report by the Committee of Interstate and Foreign Commerce (Feb 1976).
- ² *Medical Devices: A Legislative Plant, Study Group in Medical Devices* (Cooper Report), Department of Health, Education and Welfare (Sep 1970).
- ³ T. M. Judd, J. T. Lalmond, and D. G. Grant, *The Johns Hopkins Hospital High Technology Equipment (HTE) Quality Assurance Program*, JHU/APL SR 80-4 (Aug 1980).

STRUCTURAL CORNEAL ALTERATIONS FROM EXPOSURE TO INFRARED RADIATION

C. B. Barger, R. L. McCally, and R. A. Farrell

We have used histological methods to determine the endothelial damage thresholds for exposure of rabbit cornea to CO₂ laser radiation. We also have used experimental and theoretical methods to show that the peak endothelial temperature achieved at those thresholds is essentially the same as that achieved by the corneal epithelium at its damage threshold.

BACKGROUND

The cornea is the transparent front wall of the eye. From front to back, it consists of a tear layer (6 μm thick), five or six layers of cells called the epithelium (40 to 50 μm thick), the collagenous stroma (which comprises 90% of the corneal thickness), and a single layer of cells called the endothelium (about 5 μm thick). The endothelium regulates the transport of fluids across the cornea in order to maintain hydration at a proper level

so that the cornea is transparent. Endothelial failure results in swollen, opaque tissue.

The hazardous effects of CO₂ laser radiation (10.6 μm) on the cornea are well documented.^{1,2} Some 98% of this radiation is absorbed in the frontmost 40 μm of the cornea; consequently, epithelial damage has received the most attention up to now. The first indication of epithelial damage is the presence of a relatively faint, grayish-white area that appears within about one hour after exposure. Previous workers have determined threshold-lesion intensity levels for epithelial damage as a function of exposure time for exposures from about 1 ms to several minutes.^{1,2} Such threshold exposures usually raise the temperature at the epithelial surface (more precisely, 6 μm below the anterior tear surface) by some 35 to 55°C.

Heat conduction causes part of this thermal insult to spread to the endothelium^{3,4}; evidence of altered endothelial integrity following exposure at or slightly above the epithelial damage threshold has been reported.⁵ In addition, there are ever-increasing in-

This work was supported by the U.S. Army Medical Research and Development Command.

dustrial and military uses of other lasers, which operate at shorter infrared wavelengths (e.g., holmium at 2.06 μm and erbium at 1.54 μm). Radiation at those wavelengths would also be strongly absorbed by the water of the cornea although not nearly as strongly as the 10.6 μm radiation. The absorption length of the radiation in water at the shorter wavelengths is comparable to or even larger than the thickness of the cornea so that this radiation would penetrate the cornea and cause a more uniform temperature increase throughout its depth.

In general, one would expect the more uniform heating to produce endothelial damage at or below the epithelial damage threshold, especially if the endothelium were more sensitive than the epithelium to temperature increases. Human endothelial repair appears to come about when existing undamaged cells slide and enlarge to fill the gap.⁶ However, repeated exposures in an unprotected environment could lead to permanent corneal clouding because of the impaired ability to maintain normal hydration.

DISCUSSION

We tested the preliminary evidence⁵ of altered endothelial integrity resulting from exposures to CO_2 radiation near the epithelial damage threshold. To accomplish this, we determined the endothelial damage threshold exposure for three peak irradiances with TEM_{00} (Gaussian beam profile) CO_2 laser radiation. The irradiance levels were 24.5, 10.0, and 3.6 W/cm^2 . Endothelial damage was determined in the Eye Pathology Laboratory of the Wilmer Institute of the Johns Hopkins Medical Institutions by Dr. W. R. Green, using a staining method.⁴ Light micrographs of normal and damaged endothelial cells are shown in Fig. 1. Our threshold determinations are plotted in Fig. 2. These exposure times for endothelial damage thresholds are ten or more times greater than those that caused epithelial threshold damage.^{1,2} Therefore, the suggestion in Ref. 5 that endothelial damage might occur near the epithelial damage thresholds is not true for these power densities.

In order to gain a better understanding of endothelial damage caused by exposure to infrared radiation, it is important to know the endothelial temperature-time history. We elected to calculate the changes from the heat flow equation, assuming that the thermal properties of cornea can be approximated by those of water. The theoretical predictions are summarized in Refs. 3 and 4 for erbium, holmium, and CO_2 lasers. The theoretical model is tested by measuring endothelial temperature changes in excised rabbit corneas that are irradiated by a CO_2 laser operating in the TEM_{00} mode.

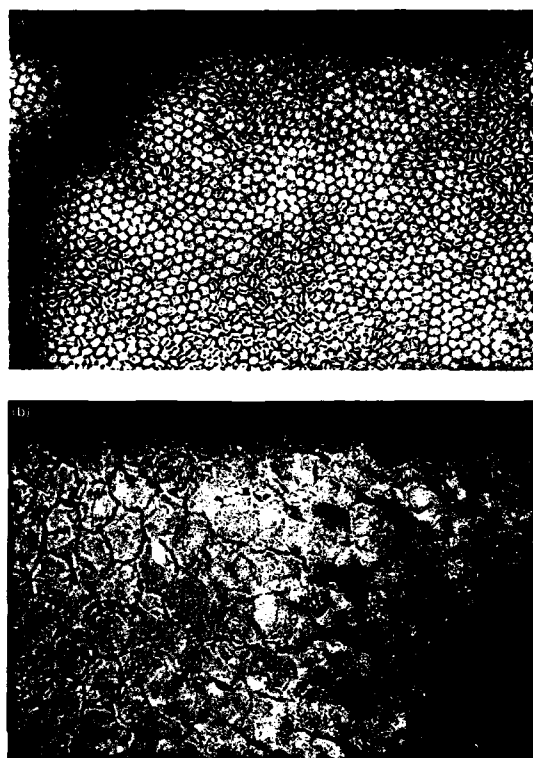


Fig. 1 Light micrographs of normal and damaged endothelial cells. (a) Apparently normal cells near the beam axis for an exposure of 10 W/cm^2 for 4.56 s (about 90% of the damage threshold time). (b) Highly magnified edge of lesion produced by an exposure of 10 W/cm^2 for 5.24 s (near the damage threshold time). Note the normal cells on the left. The borders of the damaged cells on the right vary from heavily stained to completely unstained.

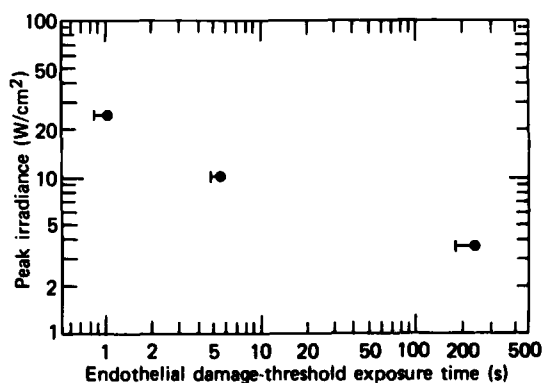


Fig. 2 Peak irradiance versus endothelial damage threshold time. Dots indicate minimum time for which damage was observed. Partial error bar extends to longest exposure for which no damage was observed. (Sixteen rabbits were used at 3.6 and 10 W/cm^2 ; five were used at 24.5 W/cm^2 .)

The calculated temperature changes are based on a Green function solution to the conduction equation,⁷ and the experimental temperatures are obtained using either a thermocouple or a liquid crystal technique. The thermocouple measures temperatures over a wide range but only at a single position in space. In contrast, the liquid crystal method has a limited practical operating range and is less precise but measures temperatures over the entire endothelial surface.

Some results of the thermocouple measurements are presented in Fig. 3. The exposure time (0.104 s) in Fig. 3a is approximately that of an epithelial damage-threshold exposure for the 24.0 W/cm² peak power density. We found that the concomitant 5 to 6°C endothelial temperature increase was insufficient to cause damage. The longer, 1.04 s, exposure shown in Fig. 3b resulted in a 45°C temperature increase. This was the shortest exposure that caused endothelial damage at this peak power density (cf. Fig. 2 and Ref. 4). The reasonable agreement between calculated and measured temperatures from both techniques assures that the theoretical values can be used to interpret endothelial damage *in vivo* and to predict results for other infrared laser systems.

The calculated temperature-time histories of the endothelium at damage-threshold exposures show that it experiences temperature elevations of 30 to 50°C. At the exposure threshold for damage to the epithelium, the temperature also increases about 40°C, depending on the position within the epithelium and the exposure time.¹ Thus the two cellular layers have similar temperature sensitivities. Because of this, we point out in Refs. 3 and 4 that the endothelium may indeed be susceptible to damage from other infrared laser systems at exposure levels for which they produce threshold epithelial damage.

REFERENCES

- ¹ D. E. Egbert and E. F. Maher, *Corneal Damage Thresholds for Infrared Laser Exposure—Experimental Data, Model Predictions, and Safety Standards*, USAF School of Aerospace Medicine, Brooks AFB, SAM-TR-77-29 (Dec 1977).
- ² A. S. Brownell and B. E. Stuck, "Ocular and Skin Hazards from CO₂ Laser Radiation," *Proc. Ninth Army Science Conf.* (Jun 1974).

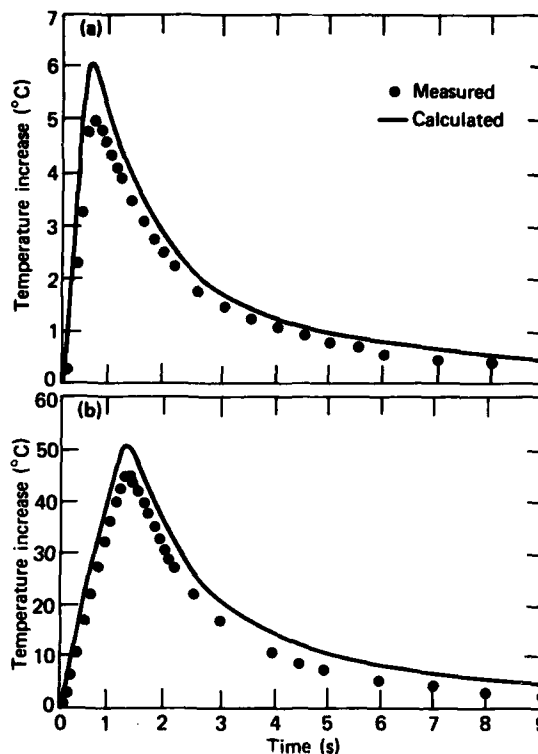


Fig. 3 Endothelial temperature increase as a function of time. The measured corneal thickness was 0.38 mm. (a) The duration was 0.104 s. (b) The duration was 1.04 s. The exposure corresponds to the threshold for endothelial damage.

- ³ C. B. Barger, R. L. McCally, and R. A. Farrell, "Calculated and Measured Endothelial Temperature Histories of Excised Rabbit Corneas Exposed to Infrared Radiation," *Exp. Eye Res.* 32, pp. 241-250 (1981).
- ⁴ C. B. Barger, R. A. Farrell, W. R. Green, and R. L. McCally, "Corneal Damage from Exposure to Infrared Radiation: Rabbit Endothelial Damage Thresholds," *Health Phys.* 40, pp. 855-862 (1981).
- ⁵ E. S. Beatrice and B. E. Stuck, "Ocular Effects of Laser Radiation: Cornea and Anterior Chamber," AGARD Lecture Series No. 79 on Laser Hazards and Safety in the Military Environment, p. 5-1 (1975).
- ⁶ D. L. Van Horn and R. A. Hyndjiuk, "Endothelial Wound Repair in Primate Cornea," *Exp. Eye Res.* 21, pp. 113-124 (1975).
- ⁷ H. C. Chang and K. G. Dedrick, "On Corneal Damage Thresholds for CO₂ Laser Radiation," *Appl. Opt.* 8, pp. 826-827 (1969).

STENOSIS HEMODYNAMICS AND ENDOTHELIAL RESPONSE

V. O'Brien, O. J. Deters, F. F. Mark, and L. W. Ehrlich (APL) and K. Sagawa and G. M. Hutchins (JHMI)

The objective of this program is to find out how blood fluid mechanics affects the local arterial wall in an effort to determine the factors influencing the development of atherosclerosis. Our three-pronged approach uses animal experiments, theoretical modeling, and laboratory experiments. During this reporting year, we measured the detailed spatial distribution of velocity components of flows in a transparent laboratory model of a stenosis (arterial occlusion).

BACKGROUND

Atherosclerosis is a life-threatening disease that takes a long time to develop to the crisis stage where an atheromatous plaque completely occludes a major artery. Clinicians are interested in the mechanisms of the development so that therapeutic intervention might prevent, or at least slow down, the growth of stenoses. Because of the focal tendency of atheromatous lesions, it has been widely accepted that local flow factors are involved in the lipid deposition process that causes narrowing of the arteries.¹ Indeed, there is evidence that extreme, acute, fluid mechanical stresses in living animals can cause marked changes in the endothelial cells (in the arterial wall), which may affect lipid deposition; however, the relationship to the chronic (long-term) lipid deposition process is not clear.¹

Because of the complexity of the problem, we have developed a multiple approach that includes animal experiments, computer modeling, and detailed flow measurements in transparent model stenoses. We chose dogs for the animal experiments because they do not develop atherosclerosis when fed their normal diet. Thus we could induce an ideal ring stenosis by surgically implanting an electromagnetic flow meter in a young dog to constrict the artery smoothly as the dog grows (Fig. 1). The procedure has several advantages. By creating ideal stenoses in healthy dogs, the lipid-free (normal) wall response can be described and correlated with the flow. The results will provide a basis for comparison to the lipid involvement when dogs in a similar situation in future experiments are fed a fatty diet and develop the disease. The local axisymmetric flow fields created in this manner reduce the fluid

mechanical part of the problem to a tractable, time-dependent, two-dimensional calculation. Finally, the flow meter for *in vivo* measurements is already in place.

It is not feasible to measure all the required flow parameters in living dogs. However, if the cyclic volume flow is recorded (via the electromagnetic flow meter) and the geometry is known (from an X-ray picture), the flow field can be synthesized completely from a theoretical flow solution. But the nonlinear equations governing the pulsatile flow can only be solved in numerical approximation.² Thus, in order to have confidence in the calculations, we have validated the method by velocity measurements in a model stenosis.³ A description of this aspect of our program follows.

DISCUSSION

A transparent model of a constricted artery was manufactured and installed in a flow system in the APL Biodynamics Laboratory. Laser light scattered from tiny tracer particles suspended in the fluid was processed to provide fine space and time resolution of the velocity components in the vicinity of the model stenosis. The measurement technique, laser Doppler velocimetry (LDV), allows time-dependent measurement of forward and reverse flows, even very close to the wall.⁴

The gravity-driven flow is provided with an adjustable return pump so that steady-state operation can be obtained at a given Reynolds number. The periodic flows are produced by a rotating valve in the flow line.

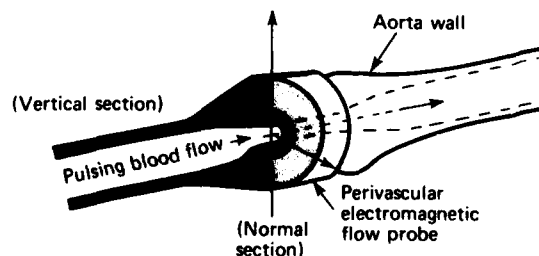


Fig. 1 Induced canine stenosis with a chronically implanted perivascular electromagnetic flow probe.

First we considered steady flows, which are simpler to measure and calculate. Among the features predicted for such flows is a separated (recirculation) region that appears at moderate Reynolds numbers in constrictions that mildly occlude the tube.^{2,3} Figure 2 shows normalized, measured, centerplane, axial velocity profiles (u); at left is the parallel inlet flow, in the center is the throat profile, and on the right is $u(r)$ at a z station within the separated region (indicated by negative velocities near the wall). The actual centerline velocity, u_c (indicated by the numerical values) is greater for the latter two stations than for the inlet value. The zero crossing and the radius of the most negative axial flow velocity can be determined at other z stations where the wall is parallel to the axis. Within the stenosis, u' , the velocity component parallel to the wall at the given z can be measured by turning the plane of the intersecting laser beams. This allows the separation point to be located and compared to the theoretical prediction where the curves $u' = 0$ and the curve of null vorticity ($\partial u' / \partial r = 0$ essentially) intersect the wall (cf. Fig. 3).

Time-dependent measurements for pulsatile flows have also been made, with the correlator operating in the signal averaging mode. The sweep is triggered each period. The incoming signal for each cycle is collected in 300 equal time bins, and 300 to 600 cycles are averaged at each measuring point in order to achieve an adequate signal-to-noise ratio. Separated regions are apparent from the negative axial velocity measurements near the wall, but these regions are time-dependent.³ The comparison with theory is not straightforward but proceeds on the assumption that the measured centerline inlet velocity is exact. This work is still in process.

In vivo measurements of the time-dependent flow, provided by the implanted electromagnetic flow meter, are used as inputs for the theoretical pulsatile flow calculations to describe the (unmeasurable) detailed flow patterns. The calculations are rather sensitive to the volume flow rate provided by the flow meter so it must be calibrated dynamically for unsteady flow. LDV data will provide this measurement to complement the quasi-steady calibration *in situ*.

REFERENCES

¹ F. B. Gessner, "Hemodynamic Theories of Atherogenesis," *Circ. Res.* 33, pp. 259-266 (1973).

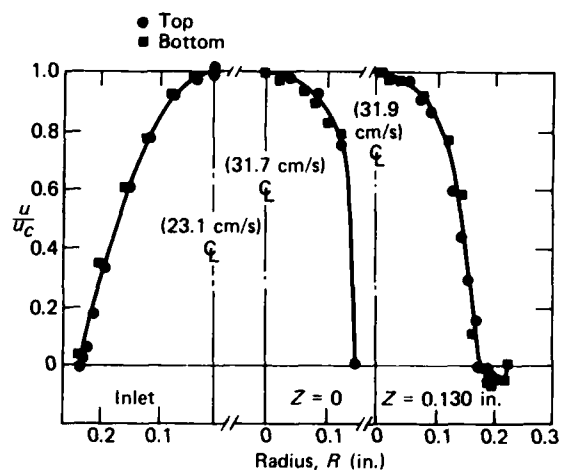


Fig. 2 LDV measurements for steady flow through an axisymmetric stenosis of 50% areal occlusion. Axial velocity profiles are presented at various locations. (Centerline velocities, u_c , are given in parentheses.)

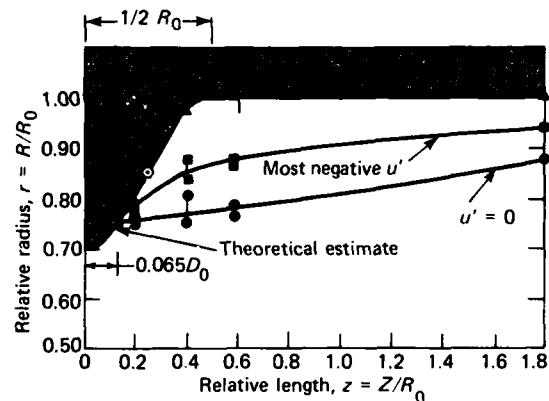


Fig. 3 Locating the separation point in the stenosis (R_0 is the inlet radius). The small solid points are measured data. The separation point is between the throat and the encircled point of inflection of the wall boundary.

² V. O'Brien and L. W. Ehrlich, "Variation of Wall Shearing Stress with Arterial Geometry," *Proc. 32nd Annual Conf. on Engineering in Medicine and Biology*, p. 145 (1979).

³ V. O'Brien and L. W. Ehrlich, "Pulsatile Flow Through a Constricted Artery," *Biofluid Mechanics 2*, D. J. Schneck (ed.), Plenum Press, New York, pp. 497-516 (1980).

⁴ O. J. Deters, C. B. Barger, G. M. Hutchins, F. F. Mark, and M. H. Friedman, "Velocities in Unsteady Flow Through Casts of Human Arteries," *Proc. 32nd Annual Conf. on Engineering in Medicine and Biology*, p. 101 (1979).

THE PROGRAMMABLE IMPLANTABLE MEDICATION SYSTEM

R. E. Fischell and W. E. Radford

The Programmable Implantable Medication System (PIMS) consists of an implantable programmable infusion pump (IPIP) and the necessary support equipment. The IPIP will be used to treat a variety of chronic diseases, one example being the delivery of insulin to the diabetic. During the past year, several significant milestones in the development of the hardware have been reached.

BACKGROUND

The technology of devices that can be implanted in the human body has progressed to where it now appears practical to provide selected patients with an

IPIP for the treatment of a variety of chronic diseases, for example, diabetes. There are about a million Americans who require one or more daily injections of insulin. The IPIP would make it possible to provide more precise metering of the insulin into the patient's body so that there would be enough in the blood immediately following meals and there would not be too much when the patient has not eaten for a long time or has had physical exercise (as is now the case with daily injections).

Other patients who might benefit from the use of IPIP therapy would be those who have (a) inoperable malignant tumors (treated locally with chemotherapeutic drugs), (b) hemophilia (treated with Factor 8), (c)

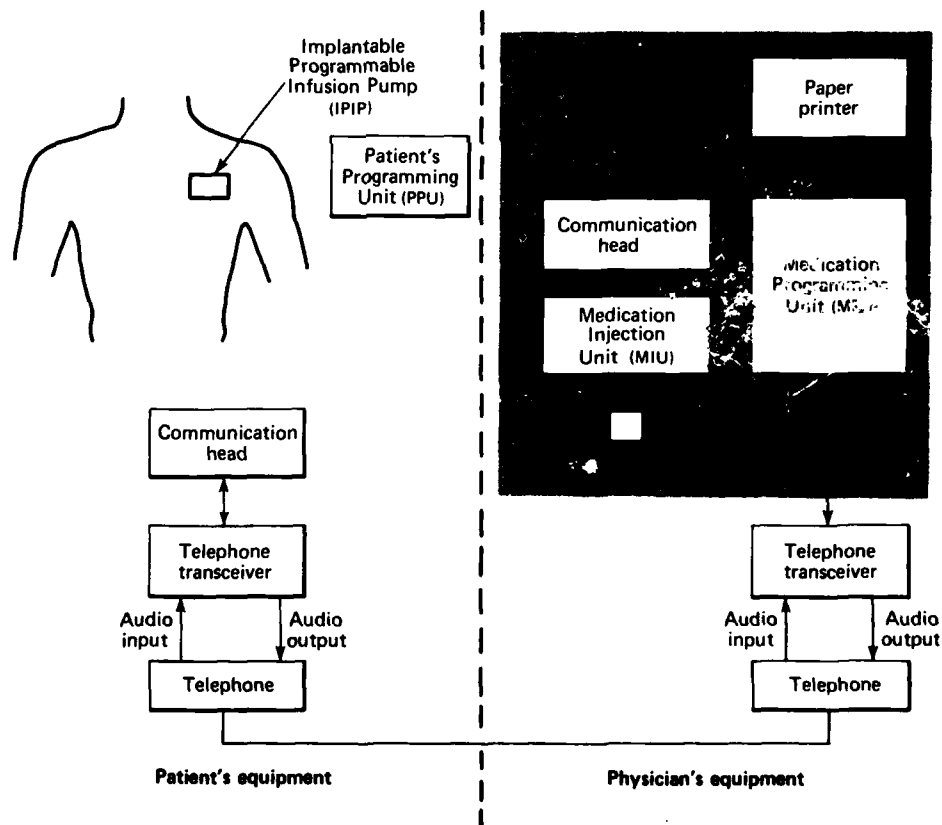


Fig. 1 Block diagram of PIMS.

recurring blood clots as in phlebitis (treated with Heparin or salicylic acid), (d) drug addiction (treated with methadone), (e) alcoholism (treated with Antabuse), (f) intractable pain (treated with opiates into the cerebrospinal fluid), (g) hypertension (treated with antihypertensive drugs), (h) epilepsy (treated with Dilantin), (i) mental illness (treated with lithium or neuroleptic drugs), and (j) thalassemia (treated with desferrioxamine).

DISCUSSION

PIMS will make use of previous work on microminiaturized command, telemetry, and programming systems for the human tissue stimulator. That technology will be combined with new concepts to provide a safe, reliable, and effective system for infusing a variety of medications into the body.

Figure 1 is a block diagram of PIMS showing both the patient's and the physician's equipment. The IPIP, the implanted device, is programmed by the physician, but additional programming can be performed (at the physician's option) by the patient himself. The patient's programming unit is a pocket-sized device used by the patient to communicate with

the IPIP. It will command the IPIP to deliver accurately metered medication dosages (such as a specific profile of insulin after a meal) into the patient. The physician will have a medication programming system, which consists of a "smart" terminal called a medication programming unit to be used by him to program the IPIP; a medication injection unit, which injects the medication fluids into the IPIP under control of the medication programming unit; and a paper printer, which provides a permanent record of the medication injection and IPIP programming. Communication between the IPIP and the medication programming unit can also take place by means of telephone transceivers, as shown.

Within the last year, an IPIP has been assembled in breadboard form and has operated according to design. Medication programming and injection units have been built, as has an operating pump that delivers about 2 μ l of liquid per stroke. Septum material for the IPIP has been tested and was shown to be able to last more than 50 years under ordinary usage. The battery required to power the IPIP has been developed and built and is now being tested. Finally, custom-built large-scale integrated circuits for the IPIP have been designed and ordered, and some have been received at APL.

FUNDAMENTAL RESEARCH

INTRODUCTION

Fundamental research has been firmly established at APL for many years as one of the principal missions of the Laboratory. These missions include the application of advanced science and technology to the enhancement of the security of the United States and the pursuit of basic research to which the Laboratory's facilities can make an especially favorable contribution. The incorporation of basic research into the Laboratory's mission recognizes that such research will play a vital role in future technological achievements and that it is needed to avoid institutional obsolescence.

Much of the basic research conducted at APL is done in the Research Center, which was formally established in 1947. Its initial objectives, still valid today, were to establish APL as a contributor to scientific knowledge, to develop and provide fundamental understanding basic to fields of present and potential interest to the Laboratory, and to enhance the professional competence of its staff by serving as a doorway to science. Since its inception, the Research Center has spawned new programs that are now carried out in other units of the Laboratory. Most notable of these are the genesis of the Space Department and the Biomedical Research Program.

Today, the Milton S. Eisenhower Research Center is comprised of 60 staff members organized into eight groups. These scientists report their research in the professional scientific literature and, typically, 60 papers are published each year. The articles in this section describe some recent accomplishments. The surface science program is represented by an article on the gases emitted during the pitting corrosion of aluminum. It provides basic insights into the mechanism of corrosion, a problem of great importance to the Navy. The article on surface diffusion and spin polarization, from the heterogeneous chemistry program, provides the framework for distinguishing between chemical reactions that occur on the surface of a material and those that occur in the bulk phase. The article on surface-enhanced Raman scattering arises from the photochemistry and spectroscopy program. This recently recognized phenomenon has potential use for probing surface states and chemical reactions on surfaces; thus a fuller understanding of its underlying mechanism is important.

The program on new methods in wave physics is represented by an article on the development of a variational principle applicable to the scattering of electromagnetic radiation from objects with random characteristics. Such variational principles provide powerful computational methods for such problems as radar scattering from the ocean surface or from chaff. This contribution is also significant because it is one result of a collaboration between the Research Center and the Fleet Systems Department. The article on vibrational frequencies of composite structures, from the mathematical sciences program, details the first rigorous computation of upper and lower bounds of the vibrational frequencies of such structures.

The research effort in materials science is represented by two articles, one on spin glasses and another on electrical switching and memory phenomena in organic semiconductor films. The spin glass research has provided a theoretical model that predicts the characteristics of the phase boundaries of amorphous magnetic alloys, predictions that agree with recent experiments. The switching in organic films, which compares favorably with that in inorganic amorphous semiconductors, is interpreted in terms of the bulk properties of the film material.

These articles represent only a few of the research areas being investigated. Programs in solid-state physics and optical physics have been described in previous *Accomplishments* volumes.

Other Research Center accomplishments are reported elsewhere in this volume. They include the work of Bird on magnetic levitation (in the Space Science and Technology Section), the work of Hunter on the propagation of fires (in the Energy, Environment, and Urban Technology Section), and the work of Barger, McCally, and Farrell on infrared damage to the cornea and of O'Brien et al. on the mechanics of pulsatile blood flow (in the Biomedical Science and Engineering Section).

GASES EVOLVED DURING THE PITTING CORROSION OF ALUMINUM

C. B. Barger and R. C. Benson

Methods of corrosion protection are often found by first understanding the chemical reactions of a metal with its environment. In an effort to gain information about the behavior of aluminum in various aqueous electrolytes, we have determined the composition of the gases evolved during the pitting corrosion of this important structural metal. The rather surprising results help elucidate pitting mechanisms and reactions.

BACKGROUND

In our initial aluminum corrosion experiments, we observed blister formation as a step in the breakdown of the passivating oxide in chloride solutions.^{1,2} Such blister formations require gas production at the oxide/metal interface. The present research examines this gas production more closely. Aluminum is known to undergo pitting corrosion in the aqueous electrolytes KCl, KSCN, and NaNO₃. We have shown that during corrosion the gases evolved from the pits are unique for each electrolyte.³ In addition, we observed that the gas evolution begins when the potential of the metal is increased above a specific value known as the pitting potential, E_p , and ceases when the potential is decreased below E_p . E_p has been determined to be about -0.8 V (all potentials are referred to the saturated calomel electrode) for 1 M Cl⁻ electrolytes and about 1.46 and 0.96 V for 1 M NaNO₃ and 1 M KSCN, respectively. The gases evolved from the NO₃⁻ and SCN⁻ electrolytes can only be explained by the direct reaction of the anion with the metal. These results may imply that Cl⁻ reacts with the metal directly.

DISCUSSION

Two separate experimental setups were used, one for the gas collection and identification experiment and one for observation through a microscope of gas evolving from the pits. For the gas collection experiment, 99.99% pure aluminum was machined into a cylinder about 1 cm high and 1 cm in diameter. It was screwed onto a Teflon holder that sealed the electrical connections from the electrolyte. For the light microscope observations, 0.25 mm thick disks of aluminum, 99.999% pure, were placed in an electrode holder as described previously.² Samples for both experiments were degreased in acetone.

Deionized water of 18 M Ω -cm resistivity and A.C.S. reagents (highest purity available) were used to prepare the electrolytes, which were deaerated with high purity argon before the gas was collected. The gas collection apparatus (a glass tube with a bell-shaped piece on the end) was evacuated and filled with electrolyte, which was subsequently displaced by the 1 to 2 cm³ of evolved gases. The gases were passed through a trap at -50°C to remove water before they entered the gas analyzer (VeeCO Model SPI-10). After the experiment, the trap was warmed to room temperature, and the gases from it were analyzed. Only water was detected.

The sample potential was controlled potentiostatically. The reference electrode was a saturated calomel electrode connected by a bridge of the electrolyte through a Luggin capillary placed about 1 mm from the sample surface.

The mass spectrum of the gas collected from pitting aluminum at a potential of 1.5 V in 1 M KCl is shown in Fig. 1a. The spectrum shows the presence of H₂ and the deaeration gas, Ar, which is always present (Ar⁺ at $m/e = 40$ and Ar⁺⁺ at $m/e = 20$, where m/e is the mass-to-charge ratio). Electrode potentials between -0.5 and +1.5 V were investigated. The gas evolution increased with increasing electrode potential (increasing current). For all potentials above E_p , only H₂ and Ar were detected. This is surprising since hydrogen production via the normal route of $2H^+ + 2e \rightarrow H_2$ should be impossible at an anode potential of 1.5 V. Indeed, oxygen production (via $2H_2O \rightarrow O_2 + 4H^+ + 4e$) is to be expected at this potential. However, in all cases, O₂ was not observed above the weak background signal. Pickering and Frankenthal⁴ had also observed hydrogen evolution at controlled high potentials (1.2 V) during the pitting corrosion of iron and stainless steels. Their explanation includes a high-resistance path resulting from a constriction in the pit caused by a gas bubble.

The mass spectrum of the gas collected from pitting aluminum in 1 M KSCN at a potential of 1.2 V is shown in Fig. 1b. The main components were H₂ and CH₄ (Fig. 1c shows the spectrum of pure CH₄), with weaker peaks at 28, 32, 33, and 34 m/e . (It should be noted that the background signal was negligible at this sensitivity.) The distinctive odor of H₂S was present, and the qualitative analysis of the solution after pitting was positive for the soluble sulfide. Hence, the 32 to 34 m/e peaks are probably due to the small amount of H₂S

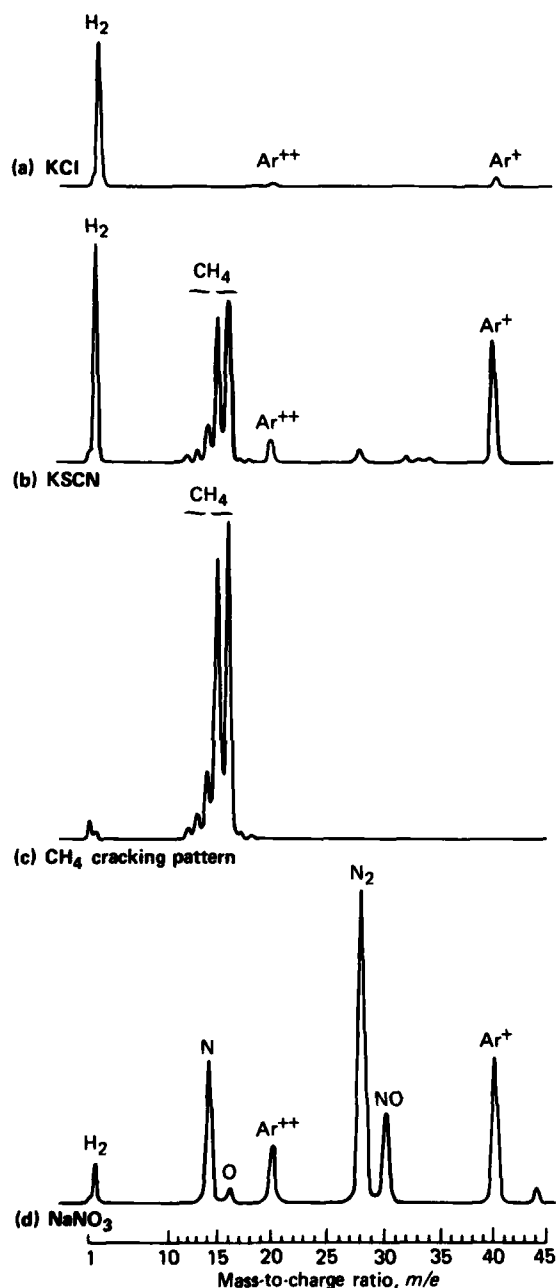


Fig. 1 Mass spectra of the gases evolved during the pitting corrosion of aluminum under the conditions indicated: (a) 1 M KCl at a potential of 1.5 V, (b) 1 M KSCN at a potential of 1.2 V, (c) spectrum of pure methane, and (d) 1 M NaNO₃ at a potential of 2.0 V.

that escaped the water. The 28 m/e peak could be either N₂ or CO.

Figure 1d shows the mass spectrum of the gases evolved from pitting aluminum in 1 M NaNO₃ at a potential of 2.0 V. The gases are H₂, N₂, NO, and a peak at 44 m/e (likely N₂O). Qualitative analyses for NH₃ in solution were positive; however, ammonia is not present in the mass spectrum, presumably because it is highly soluble in water.

The microscopic observations show that gas evolution occurs only for potentials above E_p , which suggests that it is intimately involved in the pitting process. The pathways by which these gases are formed are not known, but the fact that CH₄, H₂S, N₂, NO, and NH₃ are produced indicates that SCN⁻ and NO₃⁻ must interact directly with the metal. Furthermore, all the pitting potentials are more positive than the potential required for H₂ production, yet H₂ is evolved above E_p in each case. Thus, if H₂ is formed in the usual way, the actual potential difference across the electrified interface that controls the rate of the electrochemical reaction must fluctuate to low negative values because of bubble constriction,⁴ even though the potential on the metal itself is constant.

Although not yet understood, the suggested direct metal-ion interaction may involve the formation of intermediate species that lead to gaseous products and metal dissolution. For example, others have proposed that when aluminum is pitted in chloride solutions, intermediate aluminum chloride species are formed and then are hydrolyzed. Similarly in other solutions, aluminum carbide, sulfide, or nitride species may be formed that then hydrolyze to CH₄, H₂S, and NH₃, respectively (see the *Handbook of Chemistry and Physics*). Since these intermediate species are unstable in water, they would necessarily be formed on the metal surface, which could stabilize such transition complexes.

In summary, our results indicate that the pitting of aluminum is accompanied by evolving gas that has a composition dependent on the anion and that a primary step in the pitting mechanism involves a direct interaction of the anion with the aluminum.

REFERENCES

- C. B. Barger and R. B. Givens, "Localized Corrosion of Aluminum: Blister Formation as a Precursor of Pitting," *J. Electrochem. Soc.* 124, p. 1845 (1977).
- C. B. Barger and R. B. Givens, "Precursive Blistering in the Localized Corrosion of Aluminum," *Corrosion* 36, p. 618 (1980).
- C. B. Barger and R. C. Benson, "Analysis of the Gases Evolved During the Pitting Corrosion of Aluminum in Various Electrolytes," *J. Electrochem. Soc.* 127, p. 2528 (1980).
- H. W. Pickering and R. P. Frankenthal, "On the Mechanism of Localized Corrosion of Iron and Stainless Steel," *J. Electrochem. Soc.* 119, p. 1297 (1972).

SURFACE DIFFUSION AND SPIN POLARIZATION

L. Monchick

It is found that when two reactive molecules with unpaired spins are free to diffuse on a surface as well as to react, the resultant electron spin resonance signal is qualitatively different from the one in similar experiments in the bulk phase. This suggests a qualitative way of discriminating two-dimensional motion from three-dimensional.

BACKGROUND

Stochastic processes in two dimensions have attracted increasing interest lately for a number of reasons: reactions on surfaces are often limited by the rate at which reactants can move about the surface to find each other; in many cases, as in catalytic surfaces, the reaction can take place only if the reactants meet at some specific point on the surface, such as a crystal edge or a dislocation, that enhances the reaction probability; in biophysics, reactions in or on membranes and cell walls also involve two-dimensional stochastic motion.

There are many ways of detecting stochastic motion directly, but processes involving reaction take place in picoseconds and in microscopic domains. Thus, methods for inferring the influence of diffusion on reaction must be indirect. One such method, which has proven very successful in three-dimensional processes, is chemically induced dynamic electron polarization (CIDEP).^{1,2,3} Here one takes advantage of the fact that magnetic interactions between the spins of the electrons and the nuclei of two reacting molecules induce the reactants to interact differently from what they would under the shorter range bond-forming (valence) forces. Both spin-spin and valence interactions are felt by the reactants as they move from region to region. An externally imposed magnetic field can change the relative importance of the two interactions and thus can act as a probe of the diffusive motion, of the residual spin-electronic motion interactions, and of the short range valence forces. This is the type of process now to be considered.⁴

DISCUSSION

The CIDEP process is more complicated than classical stochastic processes because the reactants are molecular and can interact differently depending on their particular quantum states. Since the reactants are

usually formed by the breakup of a single larger molecule, the quantum state of the reactants is usually a "pure" one. This means that all interference terms that would be neglected, or averaged out, in a classical representation must be kept. The most natural description of the system is in terms of the density matrix describing the distribution of the distances between the reactants and the distribution between bonding states (electron spins antiparallel) and antibonding states (electron spins parallel). This is assumed to evolve according to the stochastic Liouville equation

$$\frac{\partial \hat{\rho}}{\partial t} = D \nabla^2 \hat{\rho} + \Omega \times \hat{\rho}, \quad (1)$$

$$\frac{\partial \rho_0}{\partial t} = D \nabla^2 \rho_0, \quad (2)$$

$$\Omega = \begin{bmatrix} \bar{a} \\ 0 \\ \bar{J} \end{bmatrix} \quad \hat{\rho} = \begin{bmatrix} \rho_x \\ \rho_y \\ \rho_z \end{bmatrix}, \quad (3)$$

where ρ_0 is a scalar and $\hat{\rho}$ a vector composed of combinations of the components of the density matrix. ρ_x and ρ_y are measures of the spin polarization and spin precession motion, and ρ_z and ρ_0 are the difference and the sum, respectively, of the populations of the bonding and antibonding states. Ω is a torque inducing a precessional motion in $\hat{\rho}$, and its components $\Omega_x = \bar{a}$ and $\Omega_z = \bar{J}$ are due to magnetic and exchange forces, respectively.

The precessional motion induced by the torque Ω is complex. Close in, where J is much larger than \bar{a} , the state vector $\hat{\rho}$ tends to precess about the z-axis as in Fig. 1a. At larger distances, $\bar{a} \gg J$, and the state vector tends to precess about the x-axis as in Fig. 1b. The stochastic motion moves the reactants about so that the state vector feels different fields at different times and a characteristic precessional motion might look like Fig. 1c.

What is measured in an experiment is the ratio of the residual spin polarization at long times and the total reactant population. This quantity can be shown⁴ to obey an integral equation with a symmetric Schmidt-Hilbert kernel. Standard analysis then shows that the residual spin polarization varies as

$$\lim_{J_0 \rightarrow \infty} P \approx \frac{(\bar{a} r_0 + \hbar^{-1})}{4\lambda^2 \bar{a}^2 a}, \quad (4)$$

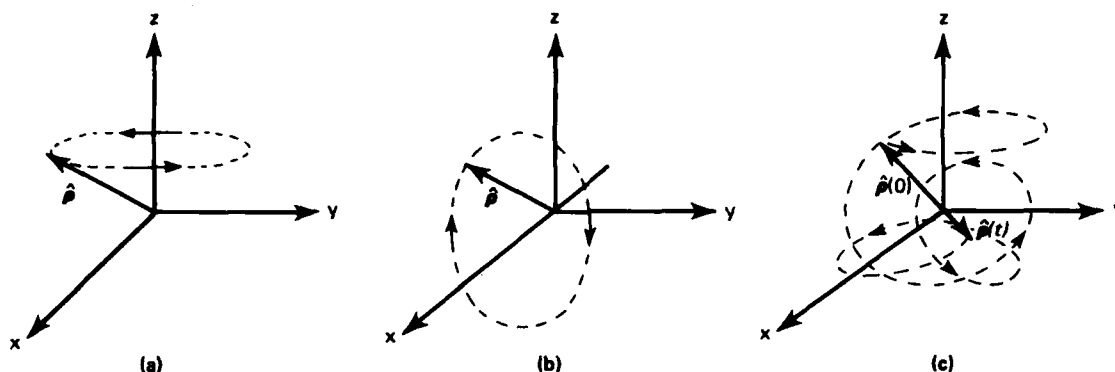


Fig. 1. Precessional motion of the state vector, $\vec{\rho}$, (a) in regions where valence forces predominate; (b) in regions where spin-orbit or spin-magnetic fields predominate; and (c) in the case where the reactants are also free to carry out stochastic displacements.

$$a = \sigma^2 \tilde{a}/D,$$

$$\vec{J} = \vec{J}_0 e^{-N/r_0},$$

where r_0 is the initial separation of the reactants and h the rate at which they react on contact. The contact distance is designated by σ , λ is a parameter characterizing the valence forces, and a is a dimensionless parameter composed of the magnetic interaction \tilde{a} , σ , and the diffusion coefficient D .

This relation differs drastically from the one deduced for three dimensions by the appearance of logarithmic terms. It seems to be a direct consequence of the fact that two- and three-dimensional stochastic motions are qualitatively different in several respects: in three dimensions, particles that collide once may sometimes collide again; in two dimensions, they are certain to do so.⁵ The different dependence on the magnetic precessive force, a , opens up the attractive possibility of a CIDEP experiment distinguishing true

two-dimensional motion on a surface from stochastic motion that really takes place in three dimensions.

REFERENCES

- ¹L. Monchick and F. J. Adrian, "On the Theory of Chemically Induced Electron Polarization (CIDEP): Vector Model and an Asymptotic Solution," *J. Chem. Phys.* **68**, pp. 4376-4383 (1978).
- ²L. Monchick, "On the Theory of Chemically Induced Electron Polarization (CIDEP): II. Potential Forced Diffusion," *J. Chem. Phys.* **70**, pp. 4887-4892 (1979).
- ³F. J. Adrian and L. Monchick, "Theory of Chemically Induced Magnetic Polarization. Effects of $S-T_2$ Mixing in Strong Magnetic Fields," *J. Chem. Phys.* **71**, pp. 2600-2610 (1979).
- ⁴L. Monchick, "Surface Diffusion and Spin Polarization," *J. Chem. Phys.* **72**, pp. 6258-6264 (1980).
- ⁵E. W. Montroll, "Random Walks on Lattices," *Proc. Symposia in Applied Mathematics XVI* (1964).

AN ELECTRODYNAMIC MECHANISM OF SURFACE ENHANCED RAMAN SCATTERING

F. J. Adrian

The Raman spectrum of certain molecules adsorbed on roughened silver, copper, and gold surfaces can be many orders of magnitude more intense than the corresponding spectrum of the isolated molecules. It is proposed that this is due to surface plasmon enhancement of both the local electric field of the exciting radiation and the radiation-induced molecular dipole moment.¹ This is consistent with the observation that silver yields large Raman enhancements over a wide range of optical frequencies, whereas the effect is weaker on copper and gold and usually is observed only with red exciting light.

BACKGROUND

The Raman effect is an inelastic light scattering process in which part of the incident photon energy excites a vibrational transition in the scattering molecule and the rest appears as a lower energy scattered photon. The effect occurs because internal vibrations of the scattering molecules modulate their polarizability, which then modulates the strength of their interactions with the incident light wave. As a result, the scattered light contains weak sidebands separated from the incident frequency by multiples of the vibration frequency. The sidebands, known as the Raman spectrum, contain important information about the molecular vibrations.²

The major disadvantage of Raman spectroscopy is that the effect is very weak, but the high intensity and monochromaticity of laser sources have alleviated this problem for bulk samples. Even so, intensity problems seem to preclude using Raman spectroscopy for surface studies where one has at best a few monolayers of scattering molecules. Attempts to increase the surface area by using roughened surfaces recently led to the serendipitous discovery that the Raman lines of certain molecules adsorbed on roughened silver, gold, and copper surfaces are many orders of magnitude more intense than the corresponding isolated molecule lines.³ Similar enhancements have been observed for molecules adsorbed on very small colloidal particles of silver and gold. Since the discovery of this spectacular surface enhanced Raman scattering (SERS) effect, extensive experimental and theoretical work has been done to understand it.

DISCUSSION

The intensity of the Raman line corresponding to the transition between vibrational states Λ_n and Λ_m is

$$I_{mn} = \frac{4}{3\pi^2 c^2} (\omega_0 - \omega_{mn})^4 \left| \frac{\partial \alpha}{\partial Q} \right|^2 \cdot |\langle \Lambda_n | Q | \Lambda_m \rangle|^2 E_0^2 \quad (1)$$

Here, E_0 is the local electric field intensity of the exciting radiation whose frequency is ω_0 , ω_{mn} is the molecular vibration frequency, Q is the generalized nuclear displacement coordinate for the vibration, and α is the frequency-dependent polarizability of the molecule. The quantity $\langle \Lambda_n | Q | \Lambda_m \rangle$ plays an important role in determining the Raman intensity but it is an intramolecular term that cannot be significantly involved in the SERS effect.

Proposed explanations of SERS fall into two classes: molecular and electrodynamic. Molecular mechanisms generally involve charge transfer states in which an electron is excited from the molecule to the metal or vice versa by the incident radiation. Such transitions can increase the polarizability; however, analysis shows that a large enough increase to explain SERS can occur only if the charge transfer states have a substantial component satisfying the "resonance Raman" condition, i.e., that the charge transfer excitation frequency approximately equals ω_0 . This possibility is precluded by the fact that the metal electrons obey the Fermi distribution and, thus, only a very small fraction of the charge transfer states can satisfy the resonance condition.

All the electrodynamic mechanisms involve enhancements of both the electric radiation field and the radiation-induced molecular dipole in the vicinity of the metal-insulator surface. For example, consider a dipole, μ , which may be either the source of the exciting electromagnetic radiation or the induced molecular dipole, located at a height, h , above a plane metal surface. In the static approximation, which is valid if the fields are calculated within a small fraction of a wavelength from the surface (as is appropriate for typical adsorbed molecules), the net field will be the resultant of μ and an image dipole, μ_{im} , located at a distance h below the metal surface.⁴ Here, $\mu_{im} = (\epsilon - \epsilon_M) \mu / (\epsilon + \epsilon_M)$, ϵ_M is the complex dielectric constant of the metal, illustrated for silver and copper in Fig. 1.⁵

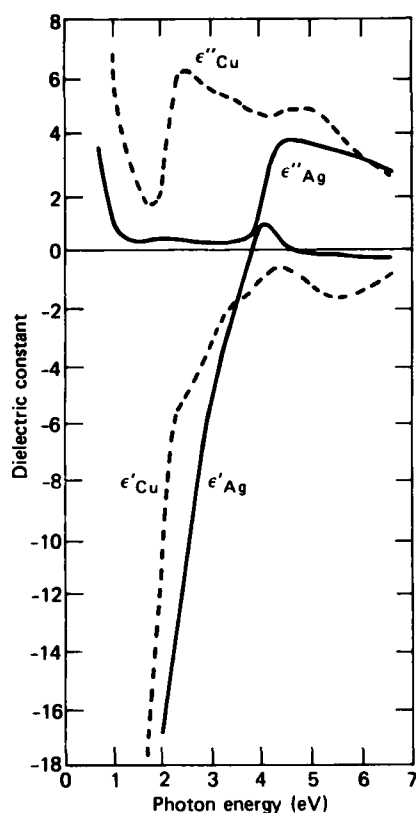


Fig. 1 Complex dielectric constants of silver and copper as functions of photon energy. ϵ'_M and ϵ''_M are the real and imaginary parts, respectively.

and ϵ is the dielectric constant of the insulating medium.

Typically, $|\epsilon'_M| \gg \epsilon$ (cf. Fig. 1); thus, for a planar surface, $\mu_{im} \approx -\mu$, and the direct field and dipole enhancements are much too small to explain SERS. It was suggested⁶ that if the molecule were sufficiently close to the surface, the field of the image of the original induced dipole would further polarize the molecule, leading to a larger image dipole, and so on until the effective molecular dipole moment became large enough to explain SERS. Although this mechanism still has adherents, its basic difficulty is that it requires the molecule to be unreasonably close to the surface; so close, in fact, that if the molecule had a one Debye unit static dipole moment, the attractive force between the final static moment and its image would be comparable to a strong chemical bond.

There is now a growing consensus, based on work at several laboratories including APL, that SERS results from very large enhancements of both the in-

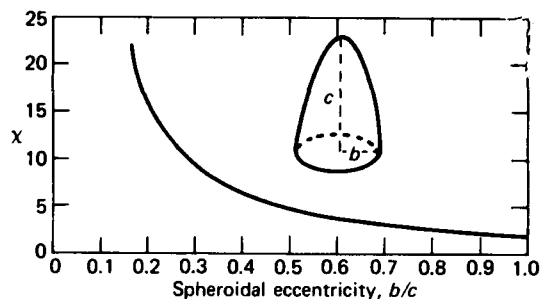


Fig. 2 Spheroidal polarization factor, χ , as a function of spheroidal eccentricity. $\chi = 2$ for a sphere ($c = b$).

cident optical electric field and the induced molecular dipole in the vicinity of convexly curved metal surfaces that are characteristic of small metal particles and protrusions on roughened metal surfaces. On such surfaces, the image dipole is effectively $\mu_{im} = \chi\mu(\epsilon - \epsilon_M)/(\epsilon_M + \chi\mu)$. On a flat surface, $\chi = 1$ as discussed above; however, for a prolate spheroidal surface bump with major semiaxis c and minor semiaxes $a = b < c$, χ increases rapidly with surface curvature (cf., Fig. 2). As seen from Fig. 1, this enables the surface plasmon resonance condition $\epsilon'_M + \chi\epsilon = 0$ to be achieved at frequencies in the visible region where $|\epsilon''_M| \ll |\epsilon'_M + \epsilon|$; consequently, very large field and Raman enhancements can occur.¹ For example, at a typical Raman excitation frequency of 500 nm ($\hbar\omega_0 = 2.5$ eV), silver has $\epsilon'_M = -8$, $\epsilon''_M = 0.34$, and large field enhancements occur on moderately prolate spheroidal surface irregularities ($b/c = 0.33$ to 0.5 for $\epsilon = 1$ to 2).

Figure 1 also illustrates why silver yields the largest Raman enhancements over the widest range of excitation frequencies. It has very small ϵ''_M over a wide range of the visible spectrum whereas ϵ'_M is larger for copper and achieves its smallest values in the red portion of the visible spectrum ($\lambda > 600$ nm or $\hbar\omega_0 > 1.9$ eV). This agrees with observations that the SERS effect is smaller for copper and often can be observed only with red excitation light despite the fact that the ω_0^4 factor in Eq. 1 would favor the more commonly used blue-green light of an argon laser.

Finally, the novel SERS phenomenon very likely is related to the well known colors exhibited by colloidal suspensions of metal particles. Surface plasmon resonance plays an important role in the light scattering that produces these colors. In fact, SERS has been observed for molecules adsorbed on these colloidal particles, the maximum in the frequency-dependent SERS corresponding closely with the maximum in the optical density.

REFERENCES

- ¹F. J. Adrian, "Surface Enhanced Raman Scattering by Surface Plasmon Enhancement of Electromagnetic Fields on a Roughened Metal Surface," *Chem. Phys. Lett.* **78**, 45-49 (1981).
- ²L. A. Woodward, *Raman Spectroscopy I*, H. A. Szymanski (ed.), Plenum Press, New York, Chap. 1 (1967).
- ³R. P. Van Duyne, *Chemical and Biological Applications of Lasers 4*, C. B. Moore (ed.), Academic Press, New York, Chap. 5 (1978).
- ⁴J. D. Jackson, *Classical Electrodynamics*, 2nd Ed., Wiley, New York, pp. 147-149 (1975).
- ⁵P. B. Johnson and R. W. Christy, "Optical Constants of the Noble Metals," *Phys. Rev. B*, **6**, p. 4370 (1970).
- ⁶F. W. King, R. P. Van Duyne, and G. C. Schatz, "Theory of Raman Scattering by Molecules Adsorbed on Electrode Surfaces," *J. Chem. Phys.* **69**, pp. 4472-4481 (1978).

VECTOR STOCHASTIC VARIATIONAL PRINCIPLES FOR ELECTROMAGNETIC WAVE SCATTERING

J. A. Krill and R. H. Andree

Vector stochastic variational principles have been derived to allow the calculation of accurate approximations of electromagnetic wave scattering from conducting dielectric objects (or surfaces) with arbitrary, random characteristics. The resulting expressions have a form that is inherently simpler to evaluate than the direct average of the corresponding deterministic variational expression. This simplification opens the way for the application of this method to practical problems such as electromagnetic scattering from precipitation, aerosols, or the ocean surface, all of which exhibit random properties.

BACKGROUND

The scattering of electromagnetic radiation from random surfaces or volumes (e.g., the ocean's surface, terrain, aerosols, chaff) influences the operating characteristics of such systems as radar, sonar, radar altimeters, and communication links. Improved understanding of random scattering phenomena may lead to better system design and operation as well as to better methods of modeling the scatterers themselves. To this end, numerous approximation techniques for calculating wave scattering have been derived and applied with varying degrees of success.

Solutions to the integral wave equation that describes scattering require knowledge of the currents

or fields on or within the scatterer. The various approximation techniques require initial estimates of these generally unknown quantities. Variational methods are particularly useful in this regard because errors in the variational approximation to the scattered field resulting from errors in the initial estimates cancel to first order. Although such methods were well known for certain deterministic scattering problems, they were not tractable for stochastic scattering because they required calculating statistical moments of a complex ratio of integrals.

A breakthrough occurred in 1977 when Hart and Farrell¹ showed that the averages of the individual integrals comprising the variational expression for the deterministic problem could themselves be combined to form an invariant expression for the average of the scattering amplitude, thereby providing for inherently more tractable calculations than the direct averages of the standard deterministic formulation.

Although the results of Ref. 1 were developed for the scattering of scalar waves by objects or surfaces on which the field satisfies homogeneous (i.e., vanishing) boundary conditions, the reasoning is completely general. We have extended the theory of Ref. 1 to account for polarization phenomena in electromagnetic wave scattering from random scatterers having arbitrary inhomogeneous and anisotropic permittivity and conductivity, for which the fields satisfy nonvanishing boundary conditions.² To accomplish this, we first had to develop deterministic variational principles for the scattering of vector waves

This work was supported in part by Indirectly Funded R&D and in part by the Army Chemical Systems Laboratory, Aberdeen.

from such objects and show that they have a form analogous to the case treated in Ref. 1. Hart and Farrell's general results were then used to develop the corresponding stochastic variational principles for the vector scattering amplitude and the differential scattering cross section. We also constructed invariant expressions for the probability distribution functions of the quantities.

DISCUSSION

The stochastic variational principles derived in Ref. 1 are based on the standard variational form for the scattering amplitude, T , for scalar waves satisfying homogeneous boundary conditions:

$$T = N_1 N_2 / D \quad (1)$$

where N_1 , N_2 , and D are surface integrals whose integrands depend on the fields at the scatterer. Hart and Farrell demonstrated that the expression

$$\langle T \rangle = \langle N_1 \rangle \langle N_2 \rangle / \langle D \rangle \quad (2)$$

is an invariant expression for the average scattering amplitude, $\langle T \rangle$. Obviously Eq. 2 is more tractable than a direct average of the ratio of integrals in Eq. 1.

Extension of this concept to electromagnetic scattering from random objects with inhomogeneous and anisotropic conductivity and permittivity required that we first develop a variational expression for deterministic scattering, because no expression analogous to Eq. 1 existed for that case. To this end, consider Fig. 1, in which an electromagnetic plane wave with amplitude A and electric field polarization direction \hat{e}_i , is incident in the direction \hat{k}_i upon an arbitrary, localized, inhomogeneous, and anisotropic scatterer with tensor permittivity $\bar{\epsilon}(r)$ and conductivity $\bar{\sigma}(r)$, where r is the position vector of a point in space. We wish to examine a vector component of the scattered electric field, propagating in the direction \hat{k}_s , far from the scatterer, along an arbitrary polarization direction \hat{e}_s . Far from the scatterer, the radiation condition requires the scattered field to have the form of a spherically outgoing wave with normalized vector amplitude T , which characterizes the polarization (i.e., vector nature) and angular dependence of the scattered field.

The scalar wave problem¹ was based on the well-known variational principle for the scalar Helmholtz equation with vanishing boundary conditions. In contrast, the vector problem of Fig. 1 involved first expressing the differential vector wave equation for the electric field in a form similar to the Schrodinger equation in quantum mechanics. In this way, the

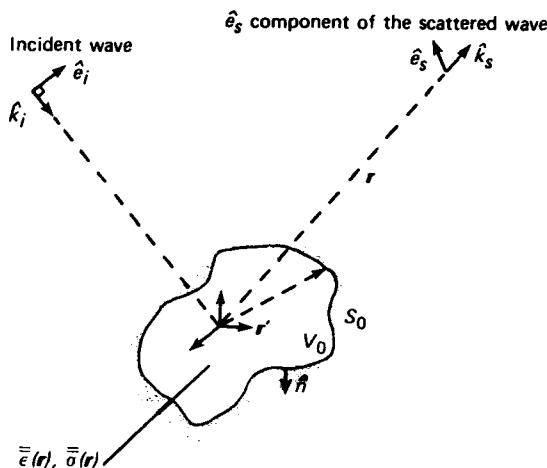


Fig. 1 Geometry for general problem of scattering from an arbitrary volume V_0 with permittivity $\bar{\epsilon}(r)$ and conductivity $\bar{\sigma}(r)$ that is suspended in free space.

scatterer is viewed as a source that is linearly proportional to the total field, and the only boundary condition is the radiation condition at infinity.

Applying a vector version of Green's theorem, one obtains an invariant expression for the vector scattering amplitude that has the form of Eq. 1, except that the integrals of Eq. 1 are now volume integrals over the scatterer with a modified dyadic Green function in the integrand of the D integral. The modification of the Green dyadic was necessary in order for the usual integral representation of the field to hold in the source region where the standard Green dyadic has a singularity. Also, variational invariance ($\delta T = 0$) for this anisotropic scatterer required a reciprocity theorem involving a second scatterer having transposed conductivity and permittivity tensors.

Vector variational principles for electromagnetic wave scattering from perfect conductors, on which the electric field satisfies homogeneous boundary conditions, were also obtained (Fig. 2). Because surface integrals result, the dyadic Green function need not be modified in this case, provided that the double surface integral D is evaluated using limiting procedures. The mathematical details for both of these problems (Figs. 1 and 2) are given in Ref. 2.

Because these deterministic vector variational principles are of the form of Eq. 1, direct extension of the results for random scattering in Ref. 1 to vector variational principles yields

$$\langle T^n \rangle = \frac{\langle N_1^n \rangle \langle N_2^n \rangle}{\langle D^n \rangle}, \quad n = 1, 2, \dots \quad (3)$$

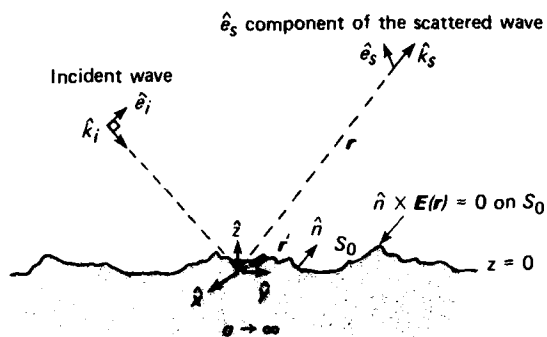


Fig. 2 Geometry of scattering of a plane wave by a perfectly conducting planar surface S_0 with a confined roughness region on which the tangential vector component of the total electric field \vec{E} vanishes.

for arbitrary statistical moments, where now $T \equiv \hat{e}_i \cdot T$ for the vector case. As noted above, the integrals N_1 , N_2 , and D involve the dyadic Green function and vector fields at the scatterer. This is an exact expression for $\langle T^n \rangle$ and, by virtue of the invariance of Eq. 1, it is variationally invariant. Analogous results can be

derived for the statistical moments of the differential scattering cross section $|T|^2$ and for the Fourier transform of the probability density function of T and $|T|^2$ (Ref. 2).

The configurations for which stochastic variational expressions of the form of Eq. 3 can be applied represent a wide variety of scattering problems. For example, precipitation and certain aerosols may be modeled as assemblies of conducting dielectric scatterers, and the surface of the ocean may be modeled as a rough planar conductor. Current work involves the demonstration of the tractability of these results by explicit calculation of the statistics of the electromagnetic waves scattered from models of random volume and rough surface phenomena that exhibit depolarization and multiple scattering characteristics.

REFERENCES

- ¹R. W. Hart and R. A. Farrell, "A Variational Principle for Scattering from Rough Surfaces," *IEEE Trans. Antennas Propag.* AP-25, pp. 708-710 (1977).
- ²J. A. Krill and R. H. Andreo, "Vector Stochastic Variational Principles for Electromagnetic Wave Scattering," *IEEE Trans. Antennas Propag.* AP-28, pp. 770-776 (1980).

VIBRATIONAL FREQUENCIES OF COMPOSITE STRUCTURES

D. W. Fox and V. G. Sigillito

A method has been developed that allows the computation of upper and lower bounds for the frequencies of vibration of composite or built-up structures. The method was recently applied, with very good results, to the structurally important situation of a plate reinforced by a single rib.

BACKGROUND

Because of the complexity of many elasticity problems, it is desirable to develop approximation methods for determining vibrational frequencies.

However, most such methods give no information on the error involved in the approximation or even whether the estimate is above or below the true value. Certain methods, such as the classical Rayleigh-Ritz procedure, always give upper bounds. Very few methods give estimates that are known to be lower bounds and, further, that can be systematically improved. One such method is that of intermediate problems, which has been successfully used together with the Rayleigh-Ritz procedure to provide tight, rigorous, lower and upper bounds for a variety of membrane, beam, and plate problems.¹⁻⁵ Recent advances in the technical development of this method⁶ have led to its first application to estimate the vibrational frequencies of more complex composite or reinforced structures.

DISCUSSION

The combined intermediate-problem/Rayleigh-Ritz method was applied to the composite structure shown in Fig. 1 to obtain lower and upper bounds on the vibrational frequencies. The structure consists of a thin rectangular elastic plate reinforced by a rib elastically bonded to it along a portion of the centerline. This elastic bond is represented by a constant modulus, K , that gives rise to an effective force, q , per unit area on the plate that has a resultant force, Q , and a moment, M . The force q is proportional to the difference between the deflection of the bottom of the rib and the top of the plate.

Additional assumptions are: (a) the reinforcing rib is narrow so that classical beam theory applies, (b) the plate is simply supported all around, and (c) the reinforcing beam is free at both ends. This model gives rise to the following coupled system of equations for the beam deflection, v , the beam torsion, θ , and the plate deflection, w :

$$\left. \begin{aligned} B \frac{d^4 v}{dx^4} - Q - \sigma \omega^2 v &= 0, & -e < x < e, \\ \frac{d^2 v}{dx^2} = 0, \frac{d^3 v}{dx^3} &= 0, & x = \pm e, \end{aligned} \right\} (1)$$

$$\left. \begin{aligned} C \frac{d^2 \theta}{dx^2} + M + \tau \omega^2 \theta &= 0, & -e < x < e, \\ \frac{d\theta}{dx} &= 0, & x = \pm e, \end{aligned} \right\} (2)$$

$$\left. \begin{aligned} D \nabla^4 w - q - \rho \omega^2 w &= 0, & -b < x < b, \\ & & -a < y < a, \\ w = 0, \nabla^2 w &= 0, & x = \pm b, \\ & & y = \pm a, \end{aligned} \right\} (3)$$

where

$$\begin{aligned} Q(x) &= - \int_{-c}^c q(x,y) dy \\ &= K \left[\int_{-c}^c w(x,y) dy - 2cv(x) \right], \\ & -e < x < e, \end{aligned}$$

$$\begin{aligned} M(x) &= - \int_{-c}^c yq(x,y) dy \\ &= K \left[\int_{-c}^c w(x,y) y dy - \frac{2c^3}{3} \theta(x) \right], \end{aligned}$$

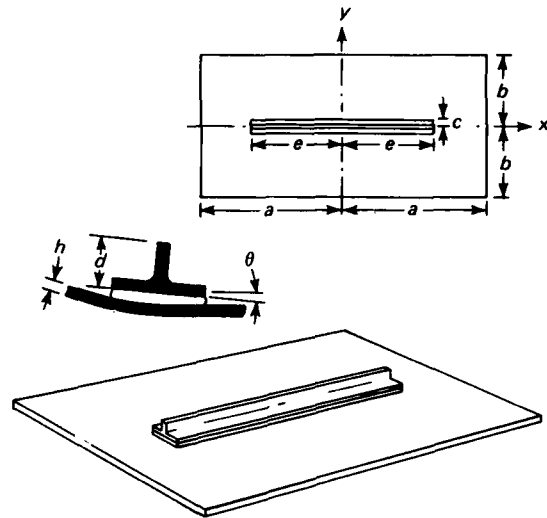


Fig. 1 The reinforced plate.

$$-e < x < e,$$

$$\begin{aligned} q(x,y) &= K [v(x) + y\theta(x) - w(x,y)], \\ & -e < x < e, \quad -c < y < c. \end{aligned} \quad (4)$$

In these equations, B and C are the beam flexural and torsional rigidity, D is the plate flexural rigidity, ρ is the plate mass per unit length, σ is the beam mass per unit length, τ is the beam mass polar moment of inertia per unit length, and ω is the symbol for the plate-beam system vibrational frequencies.

Because of the physical symmetry of the rib-reinforced plate, the solutions of the system of Eqs. 1 through 4 belong to symmetry classes that depend on whether w is odd or even in y . If w is even in y , M is independent of w ; if w is odd, Q is independent of w . Thus for solutions even in y , the system that governs the motion is 1, 3, and the first and third parts of 4 (i.e., coupled beam bending and plate deflection even in y), while for odd solutions it is 2, 3, and the second and third parts of 4 (i.e., coupled beam torsion and plate deflection odd in y). Further, there is odd-even symmetry with respect to x so that each of these symmetry classes can be decomposed into the subclasses that are even or odd with respect to x . All computations reported here were done in the even symmetry class.

The starting point of our lower bound calculations is the simpler uncoupled problem that results when K is put equal to zero. In it, the system 1 to 3 is totally uncoupled, and the frequencies and mode

shapes are easily obtained by solving the vibration problem for each piece separately. In addition, the mode shapes of the uncoupled problem are suitable functions for the Rayleigh-Ritz upper bound calculations. The lower bounds obtained from the uncoupled problem are then systematically improved by coupling the beam and plate together by allowing the coupling force to act only through the projection on a small number of approximating functions. As the number of functions is increased, the elastic bond is approximated better and better in a systematic way that results in much improved lower bounds. Technical mathematical details of the method are given in Refs. 6, 7, and 8.

Results for plates reinforced with a single rib of one-half, three-quarters, and full plate length are given in Table 1. Both the plate and rib have elastic properties typical of aluminum. For comparison, Table 2 shows the vibrational frequencies for the plate without a reinforcing rib. The main effect of the thinnest beams ($d = 0.1$) is to lower the lowest frequencies resulting from mass loading (cf. Tables 1 and 2). However, as the height of the beam is increased, the beam's influence on the plate frequencies is highly variable. This variability is particularly evident for the shortest beams. For instance, as shown in Table 1, ω_1^2 decreases

monotonically with increasing d , while ω_3^2 increases monotonically with increasing d and ω_5^2 increases with d to a point and then decreases rapidly as d increases further.

The uncovering of the unexpected nonlinear variation of vibrational frequencies as the beam height is increased demonstrates the power of the method and illustrates the unexpected complexity of the plate/beam interaction.

Table 2

EIGENVALUES FOR THE UNCOUPLED PLATE (EVEN-EVEN)

ν	Uncoupled Plate	
	$\omega_\nu^2 \times 10^{-4}$	
	$a = 10.0$	
1	3.4424	
2	23.270	
3	115.80	
4	188.50	
5	278.83	

Table 1

UPPER AND LOWER BOUNDS FOR THE REINFORCED PLATE

ν	d	$\omega_\nu^2 \times 10^{-4}$					
		$a = 10.0, b = 20.0, K = 10^4$					
		$e = 10.0$		$e = 15.0$		$e = 20.0$	
1	0.1	3.1915	3.1933	3.1482	3.1504	3.1416	3.1437
2		22.739	22.752	22.111	22.183	22.043	22.055
3		113.08	113.31	112.42	112.77	111.99	112.18
4		175.25	175.43	173.19	173.41	172.84	173.07
5		269.82	269.94	259.55	259.87	256.33	256.63
1	0.2	3.0176	3.0206	2.9566	2.9596	2.9507	2.9527
2		23.945	23.973	23.738	24.130	25.815	25.923
3		122.45	123.97	130.24	131.08	141.59	143.82
4		165.00	165.23	161.88	162.17	161.32	161.60
5		264.27	264.48	247.04	247.85	243.39	243.84
1	0.5	2.7399	2.7599	2.9409	2.9799	3.2896	3.3065
2		39.256	39.690	35.940	37.154	68.942	75.125
3		142.84	143.84	141.00	141.46	140.51	140.95
4		159.31	161.78	213.79	214.97	232.85	256.66
5		271.68	271.83	254.79	261.08	270.10	272.12
1	1.0	2.2429	2.2733	2.7997	2.9374	6.7492	7.3061
2		54.123	56.835	80.204	80.770	107.44	123.75
3		127.91	128.54	125.59	126.28	125.89	126.87
4		199.78	201.08	231.67	232.65	228.57	282.19
5		353.30	358.58	288.78	297.65	313.27	388.30

REFERENCES

- ¹J. T. Stadter, "Bounds to Eigenvalues of Rhombical Membranes," *J. Soc. Ind. Appl. Math.* **14**, pp. 324-341 (1966).
- ²N. Rubinstein and J. T. Stadter, "Bounds to Frequencies of a Simply Supported Rotating Beam," *J. Franklin Inst.* **294**, pp. 217-229 (1972).
- ³N. W. Bazley, D. W. Fox, and J. T. Stadter, "Upper and Lower Bounds for the Frequencies of Rectangular Clamped Plates," *Z. Angew. Math. Mech.* **47**, pp. 191-198 (1967).
- ⁴N. W. Bazley, D. W. Fox, and J. T. Stadter, "Upper and Lower Bounds for the Frequencies of Rectangular Cantilever Plates," *Z. Angew. Math. Mech.* **47**, pp. 251-260 (1967).
- ⁵N. W. Bazley, D. W. Fox, and J. T. Stadter, "Upper and Lower Bounds for the Frequencies of Rectangular Free Plates," *J. Appl. Math. Phys.* **18**, pp. 445-460 (1967).
- ⁶D. W. Fox and V. G. Sigillito, "Bounds for Eigenvalues of Reinforced Plates," *International Series of Numerical Mathematics* **56**, Numerische Behandlung von Differentialgleichungen, Band 3, J. Albrecht and L. Collatz (eds.), Birkhäuser Verlag, Basel (1981).
- ⁷N. W. Bazley and D. W. Fox, "Lower Bounds to Eigenvalues Using Operator Decompositions of the Form B^*B ," *Arch. Rational Mech. Anal.* **10**, pp. 352-360 (1962).
- ⁸N. W. Bazley and D. W. Fox, "Methods for Lower Bounds to Frequencies of Continuous Elastic Systems," *J. Appl. Math. Phys.* **17**, pp. 1-37 (1966).

MAGNETIC PHASES IN DISORDERED ALLOYS

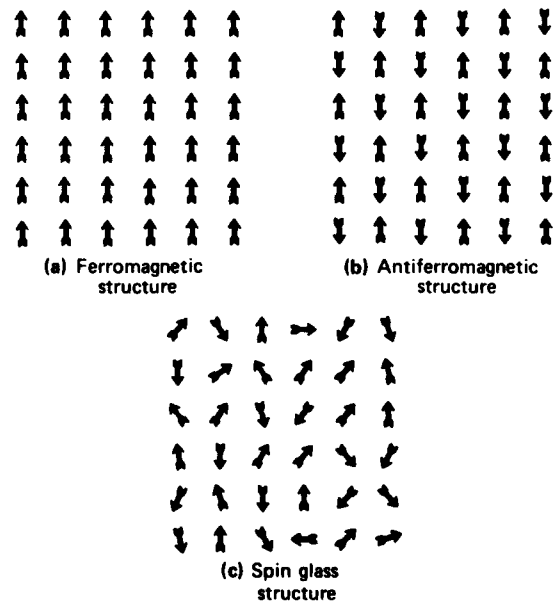
K. Moorjani

Although the existence of the novel magnetic phase, spin glass, depends on the presence of competing exchange interactions, it is the relative strength of the interactions that is demonstrated to determine the details of the spin glass/paramagnetic phase boundary. The predicted trends have been confirmed by experimental data on amorphous metal-metalloid alloys.

BACKGROUND

Spatially ordered magnetic structures can exist in a solid if the constituent atoms possess uncompensated spins, and therefore magnetic moments, that interact via exchange interactions. Schematics of two such ordered magnetic structures on a two-dimensional lattice are shown in Fig. 1a and b. In the ferromagnetic structure (Fig. 1a), the interaction between neighboring spins is such that the energy of the system is minimized when all spins point in the same direction. In a simple antiferromagnetic structure (Fig. 1b), the sign of the interaction between a spin and its neighbors is opposite to that in the ferromagnetic structure, and the ground state consists of two interpenetrating ferromagnetic lattices, with the spins on the two lattices pointing in opposite directions. Both structures possess long range spatial order.

What would be the nature of the magnetic structure in a system where both ferromagnetic and antiferromagnetic interactions are present? Depending on the relative numbers of the two types of interactions and on the way they are distributed, it is clear that it



This work was supported by the U.S. Army Research Office and Indirectly Funded R&D.

Fig. 1 Schematics of magnetic structures.

would be impossible to obtain elementary spin arrangements that would satisfy all the bonds (e.g., odd numbers of antiferromagnetic interactions around a square). This has been appropriately termed the "frustration effect" since a given spin receives conflicting signals from its neighbors and does not know the direction in which it should point to minimize its energy. For such systems, Edwards and Anderson¹ postulated the existence of a ground state where each spin "freezes" in a preferred direction that is randomly oriented and different for every spin (Fig. 1c). It is termed the spin glass state and, in contrast to ordered magnetic structures, it does not possess long range order in space. However, similar to ordered magnetic structures, it does possess long range correlations in time.

The system exhibits a phase transition to the paramagnetic state at a definite temperature, T_{sg} , at least in the mean field approximations. It should be noted that competing exchange interactions are not the only ones that can lead to the spin glass state; antiferromagnetic interaction alone on a triangular two-dimensional lattice, on a three-dimensional face-centered-cubic (FCC) structure, or on an amorphous solid will also lead to frustration and the accompanying transition to the spin glass state. This new phase has been observed in a large variety of systems, including metallic and insulating alloys.

The present work originated in order to understand the details of the spin glass/paramagnetic phase boundary as a system is continuously changed from an ordered magnetic system to a disordered one.²

DISCUSSION

Consider a random alloy $(A_x B_{1-x})_y D_{1-y}$, where A and B are magnetic species of relative concentration xy and $(1-x)y$, respectively, and D comprises nonmagnetic atoms of relative concentration $1-y$. The magnetic aspects of the alloy are represented by a Heisenberg Hamiltonian written within a cluster approximation, when an external field, H_{ext} , is present, as

$$\mathcal{H} = - \sum_m J_{Om} S_O \cdot S_m - H_{ext} \cdot S_O - H_1 \cdot \sum_m S_m \quad (1)$$

The cluster consists of a spin at the origin interacting with its nearest neighbors, m , via the exchange interaction, J_{Om} . The rest of the medium is replaced by an effective field $H_1 - H_{ext}$, which acts on atoms on the surface of the cluster and has to be determined self-consistently.

The pure A system ($x = y = 1$) is taken to be ferromagnetic, i.e., $J_{Om} = J_{AA} > 0$, while the pure B system ($x = 0, y = 1$) is assumed to be antiferromagnetic, i.e., $J_{Om} = J_{BB} < 0$. When a random alloy is formed, the interactions J_{AA} and J_{BB} retain their characteristics while the sign of the interaction J_{AB} is allowed to take on either value. The alloy being random, $J_{Om} = J$ takes on values according to the probability distribution

$$P(J) = x^2 y^2 \delta(J - J_{AA}) + (1-x)^2 y^2 \delta(J - J_{BB}) + 2x(1-x)y^2 \delta(J - J_{AB}) + (1-y^2) \delta(J), \quad (2)$$

where the first term represents the probability of an $A-A$ interaction, the second, a $B-B$ interaction, the third either $A-B$ or $B-A$ interactions, and the fourth all the interactions between the magnetic and nonmagnetic atoms.

The methodology consists of evaluating the partition function and subsequently the free energy for the Hamiltonian (Eq. 1) and then configurationally averaging the free energy over the probability distribution (Eq. 2). The order parameters for various phases (conventional magnetization for the ferromagnetic phase and long time autocorrelation of an individual spin for the spin glass phase) can then be calculated from the configurationally averaged free energy. By imposing self-consistency conditions on the order parameters, the equations determining the phase boundaries are obtained:

$$2\langle \xi^2 \rangle + 2zq\langle \xi \rangle + 3 = 0 \quad (3)$$

(ferromagnetic-paramagnetic)

and

$$\langle \xi^2 \rangle = \frac{1}{2}(2z^2 q^2 - 3) \quad (4)$$

(paramagnetic-spin glass),

where $q = (3/2z)^{1/2}$, $\xi = J/2kTq = aJ$, and z is the number of nearest neighbors. The configurationally averaged quantities $\langle \xi \rangle$ and $\langle \xi^2 \rangle$ are given by

$$\langle \xi \rangle = ay^2 J_{AA}^2 [x^2 + \beta(1-x)^2 + 2\alpha x(1-x)] \quad (5)$$

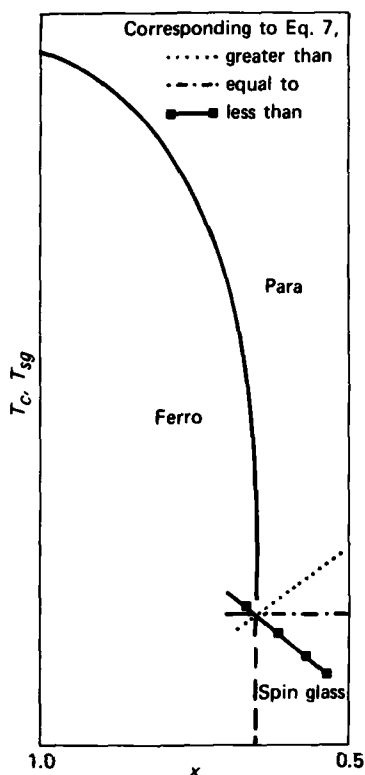


Fig. 2 Schematic phase diagram for a random alloy, for $y = 1$ and $z = 8$.

and

$$\langle \xi^2 \rangle = a^2 y^2 J_{AA}^2 [x^2 + \beta^2(1-x)^2 + 2\alpha^2 x(1-x)] \quad (6)$$

with $\alpha = J_{AB}/J_{AA}$ and $\beta = J_{BB}/J_{AA}$. The complete phase diagram of the random alloy is determined by Eqs. 3 through 6. The results are depicted in Fig. 2 for $y = 1$ and $z = 8$. The important point is that the slope dT_{sg}/dx of the paramagnetic/spin glass phase boundary in the vicinity of x_1 , the point where the three phases meet, is positive, zero, or negative depending on whether

$$|\beta| \begin{cases} \leq \left[\frac{x_1 + \alpha^2(1-2x_1)}{(1-x_1)} \right]^{1/2} \\ > \left[\frac{x_1 + \alpha^2(1-2x_1)}{(1-x_1)} \right]^{1/2} \end{cases} \quad (7)$$

These trends have been noticed in a number of amorphous metallic alloys.

REFERENCES

- S. F. Edwards and P. W. Anderson, *J. Phys. F: Met. Phys.* **5**, p. 965 (1975).
- K. Moorjani, S. K. Ghatak, K. V. Rao, B. Kramer, and H. S. Chen, *J. Phys.* **41**, p. C8-718 (1980).

SWITCHING AND MEMORY PHENOMENA IN SEMICONDUCTING CHARGE-TRANSFER COMPLEXES

T. O. Poehler and R. S. Potember

Stable and reproducible current-controlled bistable switching and memory phenomena have been observed in polycrystalline metal-organic semiconductors sandwiched between metallic electrodes. The effects are observed in films of copper or silver complexed with any one of a number of organic electron acceptor molecules. The switching effect is insensitive to

moisture and is observed over a large temperature range. It is the result of a phase transition, induced by an electric field, in the bulk of the semiconducting material and is accompanied by an abrupt increase in electrical conductivity. Depending on the acceptor molecule, either memory switching (the high conductivity persists when the field is removed) or threshold switching (the low conductivity state returns when the field drops below a threshold value) is observed. The character of the switching in going from a high to a low

This work was supported by Indirectly Funded R&D and the National Science Foundation.

impedance state in these organic charge-transfer complexes is believed to be superior in many respects to that of existing organic materials.

BACKGROUND

Electrical switching and memory phenomena are known to exist in a wide variety of inorganic semiconducting thin films. The inorganic materials include the metal oxides of nickel, silicon, aluminum, titanium, zirconium, and tantalum, all of which exhibit a voltage-controlled negative resistance when arranged in a metal-oxide-metal sandwich structure. The amorphous alloys, including chalcogenide glasses, are inorganic semiconductors that also show switching behavior. The glasses contain up to four elements, often including arsenic and/or tellurium, and exhibit a current-controlled negative resistance. There are also several reports in the literature of electrical switching in organic polymers and polycrystalline dielectrics. In all cases, the electrical characteristics are either erratic or not very reproducible. To date, no organic device has been shown to be comparable to the inorganic amorphous glasses.

DISCUSSION

Stable and reproducible current-controlled bistable electrical switching and memory phenomena are observed in polycrystalline metal-organic semiconducting films. The effects are observed in films of copper or silver complexed with the electron acceptors tetracyano-naphthoquinodimethane (TNAP), tetracyanoquinodimethane (TCNQ),¹ and TCNQ derivatives. The current-voltage characteristics of a 3.75 μm thick Cu/Cu-TNAP/Al system,² for example, reveal that there are two stable resistive states in the material (Fig. 1). A rapid switching from the high to the low impedance state is observed when an applied field across the sample surpasses a threshold value (V_{th}) of 2.7 V. This corresponds to a field strength of approximately 8.1×10^3 V/cm. At this field strength, the initial high impedance of the device, $1.25 \times 10^4 \Omega$, drops to a low value of 190 Ω . The response of those materials to a fast-rise-time rectangular pulse shows that the transition from the low to the high conductivity state occurs with a combined delay and switching time of less than 4 ns (Fig. 2). The duration of the low-impedance state before the return to the high-impedance state is shown to be controlled by the applied field, the sample thickness, and the strength of the reduction potential of the acceptor molecule.

An experiment in which an open-circuit voltage was observed in switching from the high to the low

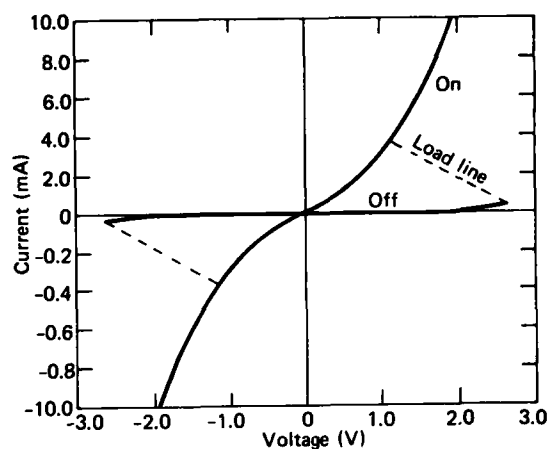


Fig. 1 Typical DC current-voltage characteristic showing high- and low-impedance states for a 3.75 μm Cu-TNAP sample.

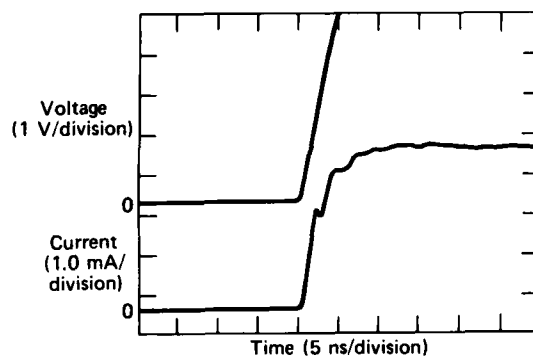


Fig. 2 Transient response to a rectangular pulse with a 4 ns rise time.

conductivity state² has helped to explain the mechanism of the observed switching phenomena because the appearance of a spontaneous electromotive force in switching between states indicates that an electrochemical reaction is responsible for the switching phenomena. In this experiment (a) voltage in excess of the threshold voltage was applied to place a Cu-TNAP sample into a high conductivity state for a short time after the applied voltage was removed, (b) the sample was then externally short circuited to eliminate capacitive effects, and finally (c) a high-input-impedance storage oscilloscope was used to measure open-circuit voltage when the sample spontaneously returned to its original high-impedance state. An open-circuit voltage of 0.3 V observed during switching to the low conductivity state shows that the mechanism by which the phase transition occurs is related to a field-

induced, solid-state, reversible, electrochemical, redox (reduction-oxidation) reaction involving the metal charge-transfer salts. It is postulated that this redox reaction produces mixed-valence species of complex salts.

We have found field-induced bistable switching in the copper and silver charge-transfer complexes TCNQ, TCNQF₄, TCNQ-(OMe)₂, TCNQ-(ME)₂, and TNAP.³ Correlations are observed between the redox potential of the various charge-transfer complexes and the electrical properties of these salts fabricated into switching devices. The first correlation is that the copper salts continually show more reproducible results and greater stability than the corresponding silver salt of the same electron acceptor. Second, a general trend is noted when one compares the reduction potential of the acceptor molecule to the field strength at the switching threshold. The relationship is summarized in Table I, which indicates that the field strength at the switching threshold is directly related to the strength of the electron acceptor, i.e., the degree of electron transfer from the metal ion to the acceptor molecules.

Finally, it appears that the nature of the low-impedance state is also related to the reduction potential of the different acceptors. For instance, devices constructed from strong electron acceptors like TCNQF₄ act as memory switches, while the switching behavior in weak electron acceptors is of the threshold type. A threshold switch is characterized by a system that immediately returns to the high-impedance state when the applied voltage is removed. Intermediate strength acceptors tend to exhibit both memory and threshold phenomena, depending on the duration or degree of power dissipation of the applied field in the low-impedance mode. The values of the reduction potentials of the various electron acceptors discussed here are calculated from solution redox potentials that

Table I
RELATIONSHIP BETWEEN REDUCTION POTENTIAL OF THE ACCEPTOR AND FIELD STRENGTH AT SWITCHING THRESHOLD

Polycrystalline Charge Transfer Complexes	Reduction Potential of the Acceptor*	Approximate Field Strength at Switching Threshold (V/cm)
Cu-TCNQ(OMe) ₂	-0.01	2.4 × 10 ³
Cu-TCNQ	+0.17	5.7 × 10 ³
Cu-TNAP	+0.20	8.2 × 10 ³
Cu-TCNQF ₄	+0.53	1.3 × 10 ⁴

*Sample potential referenced to a standard calomel electrode.

do not always reflect the contributions of the binding energy to the charge-transfer complexes in the solid state. To make more quantitative correlations in these systems, contributions from crystal structure, molecular size, and the stoichiometry of the complexes must be considered.⁴

REFERENCES

- R. S. Potember, T. O. Poehler, and D. O. Cowan, "Electrical Switching and Memory Phenomena in Cu-TCNQ Thin Films," *Appl. Phys. Lett.* **34**, p. 405 (1979).
- R. S. Potember, T. O. Poehler, A. Rappa, D. O. Cowan, and A. N. Bloch, "A Reversible Field Induced Phase Transition in Semiconducting Films of Silver and Copper TNAP Radical-Ion Salts," *J. Am. Chem. Soc.* **102**, p. 3659 (1980).
- R. S. Potember, T. O. Poehler, D. O. Cowan, and A. N. Bloch, "Electrical Switching and Memory Phenomena in Semiconducting Organic Charge-Transfer Complexes," *The Physics and Chemistry of Low Dimensional Solids*, L. Alcacer (ed.), D. Reidel Publishing Co., Dordrecht (1980).
- T. O. Poehler, R. S. Potember, D. O. Cowan, and A. N. Bloch, "Switching and Memory Phenomena in Semiconducting Charge-Transfer Complexes," *Proc. Symp. on Conducting Polymers and Related Materials* **81**, p. 189 (1980).

ENERGY, ENVIRONMENT, AND URBAN TECHNOLOGY

INTRODUCTION

Energy management is implicit in much of APL's defense work and satellite systems, and in missile propulsion in particular. Recently, APL has evaluated alternative long-range, nondepleting sources of energy to meet future national requirements. Studies of the exploitation of one aspect of solar energy, the thermal gradient between the surface and the deep ocean, indicate that this system may provide a practical and economical way to produce electricity and chemical products. APL established an ocean energy program office to assist the Department of Energy in implementing an experimental component and pilot-plant development of this concept, to be conducted primarily by industrial contractors. Two reports included in this section discuss significant testing results carried out under the direction of APL in support of this Ocean Thermal Energy Conversion (OTEC) program.

APL is assisting the Department of Energy in several additional programs: assessment of geothermal and low-head hydroelectric resources and applications in the Eastern United States; development of methods to evaluate methane gas resources and to recover this gas from landfills; development and testing of high-speed flywheels for energy storage; and a Community Annual Storage Energy System (CASES), which stores excess summer heat for use in heating buildings in winter.

APL began studying the environmental impact of energy facilities in 1971 in collaboration with The Johns Hopkins University Department of Geography and Environmental Engineering and with the Chesapeake Bay Institute. It has since evaluated for the State of Maryland the potential environmental and social impact of all power-generating facilities proposed for development in the state. The work has led to projects and contributions in a wide variety of technical areas related to the location of energy facilities, their impact, and the mitigation of that impact. Accounts of principal accomplishments in those areas are included in this section. Highlighted are a study of the effect of power plant construction on the population of striped bass in Maryland waters and a discussion of accomplishments in landfill methane recovery.

The recognition that the great cities continue to play a key role in maintaining the nation's vitality has spurred renewed interest in the institutional structures that support urban life. Through a variety of special projects, APL has participated in and contributed to programs for developing and applying modern technology to a variety of civil problems directly relevant to current urban issues. The programs have included transportation, fire research, aircraft flight safety, the siting of power plant facilities near urban centers, health-care delivery systems, and the location of leaks in buried natural-gas distribution lines. Reported in this section is some fundamental research carried out on modeling the spread of fire in a fuel-lined duct.

TESTS OF THE OTEC CORE UNIT HEAT EXCHANGER AS A CONDENSER

P. P. Pandolfini, J. L. Keirse, and J. A. Funk

APL has conceived, designed, and tested a potentially cost-effective option for heat exchangers for Ocean Thermal Energy Conversion (OTEC) power plants using shell-less, folded, 3-in. OD aluminum tubes with ammonia flowing inside. The term, "shell-less" refers to the fact that the tubes are not enclosed in a pressurized shell because the power cycle working fluid flows inside. A full-scale model (core unit) of the heat exchanger was tested successfully as a condenser over a range of conditions of interest. The experimental results of these tests, along with those of the previously completed evaporator core tests, can now be used to design the heat exchangers of an OTEC pilot plant.

BACKGROUND

In an OTEC plant, warm surface seawater will be used in evaporators to vaporize ammonia. The ammonia working fluid will drive a power turbine and then will be condensed with cold seawater drawn from a depth of 3000 ft. The electric power produced can be delivered by cable to an onshore utility grid or used on board a cruising plantship to produce energy-intensive products.

The OTEC plants will succeed commercially only if the overall system cost is low. A promising low-cost heat exchanger concept¹ uses arrays of large-diameter aluminum tubes (3-in. OD) with ammonia flowing inside. Each tube is approximately 700 ft long and is folded into horizontal passes. Seawater is pumped to head ponds above the arrays and flows vertically downward over the tubes. The use of a large-diameter tube results in a configuration with sufficient space in the vertical planes between the tube rows to permit the use of a low-cost ultrasonic cleaning system² to remove biofouling from the outside surfaces.

To test the validity of this heat exchanger concept, a full-scale core unit comprising three 3-in. OD tubes of similar length, built to APL's specifications by the Trane Co., was tested in the Argonne National Laboratory ammonia flow loop as an evaporator and, separately, as a condenser. Its performance as an evaporator, previously reported,³ was better than predicted and led to the subsequent testing of the unit as a condenser.

DISCUSSION

The core unit is illustrated in Fig. 1. For the condenser tests, ammonia vapor was introduced into the top of the unit, flowed downward through the tubes, and issued from the bottom (completely condensed) into a receiver. During the tests, the water entrance temperature was maintained at 41 to 42°F by a chiller.

The thermal performance of the test condenser was characterized by an overall heat transfer coefficient, U , the calculation of which was based on the heat duty, the areas involved in the heat exchange, the temperatures of the water at the top and bottom of the box, and the ammonia temperatures at the inlet and outlet. Theoretically, U depends on the conductive heat transfer characteristics of the water, the tube wall, and the ammonia; the values for these conductances, or film coefficients, are well established for the water and the aluminum walls. However, since the ammonia is in two-phase flow, the model for its film coefficient is less certain and depends on the geometry of the ammonia flow.

Another performance parameter that was measured was the two-phase ammonia pressure drop, Δp , in the tube from entrance to exit, which included the effects of bend losses. The prediction of the net output of the power cycle depends also on the ability to assess this loss.

Table 1 presents the range of test conditions covered, and Table 2 presents the performance measurements at nearly nominal conditions. The results indicate that the annular film coefficient model used for the ammonia side underpredicts the measured values considerably. Further analysis using a flow regime map for two-phase flow⁴ has led to a better model.

In the range of interest for OTEC condenser operations (0.49 to 0.85 lbm/s per tube), the flow is predominantly stratified. Using stratified models for the void fraction⁵ and ammonia film coefficient yields results such as those shown in Fig. 2 (in which the measurements and the calculations using the annular flow model are also shown). The use of a combination model (Fig. 2e) is indicated for ammonia flows greater than 0.85 lbm/s per tube.

The measured ammonia pressure drop through the unit is shown in Fig. 3. In general, it was higher than

This work was supported by the Department of Energy/Division of Central Solar Technology.

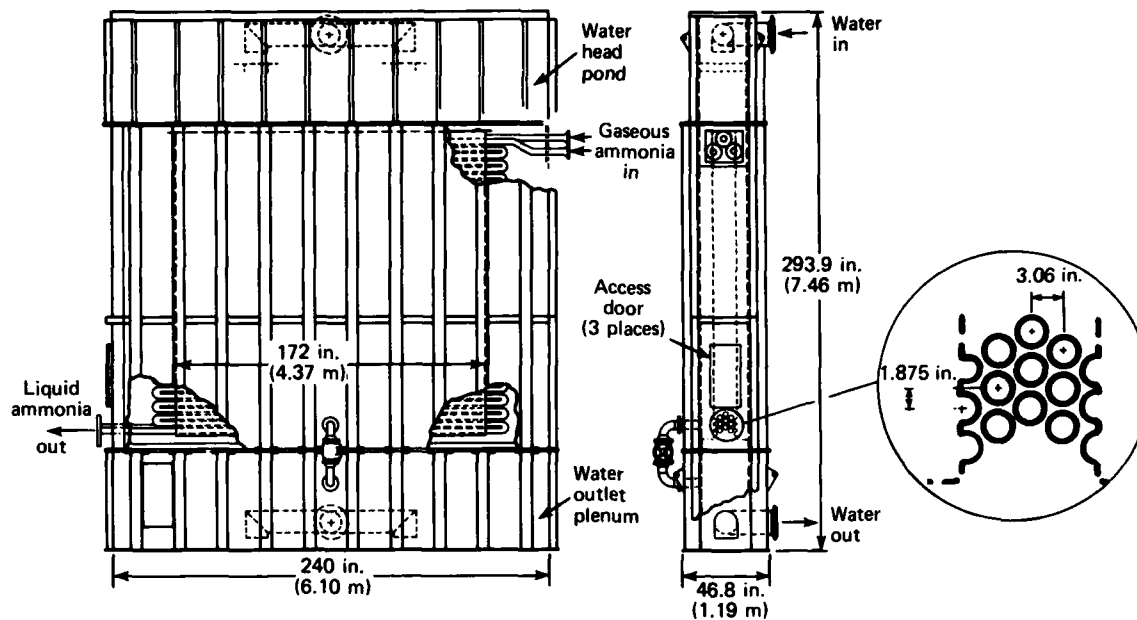


Fig. 1 Core unit of the API, folded-tube heat exchanger tested as a condenser.

Table 1

CORE UNIT CONDENSER TEST CONDITIONS

Parameter	Nominal Value	Variation
Heat duty	3.2×10^6 Btu/h (937 kW)	$2.5 - 5.0 \times 10^6$ Btu/h (732 - 1464 kW)
Water flow rate (\dot{w}_w)	3200 gal/min (12.1 m ³ /min)	1500 - 4800 gal/min (5.7 - 18.2 m ³ /min)
Water velocity (in minimum tube gap) (V_w)	2.5 ft/s (0.76 m/s)	1.2 - 3.8 ft/s (0.37 - 1.16 m/s)
Water inlet temperature	41°F (5°C)	41 - 42°F (5 - 5.6°C)
Ammonia flow per tube (\dot{w}_a)	0.6 lbm/s (0.27 kg/s)	0.43 - 2.2 lbm/s (0.20 - 1.0 kg/s)
Ammonia inlet temperature	50°F (10°C)	45 - 58°F (7.2 - 14.4°C)
Number of active tubes	3	1 and 3

Table 2

CONDENSER PERFORMANCE AT
NEARLY NOMINAL CONDITIONS

Water flow	3287 gal/min (12.7 m ³ /min)	
Ammonia flow	0.59 lbm/s/tube (0.27 kg/s/tube)	
Heat duty	3.46×10^6 Btu/h (1014 kW)	
Ammonia inlet temperature	49.3°F (9.6°C)	
Ammonia entrance quality	100%	
No. of active tubes	3	

Parameter	Predicted*	Measured
U (Btu/h-ft ² -°F) (W/m ² -K)	440 2500	510 2900
Δp (psi) (kPa)	1.8† 12.4	3.7 25.5

*Based on annular flow film coefficient for ammonia and drift flux void fraction model.

†With gravity pressure recovery; 2.6 psi (17.9 kPa) without gravity pressure recovery. Film coefficient and void fraction models have large influences on underestimation.

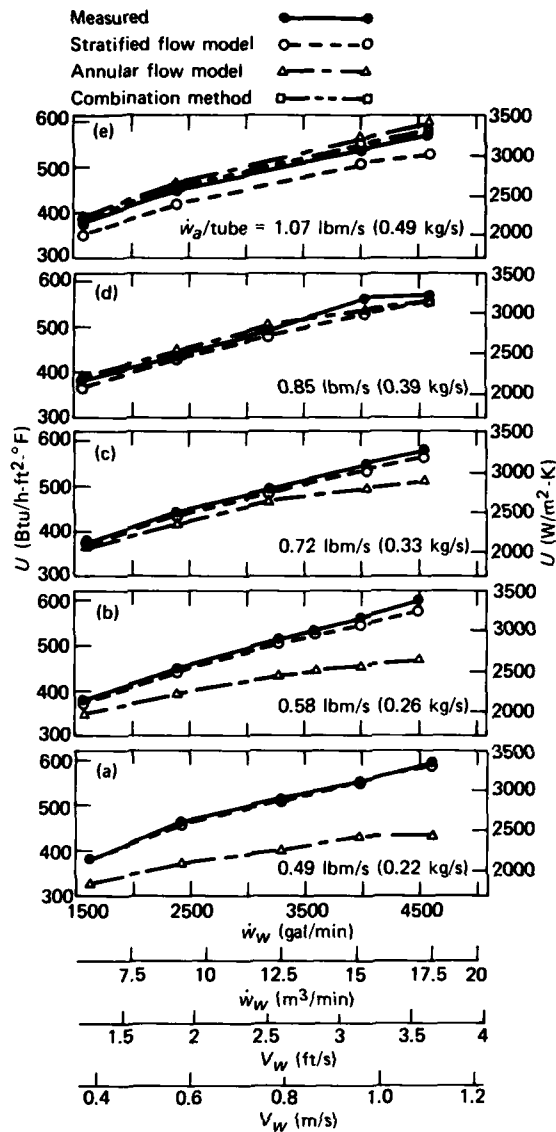


Fig. 2 Comparison of heat transfer coefficients with stratified and annular flow models for a range of ammonia flows.

predicted because its prediction was coupled directly to the ammonia film coefficient, which also was underpredicted. The components of the pressure drop are the two-phase loss in the horizontal runs, the two-phase loss in the bends, a minor deceleration gain resulting from the conversion of vapor into liquid, and a gravity head recovery as liquid is formed in the downward flow. The test data were examined with the stratified flow model that successfully explained U . The two-phase friction loss was calculated using existing

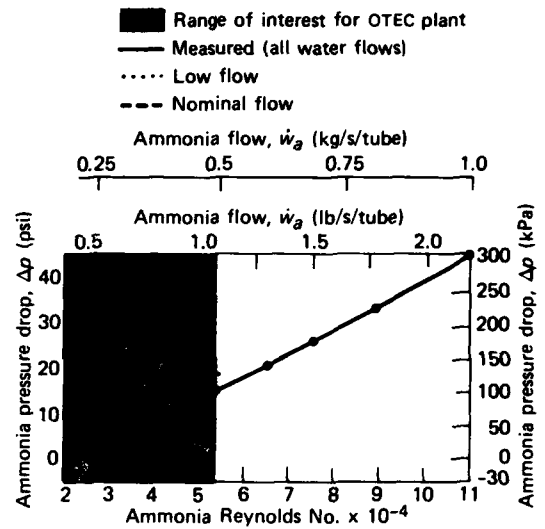


Fig. 3 Measured and predicted ammonia pressure drop versus ammonia flow rate and Reynolds number. Negative values indicate predicted pressure recovery resulting from gravity effects.

correlations for large bore pipes,⁵ the gravity head recovery was neglected because of the stratified nature of the flow, and the deceleration gain was determined using the stratified void fraction. The resulting two-phase bend loss coefficient (which is a two-phase dimensionless equivalent length for the bends) was computed by subtracting these three components from the measurement. A value of 1.5 ± 0.2 was found; it is smaller than the value that was being used (2.0).

In summary, the results of the condenser core tests for both U and Δp have been explained adequately using a stratified model for the ammonia flow. An analytical simulation of condenser performance has been modified to reflect these results. Using this data base and that generated by the evaporator core tests, the heat exchangers for a full-size OTEC pilot plantship can now be designed.

REFERENCES

1. J. F. George, D. Richards, and L. L. Perini, *A Baseline Design of an OTEC Pilot Plantship*, JHU/APL SR 78-3 (May 1979).
2. P. P. Pandolfini, W. H. Avery, and F. K. Hill, "Experiments on Cleaning of a Shell-Less Folded-Aluminum-Tube, OTEC Heat Exchanger," *Proc. 6th OTEC Conf.*, Washington, D.C., 19-22 Jan 1979.
3. P. P. Pandolfini, J. L. Keirse, and J. A. Funk, "Testing of the APL OTEC Heat Exchanger as an Evaporator," *Developments in Science and Technology*, JHU/APL DST-7, Fiscal Year 1979.
4. Y. Taitel and A. E. Dukler, "A Model for Predicting Flow Regime Transition in Horizontal and Near Horizontal Gas-Liquid Flow," *J. Am. Inst. Chem. Eng.* 22, No. 1, pp. 47-55 (1976).
5. J. F. Collier, *Convective Boiling and Condensation*, McGraw-Hill, New York (1973).

DEVELOPMENTAL TESTING OF A CONCRETE COLD WATER PIPE FOR OTEC SYSTEMS

R. W. Blevins and J. S. O'Connor

The Ocean Thermal Energy Conversion (OTEC) plantship is designed to generate electricity by using the natural temperature gradient of the tropical ocean. Large quantities of water are drawn through a pipe to the ocean surface from depths of 3000 ft in order to condense the plant's working fluid. A one-third scale model of the lightweight concrete cold water pipe (CWP) for a 40 MWe (nominal) pilot plantship was fabricated and tested to destruction. The model was 10 ft in diameter, with 2-in.-thick reinforced concrete walls and 3-in.-thick post-tensioning channels. It had an overall height of 17 ft, including the scaled hinge region in the center. The operation of the hinge joint was verified and the stiffness of the joint was determined experimentally. The model was then loaded incrementally until failure, which occurred at a load approximately 40% greater than the design load.

BACKGROUND

APL has designed a pilot plantship having a capacity of 40 MWe (net) that requires a CWP 30 ft in diameter.¹ Concrete is the least expensive of the candidate materials for the pipe, and the strength of the structure can be changed by varying the amount of steel reinforcing. However, the more common concrete formulations have two disadvantages, they are heavy and are relatively stiff. The use of a standard lightweight structural concrete (110 to 120 lb/ft³) would result in large dynamic loads in the pipe and greater deployment costs because of the equipment needed to deploy large heavy sections or the added time needed to deploy smaller sections. Dynamic analyses of the barge and CWP show that a flexible CWP is desirable.² The stresses caused by platform pipe dynamics in a rigid CWP require very thick walls, which can be quite heavy.

To circumvent these problems, a program was initiated to design and test a structural concrete that (a) would be light in weight when immersed in seawater (a unit weight of approximately 70 lb/ft³, compared to a seawater density of 64 lb/ft³); (b) would have a compressive design strength of 3000 psi; and (c) would retain the durability and the insulating characteristics of heavier concretes. A hinged CWP that would increase the flexibility and reduce the maximum stresses was

This work was supported by the Department of Energy (Division of Solar Energy Technology) and the Department of Commerce (Maritime Administration).

designed concurrently. The final lightweight, expanded-clay-aggregate concrete developed in Phase I of the project³ is heavier but stronger than was originally specified and satisfied the pipe design requirements.

The current CWP design consists of 30-ft-diameter segments, each 50 ft long, that are joined at sea to produce a 3000-ft-long pipe. A typical pipe segment is shown in Fig. 1. One segment is joined to another by slipping the flared end (the bell) of one over the narrow end (the spigot) of the other and rotating it 15° to lock the segments in position. Neoprene pads between the two sets of bearing surfaces allow 1° relative rotation of the two segments.

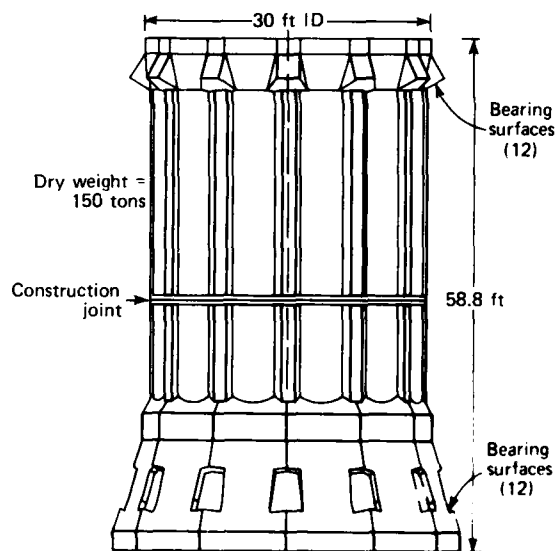


Fig. 1 Typical CWP segment.

The lightweight concrete development program was executed in two phases. The first phase³ was devoted to the development of the material itself. The second phase, devoted to a structural test of a scale model of a CWP segment, addressed five major task areas:

1. Develop the analytical models for pipe design.
2. Experimentally develop the design details of the CWP. This task included tests of bearing

pads, shear reinforcement, post-tensioning anchors, and shear tests of full-scale reinforced concrete corbels.

3. Determine whether the lightweight concrete can be successfully mixed and placed by production personnel (as opposed to laboratory technicians).
4. Verify the functional operation of the pipe joint. Experimentally determine the rotational, axial, and shear stiffness of the joint and compare them with computer predictions.
5. Verify the structural computer models used to design the pipe by testing the pipe to destruction and measuring deformations, stresses, and strains. Modify the computer models, if necessary, to resolve any discrepancies.

DISCUSSION

The model was designed using a straight geometric scaling law. Since the nonlinear stress-strain behavior of the concrete had to be known to complete tasks 2, 3, and 5 above, the model had to be constructed of lightweight concrete. Therefore, the modulus of elasticity, E , and the nonlinear stress-strain behavior are identical in the model and in the full-scale pipe. The model bearing pads have scaled stiffness properties. Strain is nondimensional and is not affected by scaling laws. If λ is the scale factor for length, then force scales by λ^2 and moment scales by λ^3 . Since this is a static test, the fact that gravity is not properly scaled has a negligible effect. The selected scale factor of one-third was based on manufacturing considerations and the space available to house the test specimen. It was felt that a 2 in. wall was the minimum that could be cast. On the other hand, any test specimen larger than one-third scale could not be tested indoors.

The test specimen was manufactured using production personnel. Figure 2 shows the completed assembly in the test fixture prior to the start of testing. A cutaway view of the test setup is shown in Fig. 3. The vertical loads are applied by four hydraulic rams acting against the end blocks and are reacted through the pipe. The steel frame structure supports only the dead load, not the test loads. Shear loads are applied by separate hydraulic rams acting on cables that extend diagonally from one end block to the other. This allows any combination of axial load, moment, and shear to be applied to the specimen by balancing the pressures in the six hydraulic rams.

The data processing system recorded 100 channels of data at each load step, including the applied loads, the deflections of the pipe (both absolute

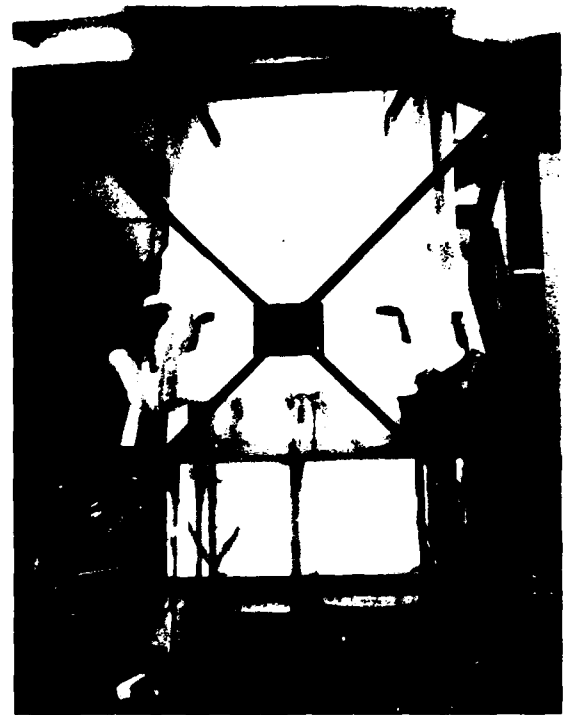


Fig. 2 Specimen in test fixture prior to testing.

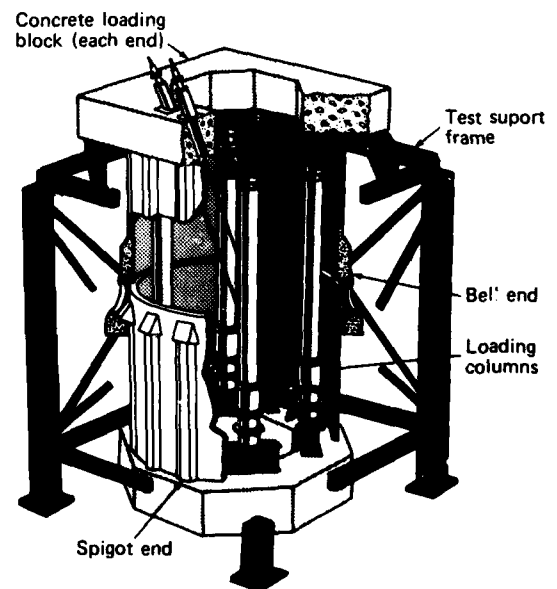


Fig. 3 Cutaway view of the test setup.

deflections and deflections of one section relative to the other), and strains in key areas of the concrete and the steel rebars (reinforcing bars).

The design loads for the test specimen were based on the plantship/CWP design as of April 1979. The maximum pipe loads were determined using the Paulling SEGPIP computer code and two Bretschneider sea spectra, for which the significant wave heights and periods were:

$$\begin{array}{ll} H_{s1} = 18.0 \text{ ft} & T_0 = 9.8 \text{ s} \\ H_{s2} = 29.0 \text{ ft} & T_0 = 18.0 \text{ s} \end{array}$$

The first condition is that beyond which the OTEC plant would be shut down; the second represents the 100-year storm condition in siting area Atlantic-1 east of Brazil. The resulting design loads are (in model scale):

Axial load	728,000 lb
Shear	24,000 lb
Rotation	0.68°
Moment	802,000 ft-lb

The test specimen was designed to these values, tested to these values, and then tested to destruction.

RESULTS AND CONCLUSIONS

Ultimate failure of the model occurred at about 140% of the ultimate design load. The failure mode was the loss of one of the circumferential post-tensioning cables in the bell segment. The loss of this cable resulted in considerable spalling and cracking in the bell area. No through cracking occurred in the cylindrical part of either pipe section. The maximum stress observed in the steel rebar was approximately 48,000 psi, still below its allowable stress of 60,000 psi.

Other than some stress concentration cracks at the corners of the cutouts, structural cracking occurred at the predicted load in the predicted locations. The rotational stiffness of the joint was approximately 24%

less than the predicted value. The data used to select the bearing pads have been reviewed and modified based on these results.

The following conclusions are drawn from the test program:

1. The analytical models used to design the test specimen have been verified for use on other designs.
2. The lightweight concrete can be mixed and placed by production personnel using normal practices and procedures. Quality assurance samples taken from the batches mixed for the scale model exhibited consistent unit weights and strengths. With the addition of a plasticizer, the concrete could be mixed to have any desired slump.
3. Normal conventions and code requirements can be used in designing with this material.
4. The lightweight aggregate must be stored in a dry, sheltered location in order to maintain its light weight. Aggregate stored in the open absorbs water, and concrete mixed with that aggregate has a higher than normal unit weight.
5. The hinge joint behaved basically as expected, although the rotational stiffness of the joint was less than expected and the center of rotation shifted slightly under the load. The concept of the joint has been verified.

REFERENCES

- ¹ J. F. George, D. Richards, and L. L. Perini, *A Baseline Design of an OTEC Pilot Plantship*, JHU/APL SR 78-3A (May 1979).
- ² J. R. Paulling, "Frequency Domain Analysis of OTEC CW Pipe and Platform Dynamics," paper No. 3543, presented at 11th Offshore Technology Conf., Houston, Tex., 30 Apr to 3 May 1979.
- ³ J. S. O'Connor (ed.), *Lightweight Concrete Development Program Phase I*, JHU/APL SR 79-1 (Apr 1979).

THE ENVIRONMENTAL ASSESSMENT GROUP'S ACCOMPLISHMENTS IN FISCAL YEAR 1980

W. D. Stanbro and L. G. Phillips

The Environmental Assessment Group is involved in a wide variety of projects in environmental impact analysis and resource assessment. This report gives a brief account of the group's principal accomplishments in fiscal year 1980. It then describes in more detail two projects that illustrate the breadth of its work.

BACKGROUND

The major activities of the Environmental Assessment Group center around the Detailed Site Evaluation section of the State of Maryland Power Plant Siting Program. The work was carried out in cooperation with the Chesapeake Bay Institute of The Johns Hopkins University. The group is responsible for evaluating the potential environmental impacts of all power plants to be built in the state. In addition to studies of particular sites, the group also conducts generic studies on problems applicable to more than one site. The group's assignment in both the site specific and generic studies covers all areas of possible effects on the natural and human environment (including air, water, and land) and economic and social effects.

Site specific activities this fiscal year have been concerned with the evaluation of a proposed 600 MWe coal-fired unit, Vienna Unit 9, that the Delmarva Power and Light Co. wants to add to its present power plant at Vienna, Md., on the Nanticoke River. Although the evaluation is still in progress, the results of major segments of the analysis have been published, including (a) the effects of air pollution from the burning of coal,¹ airborne emissions from the cooling tower,² and noise³; (b) the effects on the aquatic life of the Nanticoke^{4,5}; (c) and socio-economic aspects.^{6,7} A study is nearing completion of the potential effect on groundwater and aquatic biota of alternate techniques for disposing of waste from coal combustion and stack gas cleaning processes.⁸

Major generic studies finished this year include the possible risks near nuclear power plants,^{9,10} the environmental effects of high voltage electric transmission lines,^{11,12} the stability of the water tracing dye, Rhodamine WT, in saline waters,¹³ and the population

This work was supported by the State of Maryland, the National Park Service, the U.S. Coast Guard, Argonne National Laboratory, the Solar Energy Research Institute, and the U.S. Department of Energy.

dynamics of striped bass in the Chesapeake Bay system.¹⁴

The group has evaluated the economics of producing vacuum-deposited photovoltaic cells for the Solar Energy Research Institute¹⁵ and has developed a methodology to aid in siting storage facilities for spent nuclear fuel for the Department of Energy.¹⁶ The group has reviewed the safety of liquid natural gas transport operations within the Chesapeake Bay area for the State of Maryland Coastal Zone Unit¹⁷ and has participated in a study of the application of alternative energy technology to the U.S. Coast Guard's lighthouse system. There has also been a major effort in evaluating landfills as a source of methane. This work has been supported by the Department of Energy through the Argonne National Laboratory¹⁸ and by the National Park Service.¹⁹

DISCUSSION

Because of the many subject areas, it is impossible to describe all of them fully; therefore, we have selected two projects as examples of the group's activities: the modeling of the population dynamics of striped bass¹⁴ and the evaluation of methane production from landfills.^{18,19}

Striped Bass Population Dynamics

A major point of contention in several regulatory hearings the group has attended is the effect of power plant construction on the population of striped bass in Maryland waters. This concern is natural since striped bass support a major commercial and recreational fishery in the state. In addition, striped bass spawned in the Chesapeake Bay's tributaries are the predominant source of fish for the Atlantic Coastal fishery from New England to the Carolinas. The concern has been heightened by the precipitous drop in the yield of the fishery since the mid 1970's.

Striped bass are anadromous fish: they spend most of their lives in saltwater but swim to a freshwater portion of an estuary to spawn. Their principal spawning areas in the Chesapeake Bay system are the Potomac River, the Chesapeake and Delaware Canal, the Nanticoke River, and the Choptank River. The spawning areas of the first three bodies of water have been proposed as sites for power plant construction in recent years. Utilities are drawn to the locations by the

abundant cooling water that is available and by the desire to be located reasonably close to their load centers. Several modeling techniques are available to predict the effect of a power plant's operation on a given year's spawn. However, because of the species' complex life history, it is difficult to translate such losses into a decrease in the number of adult fish available for harvesting.

A member of the Environmental Assessment Group recently has finished a major study¹⁴ that attempts to paint a quantitative picture of the factors influencing striped bass survival and the strength of the fishery. The population dynamics of the species has been conceptualized in terms of a mathematical model, which has two parts. The first part is a model of the adult population. The factors considered were migration between the Chesapeake Bay and Atlantic coastal waters as a function of age and sex, and the mortality owing to natural factors and commercial and recreational fishing as a function of age, sex, and location (bay versus coastal). The second part is a stock-recruitment model that bridges the gap between the adults and their progeny that reach adulthood. The model considers not only the effects of spawning-population size but also environmental factors.

One of the chief difficulties in population modeling, particularly a model as detailed as this one, is the lack of reliable data. In fact, the available data are often contradictory. A major achievement of this effort has been the review and reconciliation of much of the available data. As a result, the allowed values of most model parameters have been constrained. Much of the reconciliation of data has come about through the realization that there are major differences in the migratory behavior of male and female striped bass. While it has long been suspected that the Chesapeake Bay system produced most of the striped bass in the coastal fishery, a very small proportion of the striped bass tagged in the bay showed up in the ocean. This behavior is explained by the discovery that most of the coastal fish are females that have migrated from the bay while immature without having moved into the spawning areas. The tagging studies used fish caught in the spawning areas. Those fish are predominately young males who stay in bay waters for a longer period than the females and move into the spawning areas at a younger age because they become sexually mature sooner than the females. Partly because of heavy fishing in the bay, only a small number of those males ever move into the coastal fishery.

The addition of young striped bass to the fishery is dominated by an occasional exceptionally good year, when large numbers of fish survive to the fingerling stage. Several years later, that year class is responsible for a large increase in the adult population, and the

increase is reflected in the yield of the fishery. Previous studies have suggested that the good years may be related to cold winter temperatures and high spring flows in the rivers where striped bass spawn. The postulated mechanism involves the increased availability of nutrients for the microscopic animals that provide the food for young striped bass. The last good year when a dominant year class was spawned was 1970. The size of the population and the harvest has declined sharply recently.

A major concern in the management of the fishery is the effect of the reduced spawning stock on the specie's ability to rebound, given the proper environmental conditions. The study described here has established that the size of the spawning stock may have some effect on the size of the year class; however, it remains apparent that most of the variability is due to environmental parameters. The size of the spawning stock may have only a limited bearing on the size of the spawn because of the tremendous fecundity of striped bass females. The average mature female produces 168,000 eggs per kilogram of body weight. Therefore, relatively few females are needed to produce a large number of fish if conditions are good for egg and larval survival.

The model was used in the group's power plant siting work to analyze the effects of entrainment by the proposed Vienna Unit 9. Entrainment is the destruction of eggs and larvae when they are drawn into the power plant along with the cooling water. The Vienna plant will entrain, on the average, 2% of the eggs and larvae spawned in the Nanticoke. According to the model, this will result in a loss of 4% or less of the adult fish produced from spawning in the Nanticoke. However, since the Nanticoke produces only 12% of the striped bass spawned in Maryland waters, the actual loss to the Maryland fishery is only about 0.5%.

Landfill Methane Recovery

APL has been involved with developing landfill gas recovery and utilization technology since 1977. Landfill gas, typically composed of 60% methane and 40% carbon dioxide, is formed in sanitary landfills as the deposited organic refuse decomposes. In the past few years, landfill gas has been developed into an economically competitive energy resource. It is estimated that approximately 1% of the nation's natural gas demand could be satisfied with gas recovered from landfills.

APL is currently under contract to the Department of Energy through the Argonne National Laboratory to study various aspects of landfill gas technology. Under the contract, APL recently released

the *Landfill Methane Utilization Technology Workbook*,¹⁸ which contains basic facts regarding landfill gas recovery including discussions on the generation of gas in landfills, gas collection systems, and options for control and use of the gas. Results of APL's landfill gas computer model for predicting the gas generation rate are included. The workbook also contains summaries of eight landfill gas recovery operations and information on guidelines and sources of support. A detailed discussion of legal aspects is included. The workbook concludes with a comprehensive annotated bibliography.

APL has recently completed field testing in a feasibility study¹⁹ for the National Park Service at the Kenilworth and Oxon Cove landfills in the Washington, D.C., area. The study was conducted to provide preliminary estimates of the quantity and quality of the gas at the two landfills for possible recovery. Gas wells and probes were installed at various locations and depths in the landfills, and APL has instrumented a mobile testing laboratory that contains equipment to measure the composition of the landfill gas, the internal temperature and pressure of the landfill, and the flow rates of the gas pumped out. The laboratory contains a portable gas chromatograph and digital integrator to analyze the gas for carbon dioxide, hydrogen, oxygen, nitrogen, and methane. Very little equipment is specifically designed for analyzing landfill gas, and APL is continuing to develop field testing techniques to provide accurate methods that will shorten future testing programs.

REFERENCES

- ¹J. A. Kagan, *Prediction of Air Quality Impacts for Stack Emissions from the Proposed Vienna Unit No. 9*, JHU PPSE 8-13 (Aug 1980).
- ²E. A. Davis and V. T. Freeman, *Environmental Assessment of Cooling Tower Drift and Vapor Emissions for the Proposed Vienna Unit No. 9*, JHU PPSE 8-3 (Aug 1980).
- ³M. Cwiklewski, *Prediction of Noise Impacts by the Proposed Vienna Unit No. 9*, JHU PPSE 8-2 (Feb 1980).
- ⁴E. M. Portner and L. C. Kohlenstein, *Prediction of Entrainment/Impingement Impact for Striped Bass Eggs and Larvae by the Proposed Vienna Unit No. 9*, JHU PPSE 8-1 (Nov 1979).
- ⁵W. D. Stanbro, D. A. Pyrch, and E. M. Portner, *Prediction of Chemical Concentrations in the Blowdown of the Proposed Vienna Unit No. 9*, JHU PPSE 8-4 (Feb 1980).
- ⁶C. L. Blinder, *Prediction of Socio-Economic Impacts by the Proposed Unit No. 9 at Vienna and Alternative Sites*, JHU PPSE 8-7 (Aug 1980).
- ⁷C. L. Blinder, *Land Use and Development Trends in Dorchester and Wicomico Counties*, JHU PPSE 8-12 (Aug 1980).
- ⁸E. M. Portner, et al., *Prediction of Impacts from the Solid Waste Disposal Area for the Proposed Vienna Unit No. 9*, JHU PPSE 8-5 (Dec 1980).
- ⁹T. S. Margulies, *Evaluation and Comparison of High Population Density Sites*, JHU PPSE-T-12 (Oct 1979).
- ¹⁰T. S. Margulies and T. W. Eagles, *Projected Dose Probability Distribution from Hypothetical Accidental Releases at the Calvert Cliffs Nuclear Plant*, JHU PPSE-T-15 (Aug 1980).
- ¹¹J. P. Reilly and M. Cwiklewski, "Rain Gutters Near High-Voltage Power Lines: A Study of Electric Field Induction," presented at IEEE PES Summer Meeting, Minneapolis, Minn., 13-18 Jul 1980.
- ¹²J. P. Reilly, *Spark Discharge Characteristics of Vehicles Energized by AC Electric Fields*, JHU PPSE-T-16 (Oct 1980).
- ¹³W. D. Stanbro and D. A. Pyrch, "Stability of Rhodamine WT in Saline Waters," *Water Resour. Res.* 15, No. 6, pp. 1631-1632 (1980).
- ¹⁴L. C. Kohlenstein, *Aspects of the Population Dynamics of Striped Bass [Morone saxatilis] Spawning in Maryland Tributaries of the Chesapeake Bay*, JHU PPSE-T-14 (Feb 1980).
- ¹⁵C. Feldman, et al., *Vacuum Deposited Polycrystalline Silicon Films for Solar Cell Applications, Final Report*, JHU/APL SER1/XS9/8278/4 (Dec 1980).
- ¹⁶T. S. Margulies and T. W. Eagles (APL) and the Department of Geography and Environmental Engineering (JHU), *Location Systems Analysis of Away from Reactor Spent Fuel Storage Facilities in the Eastern United States*, DOE/ET/47924-3 (Jun 1980).
- ¹⁷T. S. Margulies, *Cove Point Liquefied Natural Gas Operations, A Preliminary Review of the Risks*, JHU PPSE-T-13 (Jan 1980).
- ¹⁸R. C. Eberhart, L. Green, and G. Yoshioka, *Landfill Methane Utilization Technology Workbook*, JHU/APL CPE-7909 (Dec 1979; revised Apr 1980).
- ¹⁹L. G. Phillips and S. L. Shadel, *Landfill Gas Testing Programs at Kenilworth and Oxon Cove Landfills*, JHU/APL CPE-8001 (Jul 1980).

DUCT FIRES

L. W. Hunter

A model of the spread of fire in a circular fuel-lined duct has been developed. Extinction and acceleration limits are explored and the propagation speed is calculated. The model is the first to explain the experimentally observed behavior from basic principles.

BACKGROUND

Fire can spread rapidly over many solid fuels in narrow spaces. One important geometry is a fuel-lined duct, such as a building shaft. Other examples are electric cable conduits and two planar surfaces that face each other closely, as a stack of lumber. Fire in these situations is highly turbulent. Although the composition and velocity of the combustion gases vary with position parallel to the direction of propagation, the turbulent mixing tends to make conditions laterally uniform in an average sense. In addition, such geometries preclude the lateral plume expansion that would occur in a wall fire in an open room. These fires are one dimensional and thus are ideal for comparing theory and experiment.

Roberts and Clough¹ pioneered in experiments on duct fires. Those experiments dealt with thick-walled ducts in which heat was lost from the fire by radial conduction into the wall. The present calculation focuses on thin-walled ducts, with no radial temperature gradients in the wall. Instead, convective heat losses replace the conduction losses. Heat is lost at a rate proportional to the difference in temperature between the wall and the surroundings. The convective description keeps the problem one dimensional and is expected to reproduce the qualitative features of the experiment.

DISCUSSION

It is desired to determine the conditions under which fire spreads at a steady speed, V , and to determine the value of V in a circular duct lined with fuel over its entire circumference. The duct geometry is shown in Fig. 1.

The approach is to assume that steady fire spread has been achieved. As seen by an observer moving at the speed V , the temperature distributions do not change with time and the problem can be set up as shown in Fig. 2. The fire appears as a counterflow

This work was supported by the U.S. Nuclear Regulatory Commission.

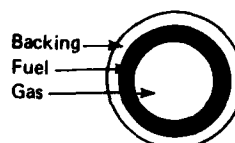


Fig. 1 Duct geometry. The solid fuel forms gaseous fuel and burns with incoming air.

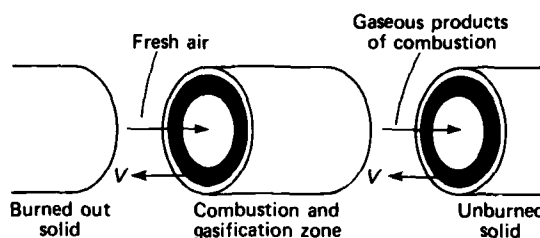


Fig. 2 Fire spreading steadily through the duct, as seen by an observer moving at the propagation speed, V .

process in which the solid flows to the left while air and combustion gases flow to the right. In the fire zone, the solid releases gaseous fuel that burns with the oxygen in the air. It is unknown in advance whether there is more fuel gas than oxygen or more oxygen than fuel gas in the combustion zone; hence, both possibilities must be considered in the analysis. It turns out that the oxygen-rich combustion is unstable. The governing equations prescribe conservation of mass and heat in both the solid and the gas phases. The equations are solved in terms of integrals that are evaluated numerically. The mathematical details are given in Ref. 2.

Conditions are varied to explore for limits in which the calculated temperatures become negative or imaginary. In those limits, the original assumption of steady fire spread is contradicted. The limits therefore show where the fire becomes unsteady and either accelerates or decelerates. On the other hand, if the calculations give positive temperatures but physically unrealistic trends in certain cases, we conclude that the propagation is steady but unstable.

The analysis is simple when the rate of heat loss from the duct to the surroundings is zero, that is, when the duct is thermally insulated. The steady propagation speed is given by an overall energy balance, which equates the input rate of chemical energy contained in the oxygen supply (left side of the equation) to the net

rate at which energy is consumed in gasifying the solid (right side):

$$Q \dot{m}_r^{(-\infty)} Y_{O_2}^{(-\infty)} / r = LPY_f V .$$

In this equation, Q is the heat of combustion per unit mass of fuel consumed, $\dot{m}_r^{(-\infty)}$ is the input mass flow rate of air, $Y_{O_2}^{(-\infty)}$ is the mass fraction of oxygen (O_2) in the air, r is the mass ratio of oxygen to fuel consumed, L is the latent heat of gasification of the solid, P is the mass of solid per unit length, and Y_f is the mass fraction of solid that gasifies. The conditions for steady propagation in the insulated duct are shown in Fig. 3. The two curves mark the highest and lowest heat release rates at which steady propagation exists. Below the straight line $Q = L$, the fire is oxygen-rich and unstable. There is also a practical upper limit arising because typically

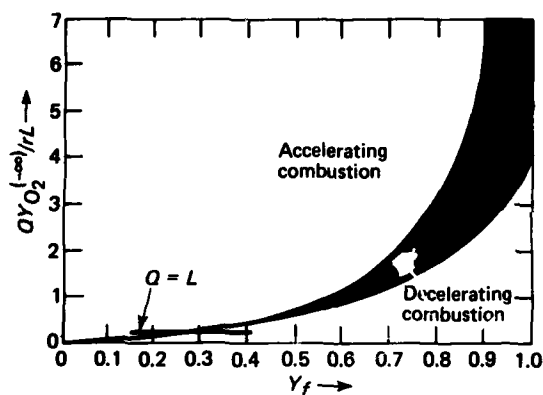


Fig. 3 Conditions for steady fire spread in an insulated duct.

$$\frac{QY_{O_2}^{(-\infty)}}{rL} \leq 2$$

in normal air. Thus, in practice, the conditions for steady combustion are actually limited to the small crosshatched region of the figure.

The analysis is more complicated with nonzero heat losses to the surroundings, but the results are simple and in agreement with the experiments by Roberts and Clough.¹ The steady propagation speed is given to reasonable accuracy by

$$\frac{rPY_f V}{\dot{m}_r^{(-\infty)} Y_{O_2}^{(-\infty)}} = 3.0 .$$

Calculations of the limits of steady propagation are presented in Ref. 2.

The duct fire calculations of Ref. 2 are encouraging and should help in the design of experiments on thin-walled ducts. Indeed, the thin ducts may be easier to examine experimentally than the thick-walled ones.

REFERENCES

- ¹A. F. Roberts and G. Clough, "The Propagation of Fires in Passages Lined with Flammable Material," *Combust. Flame* 11, p. 365 (1967).
- ²L. W. Hunter and S. Favin, "Fire Propagation in a Thermally Thin Fuel-Lined Duct with a Parallel Well-Mixed Flow," *Combust. Flame* (to be published).

SPECIAL-PURPOSE LABORATORIES AT APL

INTRODUCTION

There is a wide variety of special-purpose laboratories at APL. Some deal with fundamental research, some assess performance of Navy systems, some evaluate designs, and others assure that product quality is maintained. Aside from those laboratories committed to research, APL's facilities are generally oriented to support Navy and space programs in critical technological areas, to assess performance of weapons and space systems, or to support the operation of selected space systems.

Special-purpose laboratory operations began at APL when the Laboratory was founded. For example, facilities were established for testing the VT fuzes during the development and production phases of that program. A propulsion laboratory has been used continuously since the early days of the guided missile programs to study problems associated with ramjets and other airbreathing engines suitable for propulsion at supersonic speeds. Other laboratory facilities have been set up and operated as the needs of assigned tasks have dictated. The need for some facilities has disappeared as problems have been solved or as emphasis has changed; e.g., APL no longer is responsible for VT fuzes. The objectives that the special laboratories address are to monitor the performance of existing systems, to validate concepts and designs for new systems or equipment, to ensure quality in products prepared by APL, and to advance the state of knowledge in selected technological areas.

The Guidance System Evaluation Laboratory exemplifies the evolution of a special-purpose laboratory. Originated during the development of the semi-active homing system for Terrier and Tartar missiles, it could assess seeker operating characteristics and obtain data needed for integrating the seeker into the missile and for planning flight tests. With missile evolution, the scope of testing was expanded to include the entire guidance system. Representation of static targets quickly gave way to the simulation of targets with noise, then moving targets, and then targets with countermeasures. With the growth of missile complexity and threat severity, changes have been necessary to assure meaningful testing. Recent renovation permits testing of the latest guidance systems using on-board digital computers. Current threats involving multiple, high-speed, air-to-surface missiles attacking in intense ECM environments can be represented.

Four interests underlie the special laboratories at APL: exploration of the unknown; validation of theory, concepts, and designs; improvement of

products; and maintenance of existing products. The first provides the basis for the activities of the Research Center, with careful consideration being given to the specific areas of investigation. The second, though akin to the first, pertains to the application of technological advances to new or existing systems and is necessary to ensure that the foundation of new designs is sound. In some areas the need for experimental validation may be temporary or occasional, but in many areas (for instance, those concerned with improving communications, either man-to-machine or machine-to-machine) a continuum of operations is to be expected involving increasingly exacting levels of detail in implementation. There are many ways in which product improvements may be sought. They range from expansion of product applicability and revision to meet new goals, to improvement of control of the content of a product to ensure that performance goals are achieved. Even the reduction of the time needed to create a product is of concern (for instance, reducing the time needed to complete an assessment and generate a report). Similarly, the maintenance of existing products (such as the performance of a weapon system as determined by comprehensive system tests) can make it necessary to have laboratory systems that will provide prompt and thorough examination. The current nature of our society, which stresses technological advances while still recognizing the high cost of improvements, can be expected to stimulate the use of special-purpose laboratories.

In addition to supporting other operations at APL, special-purpose laboratories serve three basic purposes, principally for the Navy missile program and the space program, to assess the performance of the operational systems, to develop new concepts for improvements, and to evaluate new equipments and systems. In a number of instances, these laboratories operate in unique areas. Examples are the Combat Systems Evaluation Laboratory, which demonstrates and evaluates combat direction system concepts, the Guidance System Evaluation Laboratory, which assesses actual missile guidance hardware under representative RF environmental conditions, the Satellite Control and Command Center, and the Strategic System Data Processing Laboratory. Experience indicates that some special-purpose laboratories may be phased out of operation as tasks are completed or as other organizations provide the capability to carry on. However, in most instances where the special laboratories are operating on the technological frontiers of programs of continuing national interest, prior practices indicate that they will continue to evolve in step with developments in the programs they serve.

GSEL TARGET DOPPLER SIMULATOR

S. F. Buono and M. M. Soukup

A simulator has been developed that will supply a complete set of spectrally pure radio frequency (RF) signals, under automated digital control, for the test and evaluation of semiactive homing missiles. The simulator can generate three independent target Doppler signals, two missile reference signals, and one spillover signal. Advanced phase-lock loop techniques are used to generate spectrally pure signals with wide modulation bandwidth capability. Phase, frequency, and amplitude modulations are controlled by a completely automated digital interface that allows closed-loop hardware evaluations to be performed on missile guidance receivers using a hybrid analog/digital computer to simulate missile-to-target dynamics. The simulator also provides adequate fine control of the target Doppler frequencies, phases, and amplitudes to simulate a two-point target, coordinated maneuvering targets, or various electronic countermeasures (ECM) techniques such as repeaters and noise jammers. The major simulator performance parameters are listed in Table 1.

BACKGROUND

The capabilities of the APL Guidance System Evaluation Laboratory (GSEL) were expanded to test state-of-the-art missile guidance systems with "hardware-in-the-loop" flight simulations. Test requirements for the new GSEL included multiple target capability, coordinated target tactics, and stringent target

maneuvering. These were achieved with a larger test chamber, a linear phased array of target antennas (to simulate relative missile-target angular motion), and a new multitarget Doppler simulator.

Closed loop testing of semiactive homing missile guidance systems requires spectrally pure RF signals that can be modulated to simulate realistic target and missile motion. Spectrally pure signals have usually been achieved with klystrons or varactor devices that are inherently narrowband; however, current ECM tactics force modern missile homing systems to operate over significantly wider RF bandwidths. In addition, previous simulations of target and missile signals were achieved by mixing and filtering techniques. This approach was necessarily narrowband, could generate spurious signals, and was prone to cause interference or improper operation.

Therefore a requirement was established for a programmable, wideband, target Doppler simulator that would provide multiple target and missile signals. The simulator also could be modulated with special waveforms in a time frame equivalent to actual operating conditions to simulate the flight environment. For semiactive missile systems, rear reference and spillover signals as well as multiple target Doppler signals are needed.

Consequently, a programmable target Doppler simulator that operates over a wide RF band was developed. Spectral purity has been achieved by using phase lock loops in conjunction with an RF synthesizer with low phase noise. The simulator features total automatic digital control by the GSEL's Pacer hybrid computer system for closed loop testing or by a Hewlett-Packard 9835 computer for diagnostic testing.

Table 1

GSEL DOPPLER TARGET SIMULATOR
PERFORMANCE PARAMETERS

Parameter	Characteristics
Microwave frequency coverage	8 to 12.4 GHz, with 2 kHz resolution
Number of targets	3
Target power output	+ 16 dBm maximum, with 0.5 dB resolution
Doppler granularity	0.1 Hz resolution
Rear reference power output	- 16 dBm maximum, with 0.5 dB resolution
Spillover power output	0 dBm maximum, with 0.5 dB resolution

DISCUSSION

A block diagram of the system is shown in Fig. 1. A digitally controlled microwave frequency generator, which operates from 8 to 12.4 GHz, provides the basic reference signal to four phase lock loops. Each contains an offset oscillator in the loop feedback network. A crystal oscillator is used as the offset oscillator in the missile reference phase lock loop.

Each of the three target phase lock loops has digitally controlled Doppler synthesizers as offset oscillators that operate at a fixed frequency above the target Doppler frequency. As a result, each target frequency is the microwave generator frequency plus

This work was supported by NAVSEASYS COM, PMS-400B and SEA-6223.

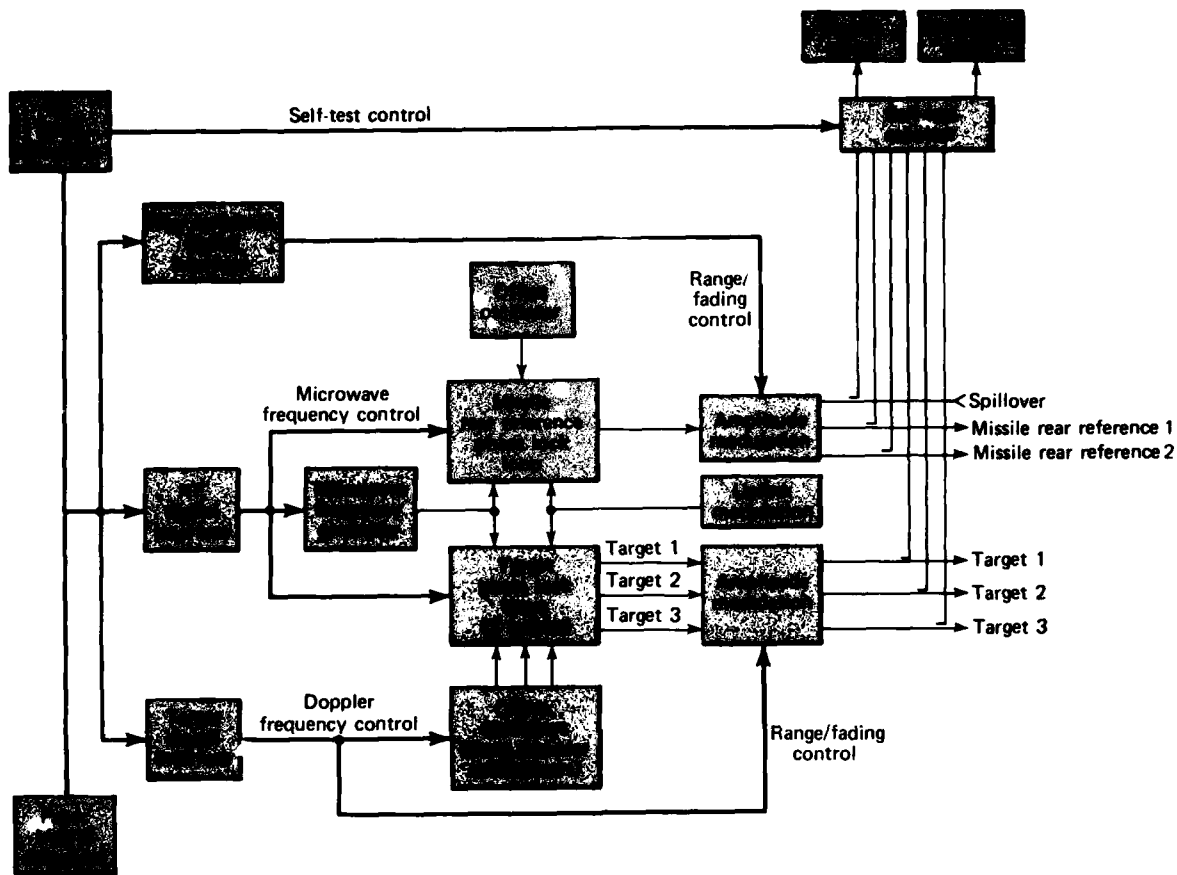


Fig. 1 Block diagram of the target Doppler simulator.

the offset oscillator frequency plus the target Doppler frequency.

The phase lock loops have been designed to provide minimum AM/FM noise for the phase locked frequency, together with the ability to track incoming target Doppler frequencies. The loops can track these Doppler frequencies at rates well above expected missile requirements. This performance has been achieved while maintaining spectrally pure signals.

The output of each phase lock loop is passed through digitally controlled microwave attenuators. In the missile's rear reference channel, the signal is split into two separate paths, which have independent control to represent illuminator-to-missile path loss and reference signal fading for each of two inputs to the missile's rear reference antennas. In addition, a portion of the missile's rear reference signal is passed through attenuators and used as a spillover signal to the missile's front antenna. Each target signal power level is controlled by three attenuators to simulate illuminator-to-target path loss, target-to-missile path loss, and a target

signal level scintillation that results from target cross section and/or multipath effects.

The required circuitry to phase modulate the signals with the missile uplink waveform (used to communicate with missiles configured for use with the Terrier and Tartar weapon systems) is included in the phase lock loop feedback networks for both the missile's rear reference and the targets.

Interface control of the Doppler generator is accomplished by a digital interface from either the GSEL's Pacer hybrid computer or the GSEL test system. Parameters under digital control for missile test operations include the microwave reference frequency, phase lock loop acquisition and track commands, target Doppler frequencies, accelerations, and signal power levels.

An HP 9835 computer is used to provide a complete self-test of the Doppler simulator, including the parameters listed in Table 1, to examine it for out-of-tolerance conditions, and to provide prompts for the

diagnosis of generator operating problems. The Doppler simulator can also be controlled by the HP 9835 computer for missile seeker open loop testing.

ACKNOWLEDGMENTS

The authors wish to acknowledge the help and cooperation of the following APL employees: R. C. LaFever, W. P. Bishop, F. N. Sansone, and D. W. Kunaniec.

AN ELECTRONICALLY CONTROLLED RF ARRAY

H. C. Davey and H. H. Knapp

A wide angle ($\pm 45^\circ$), fixed element, electronically steerable RF array system has been developed at APL for the Guidance System Evaluation Laboratory (GSEL). It is used to evaluate Standard Missile-2 seeker performance against modern maneuvering targets employing countermeasures techniques.

BACKGROUND

APL has maintained the GSEL facility for the past 16 years. It has been used to evaluate the guidance performance of successive versions of the Navy's Terrier, Tartar, and Standard Missiles. A major system in the facility was concerned with generating maneuvering targets. This was accomplished by mounting a small antenna to a wire and pulley arrangement mounted on a horizontal rail. The pulleys were driven by a servo system that, under computer control, caused the antenna to move, thereby simulating the angular location of the reflected signal from the maneuvering target. The system had several limitations. The servo-driven system limited the velocity that the simulated targets could achieve to approximately 60 degrees per second. Hysteresis effects, caused by a change in target direction, created errors in the target's angular location. The physical size of the RF

REFERENCES

- ¹M. M. Soukup, "Proposal for RF Simulator for the Advanced GSEL," JHU/APL F3D-3-040 (17 May 1976).
- ²F. M. Gardner, *Phaselock Techniques*, John Wiley and Sons, New York (1979).
- ³C. F. Fahrenkrug, "A Second-Order Phase-Lock Modulation Technique," *Microwave J.* 14 (Oct 1971).
- ⁴J. B. Payne III, "Recent Advances in Solid State Phase-Locked Microwave Signal Sources," *Microwave Syst. News* (Feb/Mar and Apr/May 1976).
- ⁵S. Wetenkamp, "Combating Phase-Lock Loop Transportation Lag," *Microwave Syst. News* (Mar 1978).
- ⁶D. Scherer, "Design Principles and Test Methods for Low Phase Noise RF and Microwave Sources," presented at Hewlett-Packard RF and Microwave Measurement Symp. and Exhibition, 1980.

darkroom that contained the antenna system limited the azimuth coverage to $\pm 18^\circ$. Also, the system was limited to a two-target capability.

With the development of Standard Missile-2, resident test capabilities began to fall short of test requirements. Consequently, the Navy approved a major upgrading of the GSEL. An important element of the new GSEL is a fixed-element RF array system.

DISCUSSION

The RF array was designed to overcome the limitations inherent in a mechanical device. An apparent target can be located between a selected pair of adjacent antennas of an array by electronically varying their relative radiated powers. Because control is electronic, target maneuvers are not limited by the antenna system. The RF array system is composed of three major subsystems: an amplitude scanner, an RF switching tree, and an array controller. A cutaway view of the upgraded GSEL is shown in Fig. 1; the major array subsystems are indicated.

Figure 2 is a photograph of the array system in the anechoic chamber. Sixty-four antennas are mounted along the top of the cylindrical wall. The switching tree components that route RF signals to selected antennas are located in the rear. The amplitude scanner and array controller cabinets are along the chamber wall. The

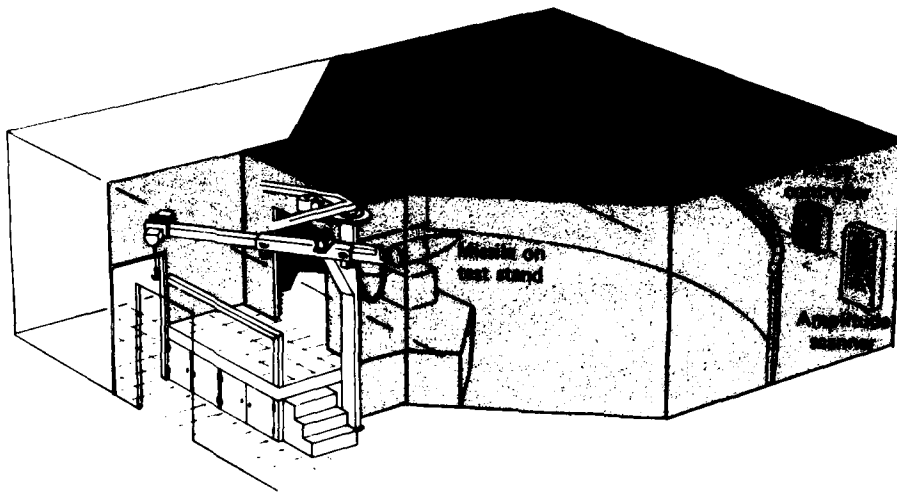


Fig. 1 Cutaway view of the upgraded GSEL.

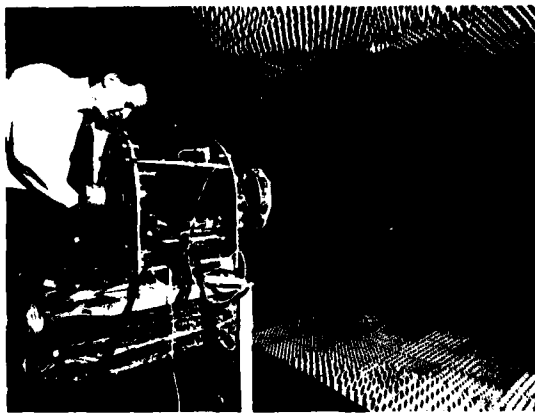


Fig. 2 Array system in anechoic chamber.

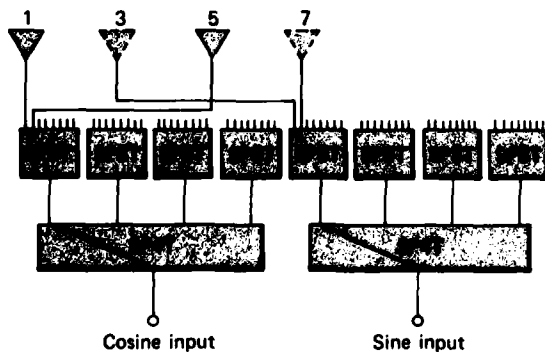


Fig. 3 RF switching tree for one array.

guidance system under test is placed at the focal point of the array.

RF radiation from selected antennas is obtained that simulates a target positioned at discrete points along the arc. First an adjacent antenna pair is selected and then the relative powers radiated from those selected antennas are adjusted. The antenna pair is designated by commands from the array controller to the switching tree (Fig. 3). RF inputs to the switching tree originate in the amplitude scanner, a controlled power divider whose outputs are determined by array controller commands. Two variables, antenna selection and RF power ratio, provide coarse and fine target positioning along the array. For example, with maximum power into the cosine input and zero power into the sine input, only antenna 1 radiates, and the target is located at antenna 1. Similarly, maximum power into the sine port and zero power at the cosine port positions the target at antenna 3. Target locations between antenna pairs are obtained by varying the power ratios between these extremes as determined by the amplitude scanner. This method of target location can be extended to include additional antenna pairs by means of the RF switching tree, thus causing linear target motion across the array.

By means of careful manufacturing procedures and the use of automated testing techniques, the array has been calibrated so that the amplitude and phase of the RF signal from each of the sixty-four paths to the focal point is within ± 0.25 dB and ± 15 electrical degrees. This tight tolerance on the system transmission loss is needed to ensure pointing errors of 1 milliradian or less across the length of the array.

The upgraded GSEL facility became operational in February 1980. Array acceptance tests have shown that the new facility can handle more sensitive testing than the previous one. It is anticipated that the RF array will continue to contribute significantly to GSEL operation in the foreseeable future.

REFERENCE

¹W. M. Gray and R. W. Witte, "Guidance System Evaluation Laboratory." *Johns Hopkins APL Tech. Dig.* 1, No. 2 (Apr-Jun 1980).

MICROPROCESSOR-CONTROLLED TERMINAL CONTROL SWITCH

C. F. Waltrip

The Computer Aided Programming (CAP) facility and the Combat Systems Evaluation Laboratory (CSEL) make computers, program development, and other resources available to authorized users. The resources are shared among users whose primary access is via computer terminals.

A major step to increase the availability of these resources was taken in 1980 with the implementation of a terminal control switch (TCS). This software-controlled switch allows interconnections to be made among computers, terminals, telecommunications lines, and other devices via serial, asynchronous links at transmission rates up through 9600 bits per second (Fig. 1).

BACKGROUND

Support of the various computer-based projects at APL requires multiple-computer systems as well as different operating systems. It is not uncommon within the CAP/CSEL facilities for four different systems to be in operation simultaneously, each controlling a separate computer.

Before 1980, the requirements of the various users of the CAP/CSEL facilities were met by permanently cabling individual computer terminals directly to specific computers. As the use of a particular computer increased, the new demand was met by cabling additional terminals to it (Fig. 2). Similarly, telecommuni-

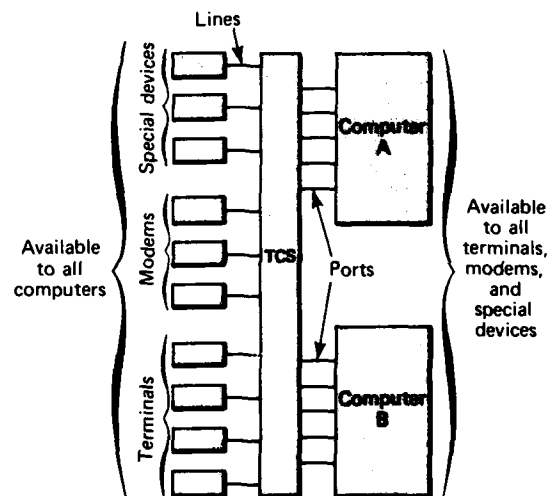


Fig. 1 Overview of TCS.

cations access as well as expansion was provided by cabling modems directly into each computer system.

Frequently the demand for access to a particular computer exceeded the number of terminals, while terminals connected to other computers were idle. It was clear that a quick, convenient way to connect any terminal to any computer was required. In this context, "convenient" meant being able to specify a computer connection from the terminal keyboard, because that

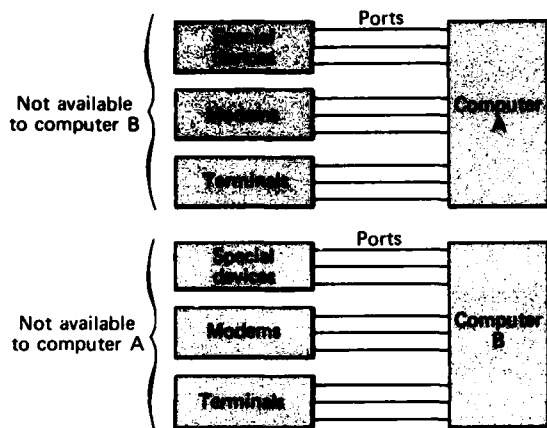


Fig. 2 Configuration prior to TCS.

would permit remote connections to be made as easily as local ones.

Remote terminals included those within the Laboratory but not adjacent to the computer facilities and also those located away from Laboratory premises for which telecommunications access was required. Remote terminals presented an additional problem in that the CAP/CSEL computers lacked the hardware to provide full modem support, and only two of the four operating systems provided software support for modems. Furthermore, only those two operating systems were equipped to provide automatic baud rate detection (the ability to determine and adapt to the specific baud rate (transmission speed) of a terminal). Baud rate detection is necessary for remote terminals because different types of remote terminals operate at different transmission speeds.

DISCUSSION

These considerations led to the following broad functional specifications for a TCS:

1. A single set of terminals was to be permanently cabled to the TCS instead of directly to separate computers.
2. Each terminal access port on each computer was to be permanently hard-wired to the TCS instead of directly to individual terminals.
3. A single set of modems was to be permanently connected to the TCS instead of directly to separate computers.
4. A user at any terminal was to be able to command the TCS from the terminal keyboard to make a connection to any computer.

A TCS meeting these specifications has been installed in the CAP/CSEL facilities. The device consists of a microprocessor-controlled time-division multiplexer. It is a Micom Micro600 model intelligent port selector that has been adapted to the requirements of the CAP/CSEL facilities. The operations of the TCS are essentially table-driven; that is, they are controlled by the contents of a predefined configuration table located in the microprocessor's memory.

The addition of the TCS to the CAP/CSEL facilities yielded the following benefits:

1. Any terminal connected to the TCS (via local, remote, or dial-in connections) can be used to specify which computer or operating system is desired. A single set of terminals and modems can serve all users, whereas a minimum of three sets of each was required previously.
2. When all the ports of a computer are in use, the user no longer encounters a busy signal, requiring continuous "retries"; he can now wait or "camp-on" until a port becomes available.
3. The TCS provides full modem hardware and software control so that these capabilities need not be satisfied by the computer hardware and software. It also provides automatic baud rate detection so that a single set of telephone lines and modems may be used by all dial-in terminals, regardless of their transmission speed. Prior to the TCS installation, at least two sets of modems and telephone lines were required.
4. When a computer is to be taken out of service for maintenance or for other reasons, access to that computer may be blocked at the TCS. Users who subsequently attempt access to it receive a stored message informing them that it is unavailable. If the computer is out of service but its operating system and data have been transferred to another computer, users are automatically routed to the other computer.
5. The TCS will disconnect any terminal from a port if there is no data activity within 20 minutes. Consequently, a computer port will not be tied up indefinitely if a user forgets to disconnect.
6. The TCS may be used by computers to establish intercomputer links. (In Fig. 3, a line is cabled to computer A, which uses this line to establish a connection through the TCS to a port on computer B.)
7. The TCS enables special-purpose devices such as graphics terminals, PROM-burners,

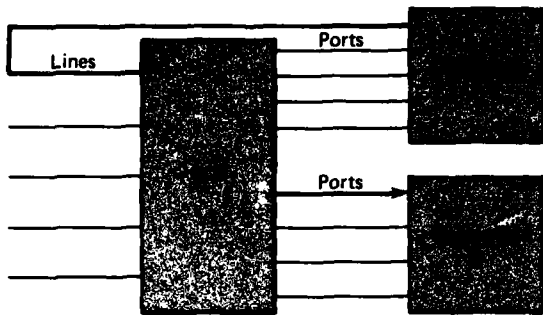


Fig. 3 Intercomputer links via TCS.

and letter-quality printers to be shared among various computers.

8. The TCS can provide statistics on terminal and computer port usage to allow the management of resource utilization, allocation, and acquisition.
9. The TCS itself has redundant logic and power supplies; all other modules are interchangeable.

REFERENCE

¹ R. L. Evans, "Optimizing Computer Access in Multi-User Systems," *Mini-Micro Syst.*, pp. 145-148 (May 1980).

PATENTS

PATENTS ACTIVITIES

The APL Patents Office is responsible for ensuring compliance with contract and grant requirements relative to patent and data rights, as imposed by the various governmental agencies that sponsor work at the Laboratory. In addition to preparing formal disclosures of inventions for the appropriate sponsors, the Patents Office prepares and prosecutes patent applications on behalf of both the University and the Department of the Navy.

The following lists indicate the invention disclosures submitted to sponsors, the patent applications prepared and filed in the United States Patent Office, and the previously filed applications that were successfully prosecuted to issuance as patents, during Fiscal Year 1980.

INVENTION DISCLOSURES

- J. L. Abita—*Microanemometer or Resistance Probe*
- J. L. Abita—*Pressure/Force Limit Switch*
- A. W. Bjerkaas, B. L. Gotwols, and G. B. Irani—*Optical Detection of the Phase Velocity of Short Gravity Waves*
- R. W. Constantine—*Foldable Aerodynamic Surface for Supersonic Anti-Ship Missile*
- R. W. Constantine—*Ramjet Powered 5 in. Diameter Guided Projectile*
- A. B. Fraser—*Hydromechanically High Pass Filtered Pressure Transducer*
- A. B. Fraser—*Spatial and Temporal Correlation of Underwater Sunlight Fluctuations in the Sea*
- A. B. Fraser—*Synchronously Detecting Transduction to Frequency Encoder*
- H. H. George and R. B. Borelli—*Threat Assessing Electronic Warfare (EW) Ranger*
- R. B. Givens and R. L. Hudson—*A Compact Electric Field Charge Measurement System*
- S. E. Grenleski, Jr., and J. L. Keirsey—*Multi-Port Dump Combustor*
- E. J. Hoffman and J. C. Loessi—*Short-Circuit-Proof DIP Test Clip*
- L. W. Hunter and C. H. Hoshall—*An Ignition Test for Plastics*
- C. A. Keller—*Apparatus and Method for Measuring the Length of an Underwater Antenna*
- C. A. Keller—*Direct Reading Fiber-Optic Monometer*
- C. A. Keller—*Method of Anodizing Tantalum Wire*
- H. A. Kues and R. H. Brown—*Current Profiling Dye Bomb*
- H. B. Land III—*Valve Position Indicator*
- J. H. Loveless—*Velocity Control Loop for Powered Wheelchairs*
- R. C. Mallalieu and H. H. Knapp—*Dual-Bridge Target Scanner*
- D. R. Marlow—*RF to IR Handover Logic Circuitry for Dual Mode Missile Guidance*

- R. C. Moore—*Clock Stopper for Static Microprocessor*
- R. C. Moore—*Current Summing Circuit for Fast D/A Converter*
- C. V. Nelson, R. F. Gasparovic, and R. V. Chappell—*Telescoping Air-Drop Oceanographic Buoy*
- J. J. Pasierb, B. F. Fuess, and L. S. Glover—*Launch Test Vehicle*
- R. F. Platte and D. Cave—*A Microprocessor Controlled Simulator of Radar Targets*
- A. S. Polk—*Water Jacketing for Test Burner*
- A. Pue—*Optimal Vehicle Following Control System*
- D. W. Rabenhorst—*High Speed TV System*
- D. W. Rabenhorst—*Improved Performance Magnetic Coupler*
- D. W. Rabenhorst—*Modular Flywheel Arrangement*
- D. W. Rabenhorst—*Series Bearing*
- K. Reinitz and L. W. Hart—*A Solid State Magnetometer*
- W. J. Roemer—*Zero Backlash, Angular Torque Transmitter*
- T. R. Small—*Flywheel Spin Stabilization Bearing*
- T. R. Small—*Soft Motor Mount*
- T. R. Small—*Superflywheel Shaft Suspension Dampener*
- S. A. Taylor—*Coherent Cancellation of Jamming*
- P. J. Waltrup, J. L. Keirsey, and W. B. Shippen—*Hyper-sonic Wide-Area Defense Missile*

PATENT APPLICATIONS

- R. H. Bauer and M. Heidkamp—*Method for Correcting Navigation Errors Due to Water Currents*
- C. Feldman, H. K. Charles, and F. G. Satkiewicz—*Method for Fabricating a Thin-Film (Si) Solar Cell with Metal Boride Bottom Electrode*
- C. Feldman, H. K. Charles, and F. G. Satkiewicz—*Thin-Film (Si) Solar Cell with Metal Boride Bottom Electrode*
- R. E. Fischell—*Recorder with Patient Alarm and Service Request Systems Suitable for Use with Automatic Implantable Defibrillator*
- R. H. Lapp—*Pivotal Support with Independent Adjusting Elements and Locking Means*
- F. Marcellino—*Low Level Circuit Continuity Tester*
- C. Philippides—*A Clock Invariant Synchronization Technique for Random Binary Sequence to NSWC*
- R. S. Potember, T. O. Pochler, and D. O. Cowan—*Organic Memory or Threshold Switch Composed of Copper or Silver Complexed with TNAP or TCNQ Electron*

PATENTS ISSUED

- C. B. Baker and J. L. Keirsey—*Hypersonic Modular Inlet*, No. 4,194,519
- W. E. Buchanan and E. F. Kiley—*Information Display Method and Apparatus for Air Traffic Control*, No. 4,196,474
- J. W. Follin and R. E. Miller—*Digital Beamsteering for a Parametric Scanning Sonar System*, No. 4,190,818
- J. B. Garrison—*Passive Acquisition System*, No. 4,173,760

- J. Gulick, J. S. Miller, and A. J. Pue—*Broadband Interferometer and Direction Finding Missile Guidance System*, No. 4,204,655
- M. L. Hill—*Method and Apparatus for Defining an Equipotential Line or Surface in the Earth's Atmosphere and Measuring the Misalignment of a Selected Line or Plane Relative to an Equipotential Line or Surface*, No. 4,199,715
- E. C. Jarrell, D. R. Marlow, and H. B. Tetens—*Target Seeker Simulator*, No. 4,215,347
- J. W. Kuck—*Pulse Doppler-Radio Proximity Fuze*, No. 4,194,203
- J. W. Kuck—*Pulse Doppler-Radio Proximity Fuze*, No. 4,195,295
- L. C. Miller, J. A. Perschy, and G. D. Smith—*Continuous Memory System*, No. 4,186,440
- J. C. Murphy and L. C. Aamodt—*Self-Calibrating Photoacoustic Apparatus for Measuring Light Intensity and Light Absorption*, No. 4,184,768
- J. C. Murphy and R. C. Cole—*Laser Interferometry Detection Method/Apparatus for Buried Structure*, No. 4,172,382
- F. N. Sansone—*Minimal Distortion Video Bandpass Filter*, No. 4,215,325

PUBLICATIONS AND PRESENTATIONS

PUBLICATIONS

- F. J. Adrian, "Principles of the Radical Pair Mechanism of Chemically Induced Nuclear and Electron Spin Polarization," *Rev. Chem. Intermed.* 3, No. 3, pp. 3-43 (1979).
- F. J. Adrian and L. Monchick, "Analytic Formula for Chemically Induced Magnetic Polarization by S-T_{1/2} Mixing in a Strong Magnetic Field," *J. Chem. Phys.* 72, No. 10, pp. 5786-5787 (1980).
- W. E. Allen, "The Magsat Power System," *Johns Hopkins APL Tech. Dig.* 3, No. 3, pp. 179-182 (1980).
- R. H. Andreo, "Variational Methods for Wave Scattering from Random Systems," *Lecture Notes in Physics — Mathematics, Methods, and Applications of Scattering Theory*, No. 130, Springer-Verlag, Berlin, pp. 92-94 (1980).
- R. H. Andreo and J. H. Krill, *Stochastic Variational Formulations of Electromagnetic Wave Scattering*, Pergamon Press, New York, pp. 565-568 (1980).
- T. P. Armstrong (Univ. Kansas) and S. M. Krimigis (APL), "Reply to Criticism by D. Hovestadt of Their Paper on Unusual Bursts Observed with Detectors Aboard IMP 8," *J. Geophys. Res.* 85, No. A7, pp. 3503-3504 (1980).
- W. H. Avery, "Ocean Thermal Energy Conversion Contribution to the Energy Needs of the United States," *Johns Hopkins APL Tech. Dig.* 1, No. 2, pp. 101-107 (1980).
- C. B. Barger, "High Vacuum Scanning Electron Microscopy as a Tool in Surface Analysis," *Johns Hopkins APL Tech. Dig.* 1, No. 1, pp. 38-44 (1980).
- W. Barron and P. Kroll (Metro Center) and W. J. Toth (APL), *GRITS: A Computer Program for the Economic Evaluation of Direct-Use Applications of Geothermal Energy*, JHU/APL QM-80-077 (GEMS-008) (Jun 1980).
- C. W. Bauschlicher, Jr. (NASA), D. M. Silver (APL), and D. R. Yarkony (JHU), "An SCF and MCSCF Description of the Low-Lying States of MgO," *J. Chem. Phys.* 73, No. 6, pp. 2867-2869 (1980).
- R. C. Beal, "Spaceborne Imaging Radar: Monitoring of Ocean Waves," *Science* 208, No. 4450, pp. 1373-1375 (1980).
- R. C. Beal, "The Potential of Spaceborne Synthetic Aperture Radar for Oceanography," *Johns Hopkins APL Tech. Dig.* 1, No. 2, pp. 148-156 (1980).
- W. G. Berl, "Albert Einstein — A Moral Visionary in a Distraught World," *J. Wash. Acad. Sci.* 69, No. 3, pp. 101-108 (1979).
- W. G. Berl and B. M. Halpin, "Human Fatalities from Unwanted Fires," *Johns Hopkins APL Tech. Dig.* 1, No. 2, pp. 129-134 (1980).
- F. S. Billig, "China — As Viewed by an Aerospace Engineer," *Johns Hopkins APL Tech. Dig.* 1, No. 3, pp. 233-239 (1980).
- F. S. Billig, P. J. Waltrup, and R. D. Stockbridge, "The Integral-Rocket, Dual-Combustion Ramjet: A New Propulsion Concept," *J. Spacecr. Rockets* 17, No. 5, pp. 416-424 (1980).
- J. F. Bird, "Sonomagnetic Pulses from Underwater Explosions and Implosions," *J. Acoust. Soc. Am.* 67, No. 2, pp. 491-495 (1980).
- J. F. Bird, R. W. Flower, and G. H. Mowbray, "Analysis of the Retina via Suprafusion Electroretinography," *Biophys. J.* 29, pp. 379-396 (1980).
- A. W. Bjerkaas and F. W. Riedel, *Proposed Model for the Elevation Spectrum of a Wind-Roughened Sea Surface*, JHU/APL TG 1328 (Dec 1979).
- H. D. Black, "The Transit System, 1977: Performance, Plans, and Potential," *Philos. Trans. R. Soc. London A294*, pp. 217-236 (1980).
- R. W. Blevins, H. L. Donnelly, J. T. Stadter, and R. O. Weiss (APL), and L. Perez y Perez (DOE), "At-Sea Test of a Large Diameter, Steel, Cold Water Pipe," *Ocean Engineering for OTEC OED-9*, ASME, pp. 47-65 (1980).
- B. I. Blum (APL) and C. J. Johns, E. E. McColligan, C. R. Smith, and D. M. Steinwachs (JHMI), "A Low Cost Ambulatory Medical Information System," *J. Clin. Eng.* 4, No. 4, pp. 372-378 (1979).
- B. I. Blum (APL) and R. E. Lenhard, Jr. (JHMI), "An Oncology Clinical Information System," *Comput. Mag.*, pp. 42-50 (Nov 1979).
- D. W. Bockemeier (MDAC/St. Louis), W. C. Caywood, P. J. Waltrup, R. D. Stockbridge, and F. S. Billig (APL), and R. S. Burford (Hercules/ABL), *Conceptual Design of the Hypersonic Wide Area Defense Missile II*, CPIA Pub., 315, pp. 387-449 (1980).
- J. Bohandy and B. F. Kim, "A Normal Mode Analysis of Free Base Porphyrin," *Spectrochim. Acta* 36A, pp. 463-466 (1980).
- H. Bouver (APL) and R. E. Bargmann (Univ. Georgia), "Comparison of Computational Algorithms for the Evaluation of the Univariate and Bivariate Normal Distribution," *Computer Science and Statistics: 12th Ann. Symp. on the Interface*, pp. 334-348 (1979).
- N. J. Brown (Univ. California) and D. M. Silver (APL), "Comparison of Reactive and Inelastic Scattering of H₂ + D₂ Using Four Semiempirical Potential Energy Surfaces," *J. Chem. Phys.* 72, No. 7, pp. 3869-3879 (1980).
- J. L. Calkins (JHMI) and B. F. Hochheimer (APL), "Retinal Light Exposure from Operation Microscopes," *Arch. Ophthalmol.* 97, pp. 2363-2367 (1979).
- J. F. Carbary, "Periodicities in the Jovian Magnetosphere: Magnetodisc Models after Voyager," *Geophys. Res. Lett.* 7, No. 1, pp. 29-32 (1980).
- J. F. Carbary and S. M. Krimigis, "Energetic Particle Activity at 5-min and 10-s Time Resolution in the Magnetotail and Its Relation to Auroral Activity," *J. Geophys. Res.* 84, No. A12, pp. 7123-7137 (1979).
- D. E. Corman, "Estimation of J-Integral Uncertainty," *Fracture Mechanics: Twelfth Conf., ASTMSTP 700, American Society for Testing and Materials*, pp. 237-250 (1980).
- L. L. Cronvich and H. P. Liepman, *Advanced Missile Technology — A Review of Technology Improvement Areas for Cruise Missiles*, NASA CR 3187 (1979).
- O. J. Deters and C. B. Barger (APL), G. M. Hutchins (JHMI), and F. F. Mark and M. H. Friedman (APL), "Velocities in Unsteady Flow through Casts of Human Arteries (Abstract)," *Proc. 32nd Ann. Conf. on Engineering in Medicine and Biology* (1979).
- O. J. Deters and M. H. Friedman, "Simple Directionally Sensitive Two-Component Laser Doppler Anemometer," *Appl. Opt.* 19, No. 8, p. 1221 (1980).
- S. C. Dillon, *Evolution of the Orbital Improvement Program*, JHU/APL TG 1320 (Feb 1979).
- G. L. Dugger, "Is There a Chance for OTEC?" *Astronaut. Aeronaut.* 17, No. 11, pp. 36-42 (1979).
- G. L. Dugger, E. J. Francis, and W. H. Avery, "Comparisons of Estimates, Sharing Potentials, Subsidies, and Uses for OTEC Facilities and Plantships," *Expanded Abstracts, Proc. 7th Ocean Energy Conf.*, paper III C/1 (1980).
- G. L. Dugger and F. K. Hill, "Use of Satellite-Derived Sea Surface Temperatures by Cruising OTEC Plants," *Proc. 6th OTEC Conf.* II (1980).

- G. L. Dugger, F. E. Naef, and J. E. Snyder III, "Ocean Thermal Energy Conversion," Chap. 19, *Solar Energy Handbook*, J. Kreider and F. Kreith (eds.), McGraw-Hill, New York (1980).
- A. Eisner, *Drag Estimation and Satellite Orbit Determination*, JHU/APL TG 1327 (Mar 1980).
- A. Eisner and S. M. Yionoulis, *Long-Period Terms in the Neutral Density of the Upper Atmosphere*, JHU/APL CP 076 (Nov 1979).
- C. Feldman, C. H. Arrington III, F. G. Satkiewicz, and N. A. Blum, "Vacuum Deposited Polycrystalline Silicon Films for Solar Cell Applications," *Solar Research Institute Quarterly Report*, 15 Sep - 31 Dec 1979, SERI/XS9/82781-1 (Mar 1980).
- R. W. Flower, "Choroidal Fluorescent Dye Filling Patterns," *Int. Ophthalmol.* 2, No. 3, pp. 143-149 (1980).
- J. W. Follin, Jr. (APL) and S. Briscoe and F. Bennett (Metro Center), *Problems of Hydroelectric Development at Existing Dams. An Analysis of Institutional, Economic, and Environmental Restraints in Pennsylvania, New Jersey, and Maryland 1*, JHU/APL QM-79-237 (Aug 1979).
- S. N. Foner and R. W. Hart, "The Milton S. Eisenhower Research Center: Its Objectives and Activities," *Johns Hopkins APL Tech. Dig.* 1, No. 1, pp. 8-33 (1980).
- G. H. Fountain, F. W. Schenkel, T. B. Coughlin, and C. A. Wingate, "The Magsat Attitude Determination System," *Johns Hopkins APL Tech. Dig.* 1, No. 3, pp. 194-200 (1980).
- D. W. Fox and V. G. Sigillito, "Bounds for Frequencies of Rib Reinforced Plates," *J. Sound Vib.* 69, No. 4, pp. 497-507 (1980).
- E. J. Francis and G. L. Dugger, "Promising Applications of OTEC," *Proc. 7th Energy Technology Conf.*, pp. 1272-1286 (1980).
- A. B. Fraser, R. E. Walker, and F. C. Jurgens, "Spatial and Temporal Correlation of Underwater Sunlight Fluctuations in the Sea," *IEEE J. Oceanic Eng.* OE-5, No. 3, pp. 195-198 (1980).
- R. K. Frazer, "Duplication of Radome Aerodynamic Heating Using the Central Receiver Test Facility Solar Furnace," *Proc. 15th Symp. on Electromagnetic Windows* (1980).
- M. H. Friedman, C. B. Bargerion, O. J. Deters, and F. F. Mark (APL) and G. M. Hutchins (JHMI), "Hemodynamic Measurements in Human Arterial Casts: Geometric Effects and Morphological Correlates," *Proc. 31st ASME Biomech. Symp.* (1979); also in *Proc. XII Int. Conf. on Medical and Biological Engineering* (1979).
- M. H. Friedman and C. B. Bargerion (APL), G. M. Hutchins (JHMI), and F. F. Mark and O. J. Peters (APL), "Hemodynamic Measurements in Human Arterial Casts and Their Correlation with Histology and Luminal Area," *J. Biomech. Eng.* 102, No. 3, pp. 247-251 (1980).
- R. M. Fristrom, "Report of the Task Force on the Flammability of Solid Polymer Cable Dielectrics, Final Report," National Research Council EL-1263, pp. 2-1 to 2-27 (Nov 1979).
- J. F. George and D. Richards, *A Baseline Design of a 40 MW OTEC Pilot Plant*, JHU/APL SR-80-1A,B (Apr 1980).
- J. F. George, D. Richards, and L. L. Perini, *A Baseline Design of an OTEC Pilot Plantship*, JHU/APL SR-78-3A,B,C (May 1979).
- A. D. Goldfinger, "Refraction of Microwave Signals by Water Vapor," *J. Geophys. Res.* 85, No. C9, pp. 4904-4912 (1980).
- A. D. Goldfinger, *SEASAT SAR Processor Signatures: Point Targets*, JHU/APL CP 078 (Apr 1980).
- J. Goldhirsh, "A Review on the Application of Nonattenuating Frequency Radars for Estimating Rain Attenuation and Space-Diversity Performance," *IEEE Trans. Geosci. Electron.* GE-17, No. 4, pp. 218-239 (1979).
- J. Goldhirsh, "Comparison of Radar Derived Slant Path Rain Attenuations with the COMSTAR Beacon Fades at 28.56 GHz for Summer and Winter Periods," *IEEE Trans. Antennas Propag.* AP-28, No. 4, pp. 577-580 (1980).
- J. Goldhirsh, "The Use of Radar at Nonattenuating Wavelengths as a Method for the Estimation of Rain Attenuation at Frequencies Above 10 GHz," *EASCON '79 Record AES 1*, pp. 48-55 (1979).
- A. C. Goodman, *Geothermal Energy Market Penetration: Development of a Model for the Residential Sector*, JHU/APL QM-79-209 (Sep 1979).
- B. L. Gotwols and G. B. Irani, "Optical Determination of the Phase Velocity of Short Gravity Waves," *J. Geophys. Res.* 85, No. C7, pp. 3964-3970 (1980).
- W. M. Gray and R. W. Witte, "Guidance System Evaluation Laboratory," *Johns Hopkins APL Tech. Dig.* 1, No. 2, pp. 144-147 (1980).
- R. A. Greenwald (Max-Planck Inst. Aeronomie), T. A. Potemra (APL), and N. A. Safflek (Boston College), "Stare and Triad Observations of Field-Aligned Current Closure and Joule Heating in the Vicinity of the Harang Discontinuity," *J. Geophys. Res.* 85, No. A2, pp. 563-568 (1980).
- G. Gücer (JHMI) and L. J. Viernstein (APL), "Clinical Evaluation of Long-Term Epidural Monitoring of Intracranial Pressure," *Surg. Neurol.* 12, pp. 373-377 (1979).
- G. Gücer (JHMI) and L. J. Viernstein (APL), "Continuous Recording of ICP in the Normal Monkey," *Intracranial Pressure IV*, K. Shulman et al. (eds.), Springer-Verlag, Berlin (1980).
- G. Gücer (JHMI) and L. J. Viernstein (APL), "Intracranial Pressure in the Normal Monkey while Awake and Asleep," *J. Neurosurg.* 51, pp. 206-210 (1979).
- G. Gücer (JHMI), L. J. Viernstein and J. G. Chubbuck (APL), and A. E. Walker (JHMI), "Clinical Evaluation of Long Term Epidural Monitoring of Intracranial Pressure," *Surg. Neurol.* 12, pp. 373-377 (1979).
- G. Gücer (JHMI) and L. J. Viernstein and W. H. Guier (APL), "A Hemodynamic Model for Relating Phasic Pressure and Flow in the Large Arteries," *IEEE Trans. Biomed. Eng.* BME-27, No. 8, pp. 479-482 (1980).
- G. Gücer (JHMI), L. J. Viernstein (APL), and A. E. Walker (JHMI), "Continuous Intracranial Pressure Recording in Adult Hydrocephalus," *Surg. Neurol.* 13, pp. 323-328 (1980).
- W. H. Guier, *A Hemodynamics Model for Relating Phase Pressure and Flows in the Arteries*, JHU/APL CP 072 (Dec 1979).
- B. W. Hamill, "Experimental Document Design: Guidebook Organization and Index Formats," *Proc. Human Factors Society, 24th Ann. Meeting*, pp. 480-482 (1980).
- D. C. Hamilton and G. Gloeckler (Univ. Maryland), S. M. Krimigis and C. O. Bostrom (APL), T. P. Armstrong (Univ. Kansas), W. I. Axford (Max-Planck Inst. Aeronomie), C. Y. Fan (Univ. Arizona), L. J. Lanzerotti (Bell Labs.), and D. M. Hunten (Univ. Arizona), "Detection of Energetic Hydrogen Molecules in Jupiter's Magnetosphere by Voyager 2: Evidence for an Ionospheric Plasma Source," *Geophys. Res. Lett.* 7, No. 10, pp. 813-816 (1980).
- R. W. Hart (ed.), *Indirectly Funded Research and Exploratory Development at the Applied Physics Laboratory, Fiscal Year 1978*, JHU/APL SR 79-2 (Dec 1979).
- M. E. Hawley, W. A. Bryden, A. N. Bloch, and D. O. Cowan (JHU), T. O. Poehler (APL), and J. P. Stokes (JHU), "Mott Transition and Magnetic Properties of HMTSF (TCNQ), (TCNQF₄)_{1-x}," *Bull. Am. Phys. Soc.* 24, No. 3, p. 232 (1979).
- K. J. Hefferman, G. H. Fountain, B. E. Tossman, and F. F. Mobley, "The Magsat Attitude Control System," *Johns Hopkins APL Tech. Dig.* 1, No. 3, pp. 188-193 (1980).

- F. K. Hill, *Biofouling and Cleaning Tests of OTEC External Flow Heat Exchanger Tubes*, JHU/APL AEO-79-50 (Nov 1979).
- B. F. Hochheimer (APL) and S. A. D'Anna and J. L. Calkins (JHMI), "Retinal Damage from Light," *Am. J. Ophthalmol.* **88**, pp. 1039-1044 (1979).
- H. Hopfield, "Improvements in the Tropospheric Refraction Correction for Range Measurement," *Philos. Trans. R. Soc. London A294*, pp. 341-352 (1980).
- A. N. Jette and J. G. Parker, "Excitation of an Elastic Half-Space by a Buried Line Source of Conical Waves," *J. Sound Vib.* **67**, No. 4, pp. 523-531 (1979).
- A. N. Jette and J. G. Parker, "Surface Displacements Accompanying the Propagation of Acoustic Waves within an Underground Pipe," *J. Sound Vib.* **69**, No. 2, pp. 265-274 (1980).
- S. M. Krimigis, "Observations of Particle Acceleration in the Earth's Magnetotail," *AIP Conf. Proc.*, No. 56, pp. 179-197 (1979).
- S. M. Krimigis (APL), T. P. Armstrong (Univ. Kansas), W. I. Axford (Max-Planck Inst. Aeronomie), C. O. Bostrom (APL), C. Y. Fan (Univ. Arizona), G. Gloeckler (Univ. Maryland), L. J. Lanzerotti (Bell Labs), D. C. Hamilton (Univ. Maryland), and R. D. Zwickl (Los Alamos Scientific Lab.), "Energetic (≈ 100 keV) Tailward Directed Ion Beam Outside the Jovian Plasma Boundary," *Geophys. Res. Lett.* **7**, No. 1, pp. 13-16 (1980).
- S. M. Krimigis (APL) and E. T. Sarris (Democritos Univ. Thrace), "Energetic Particle Bursts in the Earth's Environment," *Dynamics of the Magnetosphere*, D. Reidel, Boston, pp. 599-630 (1979).
- J. R. Kuttler and V. G. Sigillito, "Upper and Lower Bounds for Frequencies of Clamped Rhombical Plates," *J. Sound Vib.* **68**, No. 4, pp. 597-607 (1980).
- M. M. Labes, M. Jones, H. Kao, L. Nichols, and C. Hsu (Temple Univ.) and T. O. Poehler (APL), "Conductivity and Optical Properties of a Polyiodine Canal Complex (Benzophenone)₉ (KI)₂17CHCl₃," *Mol. Cryst. Liq. Cryst.* **52**, p. 115 (1979).
- L. J. Lanzerotti and C. G. MacLennan (Bell Telephone Labs.), S. M. Krimigis (APL), T. P. Armstrong (Univ. Kansas), and K. Behannon and N. F. Ness (NASA), "Statics of the Nightside Jovian Plasma Sheet," *Geophys. Res. Lett.* **7**, No. 10, pp. 817-820 (1980).
- A. L. Lew, *The Microprocessor Based Magsat Command System*, JHU/APL CP 077 (Feb 1980).
- A. L. Lew, B. C. Moore, J. R. Dozsa, and R. K. Burek, "The Magsat Telecommunications System," *Johns Hopkins APL Tech. Dig.* **1**, No. 3, pp. 183-187 (1980).
- A. T. Y. Lui, "Observations on Plasma Sheet Dynamics during Magnetospheric Substorms," *Dynamics of the Magnetosphere*, D. Reidel, Boston, pp. 563-597 (1979).
- M. Maxfield, D. O. Cowan, and A. N. Bloch (JHU) and T. O. Poehler (APL), "Synthesis of 13,13,14,14-Tetracyano-4,5,9,10-Tetrahydropyrenequinodimethane, an Electron Acceptor for Organic Metals," *Nouv. J. Chimie* **3**, No. 11, p. 647 (1979).
- C.-I. Meng, "Polar Cap Variations and the Interplanetary Magnetic Field," in *Dynamics of the Magnetosphere*, D. Reidel, Boston, pp. 23-46 (1979).
- R. A. Meyer, M. E. Zaruba, and G. M. McKhann, "Flow Cytometry of Isolated Cells from the Brain," *Anal. Quant. Cytol. J.* **2**, No. 1, pp. 66-74 (1980).
- D. G. Mitchell and E. C. Roelof, "Thermal Iron Ions in High Speed Solar Wind Streams: Detection by the IMP 7, 8 Energetic particle Experiments," *Geophys. Res. Lett.* **7**, No. 9, pp. 661-664 (1980).
- F. O. Mitchell, *Evaluation of Potential Geothermal Resource Areas*, JHU/APL QM-79-163R/GT (Rev. Jul 1980).
- F. F. Mobley, "Magsat Performance Highlights," *Johns Hopkins APL Tech. Dig.* **1**, No. 3, pp. 175-178 (1980).
- F. F. Mobley, L. D. Eckard, G. H. Fountain, and G. W. Ousley, "Magsat — A New Satellite to Survey the Earth's Magnetic Field," *IEEE Trans. Magnet. MAG-16*, No. 5, pp. 758-760 (1980).
- L. Monchick, "A Comment on the Inversion of Gas Transport Properties," *J. Chem. Phys.* **73**, No. 6, pp. 2929-2931 (1980).
- L. Monchick, "Surface Diffusion and Spin Polarization: Two Dimensional CIDEP," *J. Chem. Phys.* **72**, No. 11, pp. 6258-6264 (1980).
- L. Monchick, J. G. Parker, and T. A. Potemra, "The Role of Vibrationally Excited Oxygen in Auroral Excitation of O₂ ($^1\Delta_g$)," *J. Geophys. Res.* **85**, No. A4, pp. 1792-1794 (1980).
- M. L. Moon, "Environmental Impact of Salt Drift from a Natural Draft Cooling Tower," *Johns Hopkins APL Tech. Dig.* **1**, No. 2, pp. 120-128 (1980).
- J. C. Murphy and L. C. Aamodt, "Photothermal Spectroscopy Using Optical Beam Probing: Mirage Effect," *J. Appl. Phys.* **51**, No. 9, pp. 4580-4588 (1980).
- W. B. Newman, "Managing a Report Collection for Zero Growth," *Spec. Libraries* **71**, No. 5-6, pp. 276-282 (1980).
- R. R. Newton, "On the Fractions of Degrees in an Ancient Star Catalogue," *Q. J. R. Astron. Soc.* **20**, pp. 383-394 (1979).
- V. O'Brien, "Fully Developed Forced Convection in Rectangular Ducts and Illustrations of Some General Inequalities," *Z. Angew. Math. Phys.* **30**, pp. 913-928 (1979).
- V. O'Brien, "Pulsatile Flow through a Constricted Artery," *Bull. Am. Phys. Soc.* **24**, No. 8, p. 1130 (1979).
- V. O'Brien and L. W. Ehrlich, "Pulsatile Flow through a Constricted Artery," *Proc. 2nd Mid-Atlantic Conf. on Biofluid Mechanisms*, pp. 497-516 (1980).
- F. C. Paddison and K. Yu, "Use of Geothermal Energy in the Eastern United States," *Johns Hopkins APL Tech. Dig.* **1**, No. 2, pp. 88-100 (1980).
- D. A. Payne, "Bäcklund Transformations in Several Variables," *J. Math. Phys.* **21**, No. 7, pp. 1593-1602 (1980).
- T. E. Phillips (APL) and B. M. Hoffman, C. J. Schramm, and S. K. Wright (Northwestern Univ.), "Conductive Molecular Crystals: Metallic Behavior in Partially Oxidized Porphyrin, Tetrabenzoporphyrin, and Phthalocyanine," *Molecular Metals*, Plenum Press, New York, p. 393 (1979).
- T. E. Phillips (APL), R. P. Scaringe (Eastman Kodak), and B. M. Hoffman and J. A. Ibers (Northwestern Univ.), "Conductive Molecular Crystals: Structural, Electrical, and Magnetic Properties of Partially Oxidized Octamethyltetrabenzoporphyrinatonicel (II)," *J. Am. Chem. Soc.* **102**, No. 10, pp. 3435-3444 (1980).
- T. O. Poehler (APL) and M. E. Hawley, W. A. Bryden, J. P. Stokes, A. N. Bloch, and D. O. Cowan (JHU), "Charge Transfer Salts of Fluorinated TCNQ: Mott Insulators Isostructural with Organic Conductors," *Proc. Conf. Organic Conductors and Semiconductors*, Springer-Verlag, Berlin (1979).
- T. O. Poehler and R. S. Potember (APL) and D. O. Cowan and A. N. Bloch (JHU), "Switching and Memory Phenomena in Semiconducting Charge-Transfer Complexes," *Proc. Electrochem. Soc.* **80-1**, pp. 189-190 (1980).
- I. P. Pollack (JHMI), L. J. Viernstein (APL), and R. L. Radius (JHMI), "An Instrument for Constant-Pressure Tonography," *Exp. Eye Res.* **29**, pp. 579-585 (1979).
- R. S. Potember and T. O. Poehler (APL) and D. O. Cowan and A. N. Bloch (JHU), "Electrical Switching and Memory Phenomena in Semiconducting Organic Charge-Transfer Complexes," *The Physics and Chemistry of Low Dimensional Solids*, L. Alacer (ed.), D. Reidel, Boston, pp. 419-428 (1980).

- R. S. Potember and T. O. Poehler (APL) and D. O. Cowan and A. N. Bloch (JHU), "Electrical Switching and Memory Phenomena in Semiconducting Organic Thin Films," *Proc. Symp. on Polymer Materials for Electronic Applications* 43, pp. 380-385 (1980).
- R. S. Potember and T. O. Poehler (APL) and A. Rappa, D. O. Cowan, and A. N. Bloch (JHU), "A Reversible Field Induced Phase Transition in Semiconducting Films of Silver and Copper TNAP Radical-Ion Salts," *J. Am. Chem. Soc.* 102, Vol. 10, pp. 3659-3660 (1980).
- T. A. Potemra, "Studies of Auroral Field-Aligned Currents with Magsat," *Johns Hopkins APL Tech. Dig.* 1, No. 3, pp. 228-232 (1980).
- T. A. Potemra (APL), T. Iijima (Univ. Tokyo), and N. A. Saflekos (Boston College), "Large-Scale Characteristics of Birkeland Currents," *Dynamics of the Magnetosphere*, D. Reidel, Boston, pp. 165-199 (1979).
- T. A. Potemra, "Current Systems in the Earth's Magnetosphere," *Rev. Geophys. Space Phys.* 17, No. 4, pp. 640-656 (1979).
- T. A. Potemra, "Studies of Auroral Field-Aligned Currents with Magsat," *Johns Hopkins APL Tech. Dig.* 1, No. 3, pp. 228-232 (1980).
- T. A. Potemra, F. F. Mobley, and L. D. Eckard, "The Geomagnetic Field and Its Measurement: Introduction and Magnetic Field Satellite (Magsat) Glossary," *Johns Hopkins APL Tech. Dig.* 1, No. 3, pp. 162-170 (1980).
- W. R. Powell, "Community Annual Storage Energy System," *Johns Hopkins APL Tech. Dig.* 1, No. 2, pp. 108-113 (1980).
- W. R. Powell, "Solar Electric District Heating via CASES," *Proc. Intersociety Energy Conversion Engineering Conf.*, Seattle, pp. 904-909 (1980).
- A. J. Pue, *Control Law Implementation for Short Headway Vehicle-Follower AGT System*, JHU/APL CP 075/TPR 045 (Oct 1979).
- A. J. Pue, H. Y. Chiu, and S. J. Brown, Jr., *Operational Concepts and Implementation Techniques for Vehicle-Follower Control of AGT Systems*, JHU/APL CP 074/TPR 041 (Aug 1979).
- D. W. Rabenhorst, "Demonstration of a Low Cost Flywheel in an Energy Storage System," *Proc. 1979 Mechanical and Magnetic Energy Storage Contractors' Review Meeting*, pp. 408-414 (1979).
- D. W. Rabenhorst, "Energy Conservation with Flywheels," *Johns Hopkins APL Tech. Dig.* 1, No. 2, pp. 114-119 (1980).
- R. P. Rich, "Mechanical Proof Testing," *Comput. Lang.* 5, pp. 1-28 (1980).
- C. H. Ronnenburg and R. L. Trapp, "Automated Antenna Tests Save Time and Cut Costs," *Microwaves* 19, No. 1, pp. 66-72 (1980).
- L. J. Rueger and A. G. Bates, "Nova Satellite Time Experiment," *Radio Sci.* 14, No. 4, pp. 707-714 (1979).
- N. A. Saflekos and T. A. Potemra, "The Orientation of Birkeland Current Sheets in the Dayside Polar Region and Its Relationship to the IMF," *J. Geophys. Res.* 85, No. A5, pp. 1987-1994 (1980).
- F. G. Satkiewicz, "Secondary Ion Mass Spectrometry for the Study of Solids," *Johns Hopkins APL Tech. Dig.* 1, No. 1, pp. 45-48 (1980).
- F. W. Schenkel, *An Auroral Spectrophotometer (Vacuum Ultraviolet and Visible)*, JHU/APL CP 079 (Aug 1980).
- J. A. Schetz, F. S. Billig, and S. Favin, "Approximate Analysis of Axisymmetric Supersonic Base Flows with Injection," *AIAA J.* 18, No. 8, pp. 867-868 (1980).
- G. Schmeisser (JHMI) and W. Seamone (APL), "An Assistive Equipment Controller for Quadriplegics," *Johns Hopkins Med. J.* 148, No. 3, pp. 84-88 (1979).
- G. Schmeisser (JHMI) and W. Seamone (APL), "Low Cost Assistive Device Systems for a High Spinal Cord Injured Person in the Home Environment," *Bull. Prosthetics Res.* BPR 10-32, pp. 212-223 (1979).
- D. M. Silver, "Interaction Energy between Two Ground-State Helium Atoms Using Many-Body Perturbation Theory," *Phys. Rev. A* 21, No. 4, pp. 1106-1117 (1980).
- D. M. Silver, "Rotationally Inelastic Collisions of LiH with He. I. *Ab Initio* Potential Energy Surface," *J. Chem. Phys.* 72, No. 12, pp. 6445-6451 (1980).
- D. M. Silver (APL) and N. J. Brown (Univ. California), "Valence Bond Model Potential Energy Surface for H₄," *J. Chem. Phys.* 72, No. 7, pp. 3859-3868 (1980).
- J. F. Smola, "The Magsat Magnetometer Boom System," *Johns Hopkins APL Tech. Dig.* 1, No. 3, pp. 201-204 (1980).
- H. M. South, "High Data-Rate Recordings and Processing Systems for Hydrophone Arrays," *Proc. Oceans '80 Conf.* (1980).
- W. D. Stanbro and D. A. Pyrck, "Stability of Rhodamine WT in Saline Waters," *Water Resour. Res.* 15, No. 6, pp. 1631-1632 (1979).
- M. A. Stanford, J. C. Swartz, T. E. Phillips, and B. M. Hoffman, "Electronic Control of Ferroporphyrin Ligand-Binding Kinetics," *J. Am. Chem. Soc.* 102, No. 13, pp. 4492-4499 (1980).
- J. P. Stokes, A. N. Bloch, W. A. Bryden, D. O. Cowan, and M. E. Hawley (JHU) and T. O. Poehler (APL), "Mott Transition and Conductivity in the Organic Solid Solutions HMTSF (TCNQ)_x (TCNQF₄)_{1-x}," *Bull. Am. Phys. Soc.* 24, No. 3, p. 232 (1979).
- A. M. Stone, "Geothermal Energy — An Overview," *Johns Hopkins APL Tech. Dig.* 1, No. 2, pp. 78-87 (1980).
- H. Sulzbacher and W. Baumjohann (Univ. Münster, FRG) and T. A. Potemra (APL), "Coordinated Magnetic Observations of Morning Sector Auroral Zone Currents with Triad and the Scandinavian Magnetometer Array: A Case Study," *J. Geophys. Res.* 85, pp. 7-17 (1980).
- J. E. Tillman, *Brittle Deformation of the Manhattan Prong: Progress Report Aug 1979 - June 1980*, JHU/APL QM-80-104 (Aug 1980).
- B. E. Tossman, F. F. Mobley, G. H. Fountain, K. J. Hefferman, J. C. Ray, and C. E. Williams, "Magsat Attitude Control System, Design and Performance," *Proc. AIAA Guidance and Control Conf.*, AIAA-80-1730-CP, CP-805 (1980).
- L. J. Viernstein, "Intracranial Pressure Monitoring," *Johns Hopkins APL Tech. Dig.* 1, No. 2, pp. 135-143 (1980).
- L. J. Viernstein (APL) and I. P. Pollack (JHMI), "Validity of the Imbert-Fick Law for Constant-Pressure Tonography," *Exp. Eye Res.* 29, pp. 587-594 (1979).
- J. L. Wagner (APL) and J. D. Anderson, Jr. (Univ. Maryland), "Laser Radiation — Gasdynamic Coupling in the SF₆-Air Laminar Boundary Layer," *AIAA J.* 18, No. 3, pp. 333-334 (1980).
- W. M. Walsh, F. Wudl, G. A. Thomas, D. Nolewajek, J. J. Hauser, and P. A. Lee (Bell Labs.) and T. O. Poehler (APL), "Restoration of Metallic Behavior in Organic Conductors by Small Electric Fields," *Phys. Rev. Lett.* 45, No. 10, pp. 829-832 (1980).
- L. T. Watson (Michigan State Univ.) and D. Fenner (APL), "Algorithm 555: Chow-Yorke Algorithm for Fixed Points or Zeros of C² Maps [CS]," *ACM Trans. Math. Software* 6, No. 2, pp. 252-259 (1980).
- R. O. Weiss, R. W. Blevins, H. L. Donnelly, and J. T. Stadter (APL) and L. Perez y Perez (DOT), "At-Sea Test of a Large Diameter, Steel, Cold Water Pipe," *Ocean Engineering for OTEC, Proc. 1980 Energy-Sources Technology Conf.*, pp. 47-67 (1980).

- R. O. Weiss and J. T. Stadter, "Analysis of Contact through Finite Element Gaps," *Comput. Struct.* **10**, pp. 867-873 (1979).
- S. Wilson (Science Research Council, UK) and D. M. Silver (APL), "Diagrammatic Perturbation Theory: An Application to the Nitrogen, Carbon Monoxide, and Boron Fluoride Molecules Using a Universal Even-Tempered Basis Set," *J. Chem. Phys.* **72**, No. 3, pp. 2159-2165 (1980).
- S. Wilson (Science Research Council, UK) and D. M. Silver (APL), "On the Contribution of Higher-Order Excitations to Correlation Energies: The Ground State of the Water Molecule," *Theoret. Chim. Acta* **54**, pp. 83-91 (1979).
- S. K. Wright and C. J. Schramm (Northwestern Univ.), T. E. Phillips (APL), and D. M. Scholler and B. M. Hoffman (Northwestern Univ.), "Conductive Molecular Solids: Partial Iodine Oxidation of Octaethylporphyrins," *Synth. Metals* **1**, No. 1, p. 43 (1979).
- L. J. Zanetti and T. A. Potemra (APL), J. P. Doering and J. S. Lee (JHU), R. L. Arnoldy (Univ. New Hampshire), and R. A. Hoffman (NASA), "Coincident Particle Observations from AE-C and ATS 6 during the October 28, 1977, Geomagnetic Storm," *J. Geophys. Res.* **85**, No. A9, pp. 4563-4570 (1980).

PRESENTATIONS

- F. J. Adrian, "Nature of the Three-Electron Bond in Noble Gas Monohalides as Revealed by ESR Spectroscopy," Meeting, Greater Washington ESR Discussion Group, Georgetown Univ., 22 Feb 1980.
- F. J. Adrian, "Radical Pair Mechanism of Chemically Induced Magnetic Polarization," Seminar, Princeton Univ., 23 Oct 1979.
- R. H. Andreo, "Stochastic Variational Principles for Electromagnetic Wave Scattering from Random Systems," Meeting on Recent Development in Classical Wave Scattering: Focus on the T-Matrix Approach, Ohio State Univ., 25-27 Jun 1979.
- R. H. Andreo and J. A. Krill, "Vector Stochastic Variational Expressions for Electromagnetic Wave Scattering from Random Magnetic Objects," Workshop on Wave Propagation in Random Media, VPI&SU, 25 Mar 1980.
- R. H. Andreo and J. A. Krill, "Vector Stochastic Variational Principles: Generalizations and Computational Features," CSL Scientific Conf. on Obscuration and Aerosol Research, Aberdeen Proving Ground, 22 Jul 1980.
- W. H. Avery, "The OTEC Contribution to Energy Needs of All Regions of the U.S.," IEEE 1980 Region 6 Conf., San Diego, 21 Feb 1980.
- C. B. Barger, "Precursive Blistering in the Localized Corrosion of Aluminum," Corrosion Seminar, NSWC, White Oak, Md., 15 Jan 1980; also presented at Washington, D.C. Chapter, Electrochemical Society, 3 Apr 1980.
- C. B. Barger, R. L. McCally, and R. A. Farrell, "CO₂-Laser Damage Thresholds in the Cornea: A Critical Temperature versus a Damage Integral Mechanism," Fourth International Congress of Eye Research, New York, 30 Sep 1980.
- F. S. Billig, "A Visit to China," JHU/APL Colloq., Laurel, Md., 11 Apr 1980.
- N. A. Blum, K. Moorjani, F. Satekiewicz, and T. O. Poehler, "Mossbauer and SIMS Investigation of Amorphous Fe₃B_{1-x} Thin Films," American Physical Society Meeting, New York, Mar 1980.
- J. L. Calkins (JHMI), B. F. Hochheimer (APL), and S. A. D'Anna (JHMI), "Potential Hazards from Specific Ophthalmic Devices," Conf. on Intense Light Hazards in Ophthalmic Diagnosis and Treatment, Houston, 25 Nov 1979.
- L. L. Cronvich, "Aerodynamics of Airbreathing Missiles for U.S. Navy Surface-to-Air Application," Workshop on Aerodynamics of Missiles with Airbreathing Propulsion, London, 8-9 May 1980.
- G. L. Dugger, "Ocean Thermal Energy Conversion," First International Symp. on Non-Conventional Energy, Trieste, 27 Aug - 21 Sep 1979.
- G. L. Dugger, E. J. Francis, and W. H. Avery, "Projected Costs for Electricity and Products from OTEC Facilities and Plantships," IECEC '80, 15th Intersociety Energy Conversion Engineering Conf., "Energy to the 21st Century," Seattle, 18-22 Aug 1980.
- W. L. Ebert, "Multiple Marker Bi-Plane Cineventriculogrammetry," Interdepartmental Seminars on Cardiovascular Research, The Johns Hopkins Univ., 25 Oct 1979.
- L. W. Ehrlich, "An ad hoc SOR Method," Conf. on Elliptic Problem Solvers, Santa Fe, N. Mex., 2 Jul 1980.
- A. Eisner and S. M. Yionoulis, "Neutral Density Variations in the 900-1200 km Region of the Upper Atmosphere," International Symp. on Space Geodesy and Its Applications, Cannes, 18-21 Nov 1979.
- R. A. Farrell, R. H. Andreo, and R. L. McCally, "Cross Polarized Small-Angle Light Scattering Patterns in Cornea," Symp. on Principles and Applications of Light Scattering: ACS 2nd Chemical Congress of the North American Continent, Las Vegas, 26 Aug 1980.
- R. A. Farrell, R. H. Andreo, and R. L. McCally, "Structural Implications of Polarized Light Scattering in Cornea," Fourth International Congress for Eye Research, New York, 30 Sep 1980.
- C. Feldman, "Vacuum Deposited Polycrystalline Silicon Films for Solar Cell Applications," 14th IEEE Photovoltaic Conf., San Diego, 7-10 Jan 1980.
- R. W. Flower, "The Role of Oxygen in Retinopathy: A 14-Year APL-Wilmer Institute Cooperative Study," JHU/APL Colloq., Laurel, Md., 30 May 1980.
- D. W. Fox, "Bounds for Eigenfrequencies of Reinforced Elastic Plates," Seminar, Dept. Mathematical Sciences, The Johns Hopkins Univ., 10 Apr 1980.
- D. W. Fox, "Bounds for Eigenvalues of Reinforced Plates" and "Useful Technical Devices in Intermediate Problems," Conf. on the Numerical Treatment of Boundary and Eigenvalue Problems for Partial Differential Equations, Clausthal, West Germany, 29-30 Sep 1980.
- E. J. Francis, W. H. Avery, and G. L. Dugger, "Comparison of Cost Estimates, Sharing Potential, Subsidies, and Uses for OTEC Facilities and Plantships," 7th Ocean Energy Conf., Washington, 2-4 Jun 1980.
- J. F. George and D. Richards, "Design and Integration of a 40 MW_e Floating OTEC Pilot Plant," 7th Ocean Energy Conf., Washington, D.C., 2-4 Jun 1980.
- J. F. George and D. Richards, "Preliminary Design of a Cruising OTEC Modular Experiment," 14th Intersociety Energy Conversion Engineering Conf., Boston, 10 Aug 1979.
- J. W. Giles and H. A. Kues, "Photographic Dye Studies of Underwater Wakes," Ocean Optics VI, Naval Postgraduate School, 25 Nov 1979.
- G. Gücer (JHMI) and L. J. Viernstein (APL), "Continuous

- Recording of ICP in the Normal Monkey," American Association of Neurological Surgeons, Los Angeles, Apr 1979; also presented at the 4th International Symp. on Intracranial Pressure, Williamsburg, Va., Jun 1979.
- A. N. Jette, "Interpretation of Hyperfine Interaction and Structure of Defect Centers Using a Spin-Correlated Valence Bond Theory," Seminar, Univ. Antwerp, 4 Mar 1980; also presented at Seminar, Gesamthochschule Paderborn, FRG, 22 Apr 1980.
- A. N. Jette, "Valence Bond Study of Hyperfine Interactions and Structure of Hypervalent Radicals," Zentrum Interdisziplinäre Forschung, Univ. Bielefeld, FRG, 11 Mar 1980.
- H. A. Kues, "Retinal Nerve Fiber Enhancement Techniques," Wilmer Research Institute Meeting, Baltimore, 27 Sep 1979.
- J. R. Kuttler, "Estimating Characteristic Frequencies of Orthotropic Clamped Plates," Meeting, American Mathematical Society, San Antonio, 6 Jan 1980.
- L. Monchick, "Anisotropic Forces and Molecular Collisions," Zentrum Interdisziplinäre Forschung, Univ. Bielefeld, FRG, 20 Nov 1979; also presented at Inst. Theoretical Physics, Univ. Erlangen-Nürnberg, 3 Dec 1979.
- K. Moorjani, "Disordered Magnets," Physics Dept. Seminar, Univ. Maryland, College Park, 27 Feb 1980.
- K. Moorjani, "Magnetic Glasses," Groupe de Transition des Phases, C.N.R.S., Grenoble, France, 23 Jul 1979; also presented at 7th AIRAPT International Conf., Le Creusot, France, 30 Jul - 3 Aug 1979.
- K. Moorjani, "Magnetic Phase Diagrams of Amorphous Metallic Alloys," 4th International Conf. on Liquid and Amorphous Metals, Grenoble, France, 7-11 Jul 1980.
- K. Moorjani (APL) and S. K. Ghatak (Indian Inst. of Tech., Kharagpur), "Competing Exchange Interactions in Random Magnets," American Physical Society Meeting, Chicago, 20-21 Jan 1980.
- J. C. Murphy, "Time Dependent Processes in Photoacoustic Spectroscopy," Topical Meeting on Photoacoustic Spectroscopy, Univ. Iowa, 1-3 Aug 1979.
- V. O'Brien, "Pulsatile Blood Flow," Bioengineering Seminar, The Johns Hopkins Univ., 22 Oct 1979.
- V. O'Brien, "Pulsatile Flow in Arteries," Fluid Dynamics Reviews, Univ. Maryland, College Park, 2 May 1980.
- V. O'Brien and L. Ehrlich, "Planar Entry Flow of Viscoelastic Fluid," Workshop of Viscoelastic Flow, Brown Univ., 2 Nov 1979.
- T. O. Poehler, "Infrared Extinction in Conducting Organic Polymers and Compounds," CSL Scientific Conf. on Obscuration and Aerosol Research, Aberdeen Proving Ground, Md., 24 Jul 1980.
- T. O. Poehler, "Infrared Extinction in Organic Compounds and Polymers," CSL Scientific Conf. on Obscuration and Aerosol Research, Aberdeen Proving Ground, Md., 17-21 Sep 1979.
- T. O. Poehler, "Switching and Memory Effects in Organic Semiconducting Charge-Transfer Complexes," Chemistry Div. Symp., Naval Research Lab., Washington, D.C., 13 Feb 1980.
- T. O. Poehler, "Switching and Memory Phenomena in Semiconducting Charge Transfer Complexes," Gordon Research Conf. on Electron-Donor-Acceptor Interaction, Wolfboro, N.H., 13 Aug 1980.
- T. O. Poehler, "Switching and Memory Effects in Organic Charge Transfer Complexes," International Conf. on Low Dimensional Synthetic Metals, Copenhagen, 14 Aug 1980.
- R. S. Potember and T. O. Poehler, "Switching Phenomena and Memory in Organic Semiconductors," Chemistry Dept. Colloq., Univ. Pennsylvania, 29 Jan 1980.
- R. S. Potember and T. O. Poehler (APL) and D. O. Cowan (JHU), "Switching and Memory Phenomena in Semiconducting Charge-Transfer Complexes," Meeting, American Chemical Society, Washington, D.C., 10-13 Sep 1979.
- R. S. Potember and T. O. Poehler (APL) and A. Rappa, D. O. Cowan, and A. N. Bloch (JHU), "Electrical Switching and Memory Phenomena in Semiconducting Organic Charge-Transfer Complexes," NATO Advanced Study Inst. on Physics and Chemistry of Low Dimensional Solids, Tomar, Portugal, 27 Aug - 7 Sep 1979.
- J. C. W. Rogers, "Numerical Solution of Systems of Conservation Laws," Colloq., Dept. Mathematics, Univ. Wisconsin, Madison, 1 Apr 1980.
- J. C. W. Rogers, "The Stefan Problem," Analysis Seminar, Univ. Minnesota, 31 Mar 1980.
- J. A. Schetz, F. S. Billig, and S. Favin, "Analysis of Mixing and Combustion in a Scramjet Combustor with Co-Axial Fuel Jet," 16th AIAA/SAE/ASME Joint Propulsion Conf., Hartford, Conn., Jun 1980.
- J. A. Schetz, F. S. Billig, and S. Favin, "Approximate Analysis of Base Drag Reduction by Base and/or External Burning for Axisymmetric Supersonic Bodies," 16th AIAA/SAE/ASME Joint Propulsion Conf., Hartford, Conn., Jun 1980.
- V. G. Sigillito, "A Software Package for Elliptic Partial Differential Equations," Conf. on Elliptic Problem Solvers, Santa Fe, N. Mex., 2 Jul 1980.
- D. M. Silver, "Electron Correlation in Simple Chemical Systems," Univ. Electro-Communications, Chofu-shi, Tokyo, 16 Nov 1979.
- D. M. Silver, "Rotational Energy Transfer in LiH-He Collisions: A Comparison between Theory and Experiment," Hebrew Univ., Jerusalem, 23 Dec 1979.
- J. E. Tillman, "Differentiation of Mesozoic Fractures by Fluid Inclusion Analysis," U.S. Geological Survey Seminar, Reston, Va., 7 Feb 1980.
- J. E. Tillman, "Hydrothermal and Uplift Histories of the Northern Appalachian Basin," Eastern Section Meeting, Assoc. of Petroleum Geologists, Morgantown, W. Va., 1-4 Oct 1979.
- J. E. Tillman, "Unraveling the Cenozoic Tectonic History of the Eastern U.S.," Nuclear Regulatory Commission Seminar, Bethesda, Md., 19 Feb 1980.
- P. J. Waltrup, "Observed Pressure Oscillations in Full-Scale Subsonic Dump Combustors," and "Overview of NAVSEA Air Breathing Propulsion Programs," 1979 JANNAF Workshop on Pressure Oscillations in Ramjets, Monterey, Calif., 7-8 Sep 1979.
- P. J. Waltrup, F. S. Billig, and M. C. Evans, "Critical Considerations in the Design of Supersonic Combustion Ramjet (Scramjet) Engines," 16th AIAA/SAE/ASME Joint Propulsion Conf., Hartford, Conn., 30 Jun - 2 Jul 1980.
- G. P. Warman, J. C. Murphy, and L. C. Aamodt, "Surface Area Effects in Photoacoustic Spectroscopy," Topical Meeting on Photoacoustic Spectroscopy, Univ. Iowa, 1-3 Aug 1979.
- L. B. Weckesser, "DC93-104 Thermal Modeling Efforts," JANNAF Ramjet Combustor Insulator Thermal Modeling Workshop, Monterey, Calif., 14 Mar 1980.
- L. B. Weckesser, "Radome Aerodynamic Heating Effects on Boresight Error," 15th Symp. on Electromagnetic Windows, Atlanta, 18-20 Jun 1980.
- L. B. Weckesser and L. L. Perini, "Thermal Modeling of Combustor Insulation DC93-104," JANNAF 1980 Propulsion Meeting, Monterey, Calif., 11-13 Mar 1980.
- R. O. Weiss (APL), R. Barr (Hydronautics), J. Giannotti (Giannotti and Assoc.), W. Deuchler (Gibbs and Cox), R. Scotti (NOAA), J. Stadter (APL), and J. Walsh (VSE), "Report of the Ad Hoc OTEC CWP Committee: An Assessment of Existing Analytical Tools for Predicting CWP Stresses," 7th Ocean Energy Conf., Washington, D.C., 2-4 Jun 1980.

AUTHOR INDEX

AUTHOR INDEX

A

Adrian, F. J., 138
Andreo, R. H., 140

B

Bargeron, C. B., 123, 134
Benson, R. C., 134
Bird, J. F., 74
Blevins, R. W., 157
Bohn, P. F., 102
Boland, T. G., 102, 104
Brocklebank, D., 104, 107
Brown, C. R., 43
Brown, N. K., 102
Bugenhagen, T. G., 60
Bundsen, B., 60
Buono, S. F., 168

C

Carbary, J. F., 68
Carpenter, L. B., 60
Carter, B. K., 16
Chiu, H. Y., 37
Clevering, R. J., 18
Cole, C. E., Jr., 21

D

Davey, H. C., 170
Davidoff, A. E., 48, 54
Day, D. A., 24
Deters, O. J., 126
Diamant, A. M., 95

E

Edwards, C. R., 79
Ehrlich, L. W., 126

F

Farrell, R. A., 123
Ferguson, J. B., 48
Fischell, R. E., 128
Fox, D. W., 142
Funk, J. A., 154

G

Grady, H. M., 89
Grant, D. G., 120, 121

H

Haase, S. F., 16
Hill, M. L., 34
Hunter, I. R., 86
Hunter, L. W., 163
Hutchins, G. M., 126

I

Irzinski, E. P., 26

J

Jones, S. C., 71
Judd, T. M., 121

K

Kahn, S. A., 51
Keirse, J. L., 154
Knapp, H. H., 170
Kraus, B. M., 21
Krill, J. A., 140
Krimigis, S. M., 68
Kuehne, B. E., 37
Kundin, S. J., 89
Kuvshinoff, B. W., 109

L

Lalmond, J. T., 121
Lasky, M. D., 102

M

Mark, F. F., 126
McCally, R. L., 123
McDowell, R. B., 102
Miller, F. W., 102
Moble, F. F., 66
Monaldo, F. M., 76
Monchick, L., 136
Moorjani, K., 145
Myers, S. M., 18

N

Nelson, R. L., 48

O

O'Brien, V., 126
O'Connor, J. S., 157
Ondercin, D. G., 92

P

Pandolfini, P. P., 154
Petersen, J. W., 86
Phillips, L. G., 160
Pixler, H. D., 102
Plessner, K. T., 32
Poehler, T. O., 147
Potember, R. S., 147
Pride, B. J., 112

Q

Qualkinbush, D. N., 89

R

Radford, W. E., 128
Reichert, R. T., 40
Renich, W. T., 107, 109
Riffle, G. W., 18
Rzemien, R., 18

S

Sagawa, K., 126
Schmid, M. E., 54
Sigillito, V. G., 142
Soukup, M. M., 168
Stanbro, W. D., 160
Stewart, R. L., 51
Stovall, R. E., 104

T

Thurber, R. E., 18
Tolchin, S. G., 51
Trapp, R. L., 54

W

Wald, L. W., 32
Waltrip, C. F., 172
Wetzlar, E. C., 16

